Cell volume regulation in response to deformations

Larisa Venkova

▶ **To cite this version:**

Larisa Venkova. Cell volume regulation in response to deformations. Biophysics. Université Paris Saclay (COmUE), 2019. English. NNT : 2019SACLS396 . tel-02446596

HAL Id: tel-02446596
https://theses.hal.science/tel-02446596

Submitted on 21 Jan 2020

HAL is a multi-disciplinary open access archive for the deposit and dissemination of scientific research documents, whether they are published or not. The documents may come from teaching and research institutions in France or abroad, or from public or private research centers.

L'archive ouverte pluridisciplinaire **HAL**, est destinée au dépôt et à la diffusion de documents scientifiques de niveau recherche, publiés ou non, émanant des établissements d'enseignement et de recherche français ou étrangers, des laboratoires publics ou privés.

université PARIS-SACLAY

NNT : 2019SACLS396

Thèse de doctorat

UNIVERSITÉ PARIS SUD
Comprendre le monde, construire l'avenir

Régulation du volume cellulaire en réponse aux déformations

Thèse de doctorat de l'Université Paris-Saclay
préparée à l'Université Paris-Sud

École doctorale n°577 :
Structure et Dynamique des Systèmes Vivants (SDSV)
Spécialité de doctorat : sciences de la vie et de la santé

Thèse présentée et soutenue à Paris, le 25 Octobre 2019, par

Larisa Venkova

Composition du Jury:

Guillaume Charras Professeur, University College London	Président
Timo Betz Professeur, University Münster	Rapporteur
Pierre Nassoy DR, Institut d'Optique Graduate School	Rapporteur
Cristophe Le Clainche DR, Institut de Biologie Intégrative de la Cellule	Examinateur
Françoise Brochard-Wyart Professeur Emérite, Institut Curie	Examinatrice
Matthieu Piel DR, Institut Curie	Directeur de thèse

Contents

Résumé

L'importance de la rétroaction entre la signalisation biochimique et les propriétés physiques de la cellule et de l'environnement a été explorée dans de nombreuses études. Les cellules dans les tissus génèrent et subissent en permanence des forces mécaniques, souvent corrélées aux modifications des voies de signalisation cellulaires. Ainsi, les perturbations biochimiques à l'intérieur des cellules ainsi que les modifications de leur environnement mécanique peuvent les pousser à partir d'un état physiologique équilibré conduisant à des pathologies, par ex. cancer. Une seule cellule est un objet physique mais pas un simple matériau. Par conséquent, les propriétés physiques d'une cellule dépendent fortement du type de la cellule, de son environnement, du type et de l'échelle de temps des déformations appliquées, ainsi que de la région sous-cellulaire où la déformation est appliquée. Bien que les propriétés mécaniques de cellules individuelles puissent être modifiées lorsqu'elles se trouvent dans un tissu, la compréhension de la mécanique unicellulaire est importante car les cellules sont les entités de base qui constituent un tissu. Des processus tels que la différenciation, la migration des cellules immunitaires et les métastases du cancer dépendent fortement des propriétés mécaniques des cellules individuelles. L'une des principales questions est de savoir comment les cellules peuvent conserver leur forme en réponse aux déformations mécaniques qu'elles subissent. La modification de la forme de la cellule fait référence à toute modification de la surface ou du volume de la cellule. Nous sommes particulièrement intéressés par la régulation du volume des cellules chez un seul mammifère dans le contexte de déformations mécaniques qui n'a pratiquement pas été tentée, probablement en raison de l'absence de techniques permettant de mesurer avec précision le volume.

La représentation biophysique classique d'une cellule est la suivante: la cellule est entourée d'une membrane plasmique, contient de l'eau (environ 70% du volume cellulaire), des organites, du cytosquelette, de petites molécules organiques et inorganiques. Les canaux ioniques et aqueux sont incorporés dans la membrane et assurent le transport entre l'extérieur et l'intérieur. Le problème essentiel est que, pour les besoins physiologiques, la cellule produit en permanence des molécules osmotiquement imperméables qui conduiraient à un gonflement cellulaire car la membrane est hautement perméable à l'eau. Par conséquent, les cellules pompent constamment des ions à l'extérieur et à l'intérieur de la cellule, consommant de l'énergie ATP, ce qui maintient la différence de pression osmotique à travers la membrane presque égale à zéro. Il est important de noter que la différence de pression à travers la membrane générée même par le faible changement (<1%) de l'osmolarité externe est supérieure de quelques ordres de grandeur à la différence de pression que le cortex acto-myosine peut supporter. Par conséquent, il est

communément admis que les forces générées par le cytosquelette ne peuvent pas affecter directement le volume cellulaire. En raison de ce raisonnement, le volume des cellules est souvent considéré comme un paramètre constant lorsque les cellules sont déformées mécaniquement. Cependant, il a été suggéré que les stress du cytosquelette peuvent moduler indirectement le volume cellulaire via l'activation des canaux mécanosensibles.

Cette idée peut être testée sur l'exemple de la propagation cellulaire, de la déformation qui provoque une forme significative et de la réorganisation du cytosquelette. La propagation cellulaire est une déformation qui se produit lorsque la cellule en suspension rencontre un substrat adhésif. L'exemple naturel d'un tel événement est la propagation de cellules filles précédée d'un arrondi mitotique et d'une division cellulaire. Lorsque les cellules en suspension touchent le substrat, l'ancrage initial se produit probablement par le biais des interactions de Van der Waals, puis les cellules commencent à se répandre. La propagation cellulaire peut être divisée en deux étapes - précoce et tardive. Les premières minutes de propagation des cellules sont dominées par le saignement et après que les filopodes et les lamellipodes commencent à se former. A ce stade, la forme générale des cellules passe de sphère à calotte sphérique; les cellules étendent leurs réservoirs membranaires pour permettre l'extension de surface sans nouvelle addition de matériau membranaire. Plus tard, l'activité hémorragique diminue et les lamellipodes deviennent le type de protrusion dominant. Pour augmenter l'extension de la surface, les cellules ajoutent du matériel membranaire supplémentaire par exocytose. Le taux d'extension des lamellipodes est limité par la tension membranaire: les cellules à basse tension se propagent plus rapidement. Cela peut s'expliquer par le fait que l'augmentation de la tension membranaire inhibe l'assemblage de l'actine et l'activation de la Rac1 GTPase.

Comme pour d’autres, les déformations mécaniques du volume des cellules lors de l’étalement étaient souvent supposées constantes. Très récemment, les chercheurs ont révélé l’importance de la régulation du volume dans le contexte de la mécanique cellulaire. Il a été démontré que si la surface de contact augmente pendant l’étalement, le volume cellulaire diminue et qu’en 1 h la perte de volume est d’environ 25% par rapport au volume initial. cellules suspendues. La teneur en protéines totales n’ayant pas été affectée, les auteurs ont conclu que l’efflux d’eau au cours de l’épandage ressemblait quelque peu à la compression hyperosmotique. L'efflux d'eau est très peu probablement expliqué par la force de pression directe générée par le cytosquelette en raison de la différence de magnitude des forces osmotiques et cytosquelettiques (les calculs sont ci-dessus). Par conséquent, les auteurs ont proposé que les forces générées par le cytosquelette lors de la propagation activent le transport des ions mécanosensibles. De

façon frappante, selon les mêmes auteurs, le volume cellulaire est corrélé négativement avec la surface en expansion à l'état d'équilibre. La restriction de la zone d'extension n'intervient pas, car le volume moyen ne diffère pas d'une zone d'étalement donnée atteinte soit par l'adoucissement du substrat (gel PA), soit par la micromodélisation de la fibronectine sur un substrat rigide. Un autre groupe de recherche a obtenu la même tendance - la conclusion de la zone d'étalement détermine le volume des cellules.

Les deux études citées ci-dessus ont utilisé une reconstruction confocale 3D pour les mesures de volume. L'utilisation de la reconstruction confocale pour les objets relativement gros, tels que les cellules suspendues, n'est pas facile en raison des effets optiques. Contrairement aux articles décrits ci-dessus, un groupe de recherche utilisant une méthode de mesure du volume basée sur l'exclusion de la fluorescence a montré qu'il existait une corrélation positive entre le volume cellulaire et la surface d'étalement. Cette tendance a été obtenue pour trois lignées cellulaires différentes, sur le substrat de verre et les substrats en PDMS souple. Un autre groupe de recherche a également découvert la corrélation positive entre le volume cellulaire et la zone d'étalement. Il n'ya donc pas de réponse claire à la question de savoir si les stress du cytosquelette peuvent moduler indirectement la diffusion du volume cellulaire au cours de la propagation cellulaire, les résultats dans la littérature étant très rares et contradictoires.

Pour répondre à cette question, nous avons utilisé une méthode de mesure du volume des cellules vivantes uniques, basée sur l'exclusion de la fluorescence (FXm). En bref, nous injectons les cellules dans la chambre du PDMS à hauteur constante. Le milieu de culture contient du dextran fluorescent qui ne peut pas pénétrer dans les cellules. Par conséquent, les cellules apparaissent comme des objets sombres sur une image de fluorescence classique. La fluorescence exclue par une cellule est linéairement proportionnelle au volume de la cellule.

Nous avons observé que dans les 20 premières minutes d'étalement sur le verre recouvert de fibronectine, les cellules perdent en moyenne 4% du volume, puis continuent à se répandre à basse vitesse et augmentent de volume en raison de la croissance (~ 5% / h). Nous avons donc supposé qu'à long terme, le volume des cellules devrait être indépendant de la zone d'étalement. Pour tester cette idée, nous avons mesuré le volume cellulaire et la surface d'épandage des cellules adhérentes HeLa et RPE-1. Nous avons observé qu'au niveau d'une population, il n'existait pas de forte corrélation entre l'aire d'extension et le volume de ces lignées cellulaires. Afin de contrôler à la fois la zone d'étalement et la forme des cellules, car la forme elle-même affecte le cytosquelette acto-myosine et la contractilité cellulaire, nous avons utilisé des micro-motifs adhésifs de différentes formes et tailles: des cercles et des rectangles de différentes dimensions. Nos données ont montré que, pour les cellules étalées à l'état d'équilibre, le

volume moyen des cellules HeLa à motifs était indépendant de la taille et de la forme des motifs et n'était pas significativement différent du volume moyen des cellules à motifs. Pris ensemble, nos résultats montrent que le volume cellulaire est indépendant de la taille et de la forme de la zone d'extension au niveau d'une population de cellules étalées à l'état stable.

Sur le verre passivé (PLL-PEG), les cellules ne se sont pas étendues et le volume a augmenté à une vitesse proche du taux de croissance normal (~ 5% / h), alors que la propagation sur du verre revêtu de fibronectine dans les 10 à 20 premières minutes est accompagnée de 4% de perte de volume en moyenne (comme mentionné ci-dessus). Prises ensemble, ces données démontrent que la propagation cellulaire induit une perte de volume faible mais significative. De plus, nous avons réalisé une imagerie en phase quantitative combinée avec FXm et avons montré que pendant les 20 premières minutes d'étalement, la masse sèche des cellules étalées restait constante alors que le volume diminuait. Ces données indiquent que la perte de volume est principalement due à l'efflux d'ions / eau et non à une perte de masse sèche. Fait intéressant, au cours de la diminution du volume, la masse reste constante, mais lorsque le volume recommence à augmenter, la masse reprend également sa croissance au taux prévu.

Bien que les cellules HeLa perdent en moyenne 4% de leur volume lors de leur propagation, nous avons constaté qu'au niveau des cellules, la dynamique du volume est très diverse. Au cours de la propagation, les cellules peuvent perdre plus ou moins de volume, voire ne pas changer ni augmenter leur volume (~ 15% des cellules). Nous avons constaté que non seulement la dynamique du volume, mais aussi la dynamique de propagation, varient d'une cellule à l'autre - différentes cellules peuvent atteindre la même zone finale mais s'étendre à des vitesses différentes. Si, comme le suppose notre modèle de travail, la tension surface / surface joue un rôle important dans la modulation du volume, alors la cinétique d'étalement devrait être un paramètre crucial. Un étalement assez lent, grâce à la dynamique de l'acto-myosine et du renouvellement de la membrane plasmique, relâchant la tension membrane / surface, pourrait potentiellement se produire sans augmentation substantielle de la tension.

Pour quantifier un lien entre la vitesse d'étalement et la modulation du volume, nous avons mesuré deux paramètres: la vitesse d'étalement et le flux de volume pouvant être simplement ajustés avec un modèle linéaire à des intervalles de temps de 10 minutes.

Nous avons analysé ces paramètres pour chaque intervalle de 10 minutes dans l'heure qui a suivi l'épandage. Nous avons obtenu que la vitesse d'épandage diminue progressivement (en moyenne) et qu'après les 30 premières minutes d'écoulement en volume d'épandage, les flux ont généralement des valeurs proches de zéro et légèrement positives - les cellules continuent à se répandre à faible vitesse et

sans perte de volume et reprennent leur croissance. Par conséquent, pour une analyse plus approfondie de nous avons décidé de nous concentrer sur les 10 premières minutes d'étalement car il s'agit de la phase de déformation plus rapide.

Au cours des 10 premières minutes d'étalement, la vitesse d'étalement est en moyenne proportionnelle à la vitesse du flux de volume: plus les cellules se dispersent rapidement, plus elles perdent de volume. Les données ont également montré en dessous d'une certaine vitesse d'étalement, il n'y a pas de perte de volume significative en moyenne et le flux de volume est proche de zéro en moyenne. Le comportement moyen des cellules est donc cohérent avec notre modèle de travail, mais montre toujours une grande dispersion au niveau de la cellule unique. Cela pourrait être dû au besoin d'une analyse plus fine des courbes de cellule unique, car les cellules peuvent afficher des phases transitoires d'étalement rapide à différents moments de la première heure d'étalement. Il pourrait également provenir d'autres sources de variabilité d'une cellule à l'autre, telles que le stade du cycle cellulaire ou l'état du cortex cellulaire ou le type de protubérances formées lors de la propagation cellulaire. Cela fait une différence importante et relie la perte de volume à la contrainte à la surface due au processus d'étalement, qui devrait se détendre en quelques minutes, plutôt qu'à la forme de la cellule.

Pour tester davantage notre modèle de travail, nous avons donc décidé d'affecter les principaux acteurs de la dynamique du cytosquelette. La diminution de la polymérisation de l'actine / l'augmentation de la contractilité ont ralenti l'étalement et empêché la perte de volume, et l'inhibition de la contractilité a provoqué un étalement rapide et une perte de volume importante. Cependant, une combinaison d'inhibition de la contractilité et de la polymérisation d'actine dépendante d'Arp2 / 3 induisait un étalement rapide sans perte de volume.

Enfin, nous avons constaté qu'au début de l'étalement, lorsque les cellules sont proches d'une cape sphérique, elles maintiennent l'équilibre volume-surface en modulant à la fois le volume et la surface. La cinétique d'étalement module l'équilibre volume / surface: les cellules qui s'étalent rapidement ont tendance à perdre du volume plutôt que d'étendre la surface, et les cellules qui se propagent lentement ont tendance à s'étendre en surface sans perte de volume.

Nous pensons que cet équilibre peut être un mécanisme de protection empêchant les ruptures de la membrane: une expansion rapide pourrait provoquer un étirement de la membrane, en raison du frottement avec le cortex lors de la formation de protubérances de la membrane, entraînant des ruptures. Perdre du volume empêcherait d'atteindre la tension de rupture - un point intéressant étant que les cellules mesurent cette tension et activent les canaux ioniques en conséquence, existe-t-il des structures

spécialisées (par exemple des cavéoles) pour cela? Par contre, un étalement assez lent permet une extension de la membrane avec une augmentation moindre de la tension, grâce à de multiples mécanismes de relaxation du stress agissant à des dizaines de minutes (retournement du cortex actinique, exocytose, liaison et déliaison des protéines membranaires au cortex, etc.). . Des mécanismes permettant une relaxation plus rapide de la tension de la membrane pourraient permettre un étalement plus rapide sans perte de volume, tel que le claquage par exemple. Ce processus étant un processus stochastique, il pourrait expliquer la grande variabilité entre cellules observée en plus des tendances générales visibles sur les moyennes de population. Pour tester plus avant notre hypothèse et établir la fonction biologique de ce mécanisme de régulation du volume, nous allons essayer de trouver des conditions dans lesquelles un étalement rapide ne conduit pas à une perte de volume, idéalement non à cause d'une relaxation de tension rapide, mais à cause du capteur de tension menant au volume la perte serait absente. Nos meilleures suppositions sont les canaux ioniques impliqués dans la régulation du volume cellulaire (par exemple, le VRAC) et les structures sensibles à l'étirement, telles que les cavéoles.

Notre modèle de propagation pour les premiers stades de propagation suppose une géométrie cellulaire simple: la transition d'une sphère à une calotte sphérique. Cependant, dans cette transition, les cellules peuvent avoir une forme 3D plus complexe, par exemple une sphère avec un lamellipodium s'étendant au-dessous, il sera donc essentiel de réaliser une imagerie à haute résolution pour sécuriser les conclusions de cette étude.

Pour clôturer cette première section de résultats sur l'étalement des cellules HeLa, nous pouvons spéculer sur le mécanisme qui sous-tend l'effet de la polymérisation de l'actine et de la contractilité sur la forme et le volume des cellules. Plusieurs études ont montré que l’augmentation de la contractilité induit le ressuage cellulaire et que l’inhibition de la contractilité empêche la formation de saignement et favorise la formation de lamellipodes. De plus, il a été démontré que les cellules forment à la fois des bulles et des lamellipodes quand elles adhèrent à un substrat. Les conditions dans lesquelles les cellules formeraient plus de bulles correspondent souvent à une propagation lente et à une zone de propagation réduite, tandis que l'inhibition de la contractilité correspond à une propagation rapide sans saignement. Alors que la plupart des cellules auraient un mélange des deux, les traitements médicamenteux pourraient faire basculer la balance en un ou plusieurs autres. Dans le cas d'une extension lamellipodiale dominante, une polymérisation de l'actine ramifiée dans la zone de contact tirerait une feuille de membrane des réservoirs de membranes précédemment attachés au cortex de la cellule, conduisant à une activation des canaux ioniques et à une perte de volume. Cela correspond au traitement Y-27: il permet une propagation rapide

par l'effet combiné du ramollissement du cortex et de la promotion de l'extension du lamellipodium à base de Arp2 / 3, tout en réduisant les saignements, lesquels dépendent de la contractilité. Des cellules à propagation lente ou des saignements fréquents auraient l'effet inverse. Cela correspondrait à de faibles doses de Lat ou à un traitement par CK-666.

Le troisième cas, étalement rapide sans perte de volume, qui correspond à une inhibition combinée de la contractilité et de Arp2 / 3 (saillie lamellipodiale), pourrait être expliqué dans le même cadre de la manière suivante: une contractilité réduite favorise la propagation rapide même en l'absence d'Arp2 / 3 saillies lamellipodiales à base. Ce type de propagation pourrait conduire à une forme différente, et l'inhibition de Arp2 / 3 pourrait rétablir un certain niveau de saignement, même dans les cellules à contractilité basse, relâchant ainsi la tension de la membrane (à confirmer par imagerie). Une autre hypothèse est que, en l'absence d'un réseau d'actine Arp2 / 3, principalement constitué de filaments d'actine ramifiés courts, la membrane ne se tend pas lors de l'étalement, ou les structures de capteurs, ou directement les canaux / pompes ne sont pas activés / ouverts, empêchant ainsi le volume perte. Dans la dernière hypothèse, la membrane pourrait être étirée et des ruptures pourraient apparaître.

Notre modèle de travail, tiré des résultats des expériences de propagation cellulaire décrites ci-dessus, repose sur l'hypothèse selon laquelle la déformation cellulaire conduit à une tension surface / membrane, si le taux de déformation est plus rapide que les taux de renouvellement de la membrane plasmique et d'actine. Une façon de vérifier cette hypothèse consiste à imposer une déformation aux cellules non adhésives. Cela permettra également de tester l'implication de l'adhésion cellule / substrat dans la réponse de modulation de volume observée lors de l'étalement cellulaire.

Pour ce faire, nous avons utilisé un dispositif de confinement à 6 puits mis au point dans notre laboratoire. En bref, des cellules suspendues sont plaquées sur le fond de verre de la plaque à 6 puits. Des verres de couverture avec des piliers microfabriqués incompressibles de la hauteur souhaitée sont collés sur des pistons souples fixés au couvercle de la plaque à 6 puits. En fermant le couvercle de la plaque, nous confinons instantanément (~ des dizaines de ms) les cellules entre les surfaces inférieure et supérieure. La distance entre les deux surfaces est égale à la hauteur des piliers d'espacement. Le diamètre moyen des cellules HeLa étant d'environ 17 µm, nous avons considéré le confinement avec une hauteur de piliers de 20 µm en état non confiné et une hauteur inférieure à 17 µm en tant que confinement effectif. Un avantage de cette technique est que nous pouvons avoir six conditions expérimentales différentes sur la même plaque et fonctionner avec un grand nombre de cellules. Cependant, nous ne sommes pas en

mesure de suivre les changements dynamiques de cellules individuelles. Nous ne pouvons observer l'effet du confinement qu'au niveau de la population.

Premièrement, nous avons caractérisé la forme des cellules confinées. Comme prévu, les cellules non confinées ont une forme sphérique et les cellules confinées sont plutôt cylindriques aux bords arrondis, très similaires au confinement avec un porte-à-faux plat AFM. Nous avons mesuré le volume de cellules HeLa non adhésives confinées à différentes hauteurs. Le volume moyen des cellules a diminué avec la hauteur de confinement pour atteindre des pertes de volume importantes: les cellules confinées à 5 µm ont un volume inférieur de 35% à celui des cellules non confinées. Comme nous connaissons la hauteur de confinement et le volume moyen des cellules à partir de la mesure FXm, nous pouvons calculer la surface apparente en utilisant l'hypothèse géométrique de la forme simple d'une cellule - sphère et cylindre. L'analyse de la mesure indirecte de surface a montré que les cellules maintenaient une surface constante jusqu'à un confinement de 5 µm, tenant compte du changement de forme principalement dû à la perte de volume. Le confinement inférieur (moins de 5 µm) a induit un changement morphologique important dans les cellules HeLa, comme indiqué précédemment - les cellules présentaient une activité de saignement forte et soutenue. Cela rend beaucoup plus difficile la mesure d'une surface. Néanmoins, en supposant une surface simple (les bulles sont petites), il est apparu que la surface apparente augmentait beaucoup, ce qui signifie que l'adaptation au changement de forme impliqué dans ce cas extension de surface.

Pour tester l'hypothèse selon laquelle le lien entre la membrane plasmique et le cortex d'actine est responsable de la restriction d'expansion de la surface et ceci de la perte de volume en réponse au confinement, nous avons perturbé le cortex d'actine par traitement Lat. L'avantage de l'expérience de confinement, par rapport à l'étalement, réside dans le fait que la déformation est imposée de l'extérieur et qu'il est donc facile de comparer des cellules témoins et traitées avec Lat, alors que pour la propagation des cellules, la comparaison était rendue plus difficile car le traitement avec Lat affectait la vitesse d'étalement. Le traitement des cellules avec Lat A induit un phénotype de saignement important, les cellules traitées avec Lat confinées présentent également des saignements importants. Le traitement par Lat A n'a pas augmenté de manière significative le volume (~ 3%) des cellules non confinées, les cellules de confinement traitées avec Lat ont perdu beaucoup moins de volume que les cellules de contrôle. Ces résultats vont dans le sens de l'hypothèse selon laquelle la perte de volume lors de la déformation est due à la fixation de la membrane plasmique sur le cortex d'actine: le traitement Lat A permettrait une déformation à volume constant, car il facilite l'ouverture des réservoirs membranaires lors d'une

déformation rapide, évitant ainsi une tension de la membrane lors du confinement. L'effet de Lat A devrait donc être de rendre la cellule plus facile à se déformer (se déformerait davantage pour une force donnée).

Pour distinguer entre une fuite de cytoplasme ou une perte d'eau / d'ions, nous avons mesuré à la fois le volume et la masse sèche de cellules confinées. La masse sèche cellulaire est principalement due aux grosses molécules organiques qui composent les organites, le cytosquelette, la membrane, elle peut être mesurée en quantifiant le déphasage de la lumière traversant les cellules en utilisant une microscopie de phase quantitative. Les résultats ont montré que, lorsque les cellules sont confinées à 10 µm et 5 µm, leur volume diminue d'environ 10% à 30%, mais que leur masse sèche reste presque constante.

Nous avons également observé que l'épuisement en ATP induisait la mort cellulaire sous confinement alors que les cellules témoins avaient une viabilité de presque 100%. Pour interpréter mieux ce résultat, nous devons réaliser ces expériences avec une résolution temporelle élevée: une fragilité accrue de la cellule conduirait à une rupture immédiate lors du confinement, tandis qu'un défaut de régulation des ions actifs entraînerait une pression intracellulaire excessive ou une surface tension, conduisant à des bulles, ou des pores de la membrane sans induire une mort immédiate.

L'une des observations les plus intéressantes est l'échelle de temps de la perte de volume induite par le confinement rapide. Nos mesures sont limitées par une résolution temporelle de 30 ms, mais elles signifient que les cellules perdent plus de 10% de leur volume en moins de 30 ms. Ceci est beaucoup plus rapide que les changements de volume induits par des chocs osmotiques (décrits dans la section suivante des résultats), censés fournir une mesure du taux de perméation de volume à travers la membrane plasmique. La compression uniaxiale pourrait avoir un mécanisme différent de celui de la compression osmotique isotrope. Par exemple, on peut supposer que l'augmentation de la tension superficielle induite par le confinement pourrait entraîner une augmentation de la perméabilité de la membrane, impliquant potentiellement également l'ouverture de canaux. Une autre possibilité est que le confinement, en tirant sur la structure cohésive membrane / cortex, induisant ainsi potentiellement des mouvements rapides des protéines transmembranaires dans la bicouche lipidique, puisse induire un changement de l'ordre lipidique, ou de très petites ruptures transitoires de la membrane, permettant un efflux plus rapide de l'eau. Pour tester l'hypothèse de formation de pores / trous, nous pourrions utiliser des marqueurs de rupture membranaire, tels que CHMP4B-GFP (ESCRT III) ou l'iodure de propidium, utilisés auparavant en laboratoire pour étudier la fermeture des pores induits par laser.

Enfin, nous pensons que ce mécanisme de perte de volume peut être nécessaire à la survie des cellules en réponse à des déformations rapides et importantes. La perte de volume pourrait relâcher la tension de

surface transitoire et amener la tension aux valeurs homéostatiques qui empêcheraient l'éclatement des cellules.

Nos résultats avec la compression cellulaire ont soulevé des questions sur la perméabilité cellulaire à l'eau et la disponibilité de la membrane plasmique. Nous avons décidé d'étudier ces aspects de la modulation du volume cellulaire en utilisant le choc osmotique, méthode classique depuis des décennies pour étudier la régulation du volume cellulaire. Nos données expérimentales montrent que, pour les cellules HeLa non adhérentes, le volume exclu moyen est d'environ 30%. Cependant, nous avons observé une grande diversité au niveau d'une cellule. Fait intéressant, les grandes cellules avaient une plus grande fraction de volume exclu que les petites cellules. En outre, nous avons constaté que le volume exclu ne dépend pas de l'ampleur du choc ou de la polymérisation de l'actine.

Nous considérons que le volume final atteint par les cellules en réponse aux changements d'osmolarité pourrait être limité par la disponibilité de la membrane. Nous avons montré qu'une grande quantité de membrane de cellules non adhérentes est stockée dans des réservoirs membranaires, ce qui est cohérent avec l'observation précédente. Ces réservoirs sont liés à l'acto-myosine cortex et ne sont donc pas facilement accessibles.

Une autre explication possible de la diversité observée de la fraction osmotiquement active observée est que les cellules peuvent avoir une perméabilité membranaire différente, qui pourrait être définie par l'activité du canal ionique, pouvant par exemple varier en fonction du stade du cycle cellulaire et donc de la taille des cellules. Dans ce cas, le transport de l'eau intervenant en réponse à une modification de l'osmolarité ne pouvait être considéré comme un processus passif, ce qui était communément accepté sur le terrain.

La question suivante est de savoir si la cinétique du transport de l'eau à l'intérieur de la cellule induite par un choc osmotique est fondamentalement un processus de diffusion. Ensuite, en principe, la propagation de l'eau pourrait être limitée par la nature poroélastique du volume cytoplasmique et l'échelle de temps du mouvement de l'eau. Une autre limitation possible est la perméabilité de la membrane, c'est-à-dire la rapidité avec laquelle l'eau peut pénétrer à travers la bicouche lipidique.

Des études antérieures ont montré que le temps typique de gonflement osmotique est d'environ 1 min et qu'il ne dépend pas de la polymérisation de l'actine. Nos résultats expérimentaux ont montré que le gonflement et la contraction osmotiques avaient une échelle de temps de quelques secondes similaire aux valeurs estimées pour le mouvement de l'eau à l'intérieur de la cellule. Pour faire une déclaration

concluante, il faudrait augmenter encore la distribution des rayons cellulaires, ce qui est possible par arrêt du cycle cellulaire ou fusion cellulaire. Nous avons observé une forte augmentation de la vitesse de gonflement et une légère augmentation du temps de gonflement avec une augmentation de la magnitude du choc. Nous pourrions supposer que l'augmentation de la vitesse de gonflement pour une amplitude de choc élevée pourrait être due à une augmentation de la perméabilité de la membrane induite par une tension élevée, par ex. par activation des aquaporines. Pour tester plus avant l'hypothèse de contrainte poroélastique, nous avons perturbé le réseau d'actine, dans le but d'augmenter la taille des pores du réseau interne et d'augmenter le coefficient de diffusion. Contrairement à nos attentes, la dépolymérisation de l'actine a augmenté le temps de gonflement. L'explication possible serait que la tension générée dans le réseau d'actine est nécessaire pour activer les canaux ioniques, augmentant ainsi la perméabilité de la membrane. Si cette hypothèse était correcte, cela confirmerait l'idée que le gonflement osmotique n'est pas un processus passif.

L'adaptation réglementaire au volume suivie par le gonflement / retrait initial (RVI ou RVD) est un processus relativement long - la récupération du volume initial prend généralement des dizaines de minutes. C'est un processus actif car il repose sur l'activité des pompes à ions qui nécessitent de l'énergie. Nous avons constaté que les cellules récupéraient parfaitement leur volume (RVI) après un choc hypertonique de différentes amplitudes (mélange de milieu et de PEG400). Le comportement des cellules individuelles était uniforme. Au contraire, les cellules exposées à des chocs hypoosmotiques (mélange de milieu et d'eau) n'ont pas retrouvé leur volume initial en moyenne et ont présenté trois types de comportement: adaptation parfaite au volume initial, adaptation partielle, aucune adaptation. Le temps d'adaptation typique était plus long pour les faibles amplitudes de choc (~ 5 min) que pour les fortes amplitudes (~ 2 min). Les cellules avec l'actine dépolymérisée avaient un temps d'adaptation inférieur à celui du contrôle. Ce résultat est similaire aux données publiées précédemment et pourrait indiquer que l'état du cytosquelette d'actine peut moduler la RVD, probablement, par l'activation du transport des ions. Cette partie du projet est dans sa phase initiale et nécessite plus de données expérimentales pour être concluante. Nous n'avons pas étudié en détail le rétrécissement hyperosmotique, en nous concentrant davantage sur le gonflement hypoosmotique. Cependant, il est clair que nos résultats, qui ont pu être obtenus grâce à des mesures de volume précises de cellules individuelles vivantes réalisées avec une résolution temporelle élevée, remettent en question des hypothèses établies et communément acceptées.

Dans ce projet, nous avons étudié la modulation du volume cellulaire en réponse à des déformations mécaniques de différentes échelles de temps. Nous avons montré que les cellules diminuent, ne changent pas et n'augmentent pas le volume en fonction de la cinétique de déformation et de l'état du cortex d'actomyosine. Cela signifie que, selon le contexte, les cellules ont différentes propriétés matérielles, par exemple le coefficient de Poisson.

Il est important de noter que la régulation du volume des cellules chez les mammifères était principalement étudiée dans le contexte du choc osmotique (échelle de temps courte) ou du cycle cellulaire (échelle de temps longue). Nous avons découvert de nouveaux aspects de la compression osmotique isotrope grâce au FXm qui nous a permis de mesurer avec précision le volume des cellules avec une résolution temporelle élevée. Nous avons également constaté que les cellules réduisent le volume en réponse à la compression uniaxiale, ce qui remet en question l'hypothèse courante selon laquelle le volume des cellules est constant pendant le confinement mécanique. Nous avons montré que les cellules modulent leur volume tout en se propageant (échelle de temps intermédiaire). Pris ensemble, ces résultats fournissent de nouvelles informations pour comprendre la régulation du volume cellulaire des cellules de mammifère.

Abstract

Cell volume regulation in response to deformations

The field of biomechanics significantly progressed in the last two decades. The importance of the feedback between biochemical signaling and physical properties was revealed in many studies. Cells within tissues constantly generate and experience mechanical forces. Biochemical perturbations inside the cells as well as alterations in the mechanical environment can shift the tiny balance of normal physiological state and lead to pathologies, e.g. cancer. Although the mechanical properties of individual cells can alter when they are within the tissues, the understanding of single cell mechanics is still important. Differentiation, immune cell migration, and cancer invasion strongly depend on the mechanical properties of individual cells.

Mechanical deformations can lead to a change in cell surface area and volume. We are particularly interested in single mammalian cell volume regulation in the context of deformations of different timescales. For the moment, volume regulation in this context was out from the research interest, probably due to the difficulties of accurate measurements, and cell volume often considered as a constant parameter. We developed a method for cell volume measurements based on a fluorescent exclusion that allowed us to perform precise volume measurements of individual live cells.

In the present study, we mainly focused on cell volume regulation while dynamic spreading on a substrate (timescale – minutes). We demonstrated that there are different regimes for volume regulation while spreading: cells decrease, increase or do not change volume, and a type of the regime depends on the state of the actomyosin cortex and spreading speed. We obtained that faster-spreading cells tend to lose more volume. Our hypothesis is that during fast Arp2/3-driven lamellipodia extension actin pull on the membrane that generates tension and activation of ion transport and regulatory volume loss. Inhibition of actin polymerization or Arp2/3-dependent actin branching decreases spreading speed and volume loss. Next, we showed that inhibition of contractility increases spreading speed and volume loss. However, inhibition of Arp2/3 complex in cells with low contractility leads to fast spreading without volume loss. Our explanation is that inhibition of Arp2/3 induces cell blebbing and even fast deformation does not lead to volume loss as a cell can relax tension by membrane unfolding.

We also showed that volume regulation in response to fast mechanical compression (timescale – milliseconds) independent of adhesion also depends on the actomyosin cortex state. Control cells lose up to 30% of volume under confinement, as the cell membrane is attached to the cortex and cannot be

unfolded in response to the tension increase. Disruption of actin cortex leads to membrane detachment and prevents volume loss under confinement.

Additionally, we showed that cell volume response to the osmotic shock (timescale – seconds) is more complex than it used to be known in the literature. For instance, our data indicate that at the level of individual cells initial volume response to the change of external osmolarity is not a uniform passive process. Using osmotic shock technique, we also confirmed that cells have a large excess of membrane folded in reservoirs.

Taken together, our data show that cell volume and surface area are coupled through surface tension homeostasis and as deformations induce surface tension increase, they lead to change volume and surface area.

Acknowledgments

First, I want to thank jury members – Pierre Nassoy, Timo Betz, Guillame Charras, Françoise Brochard-Wyart and Cristophe Le Clainche who kindly accepted to examine my PhD project.

Next, I want to thank my PhD advisor Matthieu for welcoming me in his lab. I appreciate the perfect balance between freedom and supervision that was provided by Matthieu. My PhD project, which Matthieu allowed me to define by myself, was one of the most interesting things that I have done in my life.

Then I want to thank Damien for teaching me different kind of "bricolage" and support, especially in the very beginning of my PhD. Thanks to Baptiste, who did a master internship with Damien and me, we initiated a part of the project related to cell spreading. I also would like to thank other present and past lab members for their help to my project. Many thanks to Nishit, Pablo S, Juanma for the help with microscopy; to Aastha, Lucie and Alice for correcting my French and English; Pablo V, for the help with dendritic cells; to Guilherme, for the help with confinement and western blot; to Yanjun, Olivier (Jian), Li, Mathilde and Rafaele for the help with microfabrication; to Sylvain, Clotilde and Ewa for the help with FXm. Thanks to Alexis, Bianca, Mathieu, Ido, Valentin, Zahraa, Kos and Matthew for their help and productive discussions. Thanks to Nico who tied up the lab together.

Many thanks to Damien Coudreuse and Aurélien Roux who were in my thesis committee.

Thanks a lot to Pierre Recho for interesting discussions and ideas that he brought to my project.

Thanks to my PhD program ITN I met a lot of amazing scientists and had a possibility to visit Jochen Guck's lab. Thanks to FRM program I was able to prolong my PhD for one more productive year.

I would like to thank Institut Curie people and especially Mathieu Maurin, Pierre Sense, Amit Singh and Caroline Audouin. I also want to thank IPGG people – platform team, Jacques Fattaccioli, Abbelight team.

Thanks to Olivier Thouvenin and Victor Racine for their help with FXm. And thanks to all the others with whom I had a chance to collaborate.

I also want to thank my former supervisor Alexander Minin and my university MIPT for my undergrad training, which prepared me for PhD life.

Finally, many thanks to my family and friends who supported me all these years.

«Не кури, не влюбляйся, не пей вина
И на лбу себе высеки:
Жизнь тебе для того дана,
Что бы ты её отдал физике!»

Ева Ра

I. Introduction

The importance of feedback between biochemical signaling and physical properties of both the cell and the environment has been explored in many studies. Cells within tissues constantly generate and experience mechanical forces, which are often correlated with changes in cellular signaling pathways. Thus, biochemical perturbations inside the cells as well as alterations in their mechanical environment can push them from a balanced physiological state leading to pathologies, e.g. cancer. A single cell is a physical object but not a simple material. Hence, the physical properties of a cell strongly depend on the type of the cell, its environment, the type and timescale of applied deformations, and on the sub-cellular region where deformation is applied. Although mechanical properties of individual cells can be altered when they are within a tissue, the understanding of single cell mechanics is important as cells are the basic entities that comprise a tissue. Processes like differentiation, immune cell migration and cancer metastasis strongly depend on the mechanical properties of individual cells. One of the major question is how cells are able to maintain their shape in response to mechanical deformations that they undergo. Change in the cell shape refers to any changes in cell surface or volume. We are particularly interested in single mammalian cell volume regulation in the context of mechanical deformations that was mostly unattempted, probably due to the lack of techniques for accurate volume measurements.

1. What is cell made of?

To study the mechanics of single cells is important to understand what is a cell made of. The classical biophysical representation of a cell is the following: the cell is surrounded by a plasma membrane, contains water, organelles, cytoskeleton, small organic and inorganic molecules. Ion and water channels are incorporated in the membrane and provide the transport between exterior and interior. Some of the cell types exist in suspended state, others attach to the substrate or surrounding cells through specific bounding molecules (respectively mesenchymal and epithelial cells).

a. Plasma membrane

The cell membrane is primarily a lipid bilayer composed mostly of phospholipids with insertion of other lipids, such as cholesterol, and transmembrane proteins. Cylinder-shaped lipids contain a hydrophilic

(polar head group) and a hydrophobic part (fatty acyl chain). Once exposed to an aqueous solution, they compact their hydrophobic parts in the most energetically favorable way by forming a planar bilayer (Sych, Mély, and Römer 2018; Singer and Nicolson 1972). Individual lipids and transmembrane protein are able to move within the planar bilayer exhibiting both Brownian and non-Brownian motions (Saxton and Jacobson 1997). Depending on composition, lipids can be organized in liquid disordered (fluid-like) or liquid ordered (solid-like) phases that coexist. Induction of a curvature concentrates the more fluid lipid phase into a highly curved membrane (Roux et al. 2005). Total membrane area is often defined by the number of lipids and proteins it contains, but is rarely empirically measured due lack of methods that could account for membrane folding and nanoscale curvature. However, the apparent surface area is known. The relative increase of area is related to the distance between lipids. Thus, membrane tension T_t is defined as:

$$T_t = K_A \frac{\Delta A}{A_0} \qquad \textit{(Eq. 1)}$$

where A_0 is total membrane area, ΔA is relative change on membrane area, K_A is compressibility modulus.

The lipid bilayer is essentially unstretchable (Roux 2013) as it ruptures when $\Delta A/A_0$ = *2-3%.* Area compressibility modulus of pure lipid bilayer, related to bending modulus κ and membrane thickness (Picas, Rico, and Scheuring 2012), was estimated as $K_A = 0.1 - 1\ N/m$, depending on composition (Hamill and Martinac 2001).

Nevertheless, cells usually have a large excess of plasma membrane area stored in membrane reservoirs, like microvilli, caveolae, clathrin pits etc., that can be unfolded when cells undergo deformations. For instance, cells sacrifice microvilli (Pietuch, Brückner, and Janshoff 2013) in response to hypoosmotic shock, which causes cells to swell. Interestingly, for spherical cells, which start to spread on glass, apparent area compressibility modulus had a value of $\widetilde{K_A} = 0.19$ *N/m* that is similar to lipid bilayer by itself (Hamill and Martinac 2001). This indicates that although spherical cells have a large excess of membrane (Ping Ting-Beall, Needham, and Hochmuth 1993), they do not have access to it due to membrane-to-cortex attachment and hence appear as stiff as the plasma membrane itself.

However, disruption of plasma membrane integrity occurs even under normal physiological conditions (McNeil and Steinhardt 1997). Membrane fragility depends on its composition, for example, cholesterol depletion makes cells prone to rupture (Biswas et al. 2019). Cells are even able to rapidly close small membrane wound through ESCRT complex machinery (Jimenez et al. 2014).

As it was mentioned, the membrane has different types of compartments where it bent (Prinz and Hinshaw 2009), e.g. caveolae, clathrin pits, microvilli. In response to stretching or hypoosmotic shock cells disassemble caveolae (Sinha et al. 2011) that prevent increase of membrane tension. Total membrane area released by caveolae flattening was estimated as only 0.3%, therefore, the role of caveolae in response to mechanical stress could be in addition to actin (Echarri and Del Pozo 2015) and/or ion channels (Balijepalli and Kamp 2008).

Membrane renewal occurs by exo- and endocytosis, that have a typical timescale of 1 min (Rappoport and Simon 2003; Tran et al. 2015), however, total membrane exchanging takes much longer. For example, in *Dictyostelium* amoeba total membrane renewal time was estimated as 45 min (Thilo and Vogel 1980).

BAR (Bin/amphiphysin/Rvs) domain proteins, based on the degree of curvature they produce, are divided into three classes: BAR and F-BAR that produce positive curvature, I-BAR that generate negative curvature (Jarsch, Daste, and Gallop 2016). Their main function is sensing and generation of membrane curvature that mediate membrane traffic. They also were shown to link membrane to actin, induce membrane protrusions and affect membrane tension (Salzer, Kostan, and Djinović-Carugo 2017). Cell membrane is selectively permeable (N. J. Yang and Hinner 2015): water can passively diffuse through lipid bilayer but not ions. It was estimated that 4000 water molecules pass a single phospholipid per second, whereas for single Na^+ ion it is 70h (Hamill and Martinac 2001). Diffusional permeability for animal cell was estimated as P_d ~40 μm/s (Potma et al. 2012). Besides diffusion, transport can be provided by pores formation (Shinoda 2016). Although it has never been shown that the permeability should increase with tension; at high tension transient nanopores can appear in the membrane leading to liquid leakage (Karatekin et al. 2003).

b. Cytoskeleton

The cell membrane is attached to the underlying acto-myosin cortex through ERM-proteins: ezrin, radixin and moesin, that are activated by phosphorylation (Arpin et al. 2011; Fehon, McClatchey, and Bretscher 2010) of various kinases, including Rho and Src (for ezrin). Once activated ERM-proteins can link the membrane to the cytoskeleton and participate in various signaling as well as lamellipodium and microvilli formation (Clucas and Valderrama 2015). For instance, in RPE-J cells, which expresses ezrin and moesin at a low level and have sparse microvilli, overexpression of ezrin induced the formation of microvilli (Louvet-Vallée 2000).

Two main actin-myosin structures inside the cell are the cortex and the bulk cytoskeleton; their activity is regulated by small GTPases (Fig.1.1). The cortex has ~150 nm thickness and is represented by both formin-dependent elongated filaments and branched Arp2/3 nucleated actin (Chugh and Paluch 2018). The cortex is an active contractile material - myosin motors pull on actin and generate stresses. Myosin activity is regulated by ROCK and MLCK pathways. The actomyosin cortex is a very dynamic structure and is known to be a major regulator of cell shape. The elastic modulus of cortex ranges from 100 Pa for neutrophils and neurons to several hundreds kPa for fibroblasts (Stricker, Falzone, and Gardel 2010).

The bulk cytoskeleton is mostly represented by actomyosin structures, microtubules and intermediate filaments. The compressibility modulus of the cytoskeleton $K_A = 0.01\ mN/m$ is much lower (Hamill and Martinac 2001) than that for a membrane, therefore, the cytoskeleton network can be easily deformed in response to mechanical perturbations. Contractile actin networks formed of Filamentous-actin (F-actin) and crosslinkers have a non-linear elastic response: sparse networks with a small degree of cross-linking are observed to soften at large strains, whereas high F-actin density networks with a high concentration of cross-links are observed to stiffen at intermediate strains followed by a dramatic softening at larger strains (Stricker, Falzone, and Gardel 2010). Formation of F-actin from monomeric globular G-actin requires energy from ATP-hydrolysis. In the lamellipodium, the actin network is present as a dendritic structure branched and cross-linked by Arp2/3, whose nucleation activity is controlled by WASP (Cdc42 effector) and WAVE (Rac1 effector). Another type of actin structures are actomyosin stress fibers, whose formation is promoted by RhoA through its effectors, Rho-associated protein kinase (ROCK) and the formin mDia1 (Tojkander, Gateva, and Lappalainen 2012). The stiffness of the stress fiber is *E* = 12 kPa, which is reduced to 8kPa upon myosin inhibition (Stricker, Falzone, and Gardel 2010).

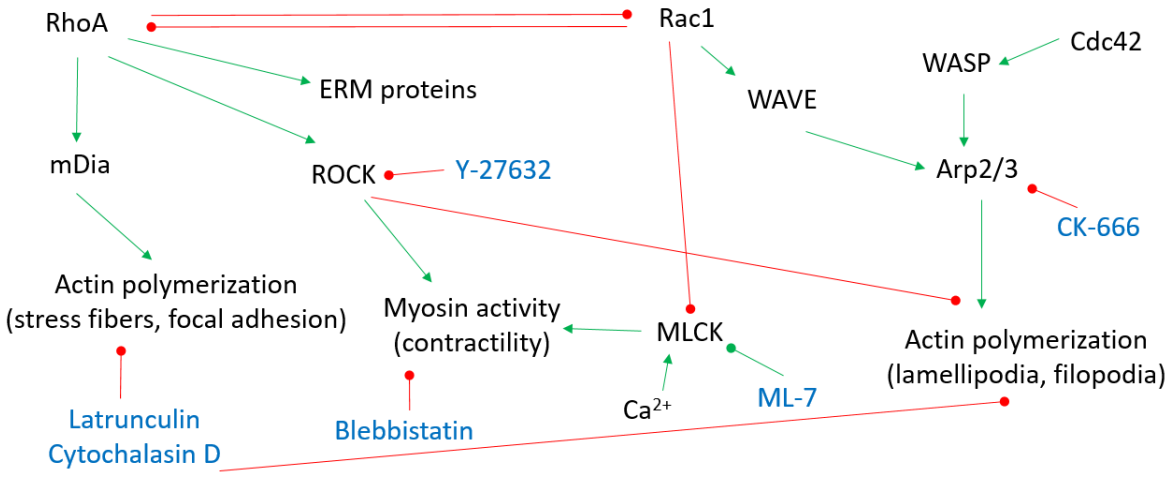

Figure 1.1: *Rho-family of small GTPases regulates acto-myosin cytoskeleton.*

c. Channels

Whereas some molecules can freely diffuse through the membrane, selective ion movement is provided by specific proteins – ion channels and ion pumps (Gadsby and Gerschel 2009) (Fig.1.2).

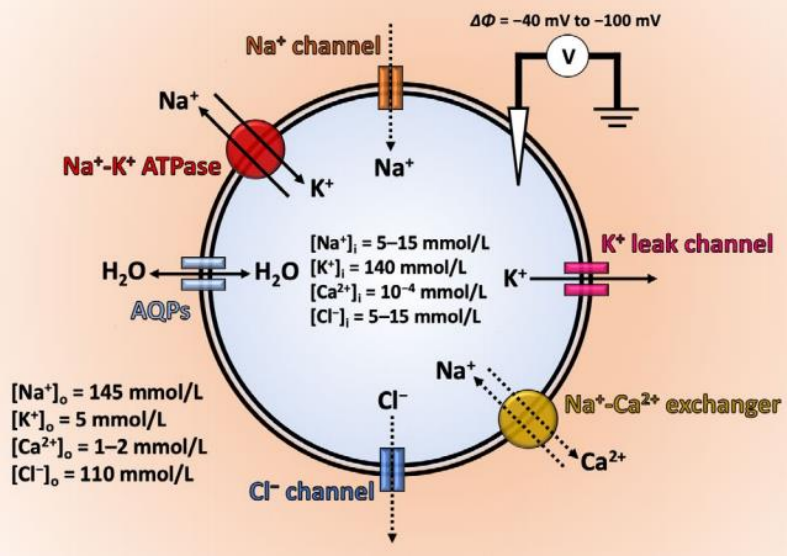

Figure 1.2: *Ion homeostasis (from* (Morishita, Watanabe, and Ichijo 2019)*)*

Ion channels provide fast passive transport along the concentration gradient. For instance, as the concentration of Na^+ is high in the cell exterior, there is a passive Na^+ transport into the cell. The opposite is with K^+, as this ion species leaks out from cells passively.

Cl^- is the only negatively charged ion species present in the cell at relatively high concentrations. Regulatory volume decrease (RVD) followed by osmotic volume increase is controlled by swelling-activated chloride efflux mediated by VRAC (volume-regulated anion channel). LRRC8 is an essential component of VRAC that was recently identified (Voss et al. 2014). The proposed mechanism of LRRC8 activation is by sensing of ionic strength that decreases when cells swell (Syeda et al. 2016). VRAC has been demonstrated to facilitate cell migration (Hoffmann, Lambert, and Pedersen 2009).

Some ion channels directly interact with actin (Sasaki, Yui, and Noda 2014; Martinac 2014), microtubules and integrins (Jiao et al. 2017). A large number of ion channels are mechanosensitive (Haswell, Phillips, and Rees 2011) (Fig.1.3), such as the widely known Piezo1 (J. Wu, Lewis, and Grandl 2017).

Piezo1, for example, is a stretch-activated channel, that induces Ca^{2+} influx and release of ATP (Miyamoto et al. 2014). ATP serves as a signaling molecule (Schwiebert and Zsembery 2003; Hamill and Martinac 2001), and Ca^{2+} serves as an important second messenger (Clapham 2007). Piezo1 is involved in cell migration, including amoeboid migration in confined environment (Nourse and Pathak 2017). In mesenchymal cells Piezo1 is highly expressed in lamellipodia and filopodia (Sugimoto et al. 2017).

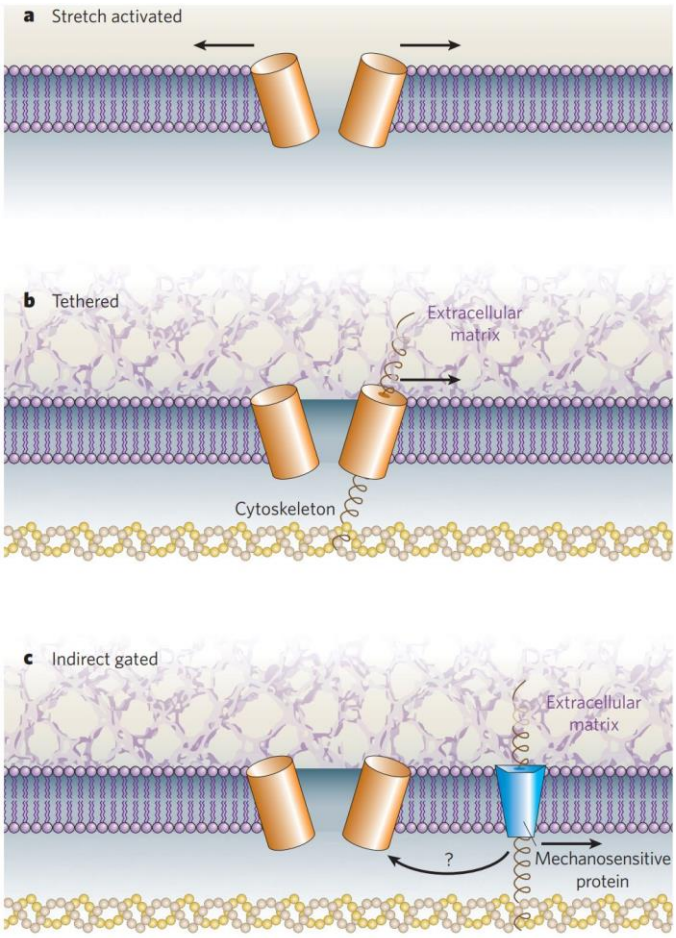

Figure 1.3: *Different models of mechanosensitive ion channels activation (from* (Lumpkin and Caterina 2007)*)*

(a): by tension in lipid bilayer; (b): by link to cytoskeleton or extracellular matrix; (c): by intermediate sensory protein

Mechanosensitive channels can play a role in volume regulation. It was shown that GsMTx4, a specific inhibitor of cationic mechanosensitive channels, and $GdCl_3$, a nonspecific blocker of stretch-activated channels (like Piezo1), blocked RVD and associated Ca^{2+} uptake (Hua et al. 2010).

Ion pumps (transporters) move ions against the concentration gradient and require energy from ATP-hydrolysis. They are responsible for maintenance of steady-state cell volume (Hoffmann, Lambert, and Pedersen 2009). One of the major players is the Na^+/K^+ pump, whose regulation prevents cell from swelling (Armstrong 2003). It pumps 3 Na^+ out of the cell and 2 K^+ in, for every single ATP molecule hydrolyzed.

Ion pumps are also important for regulatory volume recovery, Na^+/H^+ exchanger (NHE1) participates in regulatory volume increase (RVI) (Vallés et al. 2015) that counteracts cell volume decrease. Increase of NHE1 activity increases intracellular pH, which is important for cytoskeleton as actin/myosin-II activity is pH-sensitive (Vallés et al. 2015; Köhler et al. 2012) and ion transport activity (Holzer 2009). NHE-1 linked to acto-myosin via ERM-proteins (Denker and Barber 2002). NHE1 is located in the leading edge of migrating cells and has been shown to participate in migration (Hoffmann, Lambert, and Pedersen 2009).

A difference in ion concentration inside and outside the cell coming from different membrane permeability to distinct ions generates membrane potential (M. Yang and Brackenbury 2013). A dynamic membrane potential is important for cell cycle, cell-volume control, proliferation, etc. (Kadir, Stacey, and Barrett-Jolley 2018).

Another type of channel incorporated into cell membrane is the aquaporin family (AQP) (Day et al. 2014). They are known to be passive channels selective for water, that increase membrane water permeability (Mola et al. 2016). Expression of AQP4 in HeLa cells increased diffusion permeability P_d from 8 µm/s to 27 µm/s (Ibata et al. 2011). However, recent studies showed, that aquaporins also allow the transport of small organic molecules (Verkman AS 2013). It is possible, that aquaporins are gated by membrane tension (Ozu et al. 2018).

d. Cytoplasm and nucleus

In total, solid material occupies only about 30% of the cell volume (Zhou et al. 2009). Some of these solid components, like bulk cytoskeleton and macromolecular crowders (e.g. ribosomes), form poroelastic meshworks bathed in an intracellular fluid (Moeendarbary et al. 2013). It means that water movement inside the cell is limited by a porous matrix. Timescale of water movement is $\tau = R^2/D$, where R is the cell radius, and D is the diffusion coefficient; $D \sim E\varepsilon^2/\mu$, E is the elastic modulus, ε is the pore radius, μ is the cytosolic viscosity. Pore radius was estimated as ε ~15 nm and D~5 µm^2/s (G. T. Charras, Mitchison, and Mahadevan 2009). Several studies propose this poroelastic sponge-like meshwork as a key regulator of

cell volume rather than membrane-cortex (Sachs and Sivaselvan 2015). It was also shown that in response to the local dehydration, water moves faster across the thin (~6 nm) membrane than inside the cytoplasm (G. T. Charras, Mitchison, and Mahadevan 2009).

The nucleus is the biggest and stiffest organelle inside the cell (Dahl, Ribeiro, and Lammerding 2008). For mammalian cells the cytoplasmic-to-nuclear volume ratio is about 2-3 (Oney, Kurnaz, and Kurnaz 2005). Nuclear volume, unlike total cell volume, does not follow a linear relation to external osmolarity (Finan et al. 2009). The nucleus is mechanosensitive and nuclear deformations can alter gene expression (Miroshnikova, Nava, and Wickström 2017).

2. Methods to study the mechanical properties of a single cell

To understand how the cell volume would respond to mechanical deformations, we first need to understand cell material properties. The general way to study mechanical properties is to apply a given deformation and record a response. As was described above, cell is composed of many elements that have different mechanical properties. However, as we aimed to study total cell volume, we are interested in whole cell measurements and membrane-cortex interaction. Thus, we basically will discuss two parameters: stiffness and tension. The methods described below give strictly different values as mechanical response of cells depends on the applied force in order to answer: **what kind of material the cell is?**

a. Atomic force microscopy (AFM)

Cells are considered as a viscoelastic objects, depending on the time and length scale of the deformation, and AFM is mainly used to decipher both elastic and viscous responses. There are different mechanical models describing cell properties: discrete viscoelastic model, viscoelastic gels, tensegrity, soft glassy rheology model, active gels, tension model (Brückner and Janshoff 2015). At short time scale, the cell could be considered as an elastic material under global deformation, whereas at long time scale it relaxes through an active reorganization that can be seen as a viscous relaxation. For local deformations, an equivalent interpretation can be applied.

None of the existing models fully describe all the observed behavior (Haase and Pelling 2015), but they can fit experimental data well with certain assumptions. For instance, the common assumption is that Poisson's ratio of cell is constant and close to 0.5 (like rubber), which means that the cell is incompressible and conserves volume (P. H. Wu et al. 2018; Harris and Charras 2011).

However, the most commonly used nowadays is the tension model (Brückner and Janshoff 2015; Pietuch and Janshoff 2013), which relies on the assumption that a restoring force to the applied deformation originates from a constant isotropic tension *T* under a constant enclosed volume.

$$T = T_0 + \widetilde{K}_A \frac{\Delta A}{A_0} \qquad \textit{(Eq. 2)}$$

$$T_0 = T_c + T_t \qquad \textit{(Eq. 3)}$$

where T_0 is sum of cortical T_c and membrane T_t tensions; ΔA is a change of surface area related to the initial cell surface area A_0; $\widetilde{K}_A$ is the apparent area compressibility modulus, related to the compressibility modulus K_A as:

$$\widetilde{K}_A = K_A \frac{A_0}{A_0 + A_{ex}} \qquad \textit{(Eq. 4)}$$

where A_{ex} corresponds to excess of membrane area stored in reservoirs.

- Small deformations.

When the applied deformation δ is small compared to the cell radius *R*, $\frac{\delta}{R} = 1 - 10\%$, time-independent Hertz theory is valid (Paul et al. 2014), cell volume is considered as a constant. The small indentation could be applied with the small sharp or spherical or flat AFM tip. At short time scale, the force response is elastic and is used to extract the apparent cell stiffness. The range of effective Young's modulus *E* for mammalian cells is quite broad, from 1 to 100's of kPa. It depends on various parameters, both biological and physical origins. For instance, cell type, state of the acto-myosin cortex, adhesion to the substrate and region of indentation are important, as well as loading rate, depth of indentation, cantilever shape and the mechanical model.

For example, the cortex elastic modulus of non-adherent HFF cells was measured by tipless cantilever and estimated as 40 kPa (Cartagena-Rivera et al. 2016), and cortical tension was equal to 680 pN/µm (0.68 mN/m). The relation between tension *T* and elastic Young's modulus *E* was expressed as:

$$E = \frac{\pi R T^2}{2 h k_c d} \qquad \textit{(Eq. 5)}$$

where *R* is the cell radius, *h* is a cortex thickness, k_c is the cantilever spring constant and *d* is the cantilever deflection. Myosin inhibition by Blebbistatin and cortex disruption by Latrunculin (Lat; actin depolymerizing drug) reduced tension, whereas enhancement of myosin contractility by Caliculin and inhibition of Arp2/3 complex increased cortical tension.

Another representative example is a set of measurements for one cell type MCF-7. Depending on the measurement parameters, *E* differs more than tenfold (P. H. Wu et al. 2018). Measurements with small sharp cantilever also showed the difference between nuclear region (5.5 kPa) and cell edge (3.8 kPa) and showed higher values than for big spherical cantilever (0.53 kPa).

The reasoning for higher elasticity values obtained with sharp cantilever was explained by the underestimation of contact area, whereas measurement performed with spherical cantilever did not have this artifact (Harris and Charras 2011). In this study MDCK cells had E=380 Pa. Actin disruption led to two-fold decrease in elasticity, and inhibition of contractility did not affect elastic modulus. These values were in the same range as obtained with other methods like micropipette aspiration and microrheology.

In general, it is accepted that small and fast cell deformation are elastic. Only for very small deformations elastic response is rate independent (Nawaz et al. 2012). As for slow deformations, like when constant displacement δ is applied over time, cells exhibit viscous dissipation in contrast with elastic material that exerts constant force (Fig.2.1). This behavior can be fitted with time-dependent Hertz model to extract viscosity.

In the case of deformations restricted to 200 nm size, applied by a spherical bead with small forces (<30 pN) it was measured that *E* is largely determined by the acto-myosin cortex and is equal to 100 Pa in 3T3 adherent cells (Nawaz et al. 2012). This value is similar to the modulus of the purified actin network with crosslinkers (Haase and Pelling 2015). Disruption of F-actin reduced *E* to 30 Pa. At higher deformations viscous effects increased the elastic modulus.

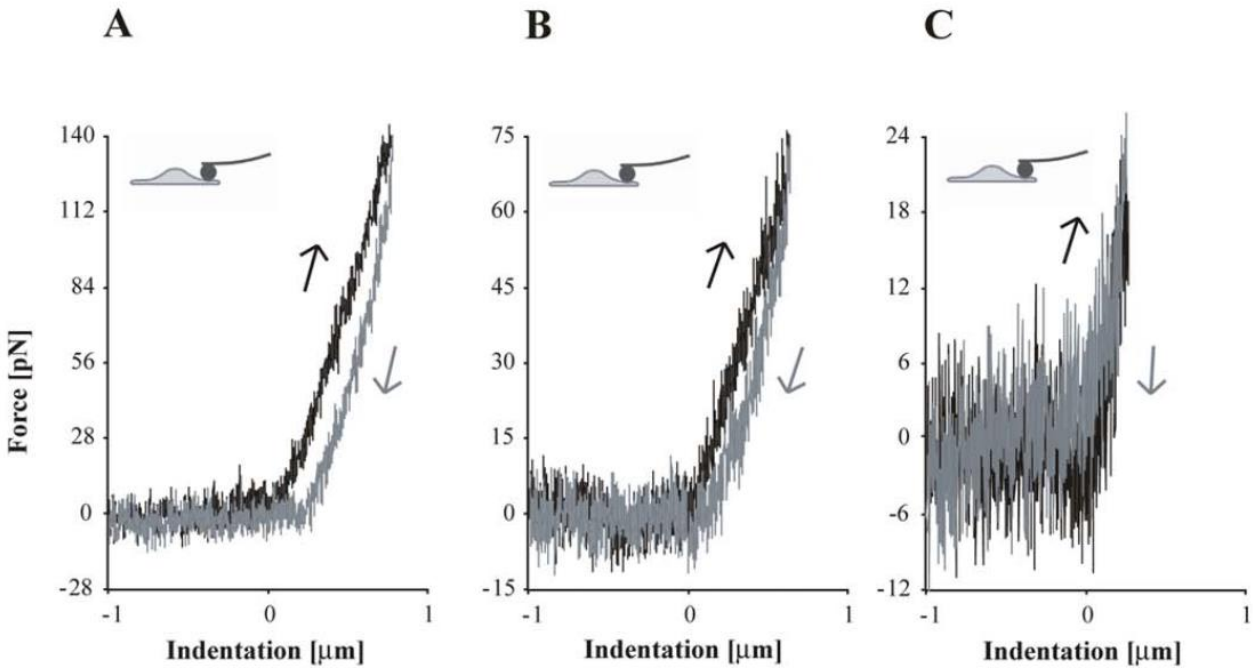

Figure 2.1: *Effect of the speed of deformation at the sub micrometer level (from (Nawaz et al. 2012))*

(a, b): At high forces indentation (black) and retraction (grey) curves are not identical, but show a considerable amount of hysteresis, that indicates a viscous regime.

(c): At small force, close to the intrinsic noise of the cantilever, hysteresis cannot be distinguished. Therefore, purely elastic response can be assumed.

Alternatively, to measure viscoelastic properties researchers often use dynamic AFM mode. However, these approaches are not very straightforward to implement and interpret.

- Large deformations

Interpretation of large deformations imposed by AFM is also very complex. Tatara theory can be applied in case of large deformations $\frac{\delta}{R} = 20 - 60\%$ for an elastic sphere. It was developed for modeling deformation of soft material like rubber, where the influence of Poisson's ratio to the calculated deformation is small (Paul et al. 2014). While for small deformations the acto-myosin cortex plays a major role, in case of large deformations membrane mechanics is also important due inextensibility of the lipid bilayer (Brückner and Janshoff 2015). In case of large deformations, the surface area should intuitively increase if the volume is constant. For GUVs (Giant Unilammelar Vesicles), this would limit the indentation

before they burst as they lack excess membrane. For GUVs compressed between two horizontal plates it was shown that at large strain elastic response is not linear due to lateral stretching of the lipid bilayer (Schäfer, Kliesch, and Janshoff 2013). It was demonstrated in the same study that reconstitution of a thick actin shell in GUVs increases their stiffness, whereas a thin actin shell does not.

Stepwise uniaxial compression of mitotic cells (Fig.2.2) shows that inhibition of myosin activity reduced cortex stiffness, but solidified it. It suggests that myosin activity fluidizes the cortex and modulates its rheological properties (E Fischer-Friedrich et al. 2016). Cortical tension of cells treated with myosin inhibitors is (0.5 mN/m) almost 3 times smaller than for control cells (1.67 mN/m). Inhibition of both myosin activity and actin polymerization significantly reduced cortical tension (0.06 mN/m). Notably, cortical tension of mitotic cells is almost 10 times higher than that of the same cells in interphase (Elisabeth Fischer-Friedrich et al. 2014). A later study also showed an increase of cortical tension in mitosis that was associated with reduction of cortex thickness (Chugh et al. 2017).

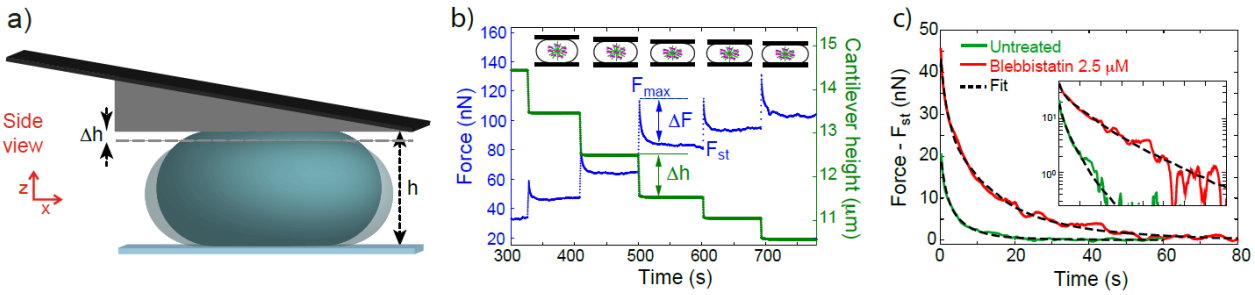

Figure 2.2: *Stepwise uniaxial compression of a mitotic cell (from* (E Fischer-Friedrich et al. 2016)*)*

(a): Scheme of experiment. In a compression step, the cantilever is lowered by a height interval (Δh).

(b): Measured force and cantilever height during confinement.

(c): Force relaxation after a step of compression

b. Micropipette aspiration

In micropipette aspiration, the cell surface is extended by aspirating a part for the cell into a micropipette. Therefore, this deformation is opposite in direction to AFM indentation. The forces range is from 10 pN to 1 nN. Aspiration of model vesicles gives a linear relationship between membrane tension and area expansion (Hamill and Martinac 2001) (Eq. 1).

After the point when a hemispherical projection is formed into the pipette, soft cells (e.g. neutrophils, RBCs) with a constant cortical tension will flow inside the pipette and stiff cells (e.g. endothelial, chondrocytes) will extend the surface into the pipette until equilibrium is reached (Hochmuth 2000). The suction pressure is proportional to cortical tension that follows from Laplace law. As suction pressure is smaller than the osmotic pressure, cell volume is considered as constant during aspiration. In this case, the cell is treated like a liquid droplet.

The cortical tension of L929 cells was estimated as 400 pN/µm (Fig.2.3) (Tinevez et al. 2009). Myosin inhibition by drug treatment decreases tension, whereas cells transfected with constitutively active version of RhoA increased tension to 1900 pN/µm.

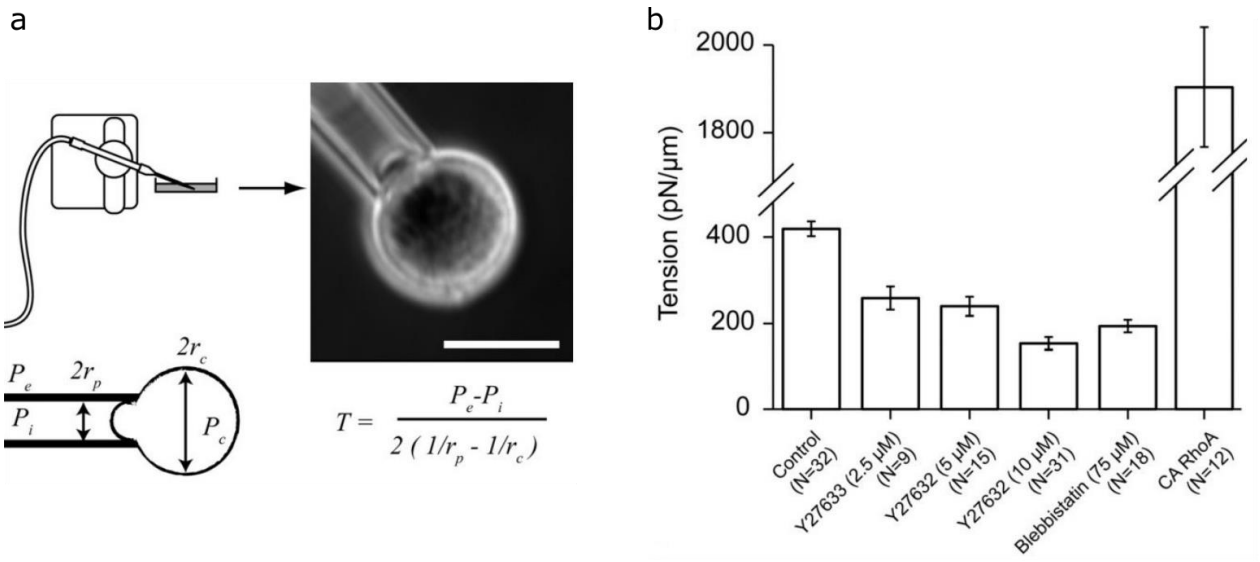

Figure 2.3: *Cortical tension measurements with micropipette aspiration (from* (Tinevez et al. 2009)*)*

(a): Scheme of experiment. Scale bar is 10 µm.

(b): Myosin inhibition decreases cortical tension, whereas myosin activation strongly increases it.

c. Tether pulling

Another common method to measure cell mechanical properties are optical tweezers with small forces in the order of 50 pN. Sometimes optical tweezers are used in combination with aspiration pipette, or tether-pulling can be done with AFM, which allows obtaining various parameters simultaneously.

When a tether is pulled from a model membrane, the tether force F_t is proportional to surface tension $\gamma_{in-plane}$ and membrane bending stiffness κ (typically 10^{-19} J):

$$F_t = 2\pi\sqrt{2\kappa T_t} \qquad \textit{(Eq. 6)}$$

since the membrane is fluid, the measure of force gives the tension of the vesicle knowing the bending rigidity. In a cell, the presence of the cortex and transmembrane protein disturbs the homogeneity of the tension. However, this tether tool can extract local measurements and the relation of the force is similar for cell, without cortex or in the cortex free regions, like blebs. In the cell with cortex the tether force also depends on membrane-to-cortex attachment $\gamma_{membrane-cortex}$. Then the measured tension is often called effective membrane tension (Diz-Muñoz, Fletcher, and Weiner 2013):

$$T_t = \gamma_{in-plane} + \gamma_{membrane-cortex} \qquad \textit{(Eq. 7)}$$

Interestingly, average membrane tension of keratocytes did not significantly change when the membrane area was increased by 30% via membrane fusion with GUVs by electroporation (Fig.2.4) (Lieber et al. 2013). This suggests that the availability of membrane area does not play a dominant role in determining membrane tension. Although, it is possible that a transient tension decrease could occur right after fusion, but then tension came back to a homeostatic value. It was also shown in the same study that partial actin disruption and Arp2/3 inhibition decrease the average membrane tension by 50% and 25% respectively.

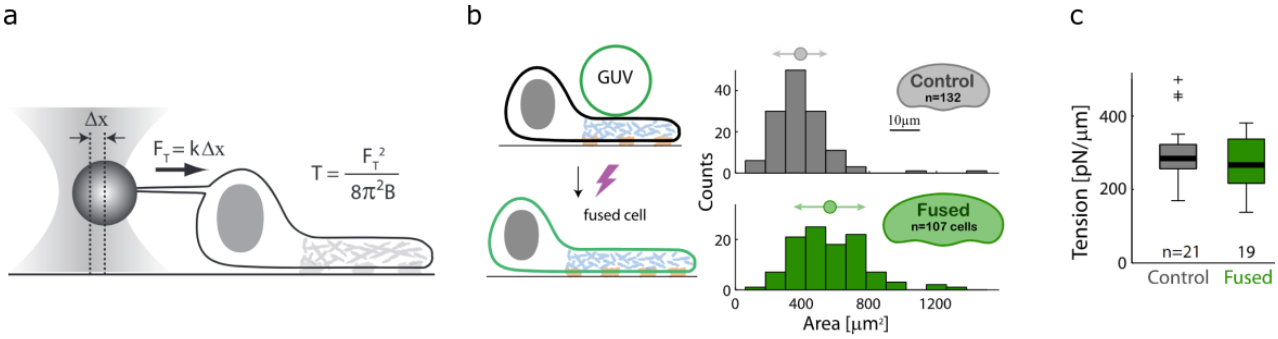

Figure 2.4: *Membrane tension in polarized keratocytes (from* (Lieber et al. 2013)*)*

(a): schematic representation of tether extraction from the rear edge

(b, c): Significant increase of available membrane area does not lead to average membrane tension decrease.

The average membrane tension at the leading edge of migrating keratocytes was estimated as 365 pN/µm (Lieber et al. 2015). However, the membrane tension at trailing edge was 30% lower. It was also recently shown, that membrane tension propagate quickly across blebs, but not in cells (Shi et al. 2018). Therefore, the common assumption that membrane tension is homogeneous across a cell is not correct. In light of such information, membrane tension is also considered as a local parameter.

d. Particle tracking

To study rheology of cytoplasm, researchers often use submicron bead-based measurements. The beads injected into cytoplasm are subjected to thermal forces and opposing viscous frictional forces. Brownian motion of the bead with radius a can be described by the diffusion coefficient proposed by Einstein: $D = k_BT/(6\pi\eta a)$, where k_BT is a thermal energy, η is liquid viscosity. When the size of the beads is larger than effective cytoskeleton mesh size, their movement, recorded at high time resolution, reflects cytoskeletal viscoelastic properties (Hale, Sun, and Wirtz 2009).

These measurements usually give low values of elastic modulus compared to AFM techniques. The value obtained for MCF-7 at 1 Hz was 4.5 Pa, at 30 Hz was 111 Pa (P. H. Wu et al. 2018). The difference between the values obtained by AFM and particle tracking can be described by the fact that these methods probe different cellular regions: AFM probes cortical structures, whereas for particle tracking, beads measure bulk cytoplasm (Hale, Sun, and Wirtz 2009). In this study, elastic modulus of 3T3 fibroblasts was found as ~0.7 Pa at 1Hz and ~8 Pa at 30 Hz. For both frequencies, actin disassembly decreased elastic modulus.

Another novel approach based on submicron particle tracking is a measure of macromolecular crowding. Effective diffusion coefficient of particles is a function of excluded volume occupied by macromolecules, mostly ribosomes (the phenomenological Doolittle equation). Ribosome concentration plays an important role in intracellular biochemistry and directly affect cell viscosity. A recent study showed that the cytoplasm of HEK-293 cells is less crowded than yeast (Delarue et al. 2018).

3. Cell volume regulation in response to deformations of different timescales

a. Steady-state volume

Even at steady-state cell volume regulation is not a simple question (Fig.3.1). The essential problem is that for physiological needs the cell contains negatively charged macromolecules and constantly produces osmotically impermeable molecules that would lead to cell swelling as the membrane is highly permeable for water (Armstrong 2003; Morishita, Watanabe, and Ichijo 2019; Hoffmann, Lambert, and Pedersen 2009). The physiological osmolarity is ~300 mOsm, then the change in osmolarity by 1 mOsm (less than 1%) will give:

$$\Delta p = cRT = 1 * 8.31 * 300 = 2493\ Pa \qquad \textit{(Eq. 8)}$$

The pressure that the cell cortex can withstand is two orders of magnitude smaller. If we assume cortical tension as $\gamma = 4 * 10^{-4} N/m$ (Tinevez et al. 2009)) and cell radius *R= 10^{-5} m*, Laplace law will give:

$$\Delta p = \frac{2\gamma}{R} = 80\ Pa \qquad \textit{(Eq. 9)}$$

This simple calculation shows that cells need an active mechanism to maintain their steady-state volume, as forces at the cell contour are not in equilibrium. Therefore, cells constantly pump ions outside and inside the cell, consuming ATP energy. This concept called pump-leak model is described by many theoretical studies (Mori 2012; Kay 2017; Essig 1968). However, some researchers argue with the idea that force balance on cell membrane plays a determining role, as sponge-like cell bulk can easily withstand osmotic pressure difference (Sachs and Sivaselvan 2015). The important argument is that some cells are able to survive in distilled water for hours.

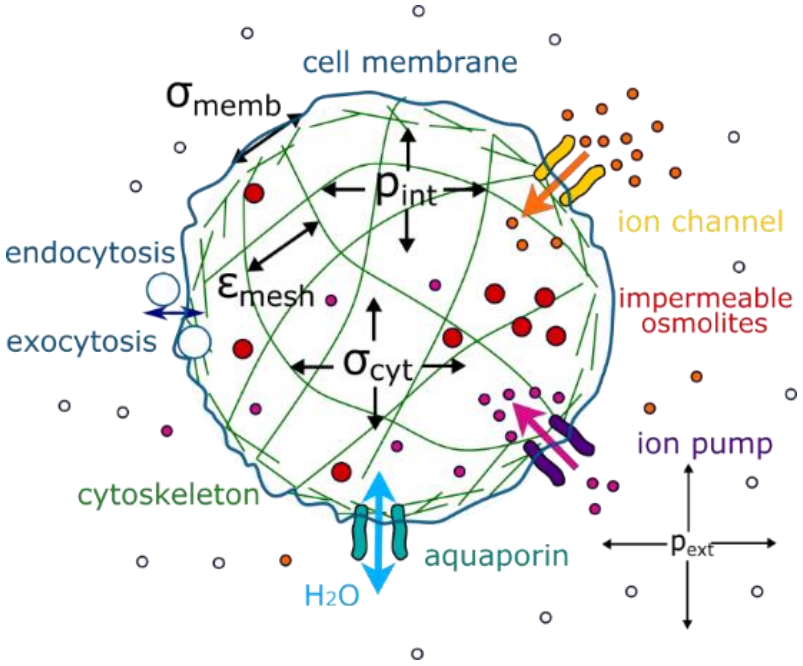

Figure 3.1: *Schematic representation of suspended cell at steady state.*

b. Osmotic shock

Osmolarity of the extracellular fluid can change under normal and pathophysiological conditions. It is well known that most of mammalian cells have a two-steps response to osmotic shock (Hoffmann, Lambert, and Pedersen 2009). When external osmolarity rapidly changes, cells passively swell/shrink with respect to osmotic pressure difference. This response can be described by the Ponder's relation (Ponder 1935), and was shown to be independent of the state of the actin cortex (Pritchard and Guilak 2004; Zhou et al. 2009):

$$\frac{V}{V_{iso}} = R\frac{P_{iso}}{P} + (1 - R) \qquad \textit{(Eq. 10)}$$

where V_{iso} and P_{iso} indicate initial volume and isotonic pressure, V indicates volume of the cell immediately after exchange of isotonic medium to the medium with osmotic pressure P; R indicates the so called osmotically active volume fraction; and *(1-R)* is an osmotically inactive volume fraction. Osmotically inactive fraction (excluded volume) represents the fraction of volume occupied by solid components (e.g. ribosomes) and water bound to them. Excluded volume for different cell lines was estimated as 15%

(Shapiro 1948; Benson, Chicone, and Critser 2011), 20% (Newton et al. 1999), 30% (Zhou et al. 2009) of the total volume. In fact, Ponder's relation is just a form of the van't Hoff law where $PV = const$.

Time of initial swelling in response to hypoosmotic shock varies in different studies, but usually takes about 1 min (Boudreault and Grygorczyk 2004; Fernández et al. 2013; Groulx et al. 2006) and does not depend on actin polymerization (Pritchard and Guilak 2004). The recent studies showed that overexpression of aquaporins significantly decreases swelling time and relative volume increase (Mola et al. 2016; Lisjak et al. 2017).

After this initial passive response, cells tend to come back to the volumes they had before the shock – this adaptation, regulatory volume decrease/increase (RVD/RVI), is known to be an active process. It requires ion channels/pumps activation and has a typical timescale of tens of minutes and is excellently reviewed in (Hoffmann, Lambert, and Pedersen 2009). RVD is usually accomplished by KCl efflux induced by parallel activation of K^+ and Cl^- channels. Osmotic swelling results in a significant increase in the cytosolic Ca^{2+} that activates Ca^{2+}-dependent K^+ channels (Okada et al. 2001). Osmotic swelling also induces release of intracellular ATP, which activates P receptors. Interestingly, human red blood cells (RBCs) do not exhibit volume adaptation, however, additional stimulation of P receptors induces significant RVD (Pafundo et al. 2010). VRACs (volume-regulated anion channels, LRRC8) mediate swelling-activated chloride efflux. LRRC8 is sensitive to ionic strength that decreases when cells swell (Syeda et al. 2016). One of the major regulators of RVI are NHE exchangers family. NHE is activated by cell shrinkage and inhibited by cell swelling. The NHE1 activation seems to be F-actin independent and less sensitive to change in ionic strength than to cell shrinkage (Hoffmann, Lambert, and Pedersen 2009). Involvement of Na^+-K^+-$2Cl^-$ cotransporters in RVI also was shown as well as organic osmolites uptake (TauT).

c. Spreading

Cell spreading is a deformation that occurs when suspended cell encounters an adhesive substrate. The natural example of such event is spreading of daughter cells preceded by mitotic rounding and cell division.

When suspended cell touch the substrate, initial anchoring probably occurs through Van der Waals interactions, and then cells start spreading. Cell spreading can be divided by two stages – early and late (Fig.3.2) (McGrath 2007). First minutes of cells spreading are dominated by blebbing, and after filopodia and lamellipodia start to form. At this stage there is a transition of overall cell shape from sphere to

spherical cap (Frisch and Thoumine 2002); cells extend their membrane reservoirs to allow area extension without new membrane material addition (Gauthier et al. 2011). Later on, blebbing activity decreases and lamellipodia become the dominant protrusion type (Fig.3.5a) (Höglund 1985). To further area extension, cells add additional membrane material via exocytosis (Gauthier et al. 2009). The rate of lamellipodia extension is limited by membrane tension (Raucher and Sheetz 2000): cells with low tension spread faster. It can be explained by the fact, that increase in membrane tension inhibit actin assembly and Rac1 GTPase activation (Houk et al. 2012). It also was shown that when membrane tension decreases/increases in cells attached to a surface, there is a correlated increase/decrease in the CLIC/GEEC pathway, bringing about a rapid endocytic response to reset the resting membrane tension (Thottacherry et al. 2018).

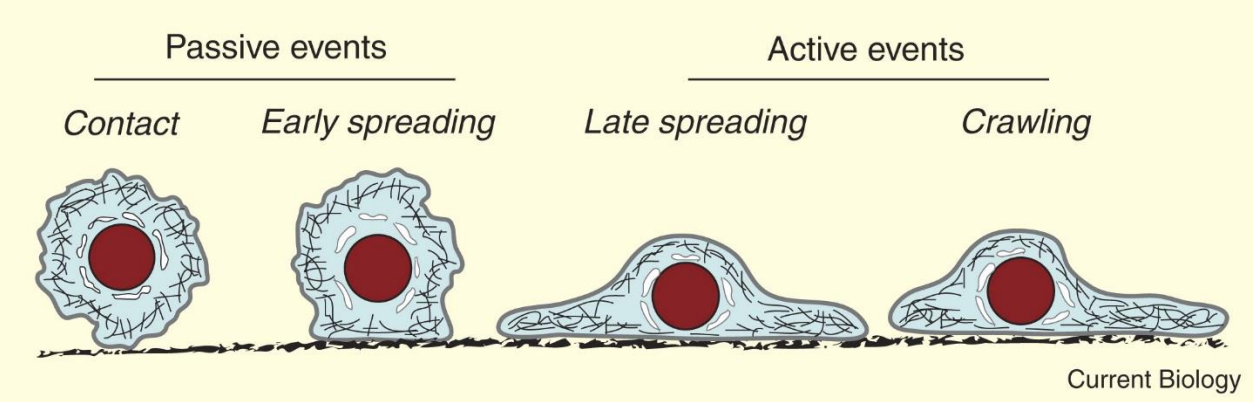

Figure 3.2: *Cell spreading stages (from* (McGrath 2007)*).*

- Early stage

At the early stage of attachment, spreading is isotropic and contact radius evolution follows a power law with slope 0.5 (Cuvelier et al. 2007). This slope is explained by the model (Fig.3.3), where adhesion energy is accommodated by energy dissipation in the thin actin shell, but not in the whole cell body. The contact zone is small compared to cell size and cell volume is considered as constant. According to this model, spreading kinetics depend on the state of actin cortex. Indeed, disruption of actin cortex by Cytochalasin D leads to linear growth of contact radius. Interestingly, microtubule disruption increases bleb formation, but does not affect contact radius evolution. At the late stage of spreading, when the cell is flattened, the slope is equal to 0.25 as dissipation occurs in the whole cell.

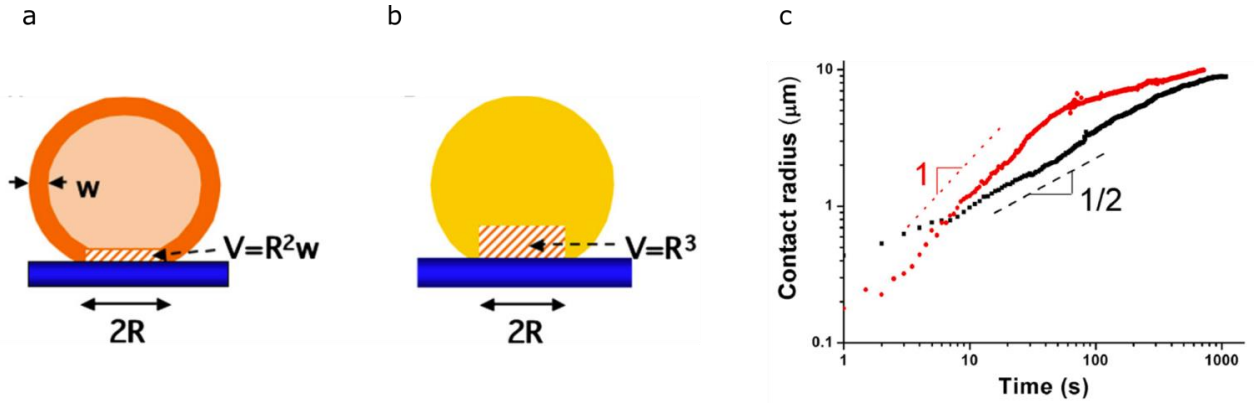

Figure 3.3: *Schematic representation of the spreading cell and contact radius evolution*

(a): Viscous dissipation occurs in actin cortex.

(b): Cell without cortex can be considered as a homogeneous viscous drop

(c): In contrast with untreated HeLa cells (black squares), Cytochalasin D-treated cells (red circles) spread more quickly and contact radius evolution is linear with time.

Later AFM measurements combined with tether pulling (Fig.3.4) showed that upon initial contact with the substrate there is a transient drop in membrane tension that is necessary for releasing membrane material forming first protrusions (Pietuch and Janshoff 2013). Suspended cells store membrane excess in reservoirs; however, cells cannot release it. Therefore, the apparent area compressibility modulus has a big value. That drop in tension is a consequence of partial cortical actin disruption and corresponds to decrease in compressibility modulus, which indicates release of membrane reservoirs. When released membrane is extended while spreading, membrane tension increases and reaches a homeostatic level. Calculation of cortical tension showed that initial values are close to zero, which reflects the absence of contraction at an early stage of spreading.

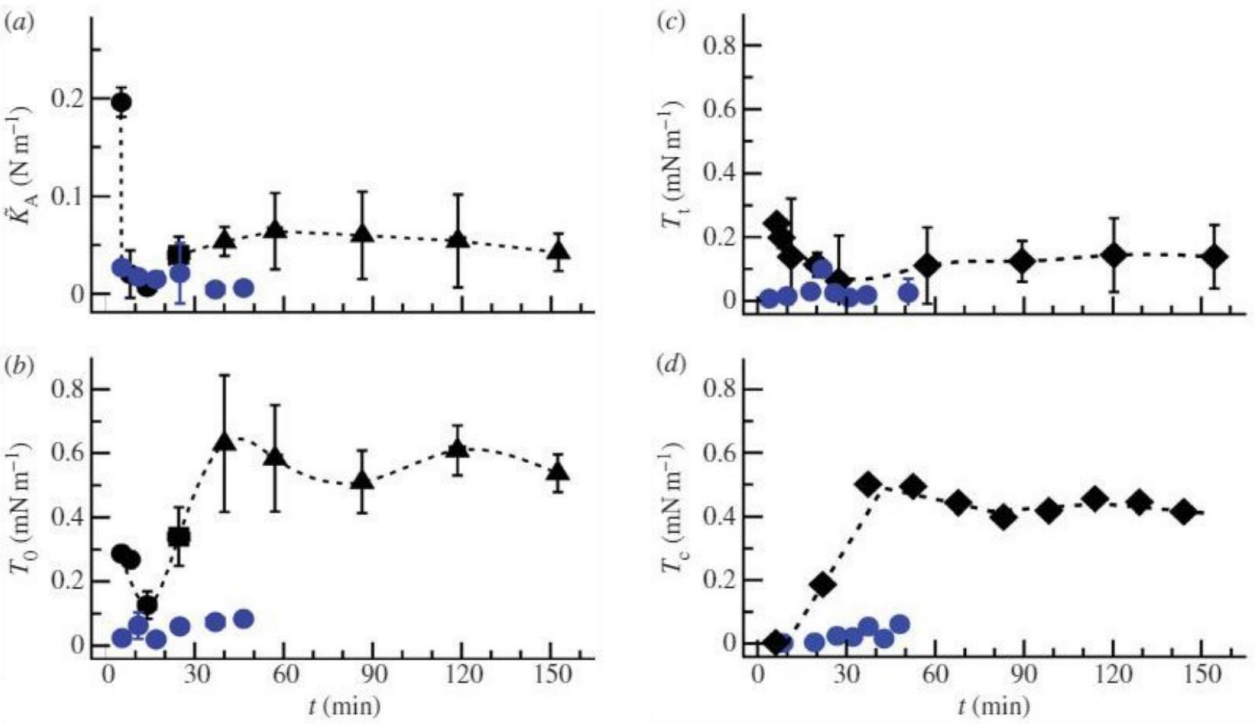

Figure 3.4: *Mechanical parameters of spreading MDCK control cells (black triangles) and Cytochalasin D-treated (blue circles) (from* (Pietuch and Janshoff 2013)*)*

Apparent area compressibility modulus (a), membrane tension obtained from indentation (b), membrane tension obtained from tether-pulling (c), calculated cortical tension (d).

- Later stage of spreading and migration

Later stage of spreading strongly depends on cytoskeleton state. Disruption of actin and microtubules induces high blebbing activity and significantly decreases spreading area that cells reach in 1 h (Fig.3.5) (L. Norman, Sengupta, and Aranda-Espinoza Helim 2011). Myosin inhibition increases spreading rate and inhibits blebbing, consistent with (G. T. Charras 2008).

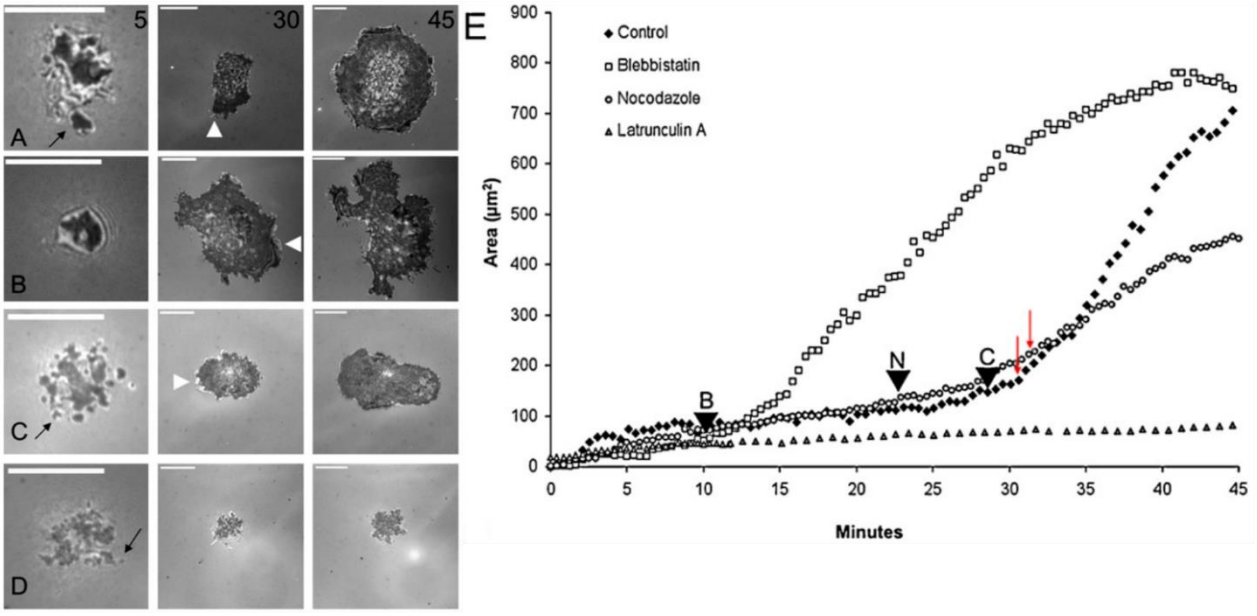

Figure 3.5: *Representative RICM images of spreading dynamics of BAECs treated with cytoskeleton drugs (from* (L. Norman, Sengupta, and Aranda-Espinoza Helim 2011)*)*

(a): control, (b): Blebbistatin,(c): nocodazole, (d): Lat A; scale bar is 10µm. Arrows indicate blebs, Arrowheads indicate lamellipodia.

(e): single cell spreading area for control and treated cells. Arrowheads indicate initial observation of lamellipodia, arrows indicate disappearance of blebs.

Inhibition of Arp2/3 complex changes actin organization in the basal plane: absence of branched actin network drive lamellipodial-to-fillopodial protrusions. Cell spreading is retarded (Henson et al. 2015). It was also shown that Arp2/3 inhibition activates cell blebbing due to reduced membrane-to-cortex attachment (Beckham et al. 2014). Inhibition of Rac1, which regulates Arp2/3 activity, suppressed lamellipodium formation and membrane ruffling and reduced adhesive area (Wells 2004), although Rac1 is not required for focal adhesion and filopodium formation (Steffen et al. 2013).

Vimentin intermediate filaments (VIF) are localized in the tail and perinuclear region of a polarized cell, whereas non-filamentous vimentin structures are present in the lamellipodium (Helfand et al. 2011). Presence of VIF inhibits lamellipodium, whereas disassembly of VIF into unit length filaments (ULF) induces membrane ruffling and lamellipodium formation.

After spreading on a substrate cells can exhibit migratory phenotype regulated by small GTPases (mesenchymal migration) (Cramer 2010). Importantly, depending on the cell type and environment some cells show amoeboid migration that does not require adhesion to the substrate (Liu et al. 2015). Variety

of ion channels and pumps involved in cell volume regulation, including VRAC, NHE1, Ca^{2+}-dependent K^+ channels and aquaporins, as well as osmotic perturbation were shown to play a role in cell migration (Hoffmann, Lambert, and Pedersen 2009). It suggests that volume regulation could be important for cell migratory properties. For instance, it was reported that cell volume inversely correlate with migration speed (Stroka et al. 2014).

- Cell volume while spreading

Like for others mechanical deformations cell volume while spreading was often assumed to be constant. Only very recently, researchers revealed the importance of volume regulation in the context of cell mechanics.

It was shown that while contact area increases during spreading, cell volume decreases, and in 1 h the volume loss is about 25% compared to the initial volume of suspended cells (Fig.3.6) (Guo et al. 2017). The total protein content was not affected, thus the authors concluded that water efflux during spreading is somewhat similar to hyperosmotic compression. The water efflux is very unlikely explained by the direct pressing force generated by cytoskeleton due to the difference of magnitudes of osmotic and cytoskeleton forces (calculations are above). Therefore, the authors proposed that forces generated by cytoskeleton while spreading activate mechanosensitive ion transportation.

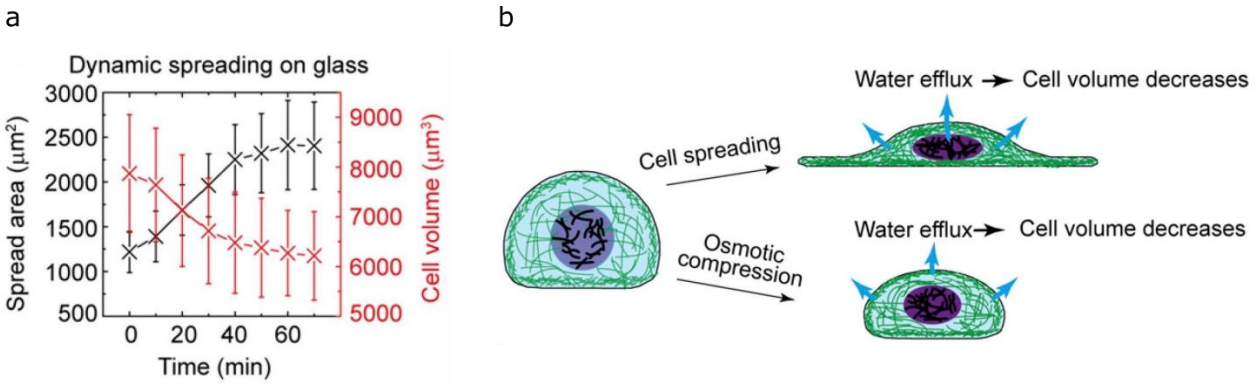

Figure 3.6: *Cell volume while dynamic spreading (from* (Guo et al. 2017)*)*

(a): average cell volume and spreading area of A7 cells dynamically attach on a stiff substrate.

(b): schematic illustration of cell volume decrease through water efflux.

Strikingly, according to the same authors, cell volume negatively correlates with spreading area at the steady state (Fig.3.7a). Spreading area restriction does not play a role, as average volume does not differ for a given spreading area reached by either substrate softening (PA gel) or fibronectin micropatterning on stiff substrate. The same trend was obtained by another research group – concluding spreading area determines cell volume (Fig.3.7b) (Xie, Yang, and Jiang 2018).

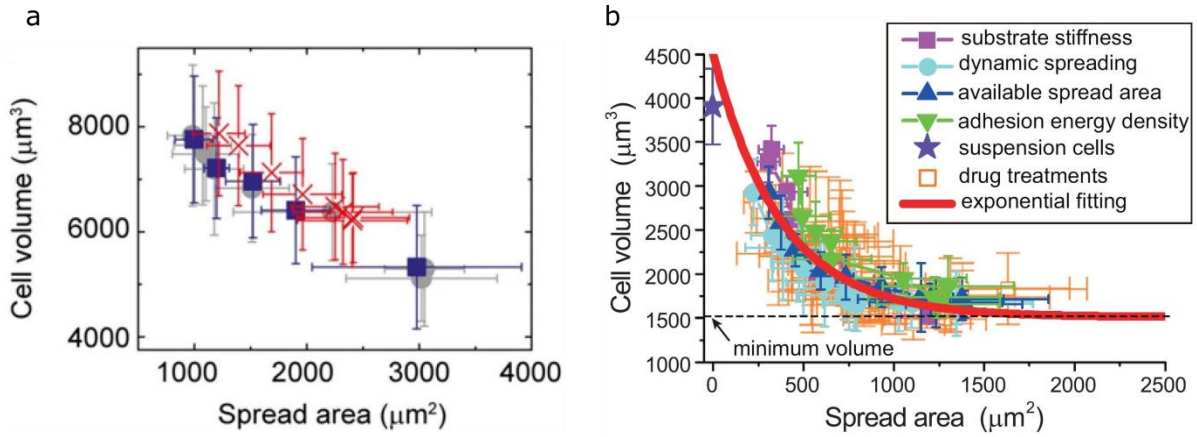

Figure 3.7: *Cell volume as a function of spreading area*

(a): Cell volume plotted as a function of the projected area, for A7 cells on substrates with different stiffness (gray), cells on a glass substrate but with different available spread area (blue), and a dynamically spreading cell (red) (from (Guo et al. 2017)*).*

(b): Cell volume of 3T3 cells plotted as a function of the projected area for different experimental conditions (from (Xie, Yang, and Jiang 2018)*)*

ATP depletion, which is supposed to inhibit active ion transport, chloride channel inhibition and inhibition of myosin by Blebbistatin treatment prevented cells from volume loss at the level of a population (Guo et al. 2017). A second study showed that inhibition of Na^+/H^+ exchanger, actin polymerization and myosin activity, decreased spreading area and increased cell volume (Fig.3.8) (Xie, Yang, and Jiang 2018).

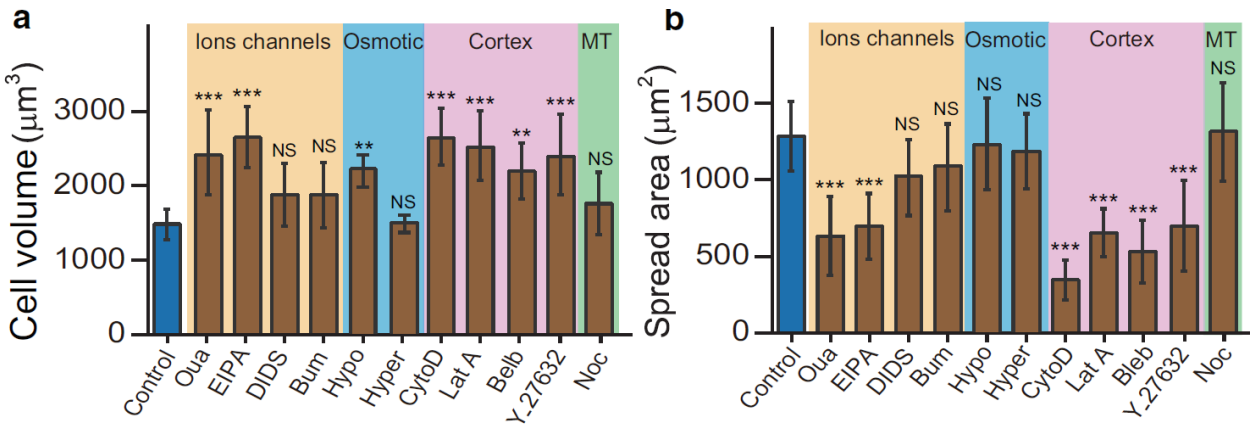

Figure 3.8: *Effect on average volume (a) and spreading area (b) of different drug treatment (from* (Xie, Yang, and Jiang 2018)*)*

Both of the studies cited above utilized 3D-confocal reconstruction for volume measurements. Using confocal reconstruction for the relatively big objects, such as suspended cell, is not easy due to the optical effects (Hell et al. 1993). Contradictory to the articles described above, a research group, that use volume measurements method based on Fluorescence exclusion (C. Cadart et al. 2017), showed that there is a positive correlation between cell volume and spreading area. This trend was obtained for three different cell lines, on the glass substrate and soft PDMS substrates (Perez Gonzalez et al. 2018). Another research group also found the positive correlation between cell volume and spreading area (Kumar and Sinha 2017).

Perhaps, nowadays, when cell volume measurements are in the zone of interest of many researchers, interpretation of the results would become as complicated as other mechanical parameter, like stiffness. First, there is a variety of methods based on different principles, and not only optical (Model 2018), although the difference between confocal and wide-field microscopy is already significant. Second, potential source of measurement error is chemical fixation as it could induce hyperosmotic shock, especially by PFA. Third, cell lines– it is well known that, for instance, HeLa cells have different phenotypes depending on the strain. Next – substrate stiffness and coating do affect cell spreading and therefore can affect cell volume. Last, drug treatment: cytoskeleton drugs, ion channels inhibitors, cell cycle synchronization can affect cell state and the ability to regulate volume.

d. Blebbing

Blebs are spherical membrane protrusions. Their appearance often correlates with high myosin activity (G. Charras and Paluch 2008). Bleb nucleation starts when there is a weak point - local rupture of the cortex (e.g. induced by local ablation) or local membrane detachment from cortex (Fig.3.9). Then hydrostatic pressure, is exerted on the cytoplasm by the cortex, which drives the fluid cytosolic flow towards the weak point, and as a result, the bleb grows. Subsequent formation of new cortical structure inside the bleb drives bleb retraction.

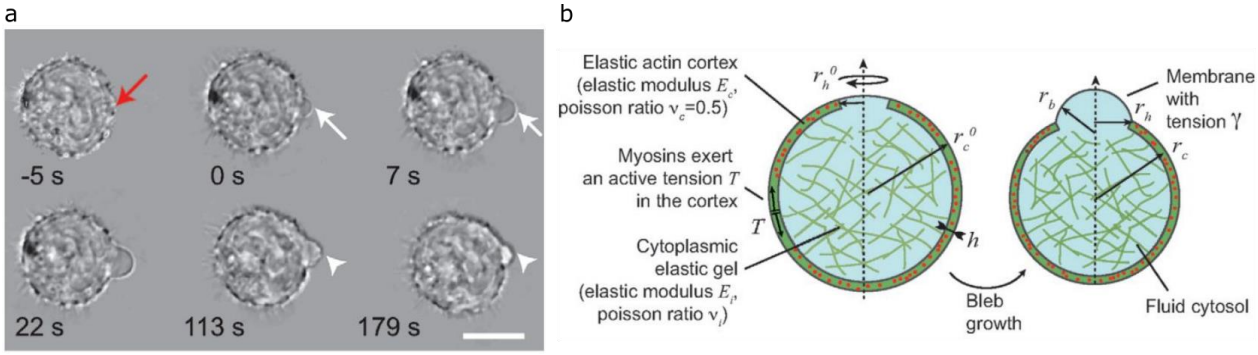

Figure 3.9: *Bleb formation (from* (Tinevez et al. 2009)*)*

(a): Laser ablation induces bleb growth that followed by retraction; (b): Elastic model of bleb growth.

Cell blebbing is an active shape fluctuation. The maximal volume of blebs, induced by laser ablation, was estimated as 6% of total cell volume (Tinevez et al. 2009). Cell volume in this study was assumed as constant.

It was proposed that bleb expansion in Zebrafish embryos is provided by aquaporin mediated water flow inside the cells and therefore leads to an increase of total cell volume, up to 10% (Taloni et al. 2015). Recently, another research group working on the same model system showed that total cell volume is conserved, and bleb expansion is just a transfer of internal cell content, but not external water uptake (Goudarzi et al. 2019).

e. Confinement

Another type of deformation that cells experience is compressive deformation by surrounding tissues. To mimic this deformation in vitro, various techniques can be used: gel on the top of the cells plated on substrate, or cells are in 3D gel; AFM with flat cantilever; confiner devices, microfabricated channels. Nature and timescale of deformation depend on the selected approach. When cells are confined by soft gel, they can deform it by exerting forces. Confinement between two stiff horizontal plates can be performed in the timescale of milliseconds or with regulated speed.

When adherent HeLa cells with the average height 6.6 µm were instantaneously confined to 5 µm (meaning that the distance between substrate glass and the top glass is 5 µm), cells were only slightly flattened (Fig.3.10) (Le Berre, Aubertin, and Piel 2012). Stronger deformation (3.5 µm confinement) induced significant cell flattening and large increase in cell surface. This increase in surface was provided by large blebs that appeared immediately after confinement due to sudden cortex extension and breakage. This was followed by bleb retraction and formation of new stable cortex in the next 5 min after confinement. Importantly, confinement deformation did not induce cell death. Moreover, confinement, especially in non-adherent environment, significantly promotes cell migration (Liu et al. 2015). However, the effect of this dramatic cell shape alteration on volume was not tested.

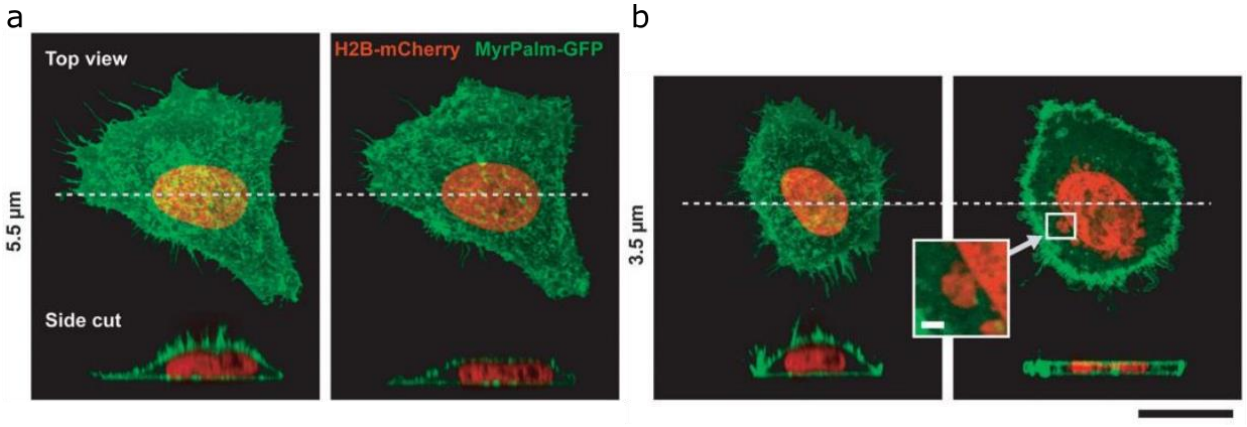

Figure 3.10: *Adherent HeLa cells before and after 5.5 µm (a) and 3.5 µm (b) confinement (from* (Le Berre, Aubertin, and Piel 2012)*)*

Left panels show the cells before confinement, right panels after confinement. 3.5 µm confinement induced nuclear blebs.

During mitosis, which last approximately 1 h, adherent cells round up and increase their volume by 30% (Zlotek-Zlotkiewicz et al. 2015). Confinement by fixed height, performed as described previously, or with polyacrylamide gel on the top of the HeLa cells prevented complete cell rounding, causing mitotic errors and delayed mitotic progression (Fig.3.11) (Lancaster et al. 2013). When cells are confined by soft 15kPa gel (mimicking tissue), forces exerted by cells are sufficient to deform the gel and partially round up. Actin cortex disruption by Cytochalasin D led to 80% of cells to have mitotic failure, inducing multipolar spindle assembly and cell death. Although actin cortex does not play a major role in mitosis of non-confined cells, it is required for compressed cells, as it enables them to sustain forces required to generate enough space for proper chromosome segregation. It is not known, if the gel compression of mitotic cells affects their volume. However, there is some evidence that compressed cells do not have mitosis-associated volume increase (Moriarty and Stroka 2018).

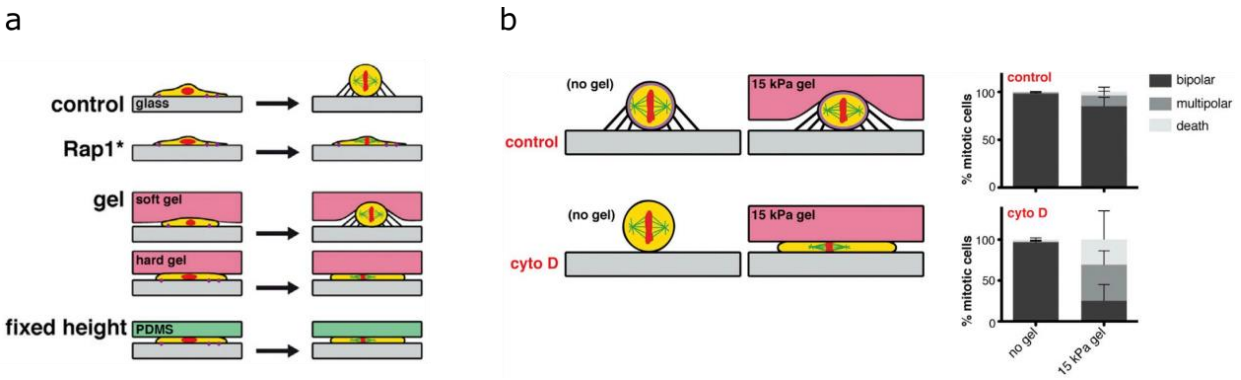

Figure 3.11: *Confinement prevents HeLa cell mitotic rounding (from* (Lancaster et al. 2013)*)*

(a): Confinement with the fixed height (<7 µm) or with polyacrylamide gel limits mitotic rounding.

(b): Actin disruption make cells unable to deform soft gel and leads to multipolar spindle assembly and cell death.

Not only the initial stiffness, but also the viscoelastic relaxation of surrounding gel was shown to be important for cell morphology at the timescale of hours (Fig.3.12). Chondrocytes encapsulated in the hydrogel with slow relaxation, were not able to expand in volume that resulted in reduced proliferation and viability (Lee et al. 2017). In contrast, in a fast relaxing hydrogel, cell volume expansion and proper cell functioning were possible.

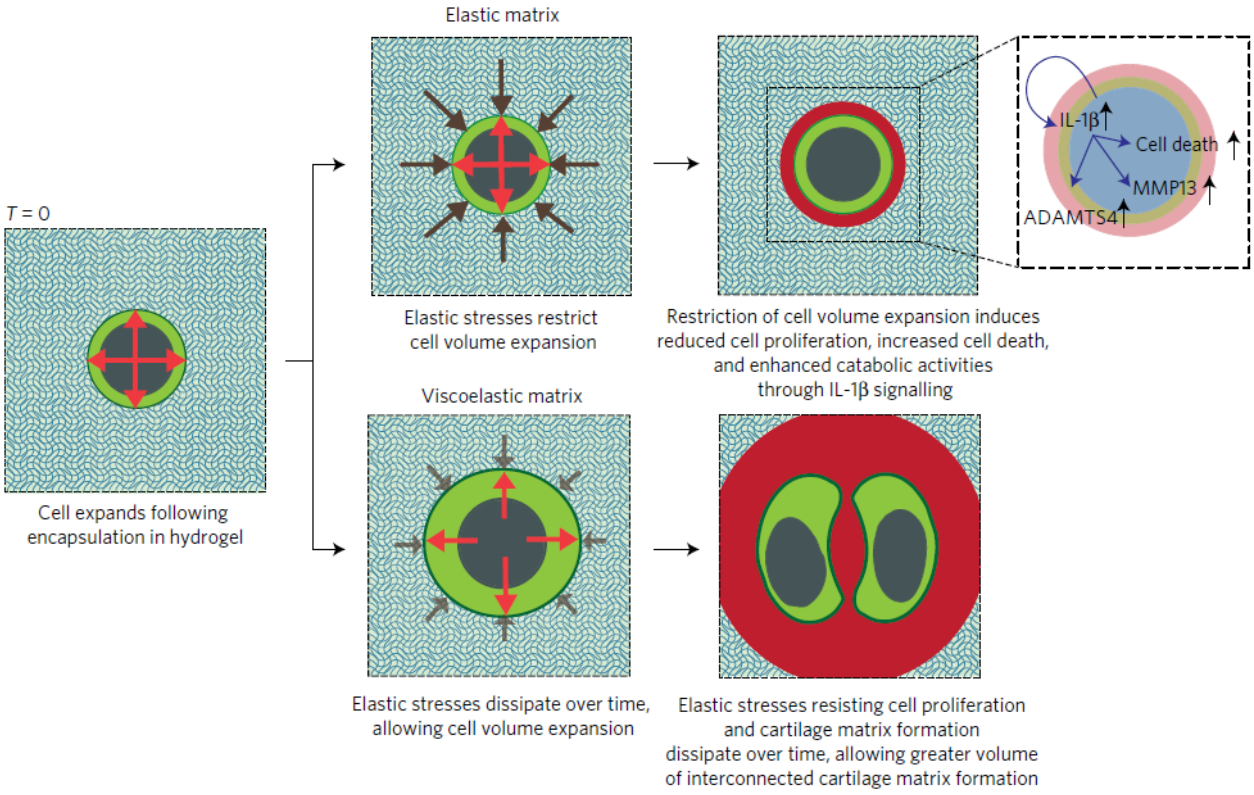

Figure 3.12: *Hydrogel stress relaxation regulates chondrocyte phenotype through restricting cell volume expansion and cartilage matrix formation (from* (Lee et al. 2017)*)*

Another mechanism of cells survival under mechanical load – Na^+ efflux through NHE1, was shown with MCF-7 under 660 Pa agarose gel (McGrail et al. 2015). Stabilization of actin filaments by Jasplakinolide treatment improved cell viability under compression and increased Na^+ efflux. On the other hand, actin depolymerization by Cytochalasin D and NHE1 inhibition by EIPA prevented Na^+ efflux and increased the percentage of dead cells. However, actin depolymerization and NHE1 inhibition did not change viability of non-compressed cells. This demonstrates that survival under confinement requires tonicity modulation.

Sudden confinement can also have an effect on cell volume. It was shown that 15% compression of cartilage extracellular matrix with the strain rate 0.005 s^{-1} induced 11% volume loss of chondrocytes (Fig.3.13) (Guilak 1995). Cytochalasin D treatment did not change volume of non-confined cells, however, confinement of treated cells led to 13% volume loss.

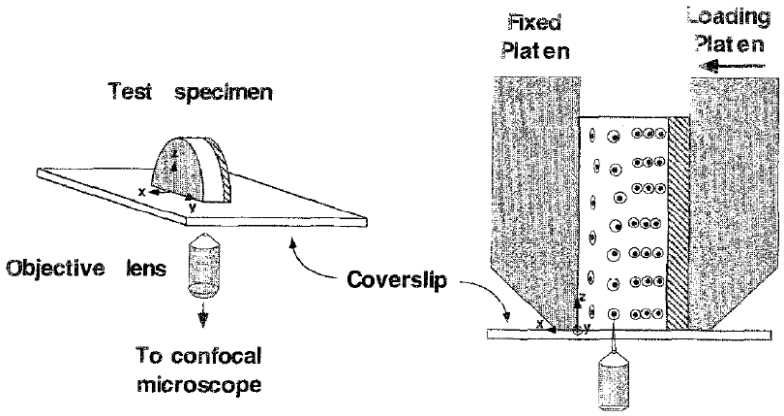

Figure 3.13: *Experimental setup for chondrocytes compression within an explant of articular cartilage (from* (Guilak 1995)*)*

Interestingly, sudden increase of hydrostatic pressure in the medium was shown to trigger Na^+ and K^+ efflux and cell volume decrease within 30 min. Pressure release was followed by volume and Na^+, K^+ concentration recovery (Hui et al. 2014).

Modeling of dynamic AFM compression with a constant indentation speed found that the indentation force strongly depends on indentation speed, especially for large deformations (Jiang and Sun 2013). When the speed is in the same range as the speed of water transport, cortical stress increases. It leads to mechanosensitive ion channel activation and water efflux. Thus, cell volume decreases and the indentation force is small. In contrast, if the indentation is faster (>1 μm/s) than the ion and water transport, those fluxes are negligible and the cell volume does not change.

II. Methods

1. Cell culture and drug treatment

HeLa EMBL, HeLa LifeAct-mcherry, HeLa-MYH9-GFP-LifeAct-mcherry, HeLa Myrpalm-GFP-Lifeact-mcherry and RPE-1 cells were maintained in Dulbecco's Modified Eagle Medium with nutrient mixture Glutamax (DMEM/Glutamax; GIBCO) supplemented with 10% (v/v) FBS (Life Technologies) and 1% 100× penicillin-streptomycin solution (Life Technologies), and stored at 37 °C and 5% CO_2.

Fresh red blood cells (RBCs) were taken from healthy donor and resuspended in PBS + 1% BSA. To preswell RBCs 50% of H2O was added to suspension before confinement.

Bone marrow derived dendritic cells (DCs) were obtain by differentiation of bone morrow precursors for 10 days in DCs medium (IMDM-Glutamax, FCS 10%, pen-strep 100 U ml−1, and 2-ME 50 µM) supplemented with granulocyte-macrophage colony stimulating factor (GM-CSF)-containing supernatant (50 ng ml^{-1}) obtained from transfected J558 cell line, as previously described (Barbier et al. 2019).

Incubation with drugs were done for suspended cells 30 min prior experiment, except Latrunculin A added right before experiment to the cells incubated 30 min in medium.

Latrunculin A (Sigma-Aldrich), CK-666 (Sigma-Aldrich), EIPA (Tocris Bioscience) were dissolved in DMSO (Sigma-Aldrich).

Y-27632 (Tocris Bioscience) (called Y-27 in the text), $GdCl_3$ (Sigma-Aldrich) were dissolved in H_2O.

CellMask (Invitrogen) staining was performed in warm PBS solution (1 µl of dye to 1000 µl PBS).

For volume measurements 10 kDa dextran conjugated with different fluorophores were used : fluorescein isothiocyanate–dextran (Sigma-Aldrich), Texas Red (ThermoFisher), Alexa Fluor 647 (ThermoFisher).

For glass coating we used bovine plasma fibronectin (Sigma-Aldrich), PLL-PEG (SuSoS) or PLL (Sigma-Aldrich).

2. Measurements of ATP depletion effect on cell viability

Cells were detached with Trypsin and resuspended with glucose free DMEM (A14430-01, Life Technologies) supplemented with dialyzed serum (Sigma-Aldrich F0392) to a final concentration of 1% (v/v). Cells were incubated 30 min prior experiment in this medium with addition of fluorescent dextran, 10 mM NaN_3 (Sigma-Aldrich) and 6 mM deoxyglucose (Sigma-Aldrich) and propidium iodide (1 µg/ml) (Sigma-Aldrich).

3. Monitoring of cell volume and contact area while spreading

Volume measurements used in the study are based on Fluorescence exclusion method (FXm) explained in details in (C. Cadart et al. 2017) and used in (Clotilde Cadart et al. 2018; Zlotek-Zlotkiewicz et al. 2015). The volume measurement were coupled with a spreading area measurement performed by Reflection Interference Reflection Microscopy (IRM) (Rädler and Sackmann 1993; Limozin and Sengupta 2009). Microscopy was performed at 37 °C with 5% CO_2 atmosphere.

a. Chambers and cell preparation

The typical height of PDMS chambers was 21.2 µm.

Chambers were incubated with 50 µg/ml fibronectin (Sigma-Aldrich) in PBS for 1 h, washed with regular culture medium and incubated overnight with medium. Cells were detached with warm EDTA (Gibco) and resuspended in medium collected from cells supplemented with 1 mg/ml fluorescent dextran (Sigma-Aldrich). Cells were incubated for 30 min in the tubes (with drugs presence if necessary) before injection into a chamber. This experimental conditions facilitate cell spreading.

In case of measurements of non-adherent cells, we used PLL-PEG coating (0.1 mg/ml solution in HEPES). Chambers were washed and incubated overnight with culture medium without FBS. Cells were detached with Trypsin and resuspended in regular medium supplemented with 1 mg/ml fluorescent dextran. Cells were incubated for 30 min in the tubes (with drugs presence if necessary) before injection into a chamber.

b. Imaging

Imaging was started immediately after cell injection into the chamber with 1 min time interval. Imaging was performed using a ZEISS Z1 Observer epi-fluorescence microscope equipped with an Orca-Flash 4 Camera (Hamamatsu) and the software Metamorph (Molecular Device). The objective 20X Plan-Apochromat objective, NA0.8 was used as a compromise between low magnification requiring for the volume measurements and high NA favorable for IRM (Fig.3.1). The filter was used according to the fluorophore conjugated with dextran. The imaging of the spreading area were made by IRM relying on the interferences that appear between the different rays reflected by the interfaces between the glass, the media and the membranes of the cell. The wavelength used for this measurement was 625 nm, which allows a correct contrast.

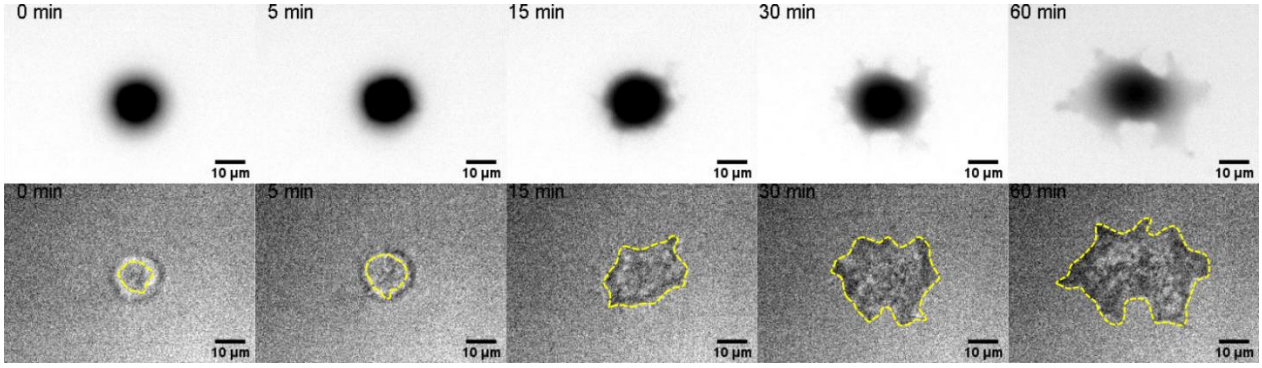

Figure 3.1*: Typical FXm (top) and RICM (bottom) images of single HeLa cell spreading*

c. Raw data extraction

The volume extraction was performed with a MatLab software (see (C. Cadart et al. 2017)).

The analysis of spreading area was performed manually using the ImageJ software. The borders of the cell are delimited manually and then the area, and different shape descriptors are extracted from the images.

d. Computation of apparent surface area

Non-adherent cells have a spherical shape. Although a lot of membrane is stored in membrane reservoirs, we can extract apparent (projected) surface S_0 of sphere with given volume V_0 obtained from cell volume

measurements. At the early stage of spreading cells have a shape of spherical cap with volume *V* and apparent surface *S* (Fig.3.2).

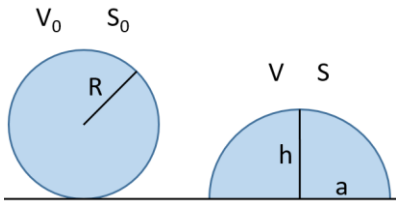

***Figure 3.2**: Scheme of sphere to spherical cap transition*

For sphere with radius R and hemisphere (a=h when contact angle is 90°):

$$V_0 = 4/3\pi R^3\ ,\ S_0 = 4\pi R^2\ ,\ V = 2/3\pi a^3\ , S = 3\pi a^2 \qquad \textit{(Eq. 11)}$$

Then increase of surface area due to transition from sphere to spherical cap with constant volume V_0=V:

$$\frac{S}{S_0} = \frac{3\pi * 2^{2/3} * R^2}{4\pi R^2} \approx 1.19 \qquad \textit{(Eq. 12)}$$

Decrease of volume when transition occur with constant surface S_0=S:

$$\frac{V}{V_0} = \frac{\frac{2}{3}\pi R^3 * (\frac{4}{3})^{3/2}}{\frac{4}{3}\pi R^3} \approx 0.77 \qquad \textit{(Eq. 13)}$$

Next we wanted to compute the surface of the spherical cap for any contact angle with given volume V measured by FXm and contact area A measured by IRM. The moments when the spreading area A is equal to the cross-section area of the cell in initial non-spread state (a=R) typically correspond to the start of protrusion formation. Therefore, for computation we used the cell spreading area that was equal or just exceeding initial cross-area of non-adherent cells and volume corresponding to this time point.

$$V = \frac{\pi h}{6}(3a^2 + h^2)\ , = \pi a^2\ , S = 2\pi a^2 + \pi h^2 \quad \textit{(Eq. 14)}$$

Thus to compute the surface we first need to compute h(V, A):

$$h^3 + 3a^2 h - \frac{6V}{\pi} = 0 \qquad \textit{(Eq. 15)}$$

Coefficients can be replaced as $p = 3a^2$ and $q = -\frac{6V}{\pi}$, then we can utilize the Cardano formula:

$$Q = (\frac{p}{3})^3 + (\frac{q}{2})^2 \qquad \textit{(Eq. 16)}$$

As Q>0 the equation has three solutions and only one of them belongs to real numbers, then:

$$h = \sqrt[3]{-\frac{q}{2} + \sqrt{Q}} + \sqrt[3]{-\frac{q}{2} - \sqrt{Q}} \quad \textit{(Eq. 17)}$$

e. Computation of spreading speed and volume flux

For HeLa cells speed of spreading $\frac{dA}{dt}$ and volume flux $\frac{dV}{dt}$ was calculated as linear slope in the first 10 min after measurable cell to substrate contact. For RPE-1 cells $\frac{dA_b}{dt_b}$ and $\frac{dV_b}{dt_b}$ were calculated as linear slopes in the 10 min (or less, if it happen early) prior time point when spreading area is equal to the cross-section area of the cell in initial non-spread state; and $\frac{dA_a}{dt_a}$ and $\frac{dV_a}{dt_a}$ in the first 10 min after that time point.

4. Cell volume measurements under confinement

We used both a static 6-well confiner (Fig.4.1) and dynamic confiner according to experimental procedure described in (Le Berre et al. 2014). Imaging was performed using a ZEISS Z1 Observer epi-fluorescence microscope equipped with an Orca-Flash 4 Camera (Hamamatsu) and the software Metamorph (Molecular Device). The objective is a 20X Long-Distance objective, with a 0.4 Numerical Aperture (NA), as low NA is required to prevent measurement variations due to relative of the focal plane to the middle of the object.

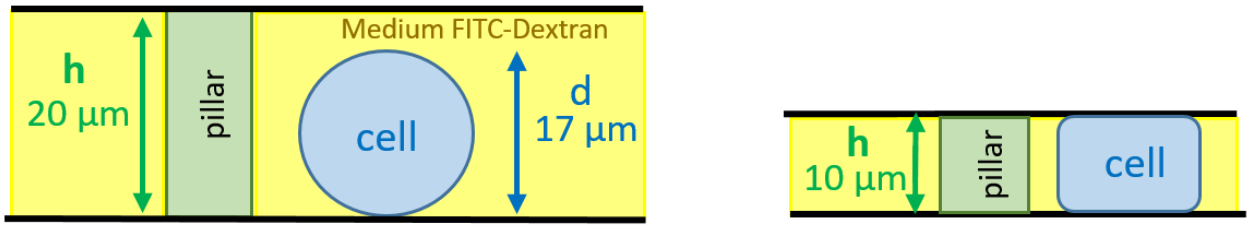

***Figure 4.1**: The principal scheme of confinement experiment. Ig height of the pillar is more than cell diameter, cells are not confined.*

a. Static 6-well confiner

As we wanted to minimize cell adhesion cells were detached with Trypsin and resuspended in the fresh medium with fluorescent dextran. ~10 µl of cell suspension were added to the glass bottom of each well.

For each 6-well plate we used at least 3 different height of the pillars in the range from 3 µm to 20 µm. 20 µm was used as a control non-confined state since the mean cell diameter is about 17 µm. That allowed us to exclude from the measurements positions where actual confinement height was different from desired. Average background intensity *I* of each fluorescent image with substraction of camera offset was plotted as a function of the pillars height *h* for each experiment (Fig.4.2). Images with background intensity significantly deviating from the linear slope α were excluded from further analysis. Alternatively actual height can be extracted as $h = I/\alpha$ (C. Cadart et al. 2017).

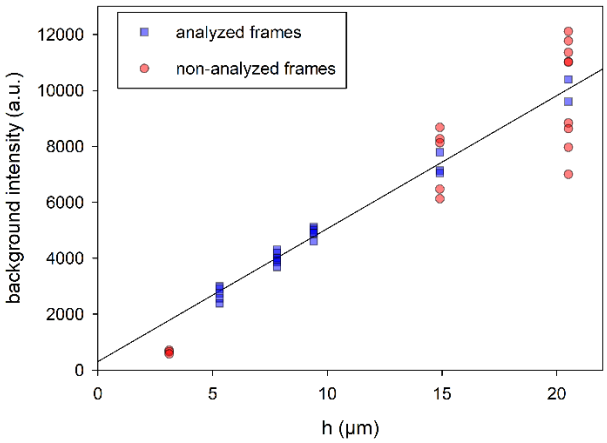

Figure 4.2*: Example of experiment where 6 different pillar heights were used: average background intensity for each position plotted versus known pillars height. Blue squares indicate positions that were used for further volume analysis, red circles indicate positions excluded from analysis.*

The volume extraction was performed with a MatLab software (see (C. Cadart et al. 2017)).

The apparent surface of confined cells was computed as $S = 2\pi rh + 2\pi r^2$, the radius r was extracted from measured volume $V = \pi r^2 h$.

b. Dynamic confiner

The dynamic confiner allows following the same cells before and after confinement. Non-adherent cells tend to escape the field of view once confined as they are pushed by liquid fluxes. To avoid cell escape we coated the bottom glass with PLL – cells were stick to the glass.

FXm requires cells to be under the roof with a constant height. The dynamic confiner normally used in our lab does not allow access to the distance between bottom glass and roof when confinement is not completed, when confinement is completed this distance should be equal to the pillars height (similar with the static confiner). However, when the applied pressure is large, actual distance can become smaller due to PDMS compression. To overcome these issues we made a new confiner setup that additionally contains small reference pillars (2 µm) that allowed actual height calculations before and after confinement (Fig.4.3).

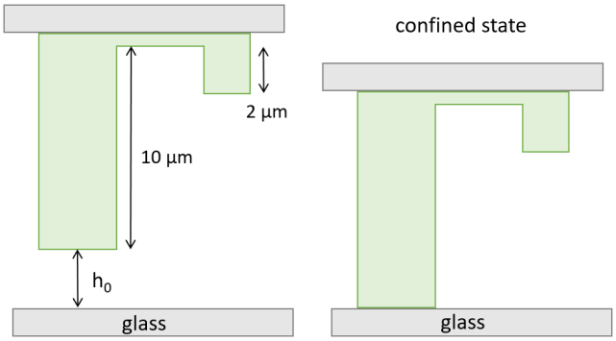

Figure 4.3*: The principal scheme of experiment with dynamic confiner, dimensions are not shown in scale. Left – before confinement, right – after confinement.*

We know the actual volume of small pillars V from they geometry. Then for both non-confined and confined states we can compute α through integrated density (sum of pixel values) of small pillars $IntDen_{sp}$ and background $IntDen_b$:

$$\alpha = \frac{IntDen_b - IntDen_{sp}}{V} \qquad \textit{(Eq. 18)}$$

The actual height then is calculated with α and the mean intensities of background I_b and the mean intensity under the big pillar in the confined state I_{bp}, which provides an actual offset:

$$h = \frac{I_b - I_{bp}}{\alpha} \qquad \textit{(Eq. 19)}$$

5. Micropatterning

Cells were patterned using the existed technique (Thery 2010). Glass coverslips were sonicated and washed in ethanol for 10 min. Following drying, the glasses were activated by plasma and incubated in 0.1mg/mL PLL-PEG diluted in 10mM HEPES buffer (pH = 7.4) for 1 h. Afterwards, chromium synthetic quartz photomasks (Toppan Photomasks Inc.) designed with the desired patterns were washed with ethanol, dried and activated with UV during 5 min. Then the glass were placed on the mask using a drop of milliQ water (typically 5µL, in order to allow a close contact between the glass and the mask). The coated glass and the mask were exposed to a UV lamp for 5 minutes. This step "burns**"** the PLL-PEG on the site of the pattern. The glasses, after being washed with milliQ water and dried, were incubated during 30 min with fibronectin (Sigma-Aldrich) and 5 µl/ml fibrinogen conjugated with Alexa 647 Fluor solution, diluted in PBS. Then the glasses were and dried. Then the glasses were sticked on 6-well plate with 20mm holes in the bottom (MatTek Corporation), using a silicone bio-compatible glue.

One the next day, cells were detached with warm EDTA and resuspended in medium collected from cells. Cell suspension was injected in the 6-well plate with micropatterns and incubated at 37 °C and 5% CO_2. When cells started to adhere, the culture medium was gently replaced in order to remove the excess of cells and avoid crowding on the patterns. Then cells were incubated for 4h that allowed them to spread on the micropatterns.

Volume measurements were performed with 6-well confiner device, which will as described before.

6. Cell volume measurements of dendritic cells (DCs) in collagen gel

Collagen mix (should be prepared on ice to delay polymerization):

1) 25 µl 10X PBS

2) 25 µl medium

3) 55 µl collagen

4) 140 µl medium with DCs ($2*10^6$/ml) + 5 µl FITC-dextran

5) 1.3 µl NaOH

Immediately after mixing suspension was added into PDMS-chamber for volume measurements with height 12 µm. Microscopy was started ~10 min after injection. Imaging was performed using a ZEISS Z1 Observer epi-fluorescence microscope.

7. Cell volume measurements during osmotic shock

Cells were detached with Trypsin and resuspended with isoosmotic medium supplemented with fluorescent dextran. Chambers were coated with PLL, this prevented cell detachment during changing medium, cell also were staying round during experiment.

Microscopy was started a few minutes after cells injection, when flow was equilibrated. Acquisition was performed with time frame 30 s. Isoosmotic medium was exchanged to the medium with the desired osmolarity typically 2.5 min after beginning of acquisition. Full medium exchange in the chamber takes 2.1 s. Imaging was performed using a ZEISS Z1 Observer epi-fluorescence microscope 20X NA0.4.

Osmolarity of working solutions was measured by an osmometer Type 15M (Löser Messtechnik).

8. Side-view microscopy

The glass slide was attached to the glass bottom dish by UV-glue, the position of glass was slightly tilted from perpendicular to the dish bottom (Fig.8.1). Glass was coated with fibronectin and washed with medium. Cells were detached with EDTA and resuspended in warm medium collected from cells and incubated 30 min. Then a drop of cells was added to the dish, close to the angle between dish bottom and attached glass. Dish was placed to the incubator for 2 minutes to allow cell initial attachment to the tilted glass. Then 2 ml of medium collected from cells were added to the dish and microscopy started with time frame 1 min. Imaging was performed using a ZEISS Z1 Observer epi-fluorescence microscope 20X NA0.4.

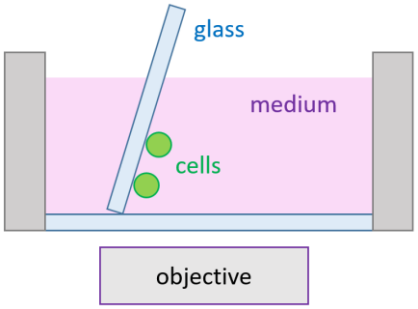

***Figure 8.1**: The principal scheme of experiment.*

9. Spinning disk microscopy

Qualitative imaging for osmotic shock and confinement experiments was performed with spinning disk set-up (Leica DMi8). 63X and 100X oil objectives were used.

10. Mass measurements

Mass measurements using Phasics camera require an objective without a phase ring (higher magnification gives lesser error but to combine with volume measurements, 20X Sflour objective was used). After the experiment is finished the reference image should be recorded. The reference can be recorded by trypsinising and flushing the cells very gently, without moving the stage, and taking images of all the stage positions. On the other hand, it can be quite challenging to remove the cells completely. In that case, the reference image can be acquired by taking 32 images by moving the stage very quickly (every 1 second).

We obtain interferograms from the the phasics camera. The camera itself contains a 2-D diffraction grating (modified Hartmann mask), which is placed before the sensor to replicate the incident wavefront. In this case, four identical replicas are created and two gradients along two perpendicular directions are measured and integrated to determine the field intensity and phase.

The measured wavefront is equal to the optical path difference (OPD) which is defined as:

$$OPD(x,y) = \int_0^h (n(x,y) - n_{medium})dz \qquad \textit{(Eq. 20)}$$

Where n is the local sample refractive index, n_{medium} is the surrounding medium refractive index, z is the coordinate along the optical axis and h is the thickness of the sample.The measured OPD is the OPD induced by sample and the medium and hence we also calculate the OPD without the sample, and subtract from the total OPD to measure the OPD contributed by the sample alone.The OPD is integrated all over the sample and expressed as the unit of volume, OVD (optical volume difference). This is linked to the dry mass by multiplying it with a specific refractive increment. For mammalian cells, this is 0.18 μm^3/pg. Image analysis was done with custom Matlab code.

III. Results

The cell volume is a vitally essential parameter as it plays a very important role in various biological processes like genetic expression (Burg and Garcia-Perez 1992), molecular crowding (Klumpp et al. 2013), protein interactions (Sukenik, Ren, and Gruebele 2017), stem cells differentiation (Lee, Stowers, and Chaudhuri 2019) and can be deregulated in different pathological conditions including cancer (Stine F Pedersen et al. 2013). However, mammalian cell volume regulation is still a poorly investigated field. Volume regulation of animal cells was mostly studied in the context of osmotic shock (Hoffmann, Lambert, and Pedersen 2009) at the level of cell population due to the complexity of precise single live cell volume measurements. The poor precision of existing techniques also limited investigation of long timescale process like cell cycle (timescale of hours) in mammalian cells and made the field debated (Ginzberg, Kafri, and Kirschner 2015).

Due to the complexity of volume measurements with high temporal resolution or the low throughput cell volume was commonly accepted as a constant parameter at the timescale of mechanical deformations as spreading on substratum (Cuvelier et al. 2007) or AFM compression (Harris and Charras 2011). Only recently experimental studies showed that cells lose volume with cell spreading area increase (Guo et al. 2017; Xie, Yang, and Jiang 2018), another work showed the opposite result (Perez Gonzalez et al. 2018); one theoretical work also predicted cell volume loss in response to slow AFM compression (Jiang and Sun 2013).

To study cell volume regulation at the different timescales we develop the technique based on fluorescence exclusion (FXm) (C. Cadart et al. 2017) originally proposed in 2011 (Bottier et al. 2011). This method allowed our lab to study cell volume regulation in the context of mitosis (Zlotek-Zlotkiewicz et al. 2015) and cell cycle (Clotilde Cadart et al. 2018).

In this project, we wanted to study cell volume regulation in response to mechanical deformations. We decided to focus on cell spreading on adhesive substrate and fast compression between two horizontal plates.

We found that cell volume does not primarily depend on the size of spreading area as was proposed in the previous studies. Instead, we showed that there is a complex cell volume modulation during cell spreading: cells decrease, do not change or increase volume. The regime of cell volume modulation is defined by the kinetics of spreading deformation – fast spreading induces water and/or ions loss while dry mass remains

constant; and the state of the acto-myosin cortex. Fast compression independent of adhesion also induced volume loss that can be prevented by depolymerization of the actin cortex, which was consistent with our observation for cell spreading. Additionally, we addressed a question of membrane to water permeability in the context of cell shape deformations, and used osmotic shock technique. We found that although, at the level of population, cells respond to osmotic shock as it was described in classical studies, there is a large diversity at the level of single cells.

1. Dynamic cell spreading

a. HeLa cells lose 5% of volume on average while spreading

When a liquid drop is placed on a wetting solid surface it spreads at constant volume. The contact area increases until equilibrium contact angle given by the Young's law is reached (Bonn et al. 2009). Similarly, sticky GUVs spread on a substrate until an equilibrium state defined by the adhesion energy and the membrane tension is reached (Cuvelier and Nassoy 2004). Notably, if a sticky GUV with aquaporin incorporated in the bilayer at the steady-state is exposed to hyperosmotic shock, the volume decrease will lead to consequent free membrane release and trigger further spreading (Berthaud et al. 2016). Contrary to GUVs, cells have a lot of free membrane stored in membrane reservoirs and various types of folds and protrusions (Guilak, Erickson, and Ting-Beall 2002; Ping Ting-Beall, Needham, and Hochmuth 1993). It is known that cells increase their membrane surface area while spreading on a substrate, by flattening of membrane folds and addition of new membrane (Gauthier et al. 2009). Despite all these membrane reservoirs and despite the viscoelastic nature of the acto-myosin cortex, cell extension is limited by membrane tension (Raucher and Sheetz 2000). Because cortical and/or membrane tension are known to activate ion transport (Lumpkin and Caterina 2007) and mechanosensitive channels play a role in volume regulation (Hua et al. 2010), we decided to measure the cell volume during spreading and ask whether cells rather extend their surface area or modulate their volume when they change shape due to adhesion on a flat substrate. We started with HeLa cells, and we then studied a second cell type in details (RPE1, see section **e** below).

Suspended HeLa cells were injected into a volume measurement chambers with glass bottom coated with fibronectin to promote spreading, or passivated by PLL-PEG that would prevent adhesion, and spreading (the detailed experimental procedure is described in Material and methods). Cells started to adhere as soon as flow in the chamber was equilibrated. Therefore, we followed the cell volume by Fluorescence exclusion method (FXm, (C. Cadart et al. 2017)) and spreading area by interference reflection microscopy (IRM, (Limozin and Sengupta 2009)) with a frame rate of 1 min immediately after flow equilibration in the chamber. We used an air 20X objective NA0.8. As we wanted to measure volume and spreading area of the same cells, this objective was a best compromise for the two methods (FXm is best at lower magnification and small aperture and IRM is best at high magnification and high aperture). The volume of individual cells was normalized by the volume at the first time point, then the volume of all the cells in the experiment was averaged for each time point.

On passivated glass (PLL-PEG), cells did not spread and the volume increased at a rate close to the regular growth rate (~5%/h) (Fig. 1.1a). On a fibronectin-coated glass, cells were spreading with a linear increase of the contact area (Fig. 1.1b,c) as was previously described (Cuvelier et al. 2007). We obtained that cells in average lost ~4% of volume during spreading (Fig. 1.1a) on fibronectin-coated glass in the first 10-20 min after injection. Taken together these data demonstrate that cell spreading induced a small but significant volume loss. A similar qualitative trend was recently observed by two research groups (Guo et al. 2017; Xie, Yang, and Jiang 2018), however, in their case cells lost 25% or 40% of volume on average. The difference could be explained by the experimental procedure. In the studies cited above cells were synchronized by starvation in serum-free medium or chemically that block cell growth. In our experiments, we used medium supplemented with serum and after initial volume loss cells started to increase volume with the speed similar to the speed of volume growth during cell cycle (~5%/h).

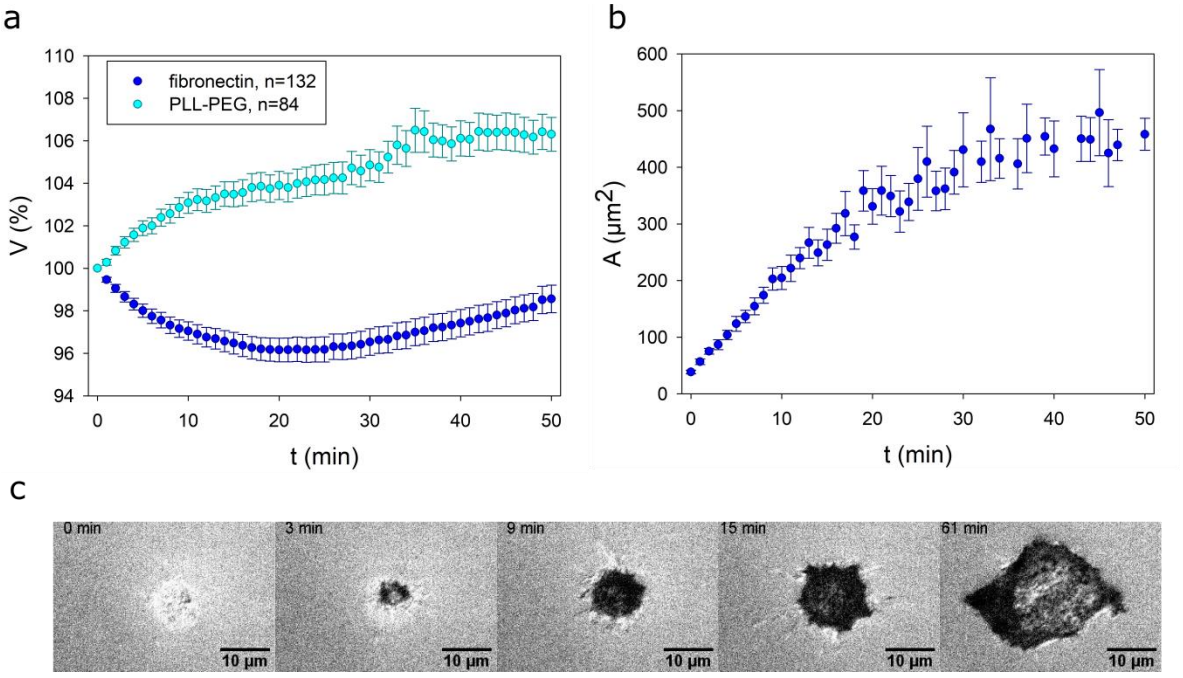

Figure 1.1 *Average HeLa volume and contact area during cell spreading of a typical experiment.*

(a): Average normalized volume of cell population plated on a substrate with different coating – fibronectin (blue), PLL-PEG (cyan). Error bars represent standard error.

(b): Averaged spreading area of cells plated on fibronectin-coated glass during spreading. Error bars represent standard error.

(c): Typical IRM images of spreading dynamic of individual cell placed on fibronectin-coated glass performed with 63X objective.

Additionally, we performed quantitative phase imaging (Aknoun et al. 2015) combined with FXm and showed that in the first 20 min of spreading cell dry mass remains constant while volume decreases (Fig. 1.2). These data indicate that volume loss is driven mainly by ion/water efflux and not by a loss of dry mass. Interestingly, during volume decrease, mass remains constant, but as volume starts to increase again, mass also resumes growth at the expected rate. This observation suggests that mass growth rate could be coupled to either volume increase or to cell density, an hypothesis often formulated (C Cadart et al. 2019) but never verified experimentally in mammalian cells. This relates to another project, which will not be detailed further here.

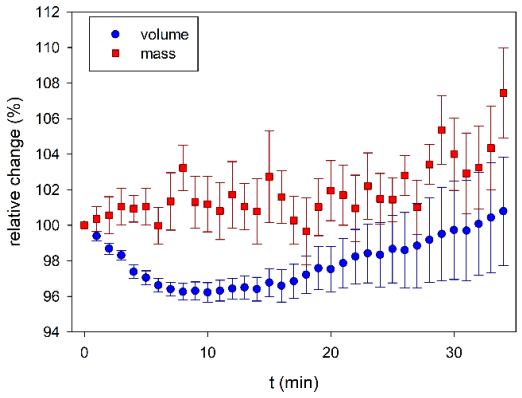

Figure 1.2 *Average cell volume (blue) and dry mass (red) during cell spreading. In the first 10 min of spreading cells lost ~4% of volume on average, while dry mass remained constant. n=17, error bars represent standard error.*

b. Diversity in single cell behavior. Fast spreading induces fast volume loss

Although in average HeLa cells lose 5% of volume while spreading, we noticed that at the single cell level volume dynamic is very diverse (Fig. 1.3). During spreading cells can lose more or less volume (Fig. 1.4a), or even do not change or increase their volume (~15% of cells).

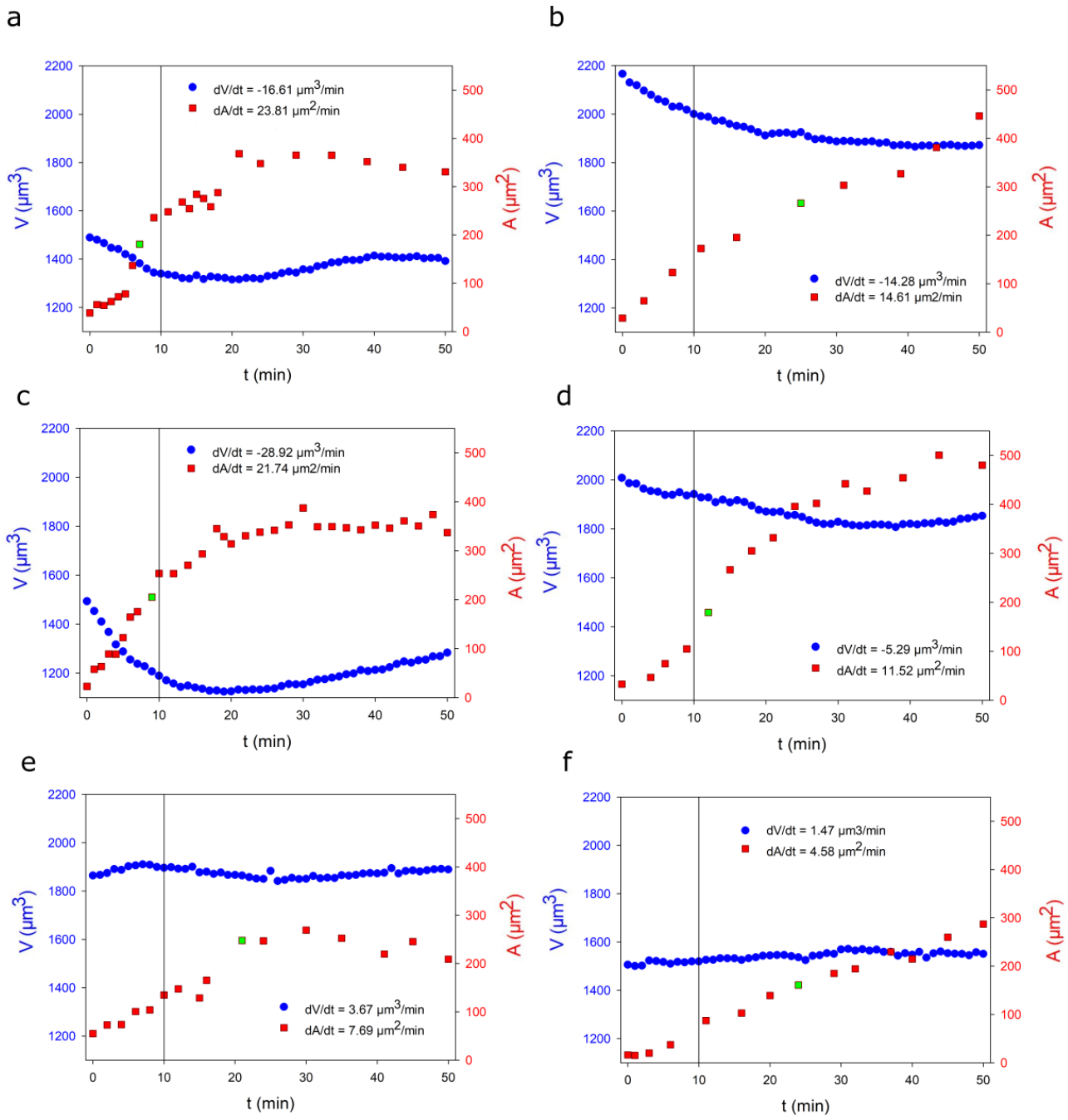

Figure 1.3 *Examples of individual cells spreading on fibronectin-coated glass. Volume (blue), spreading area (red/green), from the beginning of spreading, green points indicate spreading area equal to initial spherical cell cross-section.* $\frac{dA}{dt}$ *and* $\frac{dV}{dt}$ *are values of linear slopes fitted for the first 10 min of spreading. Cells lose volume (a-d) or do not change/increase volume (e,f) while spreading area increases.*

In order to be quantitative and understand what drives volume loss during cell spreading we first described parameters related to the time points when cells reached minimal volume. 45% of the cells reach minimal volume in the first 25 min of spreading (Fig. 1.4a) and maximal volume loss (in %) does not depend on the initial size of the cell, correlation coefficient R=0.07 (Fig. 1.4b). As cell volume increases with cell cycle progression, we also concluded that the volume loss (in %) was independent of the cell cycle stage. We also noticed that there was a correlation R=0.54 between the maximal volume loss and spreading area reached by this moment (Fig. 1.4c). These results suggest that the more cells spread, the more volume they lose, meaning that large change of cell shape induces large volume loss. However, spreading area itself, although an obvious parameter, is not enough to explain volume loss at the single cell level (Fig. 1.3e,f).

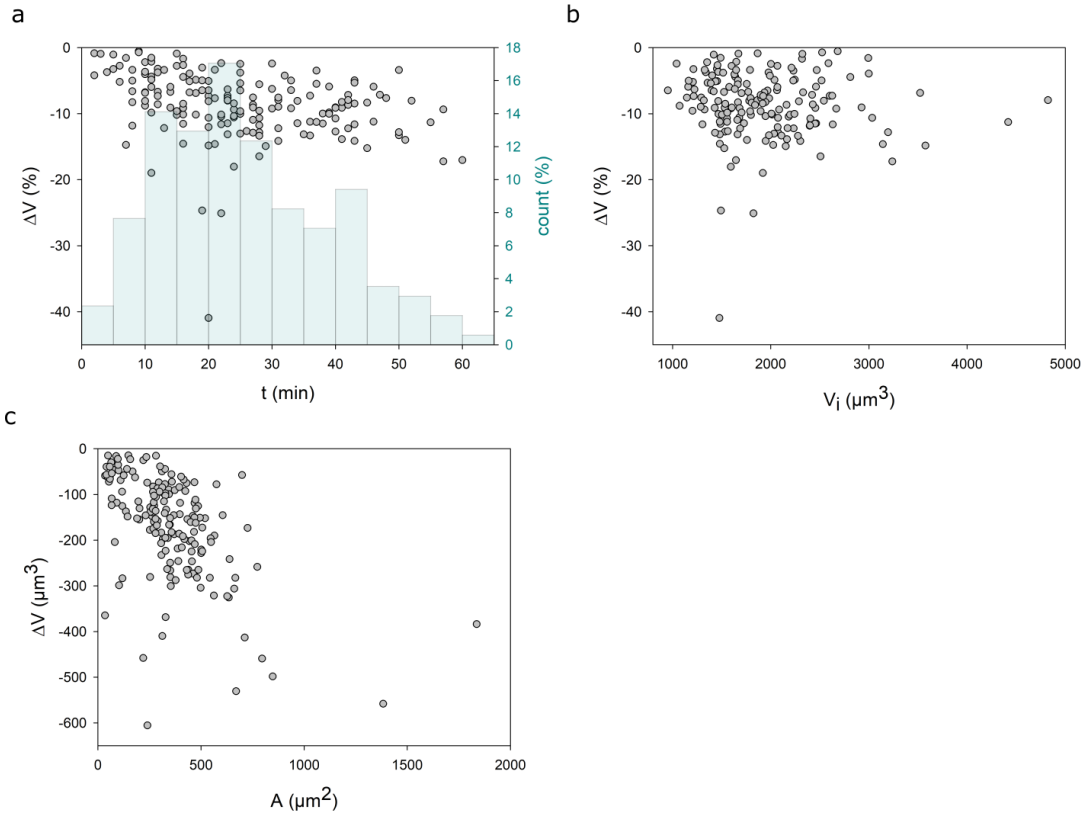

Figure 1.4 *Relation between maximal values of volume loss and initial volume (a), time of maximal volume loss (b), spreading area, reached by this time (c).*

(a): Relative volume change respected to the minimal volume values that cells reach plotted versus corresponding time points. Histogram shows count of cells reached the minimal volume at the given time interval.

(b): Relative maximal volume loss plotted as a function of initial absolute volume, n=170.

(c): Relative maximal volume loss plotted as a function of spreading area reached by that moment.

To get a better understanding of volume versus surface area dynamics, we estimated the total surface area of the cell in the initial stages of spreading. It was shown (Frisch and Thoumine 2002) and confirmed with our own data (Fig. 1.5a) that at the early stage of spreading cell shape can be described as a spherical cap. There are two extreme cases of a sphere to a spherical cap transition with a contact angle of cells with a surface equal to 90° (Fig. 1.5b):

1) with constant volume $V_t - V_0 = 0$ with projected surface increase $S_t - S_0 = 19\%$ (liquid drop model)

2) with constant projected surface $S_t - S_0 = 0$ with volume decrease $V_t - V_0 = -23\%$

The moments when spreading area is equal to cross-section area of cell in initial non-spread state typically correspond to the start of protrusion formation. The example is shown in Fig. 1.1c at the time 9 min from the beginning of spreading. Typically this transition occurs in the first 20 min of spreading (Fig. 1.3, green points), and with known volume and spreading area, we thus had access to the projected surface area by basic geometrical calculations. We obtained that individual cells can either lose volume without surface increase or extend surface without volume loss and the values of surface extension/volume loss are close to the theoretical ones (Fig. 1.5c). However, most of the cells display an intermediate phenotype and they both lose some volume and increase their surface area during the initial stages of spreading. Here we can speculate that in such short timescale cells operate with constant available membrane (without new membrane insertion). Because initial spreading can induce transient cortical tension increase (Pietuch and Janshoff 2013), volume loss could be the result of activation of ion channels/pumps while increased surface area would result from the opening/unfolding of membrane reservoirs (Fig. 1.5d). We thus draw a simple working model to guide the next steps of our study: spreading dynamics, which results from the combined effects of adhesion and cytoskeleton dynamics, induces a strong cell shape change which is accommodated thanks to a balance between volume regulatory decrease induced by surface/membrane tension activated ion channels and pumps and the opening/unfolding/detachment of cortex bound plasma membrane.

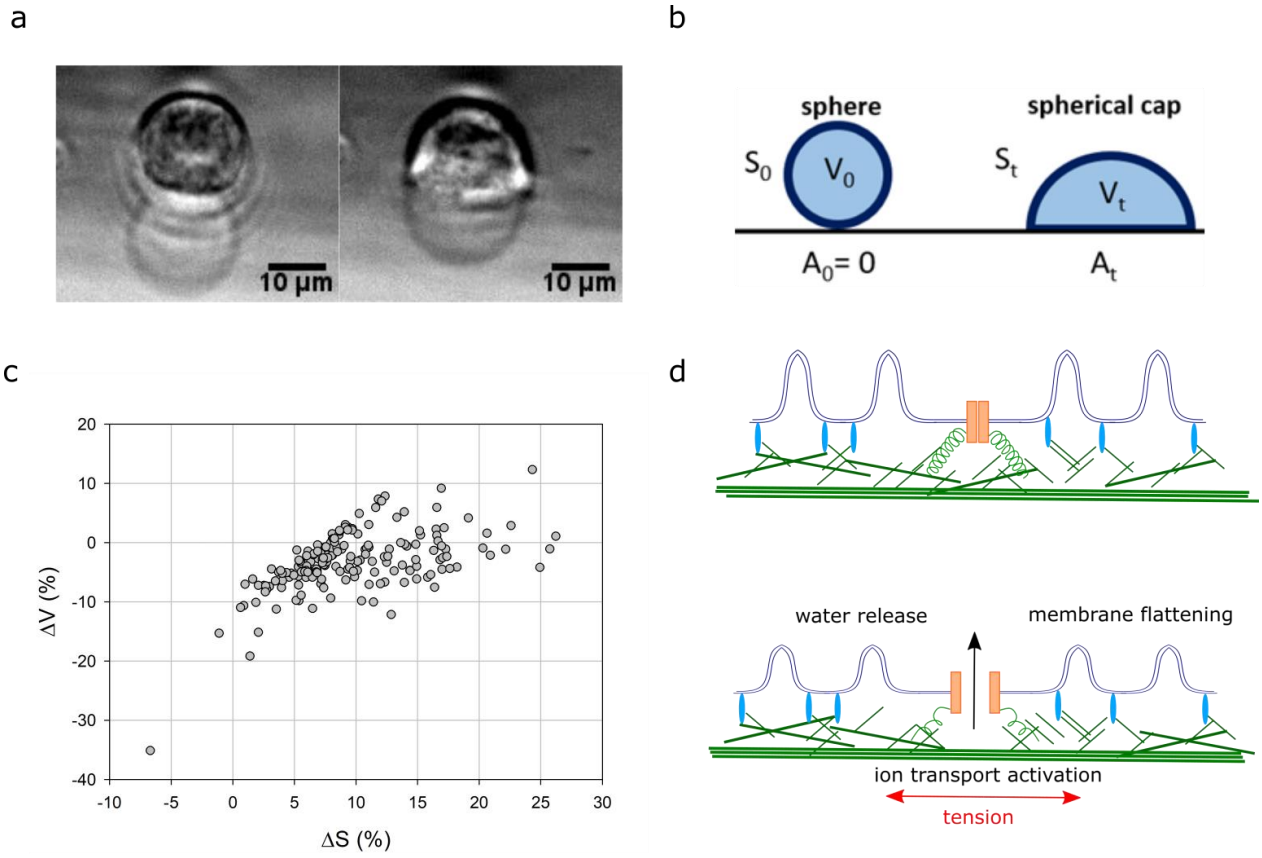

Figure 1.5 *Cell volume and projected surface area during a sphere to a spherical cap transition.*

Transmitted light image of cell spreading viewed from the side (a) and schematic representation (b) of a sphere to a spherical cap transition while spreading.

(c): Volume-surface balance for individual cells, n=189.

(d): Schematic representation of a hypothetical model of volume loss induced by spreading deformation. Folded membrane (dark blue), containing ion channels (orange) attached to the actin cortex (green) by ERM-proteins (light blue). Deformation associated to spreading induces transient tension increase in the acto-myosin cortex and consequent membrane stretching, that both activate mechanosensitive channels, also potentially involving specialised structures like caveolae (Sinha et al. 2011). This results in both osmotically driven volume decrease and membane extension by flattening of the folds.

We noticed that not only volume dynamics, but also spreading dynamics varies from cell to cell – different cells can reach the same final area but spread at different speeds. If, as hypothesized in our working model, membrane/surface tension plays an important role in volume modulation, then the kinetics of spreading should be a crucial parameter. A slow enough spreading, thanks to the dynamics of acto-myosin and plasma membrane turnover, relaxing membrane/surface tension, could potentially occur without any substantial tension increase.

To quantify a link between spreading speed and volume modulation, we measured two parameters: spreading speed $\frac{dA}{dt}$ (μm^2/min) and volume flux $\frac{dV}{dt}$ (μm^3/min; when $\frac{dV}{dt} > 0$ cell increases volume, when $\frac{dV}{dt} < 0$ cell loses volume) that can be simply fitted with a linear model at 10 min time intervals (Fig. 1.6a). We analyzed $\frac{dA}{dt}$ and $\frac{dV}{dt}$ for each interval within 1 h of spreading (Fig. 1.6b). Volume and area of individual cells were fitted with linear slopes at the 10 min time intervals and then the average value of $\frac{dV}{dt}$ for each intervals was plotted as a function of average $\frac{dA}{dt}$. We obtained that $\frac{dA}{dt}$ progressively decreases (on average) that and after the first 30 min of spreading $\frac{dV}{dt}$ mostly has values close to zero and slightly positive – cells continue to spread with low speed and without volume loss and resume growth. Therefore, for the further analysis of $\frac{dA}{dt}$ and $\frac{dV}{dt}$ we decided to focus on the first 10 min of spreading as it refers to the faster phase of deformation.

At the first 10 min of spreading, on average, the speed of spreading is proportional to the speed of volume flux: the faster cells spread the faster they lose volume (Fig. 1.6c). The data also showed below a certain spreading speed (~10 μm^2/min), there is no significant volume loss on average and the volume flux is close to zero on average. The average behavior of cells is thus consistent with our working model, but still shows a large dispersion at the single cell level. This could be due to the need for a more refined analysis of the single cell curves, because cells can display transient phases of fast spreading at different times in the first hour of spreading. It could also come from other sources of cell-to-cell variability, such as the cell cycle stage or the state of the cell cortex or the type of protrusions formed during cell spreading. To further test our working model, we thus decided to affect the main players of the cytoskeleton dynamics.

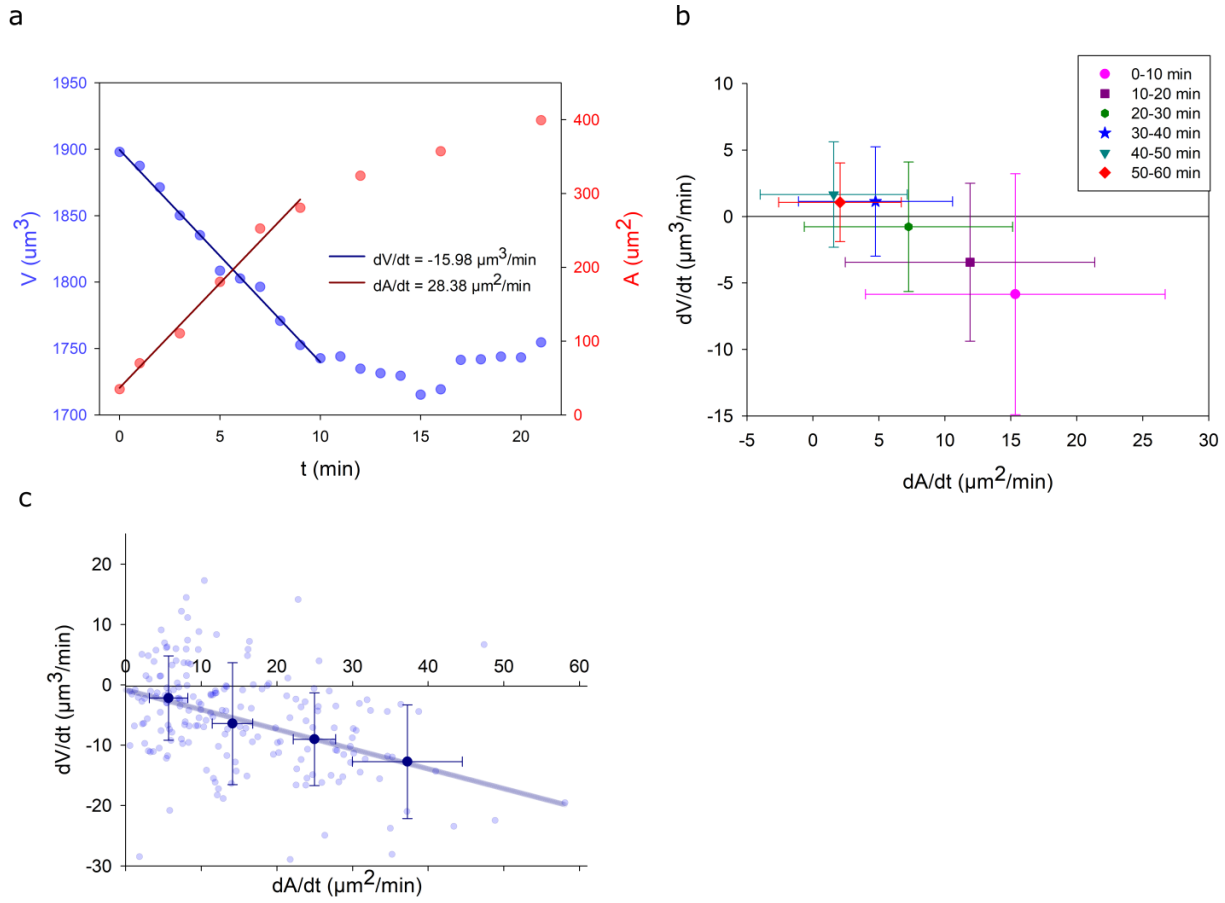

Figure 1.6 *Speed of spreading and speed of water flux.*

(a): Example of $\frac{dA}{dt}$ and $\frac{dV}{dt}$ *calculation for individual cell (linear slope).*

(c): Individual points (light blue) shows the speed of volume flux plotted as a function of spreading speed for individual cells, n=195. Dark blue points show median values of $\frac{dV}{dt}$ *for the different* $\frac{dA}{dt}$ *intervals. Median values fitted with linear slope, R=-0.98. Error bars represent standard deviation.*

(b): Average value of $\frac{dV}{dt}$ *for each intervals was plotted as a function of average* $\frac{dA}{dt}$*. n=195, Error bars represent standard deviation.*

c. Effect of cytoskeleton perturbations and modulation of ion transport activity

Cytoskeleton rearrangements play a major role in cell spreading: actin polymerization drives spreading and myosin activity resist to it (Wakatsuki 2003). For example, we observed homogeneous actin distribution for suspended cells and during spreading actin was accumulating close to the contact area

(Fig. 1.7). Thus, to further check our hypothesis that the speed of spreading deformation regulate volume loss while spreading, we decided to modulate the speed of spreading on fibronectin-coated glass by acto-myosin cytoskeleton perturbations: actin depolymerization, inhibition of Arp2/3, inhibition of contractility.

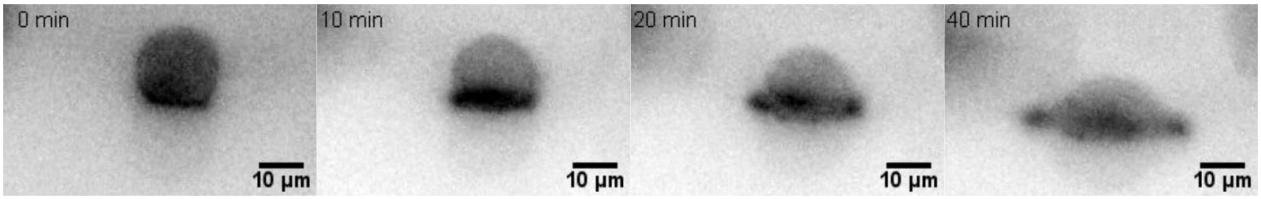

Figure 1.7 *LifeAct distribution (black) in spreading cell at different time points, side-view. Before spreading (time zero), actin is distributed homegenously on the cell surface. After initial spreading, actine accumulates at the contact area (10 min).*

- Inhibition of actin polymerization

Although the early stage of spreading was shown to be passive (Cuvelier et al. 2007), later stages of spreading, including lamellipodia formation, require actin polymerization. Therefore, we decided to check the effect of actin disruption by Latrunculin A (Lat) treatment on average volume dynamics during spreading. Cells treated with a high dose of Lat (2 µM) were blebbing without spreading and, similarly to cells platted on PEG substrates (non-adhesive), did not exhibit loss of volume, but rather an increase, in the first 30min after platting (Fig. 1.8a). On longer timescales, treated cells lost volume, without spreading, which could be due to the known long term effect of Lat on cell growth(Spector et al. 1989).

Cells treated with a low dose of Lat (100 nM) were also blebbing, and spread at a slower speed than control cells. They lost only 2% of volume on average (Fig. 1.8a,b). Analysis of individual trajectories showed that 27% of cells did not lose volume while spreading (more than control cells, 15%). Further analysis showed that Lat treated cells tend to rather increase their surface area than decrease volume as they spread (Fig. 1.8c). Analysis of $\frac{dA}{dt}$ and the average spreading area showed that Lat treatment slowed down spreading (Fig. 1.8b,e), if compare with control cells. Volume flux (Fig. 1.8f) was proportional to the speed of spreading and similar to control cells that were spreading within a low range of speed (Fig. 1.8d), confirming that $\frac{dV}{dt}$ depended on $\frac{dA}{dt}$.

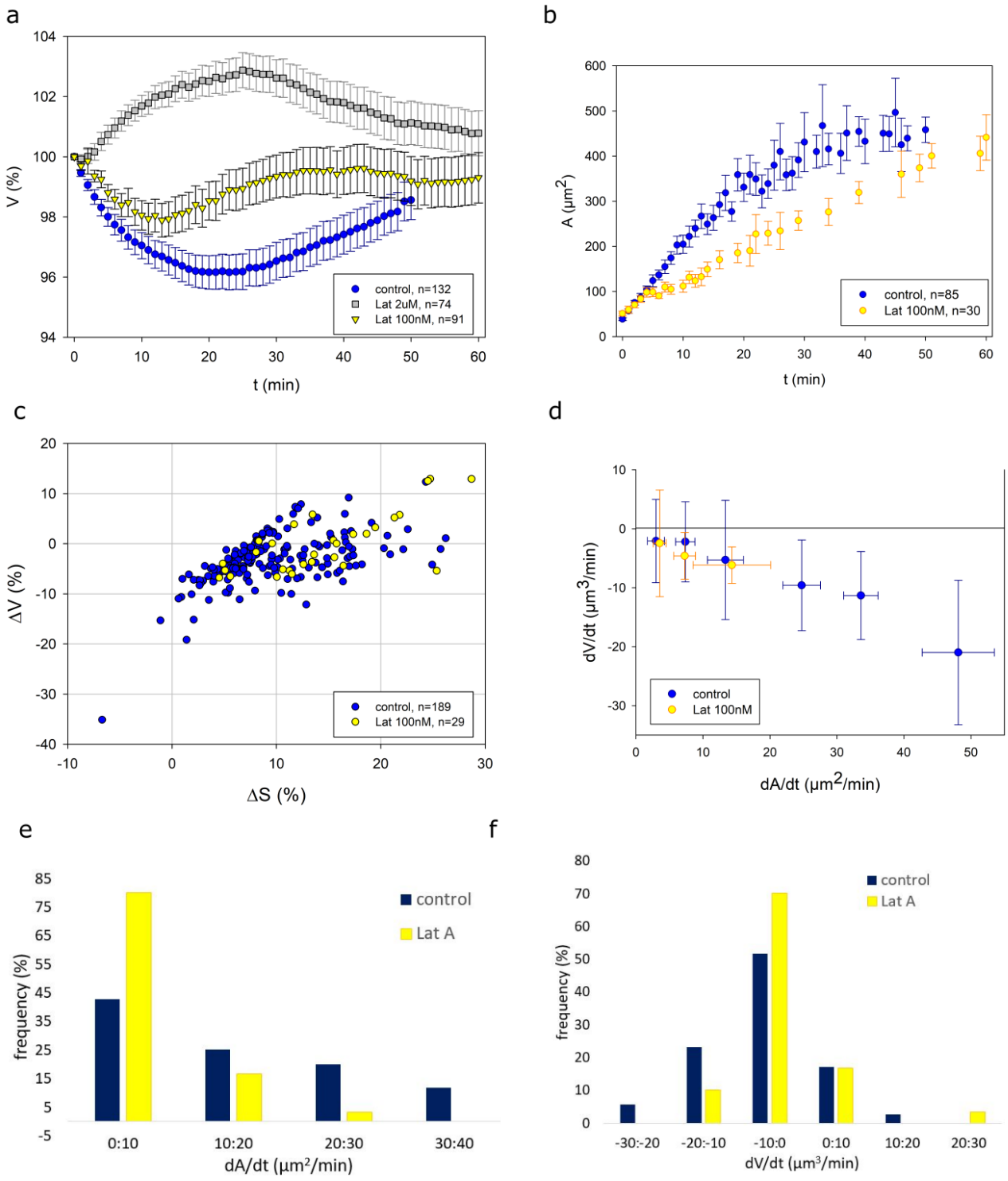

Figure 1.8 *Effect of actin disruption by Lat on spreading and volume.*

(a): Average volume of control cells (blue), treated with Lat 100nM (yellow) and 2μM (gray) of a typical experiment. In the first 20 min of experiment cells treated with 2 μM Lat did not spread and did not lose volume; cells treated with 100 nM Lat lost less volume than control. Error bars represent standard error.

(b): Average spreading area of control and Lat 100 nM treated cells of a typical experiment. A low dose of Lat delays spreading. Error bars represent standard error.

(c): Volume-surface balance for control and 100 nM treated cells.

(d): Median values of $\frac{dV}{dt}$ *for the different* $\frac{dA}{dt}$ *intervals. Error bars represent standard deviation.*

Distribution of $\frac{dA}{dt}$ *(e) and* $\frac{dV}{dt}$ *(f) for control and Lat 100nM treated cells.*

- Inhibition of Arp2/3

To obtain a more specific perturbation of actin dynamics, we chose to affect Arp2/3, the nucleator of branched actin networks, responsible for lamellipodial formation and thus important for fast cell spreading. Cells treated with CK-666 (100 µM) lost less volume than control cells on average (~2%) and had a smaller spreading area (Fig. 1.9a,b, g). CK-666 treatment reduced volume loss by reducing both $\frac{dA}{dt}$ and $\frac{dV}{dt}$ in the similar manner than treatment with low dose of Lat: volume flux remained proportional to the spreading speed (Fig. 1.9d-f).

The slowing down of spreading by CK-666 and Lat is consistent with previous research and could be explained by inhibition of actin polymerization and contractility increase (Q. Yang et al. 2012; Bun et al. 2018) and assembly of a different actin architecture (Henson et al. 2015), less favorable to fast spreading.

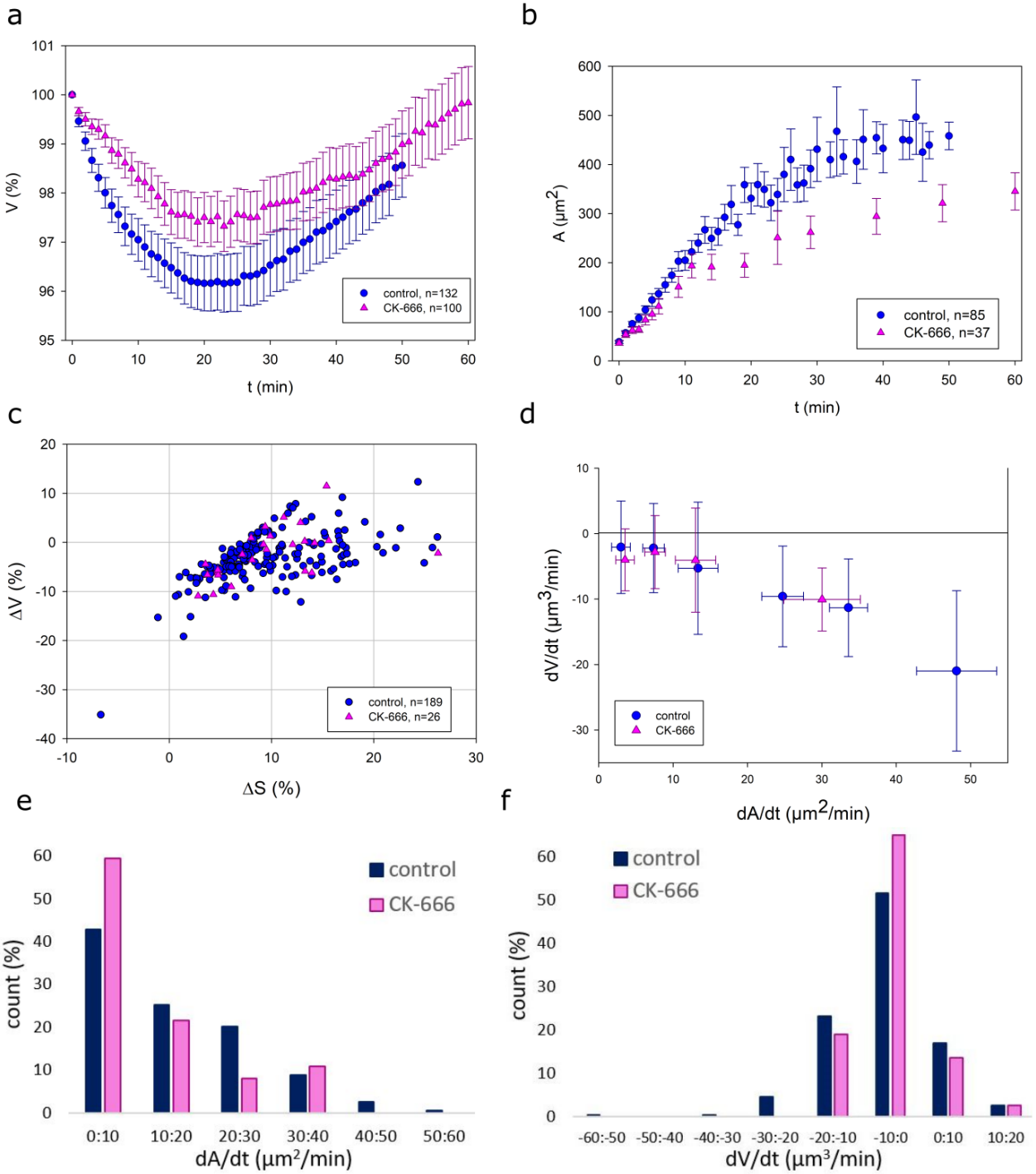

Figure 1.9 *Effect of Arp2/3 inhibition by CK-666 on spreading and volume.*

(a,b): Average volume and area of control cells (blue) and CK-666 treated (pink) of a typical experiment.; cells treated with CK-666 lost less volume than control. Error bars represent standard error.

(c): Volume-surface balance for control and CK-666 treated cells.

(d): Median values of $\frac{dV}{dt}$ *for the different* $\frac{dA}{dt}$ *intervals. Error bars represent standard deviation.*

Distribution of $\frac{dA}{dt}$ (e) and $\frac{dV}{dt}$ (f) for control and CK-666 treated cells.

g

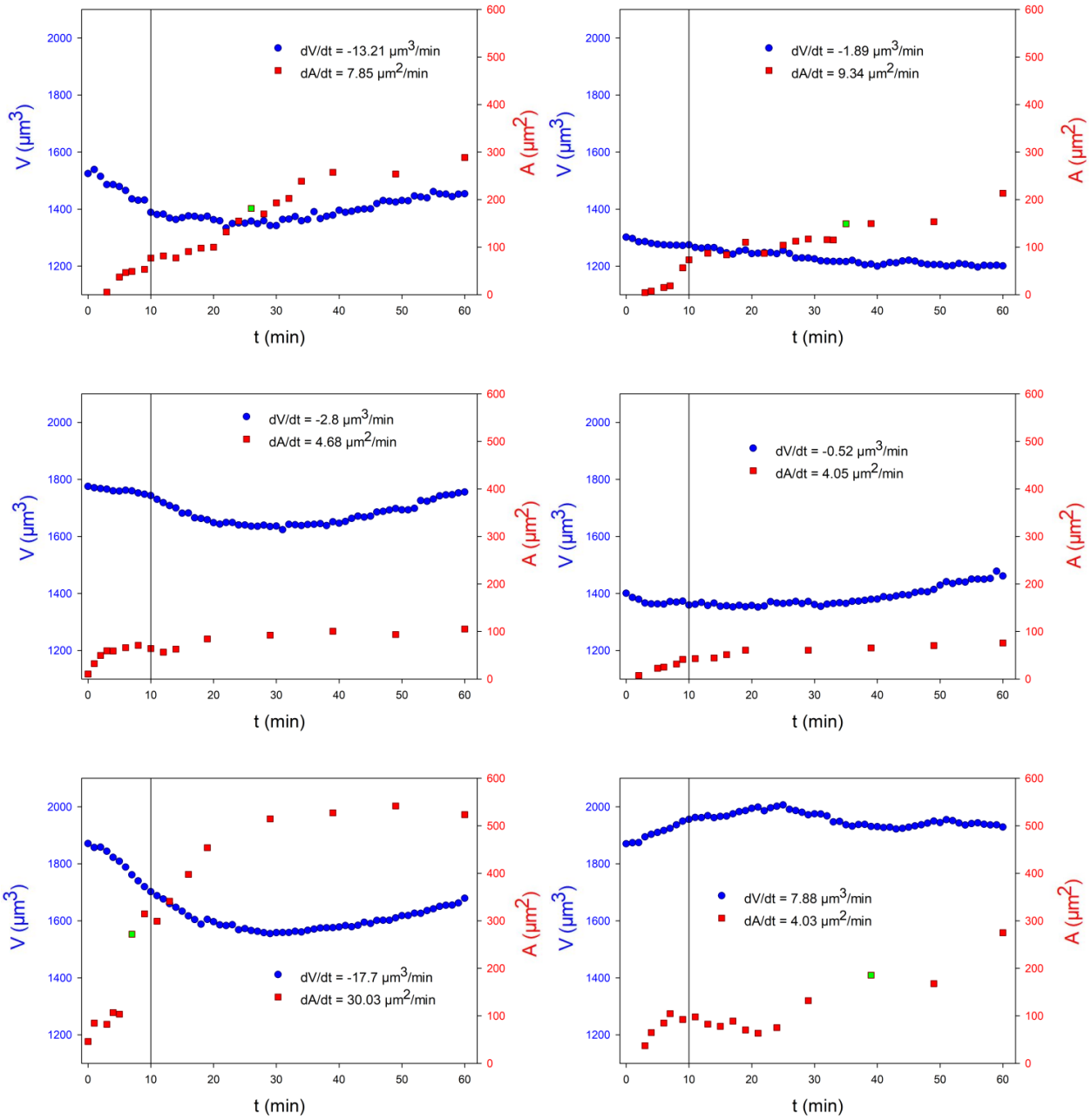

(g): examples of single cell volume/area dynamics.

- Inhibition of contractility

Contrary to Arp2/3, which promotes spreading, contractility, mostly driven by Myosin II activity, by making the cell cortex stiffer, and by increasing surface tension, tends to antagonize fast spreading. To inhibit contractility we treated cells with Y-27 (100 µM), an inhibitor of ROCK kinase which targets myosin light-chain phosphatase. Whereas cells treated with Y-27 and placed on non-adhesive substrate did not lose volume, like control cells, treated cells placed on fibronectin lost 15% of volume in average, which is three times more than control cells (Fig. 1.10a,g). Spreading area of treated cells was larger than for control cells (Fig. 1.10b). Y-27 dramatically affected single cell volume dynamic – only 3% of cells exhibit spreading without volume loss. The volume-surface balance was shifted – treated cells rather lost volume than increase surface area at the early stage of spreading (Fig. 1.10c). Y-27 also significantly shifted distributions of $\frac{dA}{dt}$ and $\frac{dV}{dt}$, treated cells were spreading faster than control cells and loosing volume faster (Fig. 1.10d-f). Interestingly, Y-27 treated cells had the same values of $\frac{dV}{dt}$ for the different ranges of $\frac{dA}{dt}$. Here we can speculate, that as Y-27 treated cells have lower homeostatic membrane tension than control (Tinevez et al. 2009), even small deformation would induce an increase in tension higher than homeostatic value, which lead to maximal volume flux. Another interpretation is that reducing contractility (and maybe also other effects of ROCK inhibition by Y-27), by affecting the capacity of cells to bleb (G. T. Charras 2008), lowers the rate of deformation needed to produce membrane tension and activate the volume regulation mechanisms. All these would thus be in the saturation regime, all spreading fast enough to fully activate the volume regulatory mechanisms. This point of view can be supported by the fact that the very large variability of behaviors observed in control cells, is mostly lost for Y-27 treated cells: their behavior is much more similar from one cell to the other, when considering single cell volume trajectories. This could be because in control cells some stochastic events, such as blebbing, occur frequently during the spreading process (L. L. Norman et al. 2010), making the volume behavior very variable from one cell to another.

To complete this aspect of the study, which shows a strong effect of contractility on volume loss, it will be necessary to also assess the effect of Blebbistatin, a more direct inhibitor of Myosin II, and ML-7 which targets MLCK (myosin light chain kinase), another pathway which modulate Myosin II activity, in part independently of ROCK (the target of Y-27).

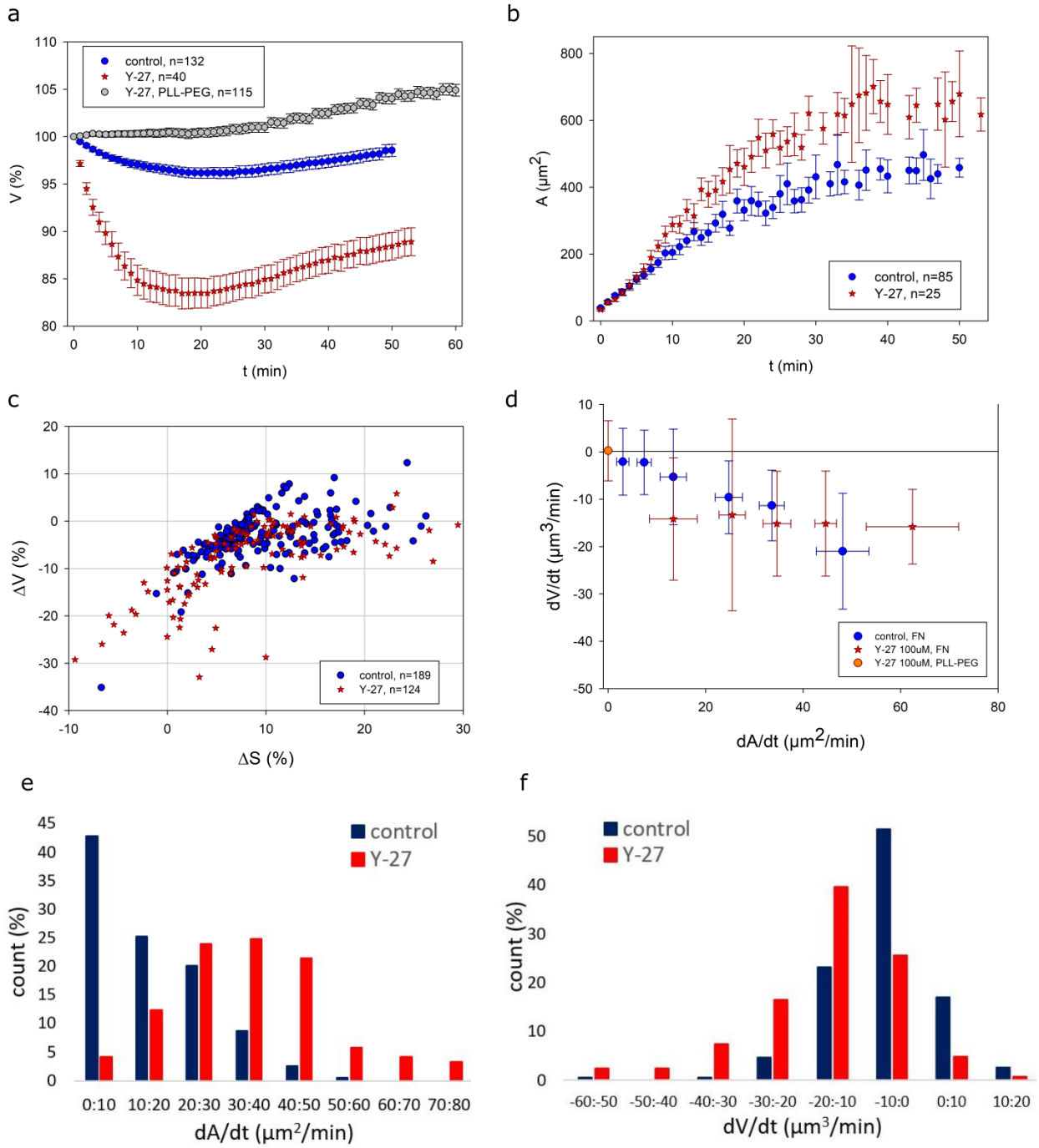

Figure 1.10 *Effect of contractility inhibition by Y-27 on spreading and volume.*

(a,b): Average volume and area of control cells (blue) and Y-27 treated (red) of typical experiment placed on fibronectin; cells treated with Y-27 spread more and lost more volume than control. Y-27 treated cells placed on PLL-PEG did not spread and did not lose volume. Error bars represent standard error.

(c): Volume-surface balance for control and Y-27 treated cells. Y-27 treated cells tend to spread with the constant projected area.

(d): Median values of $\frac{dV}{dt}$ for the different $\frac{dA}{dt}$ intervals. Orange point represents $\frac{dV}{dt}$ for Y-27 treated cells placed on PLL-PEG. Error bars represent standard deviation.

Distribution of $\frac{dA}{dt}$ (e) and $\frac{dV}{dt}$ (f) for control and Y-27 treated cells.

g

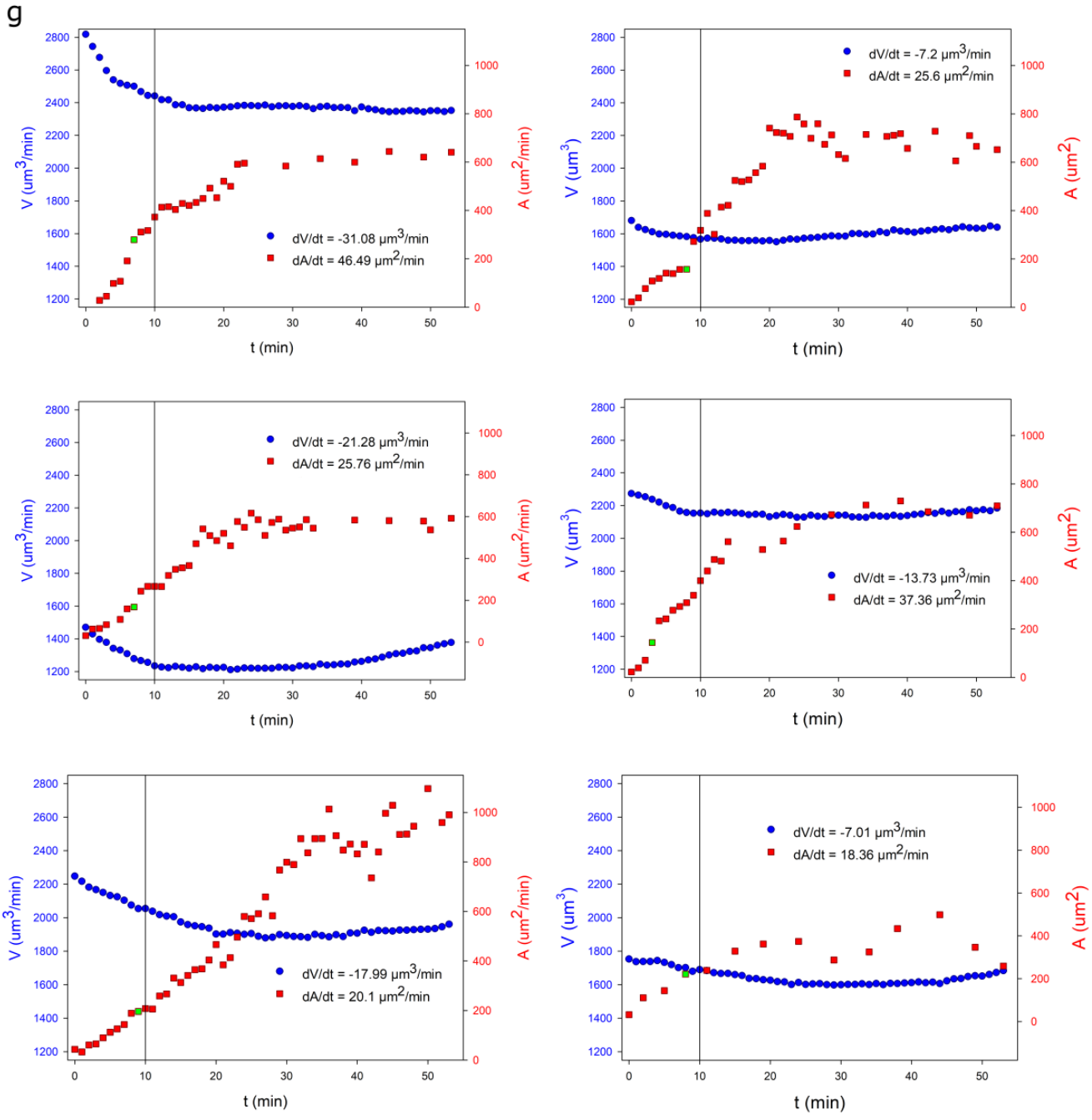

(g): examples of single cell volume/area dynamics.

Ca^{2+} ions are major regulators of contractility, acting via the CaM/MLCK pathway (Clapham 2007). Intracellular calcium increase can be mediated by release from internal stores like the ER (endoplasmic reticulum), or from the opening of channels on the plasma membrane, some of which are known to be stretch-activated channels, like Piezo channels. Such channels are known to activate during cell migration (Nourse and Pathak 2017) and extension of lamellipodia (Sugimoto et al. 2017) and could thus be activated during cell spreading. We thus used gadolinium chloride ($GdCl_3$, 100 µM), a general stretch-activated calcium channel blocker. $GdCl_3$ treated cells lost 7% of volume on average but achieved almost the same area as Y-27 treated cells (Fig. 1.11a,b). $GdCl_3$ had an intermediate effect to $\frac{dA}{dt}$ and $\frac{dV}{dt}$, compare to control and Y-27 treatment (Fig. 1.11c,d), which could be explained by the partial effect of inhibiting stretch activated Ca^{2+} influx on inhibition of cell contractility. Calcium concentration in the cell is always orders of magnitude lower than other ions and thus could not have any direct effect on cell volume, but it could also act indirectly on other molecular pathways in addition to contractility (Clapham 2007). Our result is consistent with a primary role of Ca^{2+} ions and stretch-activated calcium channels in regulation of contractility, having thus an indirect effect on volume loss during spreading. To complete this aspect of the study, we will deplete intracellular Ca^{2+} by BAPTA-AM treatment, versus BAPTA treatment, which affects only entry of extra-cellular calcium and should be similar to $GdCl_3$ treatment while spreading.

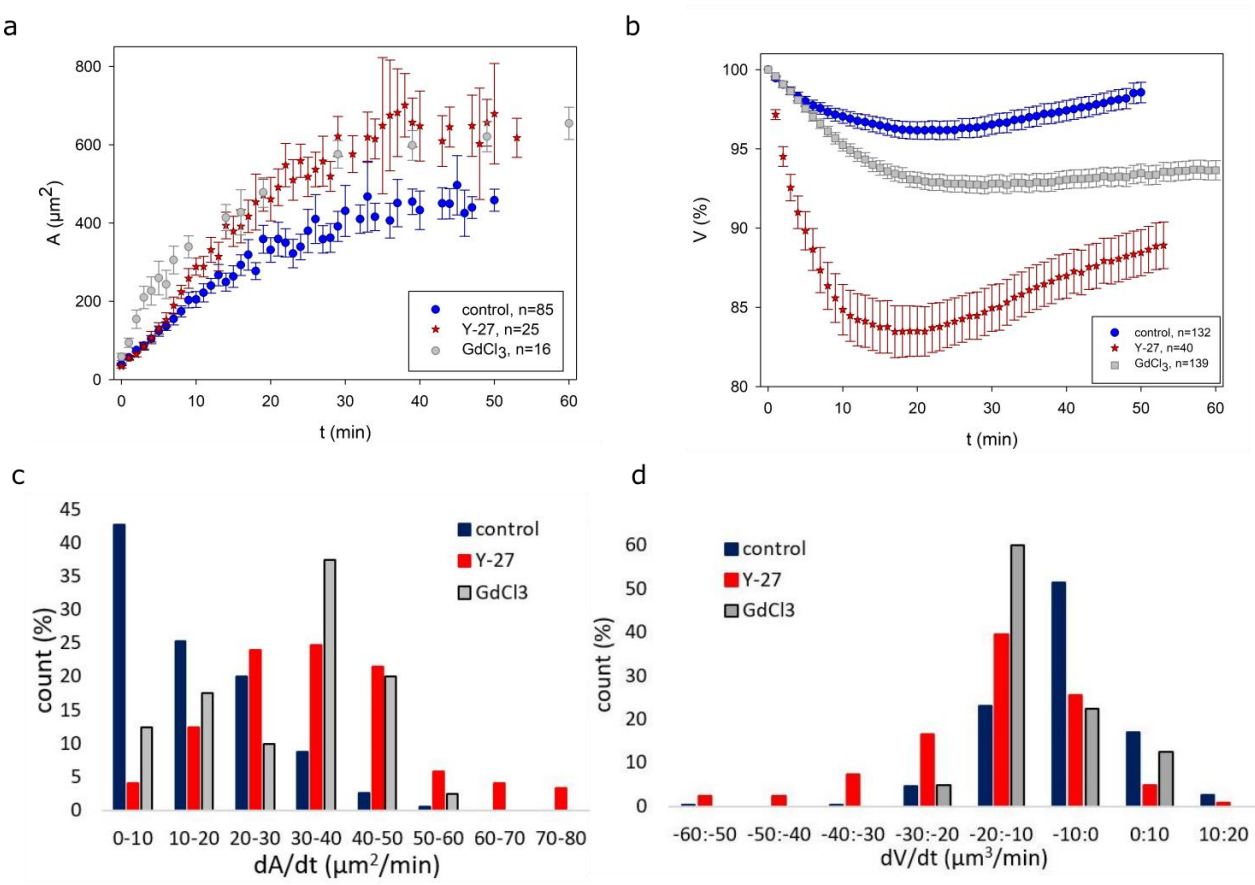

Figure 1.11 *Effect of contractility inhibition by $GdCl_3$ on spreading and volume.*

(a,b): Average volume and area of control cells (blue), $GdCl_3$ (grey) and Y-27 treated (red) of a typical experiment; cells treated with $GdCl_3$ were spread similar with Y-27 treated cells and lost more volume than control. Error bars represent standard error.

(c,d): Distribution of $\frac{dA}{dt}$ and $\frac{dV}{dt}$ for control $GdCl_3$ and Y-27 treated cells.

- Modulation of fast spreading without volume loss

Our results so far showed that we can modulate volume loss associated to cell spreading by affecting the cell cytoskeleton, with the general rule that faster spreading cells tend to lose more volume. We wondered if it is possible to break this rule, for example having fast spreading cells that do not lose volume while spreading. To achieve this, we reasoned that on one hand, reducing contractility increases spreading speed by making cells softer, but also that it is known to indirectly activate cell protrusion activity due to mutual negative interactions between the RhoA (contractility) and Rac1 (protrusion) pathways. We thus examined the effect of inhibition of Arp2/3 in cells with low contractility by a combination of CK-666 and Y-27

treatment, which does not affect cell viability at all contrary to other combinations of drugs. Double treated cells spread fast, like cells treated only with Y-27 (Fig. 1.12b, g), but they did it without volume loss, just like cells treated only with CK-666: double treated cells lost 2% of volume on average, and 25% of cells did not lose volume while spreading (Fig. 1.12a). At the early stage of spreading, cells increased surface area rather than losing volume (Fig. 1.12c), even if they were spreading fast. Distribution of $\frac{dA}{dt}$ was similar to Y-27 treated cells (Fig. 1.12e), however, distribution of $\frac{dV}{dt}$ was shifted towards even positive values (Fig. 1.12f). This result shows that fast spreading can occur without volume loss (Fig. 1.12d). It allows us to start drawing a working model consistent with this ensemble of results (see next chapter for a more detailed version of the model): reducing contractility allows fast spreading, which, in cells treated with Y-27 only, is accompanied with increased lamellipodial expansion. This would lead to fast and large volume decrease because inhibition of contractility on one hand can prevent membrane tension relaxation by bleb formation and on the other hand can increase tension due to fast pulling, from the cell cortex, of the membrane area needed to form the extending lamellipodium. Additional inhibition of branched actin polymerization would then prevent volume loss, either because it prevents membrane stretching by expansion of the thin lamellipodial protrusion produced by branched actin. Alternatively Arp2/3 inhibition rescues blebbing or any other sort of membrane detachment from the underlying cortex, which would help relaxing membrane tension during spreading. This could be because branched actin produces more friction on the plasma membrane, and thus more tension when it expands/unfolds during cell spreading; or because branched actin is required to activate ion transport (Chifflet and Hernández 2012) and consequent volume loss; or because it binds to particular membrane associated structures associated to ion pumps and involved in cell volume modulation (e.g. caveolae (Balijepalli and Kamp 2008)).

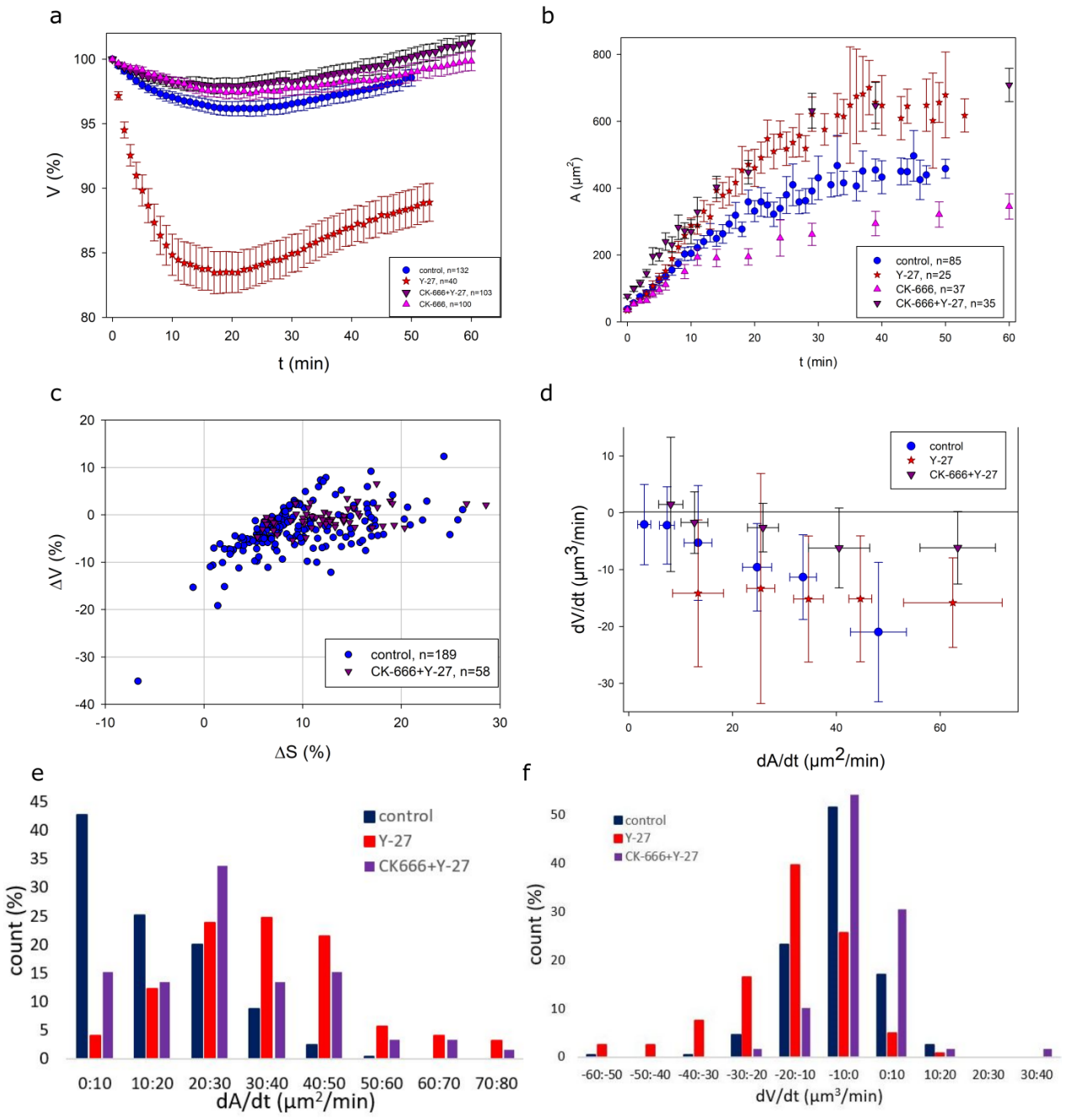

Figure 1.12 *Effect of contractility and Arp2/3 inhibition on spreading and volume by combined CK-666 and Y-27 treatment.*

(a,b): Average volume and area of control cells (blue), CK-666 (pink), Y-27 (red) and CK-666+Y-27 treated cells of a typical experiment; cells treated with CK-666+Y-27 had a similar spreading dynamics with Y-27 treated cells, however, they did not lose volume. Error bars represent standard error.

(c): Volume-surface balance for control and CK-666+Y-27 treated cells.

(d): Median values of $\frac{dV}{dt}$ *for the different* $\frac{dA}{dt}$ *intervals. Error bars represent standard deviation.*

Distribution of $\frac{dA}{dt}$ (e) and $\frac{dV}{dt}$ (f) for control, Y-27 and CK-66+ Y-27 treated cells.

g

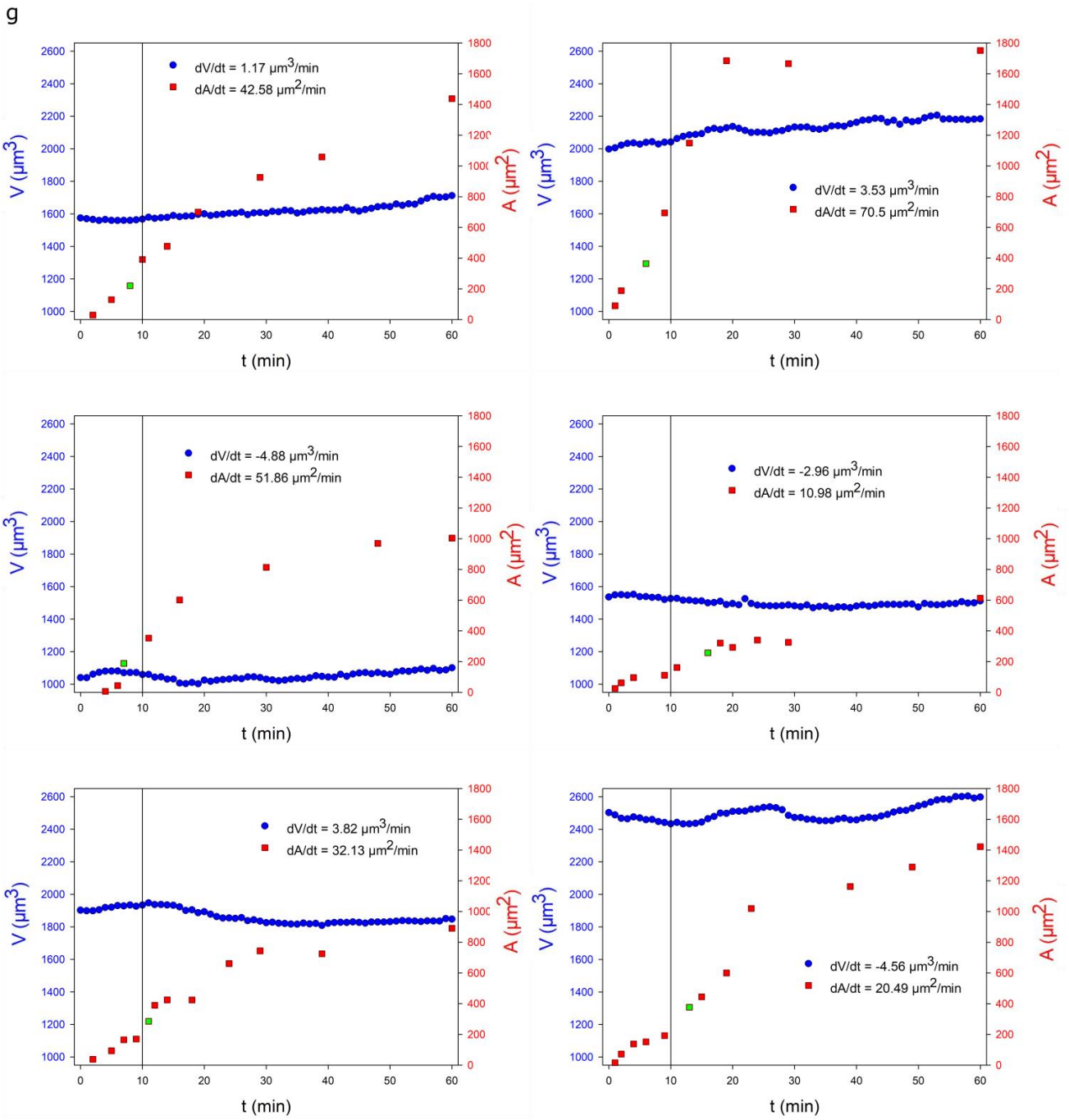

(g): examples of single cell volume/area dynamics.

d. Summary of results on spreading HeLa cells and working model

We found that cell spreading induced volume loss, which was consistent with previously published data (Guo et al. 2017). Although, either due to artifact of single cell volume reconstruction from 3D confocal images, or to the starved state of cells used in previous studies, we found that they might have strongly overestimated the amount of volume loss associated to cell spreading. 30 to 40% versus 4% in our case – note that the values are close the maximal possible volume loss (Zhou et al. 2009) upon hyperosmotic shock and should lead to cells almost devoid of free water. It would mean that cells are extremely crowded, that would affect their functioning (Delarue et al. 2018), which is not the case for spread cells. If this observation was not an artifact of the measurement method used, it could be that the cells they used were strongly diluted prior to spreading, potentially due to the starvation treatment.

We also made the new observation that speed of volume loss was proportional to the speed of spreading rather than to the extent of spreading, as proposed in previous studies (Fig. 1.13a) – the faster cells spread, the more volume they lost; and if spreading is slow, cells can spread to large areas without loss of volume. This makes an important difference and relates the volume loss to the stress in the surface due to the spreading process, which should relax within minutes, rather than to the shape of the cell. Decrease of actin polymerization/increase of contractility slowed down spreading and prevented volume loss, and inhibition of contractility induced fast spreading and large volume loss. However, a combination of inhibition of contractility and of Arp2/3-dependent actin polymerization induced fast spreading without volume loss.

Finally, we found that at early stages of spreading, when the cell shape is close to a spherical cap, cells maintain volume-surface balance by modulating both volume and surface area (Fig. 1.13b – note that here surface area is not the total plasma membrane area, which is much larger due to numerous membrane folds; see part 4 of results, on osmotic shocks). The kinetics of spreading modulate the volume/surface balance: cells that spread fast tend to lose volume rather than extend the surface area, and cells that spread slow tend to extend surface without volume loss.

We speculate that this balance can be a protective mechanism preventing membrane ruptures: fast spreading could induce membrane stretching, due to friction with the cortex as membrane protrusions form, leading to ruptures. Loosing volume would prevent reaching the rupture tension – an interesting point related to that is how cells measure this tension and activate ion channels accordingly, are there specialized structures (e.g. caveolae) for that? On the other hand, slow enough spreading allows

membrane extension with less increase in tension, thanks to multiple stress relaxation mechanisms acting at the tens of minutes timescale (actin cortex turnover, exocytosis, binding and unbinding of membrane proteins to the cortex, etc…). Mechanisms allowing faster membrane tension relaxation could allow faster spreading without volume loss, such as blebbing for example. Blebbing being a stochastic process, it could explain the large cell-to-cell variability observed on top of the general trends visible on population averages. To further test our hypothesis and establish the biological function of this volume regulation mechanism, we will try to find conditions in which fast spreading does not lead to volume loss, ideally not because of fast tension relaxation, but because the sensor of tension leading to volume loss would be absent. Our best guesses are ion channels involved in cell volume regulation (e.g. VRAC), and stretch-sensitive structures such as caveolae.

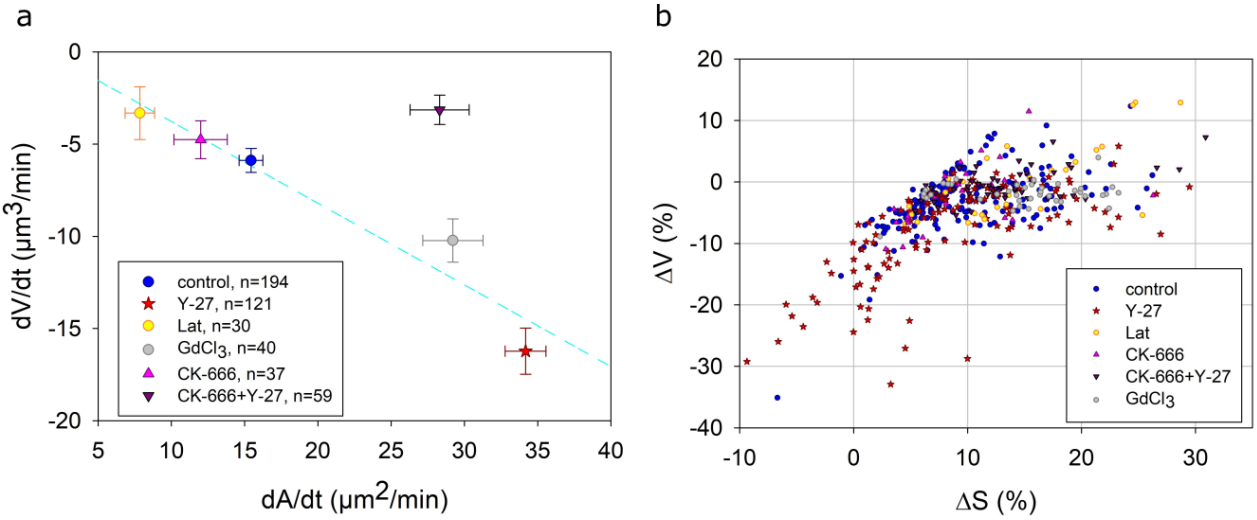

Figure 1.13 *Speed of volume flux as a function of spreading speed (a) and volume-surface balance (b) for the different drug treatment.*

(a): Mean values of $\frac{dV}{dt}$ *plotted as a function of* $\frac{dA}{dt}$ *for control and different drug treatments. Data are fitted with linear slope (R=-0.96), except CK-666+Y-27. Error bars represent standard error.*

(b): Relative volume change plotted versus relative projected surface area change.

Our spreading model for early stage of spreading assumes simple cell geometry: the transition from a sphere to a spherical cap. However, within this transition cells can have more complex 3D-shape (Fouchard et al. 2014), for example a sphere with a lamellipodium extending below, it will thus be essential to perform high resolution imaging to secure the conclusions of this study (Figure 1.14a shows preliminary results).

To close this first results section on spreading of HeLa cells, we can speculate on the mechanism, which underlies the effect of actin polymerization and contractility on cell shape and volume. Several studies showed that increase of contractility induces cell blebbing and contractility inhibition prevents bleb formation and promotes lamellipodia. Moreover, it was shown that cells form both blebs and lamellipodia when they adhere on a substrate. Conditions in which cells would form more blebs often correspond to slow spreading and reduced spreading area, while contractility inhibition corresponds to fast spreading without blebbing (L. Norman, Sengupta, and Aranda-Espinoza Helim 2011). While most cells would have a mix of the two, drug treatments could switch the balance to more of one or the other (Fig. 1.14b). In the case of dominant lamellipodial extension, branched actin polymerization in the contact area would pull a membrane sheet from the membranes reservoirs previously attached to the cortex of the cell, leading to ion channels activation and volume loss. This would correspond to the Y-27 treatment: it allows fast spreading by the combined effect of softening of the cortex and promotion of Arp2/3 based lamellipodium extension, while at the same time reducing blebbing events, which are dependent on contractility. Slow spreading cells or frequent blebbing would have the opposite effect. This would correspond to low doses of Lat, or treatment with CK-666.

The third case, fast spreading without volume loss, which corresponds to combined inhibition of contractility and Arp2/3 (lamellipodial protrusion), could be explain in the same framework in the following way: decreased contractility promotes fast spreading even in the absence of Arp2/3 based lamellipodial protrusions (Henson et al. 2015). This type of spreading might lead to a different shape, and Arp2/3 inhibition might restore some level of blebbing even in low contractile cells, thus releasing membrane tension (this is to confirm by imaging). Another hypothesis is that, in the absence of an Arp2/3 actin network, mostly formed of short branched actin filaments (Fritzsche et al. 2016) the membrane does not get tensed upon spreading, or sensor structures, or directly channels/pumps do not get activated/open (Chifflet and Hernández 2012), preventing volume loss. In the last hypothesis, the membrane could get stretched and ruptures could appear.

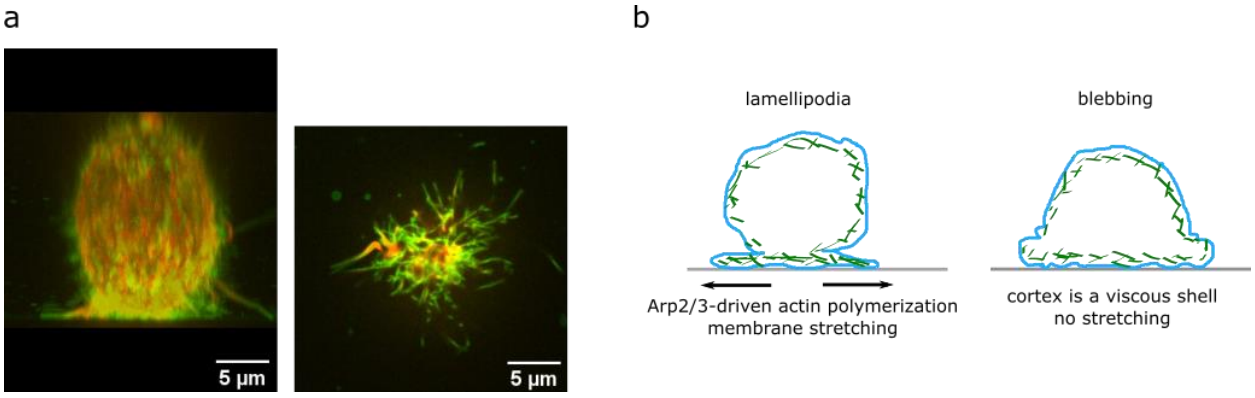

Figure 1.14 *Cell shape during the early stage of spreading*

(a): Spinning-disk 3D-reconstruction of cell shape (left) and single Z-plane of contact area (right) for control cell representing spreading driven by lamellipodia extension performed with 100x.

(b): Two possible way of spreading – through Arp2/3-dependent lamellipodia extension or through blebbing.

e. Volume modulation during spreading of RPE-1 cells.

To extend our finding to other cell types, we studied spreading of RPE-1 cells, which is known to have a lower basal contractility than HeLa cells (Liu et al. 2015). We first established the same basic volume modulation behavior during spreading (Fig. 1.15a,b,c). Cells placed on PLL-PEG did not spread and did not exhibit volume loss, instead, volume was increasing with the speed similar to cell growth, ~3.5%/hr. Cells plated on fibronectin displayed, in the initial phase of spreading, an almost opposite behavior to HeLa cells: during the first 10 min they increased their volume by 3% on average. After this brief phase of increase, the volume decreased by about the same extent and at the same speed as in HeLa cells, reaching about 95% of initial volume in the following 20 minutes (Fig.1.15b). Importantly, the phase of volume loss actually corresponded to the phase of lamellipodial extension (see IRM images in Fig. 1.15a, 10 first minutes are just adhesion of the cell body and after 10 minutes lamellipodia form). Analysis of individual trajectories showed that, indeed, a majority of cells (82%) increased volume at the early stage of spreading and then volume decrease corresponded to lamellipodia formation (confirming our previous observations). Accordingly, cells tended to extend surface rather than lose volume at the early stage of spreading (Fig.1.15d).

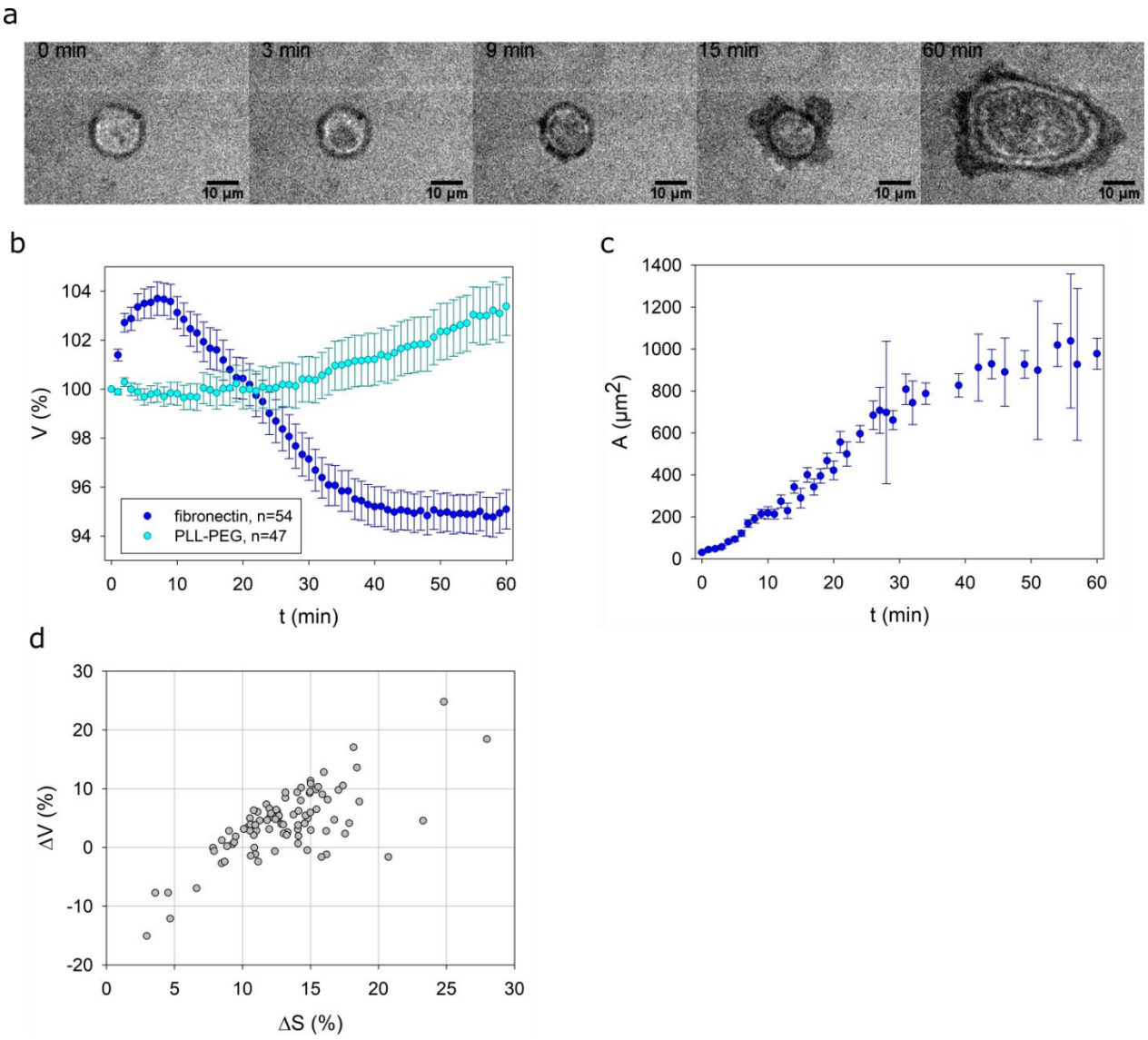

Figure 1.15 *Average RPE-1 volume and contact area during cell spreading of a typical experiment.*

(a): IRM images of spreading dynamic of individual cell placed on fibronectin.

(b): Average volume of cell placed on a substrate with different coating – fibronectin (blue), PLL-PEG (cyan). Error bars represent standard error.

(c): Averaged spreading area of cells plated on fibronectin during spreading. Error bars represent standard error.

(d): Volume-surface balance at the early stage of spreading.

We next performed the kinetic analysis, measuring the speed of spreading and volume flux before the initiation of lamellipodia formation ($\frac{dA_b}{dt_b}$ and $\frac{dV_b}{dt_b}$) and in the next 10 min after ($\frac{dA_a}{dt_a}$ and $\frac{dV_a}{dt_a}$) (Fig. 1.16a).

We obtained that after the start of lamellipodia formation $\frac{dA_a}{dt_a}$ and $\frac{dV_a}{dt_a}$ followed the same trend as HeLa cells, negative correlation. This suggest that the second phase of spreading of RPE-1 cells resembles what we observed from time zero in HeLa cells, and that RPE-1 cells have a special initial behavior while they start adhering on the substrate, which correlates with a transient volume increase. The kinetics analysis shows that during this initial phase, faster spreading cells increase their volume more and that below a certain spreading speed, there is no volume change at all, just like in the next phase of lamellipodial extension. This suggests that the volume change observed in the early phase might also depend on some mechanical activation of ion channels, but acting the opposite way. We noticed that RPE-1 cells display numerous blebs at this initial stage of spreading (Fig. 1.16b), suggesting a high contractility. Because cells did not show this behavior on PLL-PEG surfaces, we can hypothesize that it is due to the binding of integrin receptors on their integrin ligand, which is known to induce a contractile response in many cell types. It was shown before that high contractility can induce small volume increase (Taloni et al. 2015; Guillaume T. Charras et al. 2005). One potential interpretation of this result is that initial integrin engagement on fibronectin induces a contractile response, leading to blebbing and transient volume increase, before the cell initiates lamellipodial extension associated to volume decrease. HeLa cells would not display this initial phase because they have a constitutive high contractility, even in the absence of integrin binding to its ligand.

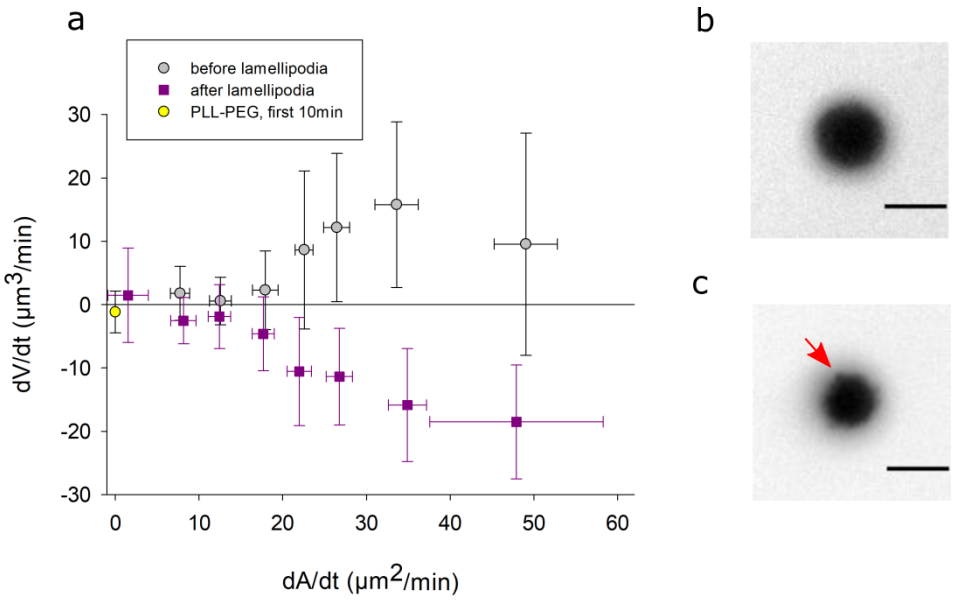

Figure 1.16 *Speed of volume flux as a function of spreading speed*

(a): $\frac{dA_b}{dt_b}$ *and* $\frac{dV_b}{dt_b}$ *(gray) before the start of lamellipodia formation and in the next 10 min after* $\frac{dA_a}{dt_a}$ *and* $\frac{dV_a}{dt_a}$ *(purple). Error bars represent standard deviation.*

FXm images of HeLa (b) and RPE-1 (c) cells at the early stage of spreading. Scale bar 10 µm. Red arrow indicates bleb.

To examine further this hypothesis we inhibited contractility with Y-27 treatment and also affected Arp2/3 (CK-666 treatment), to prevent lamellipodial extension. According to our expectations, inhibition of contractility by Y-27 treatment prevented volume increase at the early stage of spreading and did not affect further lamellipodia formation, leading to similar spreading speed and volume loss as control cells (Fig. 1.17a,b).

Arp2/3 inhibition did not affect initial volume increase, but reduced spreading area and prevented volume loss (Fig. 1.17a,b). This shows that RPE-1 cells have two phases of spreading, a first phase associated to contractility dependent volume increase, not observed in HeLa cells, and a second phase with lamellipodium dependent volume decrease, similar to HeLa cells.

Further analysis showed that, during the early stage of spreading, CK-666 treated cells, similar to control cells, displayed a positive correlation between $\frac{dA_b}{dt_b}$ and $\frac{dV_b}{dt_b}$, whereas Y-27 treated cells had $\frac{dV_b}{dt_b}$ almost equal to 0, even for a high values of $\frac{dA_b}{dt_b}$ (Fig. 1.17c). After the start of lamellipodia formation we observed

a trend similar to HeLa cells: a negative correlation between $\frac{dA_a}{dt_a}$ and $\frac{dV_a}{dt_a}$. This result confirmed our initial observation on HeLa cells, while introducing a second element: increase in contractility might induce an increase in volume (this is a point we need to check more directly). Potential way to check it is to observe integrin-independent cell spreading on PLL-coated substrate. Another difference is the extent of volume loss upon contractility inhibition, which is not as big in RPE-1 as in HeLa cells.

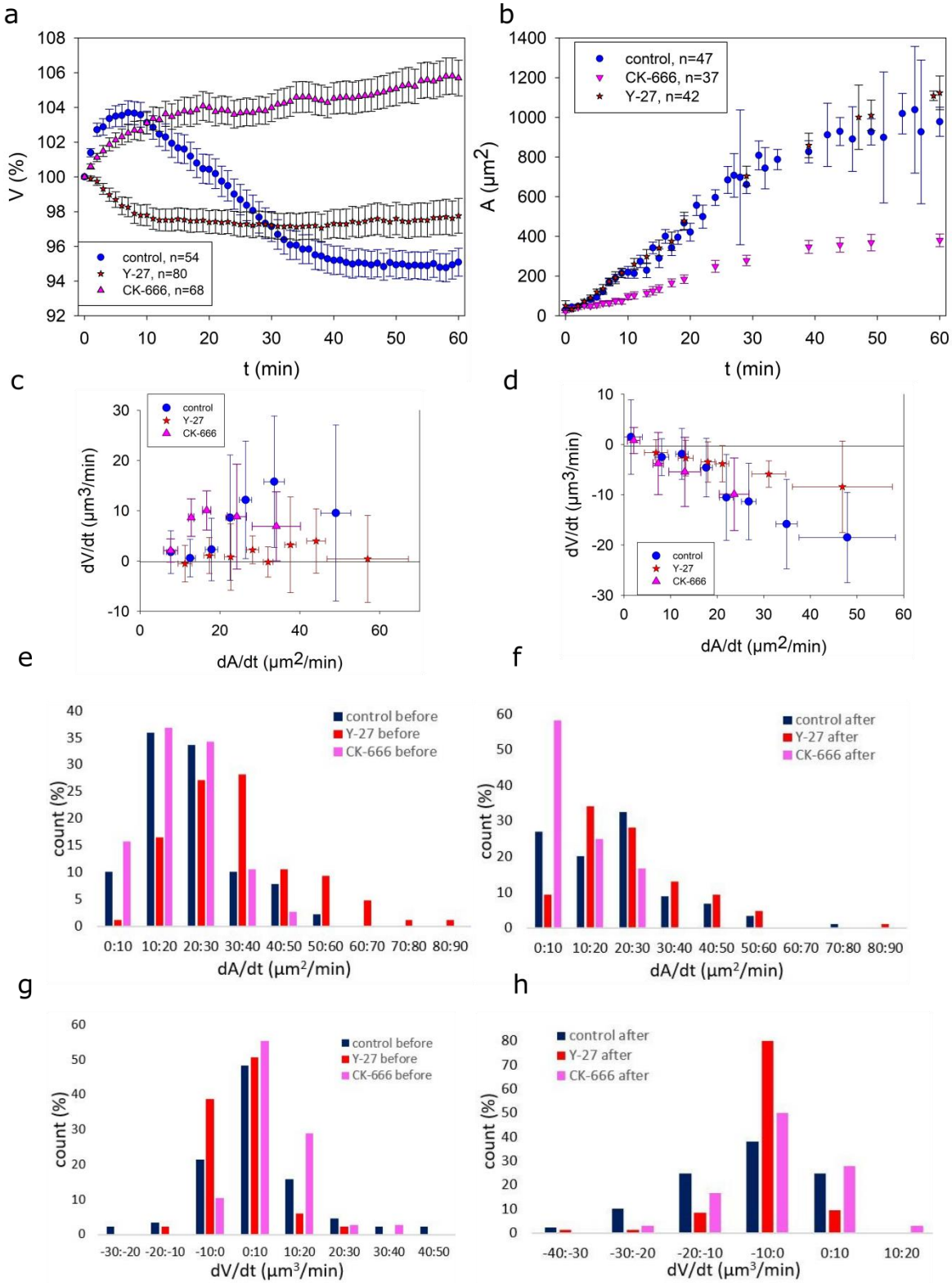

Figure 1.17 *Effect of contractility or Arp2/3 inhibition on cell volume during spreading.*

(a): Average volume of control (blue), Y-27 (red) and CK-666 (pink) treated cells (typical experiment). Y-27 treated did not increase volume while spreading, CK-666 did not lose volume. Error bars represent standard error.

(b): Average spreading area of a typical experiment. Y-27 treated cells had the same spreading area as control cells, CK-666 treated cells had a reduced spreading area. Error bars represent standard error.

(c): Median values of $\frac{dA_b}{dt_b}$ *and* $\frac{dV_b}{dt_b}$ *(d): Median values of* $\frac{dA_a}{dt_a}$ and $\frac{dV_a}{dt_a}$.

(e, g): Distributions of $\frac{dA_b}{dt_b}$ *and* $\frac{dV_b}{dt_b}$ before lamellipodia formation.

(f, h): Distributions of $\frac{dA_a}{dt_a}$ and $\frac{dV_a}{dt_a}$ in 10min after lamellipodia formation.

Although volume dynamic of spreading RPE-1 is more complex than for HeLa cells as it includes two stages (before and after lamellipodia formation), the general correlation that we observed for HeLa cells is still applicable for both stages. We observed that increase of spreading speed enhances volume loss/decrease (Fig. 1.18). Initial volume increase observed for control cells is a totally unexpected phenomenon, which would correspond to an auxetic behavior (a negative Poisson's ratio), which was already reported for the cell nucleus (Pagliara et al. 2014). It might be due to an induction of contractility via integrin signaling, concomitant to the initiation of the adhesion process. We hypnotized that at this stage cell spreading might be accompanied by a high level of blebbing. During the second stage, spreading would mostly correspond to lamellipodia extension, which would induce volume loss. To test these hypotheses, we will need to perform extensive imaging of RPE-1 cells during spreading.

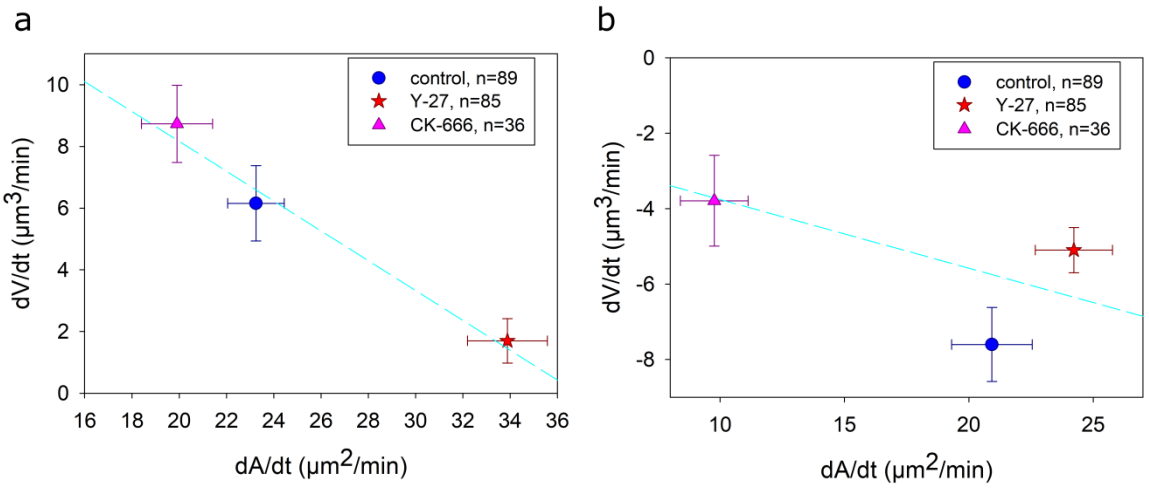

Figure 1.18 *Speed of volume flux as a function of spreading speed before lamellipodia formation (a) and in the 10 min following lamellipodia initiation (b).*

f. Na+/H+ exchanger (NHE1) inhibition

Ion transport plays a major role in classical studies of cell volume regulation. The number of involved channels would require a dedicated study, but one transporter is a classical target in studies of cell volume regulation: NHE1, the sodium/proton exchanger, which is important for regulation of cell pH (Vallés et al. 2015), was shown to be activated by osmotic cell shrinkage and participate in regulatory volume increase (Hoffmann, Lambert, and Pedersen 2009). Therefore, as a first candidate to perturb ion fluxes, we decided to examine the role of NHE1 in cell volume regulation during spreading using its inhibitor EIPA (50 µM).

We started with HeLa cells: EIPA had a slight effect on average volume dynamics, cells lost ~3% of volume during spreading with the same area as control cells (Fig. 1.19a,b), and did not change the proportion of cells that were spreading without volume loss (17%). At the early stage of spreading treated cells tend to increase their surface, more than control cells (Fig. 1.19c). The average effect of EIPA on cell volume and area was not significant, but it slightly shifted the linear proportion between $\frac{dA}{dt}$ and $\frac{dV}{dt}$ (Fig. 1.19d-f). Inhibition of NHE1 can have an indirect effect on actin. For example, its known effect as a macropinocytosis inhibitor is thought to be mostly through inhibition of branched actin nucleation (Koivusalo et al. 2010). However, unlike CK-666, EIPA treatment did not affect $\frac{dA}{dt}$ nor spreading area.

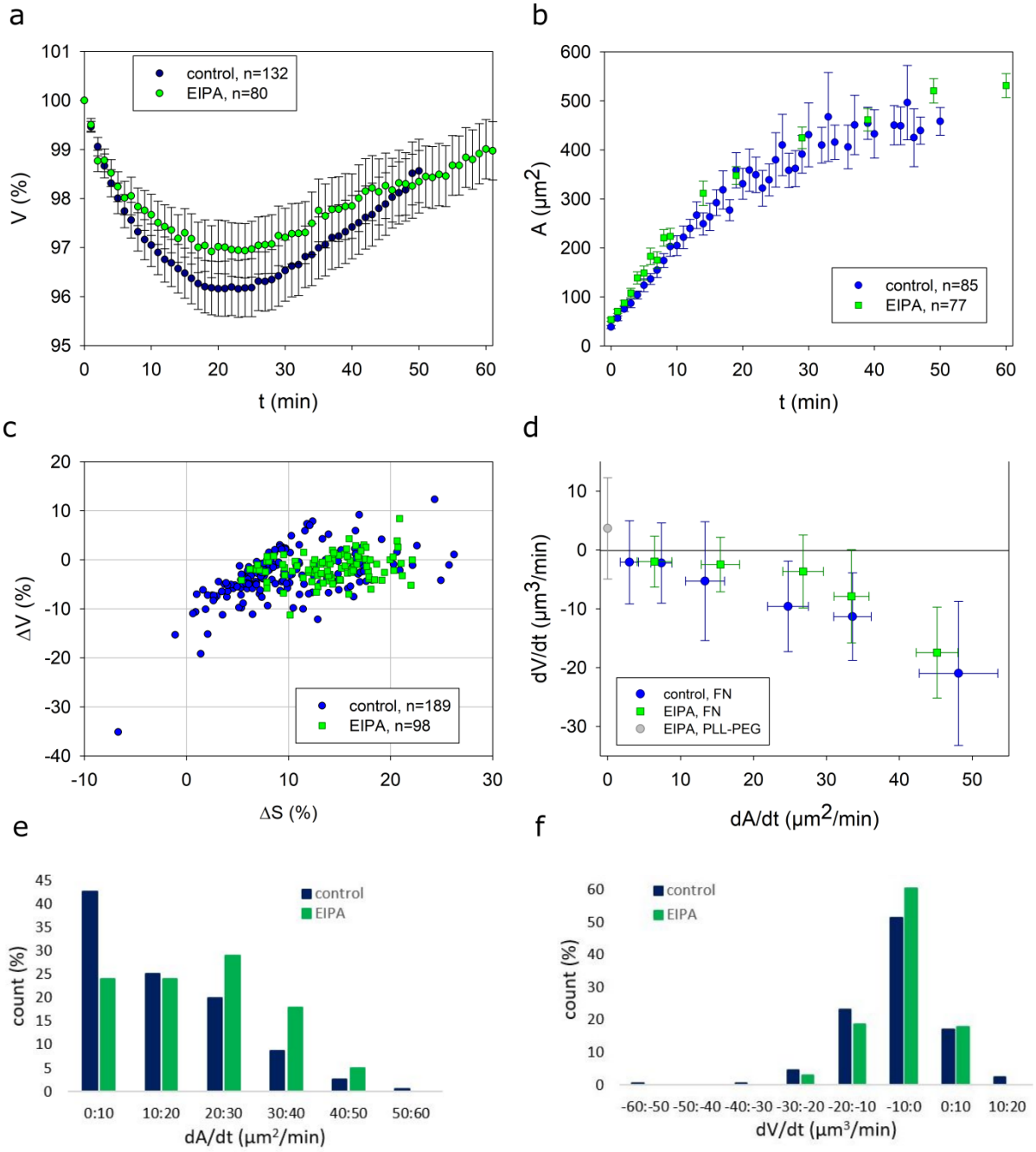

Figure 1.19 *Effect of NHE1 inhibition by EIPA on spreading and volume of HeLa cells.*

(a, b): Average volume and area of control cells (blue) and EIPA treated (green) of typical experiment placed on fibronectin; EIPA treatment slightly reduced volume loss and did not affect the spreading area. Error bars represent standard error.

(c): Volume-surface balance for control and EIPA treated cells..

(d): Median values of $\frac{dV}{dt}$ for the different $\frac{dA}{dt}$ intervals. Grey point represent $\frac{dV}{dt}$ for EIPA treated cells placed on PLL-PEG. For the same intervals of $\frac{dA}{dt}$ EIPA treated cells lost less volume. Error bars represent standard deviation.

Distribution of $\frac{dA}{dt}$ (e) and $\frac{dV}{dt}$ (f) for control and EIPA treated cells.

Because we noticed that the balance between $\frac{dA}{dt}$ and $\frac{dV}{dt}$ was slightly shifted upon NHE inhibition, and that treated cells showed more surface extension than volume loss (Fig. 1.19c), we decided to inhibit NHE1 in fast spreading cells upon Y-27 treatment. Surprisingly, 38% of cells treated with EIPA+Y-27 were spreading without any volume loss, and in average cells did not lose volume during spreading (Fig. 1.20a), showing a volume curve very similar to non-spreading cells, or to cells treated with Y-27 and CK666. However, cells were spreading as much as Y-27 treated cells (Fig. 1.20b). Surface-volume balance at the early stage of spreading was significantly shifted towards surface extension without volume loss (Fig. 1.20c). Cells treated with EIPA+Y-27 had the same spreading speed as Y-27 treated cells (Fig. 1.20e), however, the distribution of $\frac{dV}{dt}$ was mostly in a positive range which means volume increase (Fig. 1.20f). Further analysis showed that for EIPA+Y-27 treated cells $\frac{dV}{dt}$ had a negative value only for cells showing a very large $\frac{dA}{dt}$ (Fig. 1.20d). This result showed that the balance between spreading speed and volume loss could be shifted, although the mechanism is not clear – it could be an indirect effect on branched actin with an additional effect on ion pumps. The important result is that this simple treatment populates a totally different region of the volume/surface balance diagram during cell spreading.

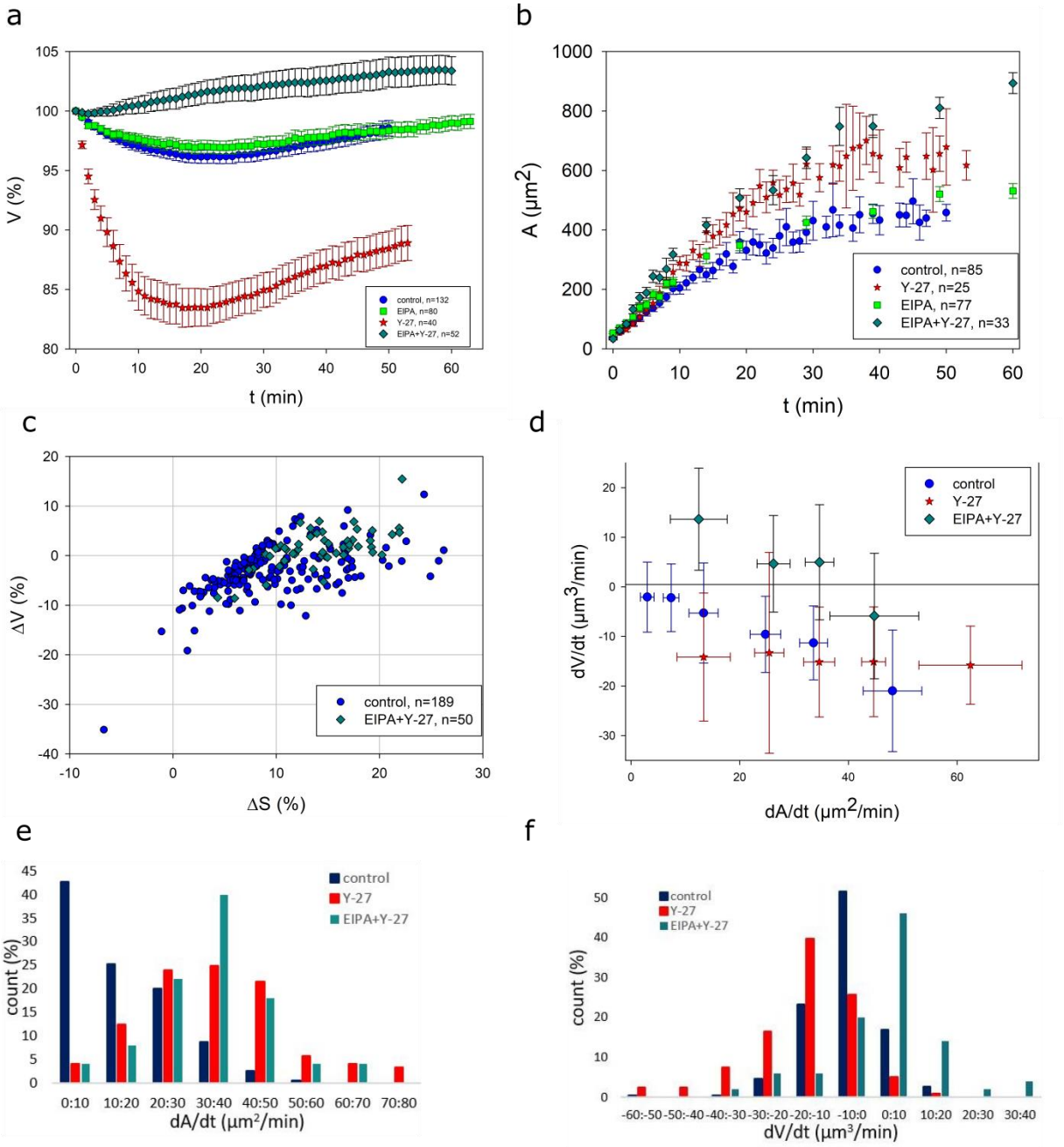

Figure 1.20 *Effect of contractility and NHE1 inhibition on spreading and volume of HeLa cells by combined EIPA and Y-27 treatment.*

(a,b): Average volume and area of control cells (blue), EIPA (green), Y-27 (red) and EIPA+Y-27 (dark cyan) treated cells of a typical experiment; cells treated with EIPA+Y-27 had a similar spreading dynamics with Y-27 treated cells, however, they did not lose volume. Error bars represent standard error.

(c): Volume-surface balance for control and EIPA+Y-27 treated cells.

(d): Median values of $\frac{dV}{dt}$ *for the different* $\frac{dA}{dt}$ *intervals. Error bars represent standard deviation.*

Distribution of $\frac{dA}{dt}$ (e) and $\frac{dV}{dt}$ (f) for control, Y-27 and EIPA+Y-27 treated cells.

Next, we also treated RPE-1 cells with EIPA and EIPA+Y-27 (preliminary data). Treated cells on average increased their volume during spreading (Fig. 1.21a). The treatment totally suppressed the volume loss phase, which accompanies the phase of lamellipodial extension in control cells. EIPA and EIPA+Y-27 treated cells had a spreading dynamics similar to CK-666 treated cells (Fig1.21b). This suggests that, at least for RPE-1 cells, the effect of EIPA treatment on spreading and cell volume regulation could be indirectly due to an inhibition of branched actin, similar to CK-666 treatment. However, this part requires more experimental data to be fully conclusive.

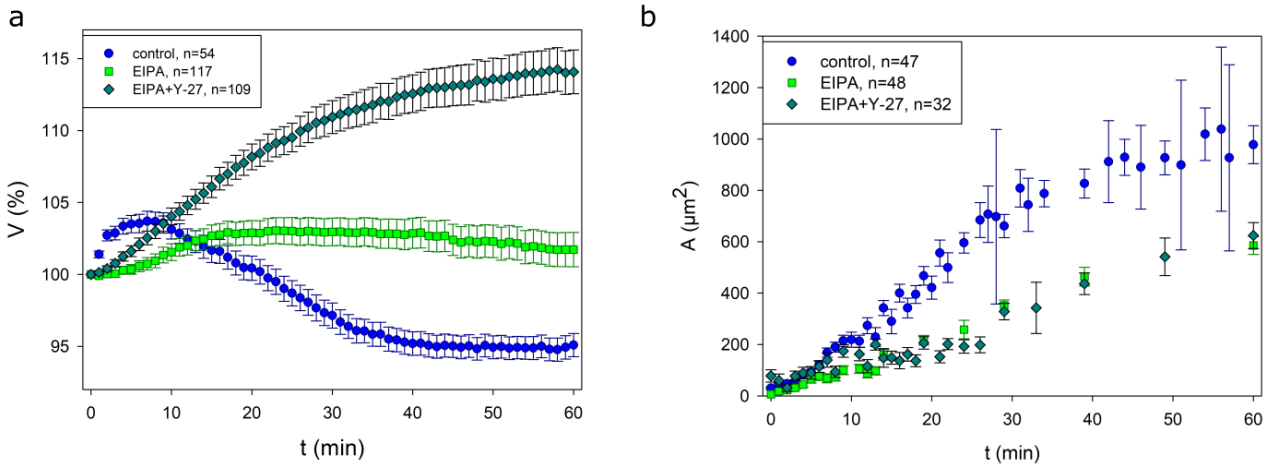

Figure 1.21 *Effect of contractility and/or NHE1 inhibition on spreading and volume of RPE-1 cells by combined EIPA and Y-27 treatment.*

(a): Average volume of control cells (blue), EIPA (green), and EIPA+Y-27 (dark cyan). EIPA treated cells did not lose volume while spreading and EIPA+Y-27 treated cells significantly increased volume while spreading. Error bars represent standard error.

(b): Average area. EIPA and EIPA+Y-27 treated cells had reduced spreading area if compared with control cells. Error bars represent standard error.

g. General conclusion on analysis of single cell spreading experiments

We demonstrated that cells modulate their volume during spreading and that this modulation depends on the spreading kinetics and the state of the acto-myosin cortex:

1) Cell spreading induces volume loss at constant dry mass.

2) For HeLa cells, volume flux depends almost linearly on the speed of spreading. Slow spreading cells do not lose volume (or even increase volume at the cell growth rate), similarly to non-spreading cells, while fast spreading cells, upon contractility inhibition, can lose up to 15% of their volume in a few tens of minutes.

For RPE-1 cells volume proportionally increases with the speed of spreading at the early stage of spreading – this phenomenon can be related to the high contractility specific for this stage and requires further investigation. Late stage of spreading has a similar trend as in HeLa cells.

3) Inhibition of actin polymerization or inhibition of Arp2/3 decreases spreading speed, reducing volume loss. Branched actin might have a specific effect on volume loss, either due to the type of structure it induces (fast extension of thin membrane sheets such as lamellipodia), or because of a more direct effect on ion channels/pumps or associated structures (caveolae).

4) Inhibition of contractility increases spreading speed and, consequently, volume loss.

5) Inhibition of branched actin in low contractile cells leads to fast spreading without volume loss.

6) Inhibition of NHE1 in low contractile cells leads to a similar phenotype of fast spreading without volume loss.

The effect of NHE1 inhibition is not completely clear for us. There are two opposite hypothesis to explain the similarity between the effect of NHE1 and Arp2/3 inhibition.

Hypothesis 1: Arp2/3 inhibition prevents formation of branched actin and associated membrane structures, such as lamellipodia, during spreading (Henson et al. 2015). And lamellipodial structures are causing the membrane tension responsible for ion channels/pumps activation. Arp2/3 inhibition is also often accompanied by increase in contractility and blebbing, which could also contribute to decrease membrane tension. Similarly, but for a different reason, NHE1 inhibition could also indirectly prevents the formation of branched actin, because it changes intracellular pH for example (Vallés et al. 2015; Köhler et al. 2012). In this hypothesis, both Arp2/3 and NHE1 inhibition prevent the formation of lamellipodia and thus prevent the build up of membrane tension during spreading. As a consequence, there is no volume loss.

Hypothesis 2: NHE1 inhibition affects intracellular pH, and, therefore, could affect activity of ion transport (Holzer 2009); Arp2/3 inhibition affects the activation of ion channels/pumps (Fritzsche et al. 2016). In this case, fast spreading without volume loss is observed because NHE1 and branched actin are both required

for ion transport activation. However, there is still an increase in surface/membrane tension upon spreading.

If this second hypothesis was true, then this would be a good context in which the function of the volume loss could be studied, as it would lead to a context of high membrane tension not compensated by volume loss because the volume regulation pathway would be inhibited. One potential defect could be the appearance of transient membrane rupture events in the fast spreading cells. This is an hypothesis which can be tested experimentally, using the tools we developed to observe formation and repair of plasma membrane holes (Jimenez et al. 2014).

Because the effect of EIPA+Y-27 treatment is robust and reproduced for two cell lines, it will require further investigations. For example, this treatment can totally change steady-state ion permeability. It would be interesting to access membrane potential/ion concentration during spreading.

2. Cell population analysis of the coupling between shape and volume

a. The volume of a cell is independent of the size and shape of its spreading area

We observed that in the first 20 min of spreading cells lose 4% of volume on average, and then cells continue to spread with low speed and increase their volume due to the growth (~5%/h). Thus, we assumed that at the long timescale cell volume should be independent of the spreading area.

To test this idea we measured cell volume and spreading area (Fig. 2.1) for adherent HeLa and RPE-1 cells (cell were injected in fibronectin-coated chamber 4 h before the measurements). Indeed, we observed that at the level of a population there is no strong correlation between spreading area and volume for HeLa (correlation coefficient R=0.35) and RPE-1 (R=0.27).

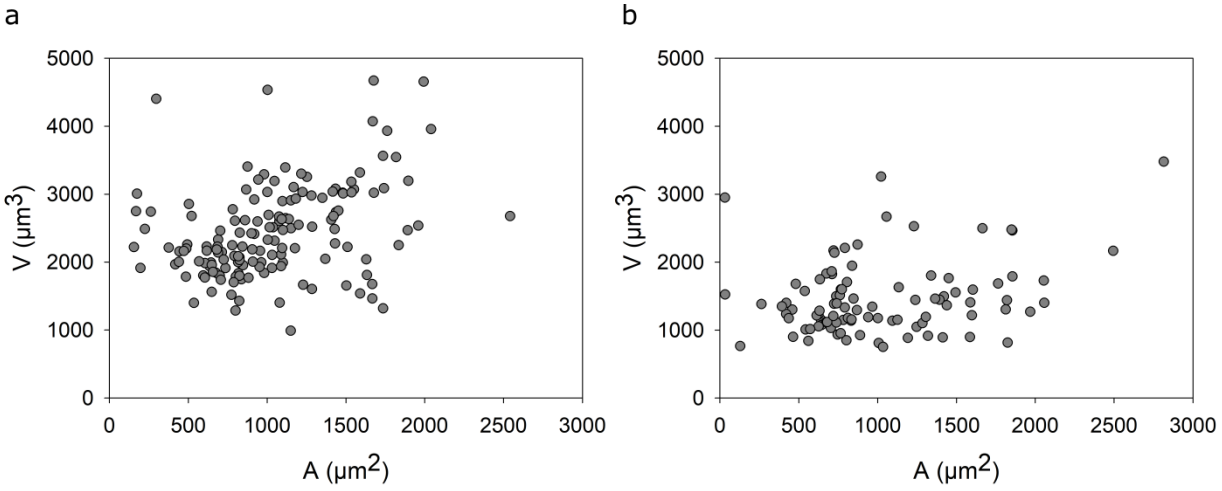

Figure 2.1 *Volume and spreading area of adherent HeLa (a) and RPE-1 (b) cells.*

If we assume that the volume $V = const$ is independent of the spreading area A and spreading is radial, thus $A \sim p^2$ (p is the perimeter of the spreading area),

$$\frac{V}{A} \sim \frac{const}{p^2} \qquad \textit{(Eq. 21)}$$

$$\log\left(\frac{V}{A}\right) \sim -2\log(p) \qquad \textit{(Eq. 22)}$$

then, the ratio between volume and area should follow a power law with slope -2. Experimental data are in good agreement with this model (Fig. 2.2), which supports the hypothesis that the volume is independent of the spreading area for steady state spread cells.

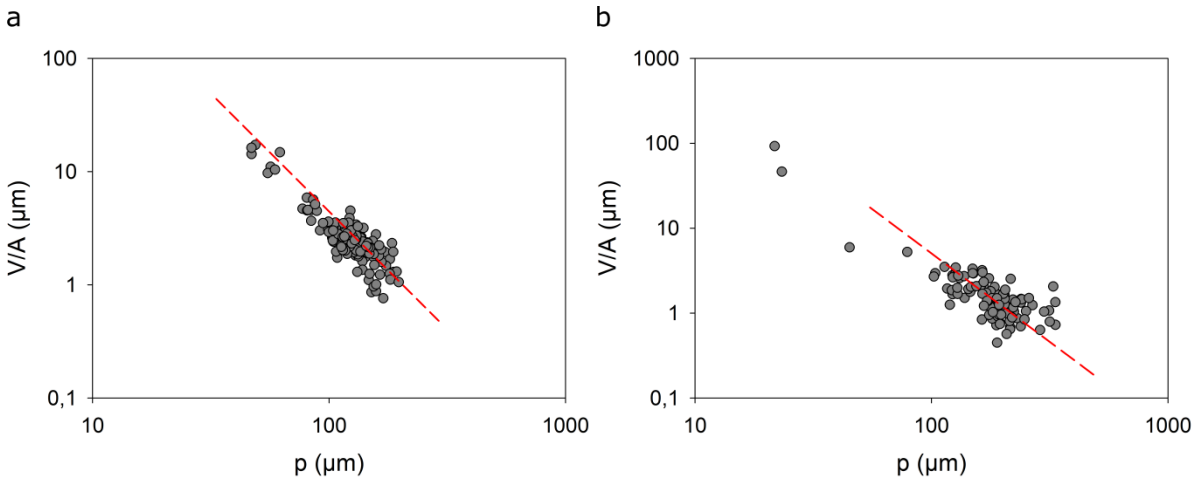

Figure 2.2 *Volume to spreading area ratio as a function of the perimeter of adherent HeLa (a) and RPE-1 (b) cells. Dash red lines represent theoretical slope -2.*

In order to control both the spreading area and the shape of cells, because the shape itself affects the acto-myosin cytoskeleton and the cell contractility (Thery 2010; Rape, Guo, and Wang 2011), we used adhesive micropatterns of different shapes and sizes: circles and rectangles with different dimensions. Our data showed that, for steady state spread cells, the average volume of patterned HeLa cells was independent of the size and shape of the patterns and was not significantly different from the average volume of non-patterned cells.

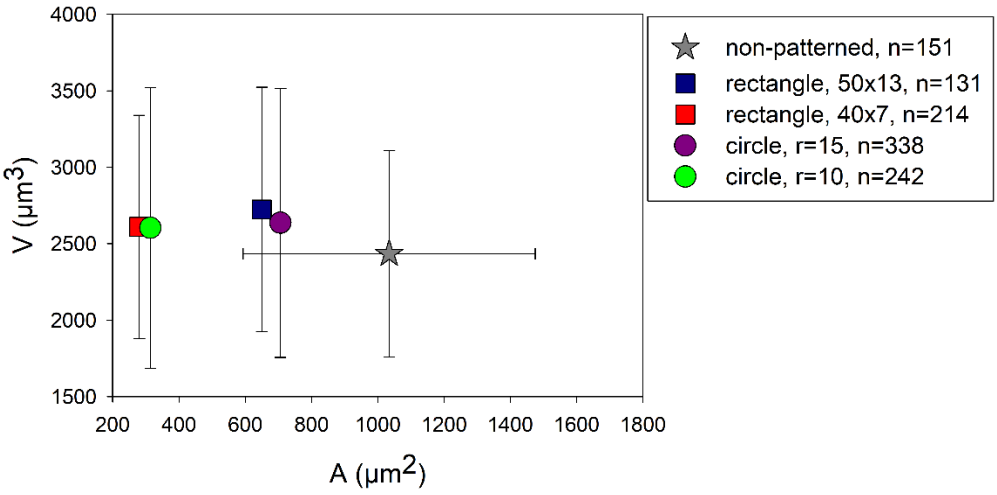

Figure 2.2 *Average volume of cells grown at different patterns (circles and rectangles) and non-patterned cells. Error bars represent standard deviation.*

b. Conclusion on steady state spread cells

Taken together our results show that cell volume is independent of the size and shape of the spreading area at the level of a population of steady state spread cells. This would be expected from our previous experiments on dynamically spreading cells, which showed that volume loss is related to the kinetics of spreading and not to the absolute spreading area.

There are a few recent studies describing the relationship between cell volume and spreading area at the level of a population of steady state spread cells with contradictory results. Two research groups found a negative correlation between volume and area (Guo et al. 2017; Xie, Yang, and Jiang 2018), another one found a positive correlation (Perez Gonzalez et al. 2018), whereas in our case there is no correlation. There are several hypothesis to explain these differences: methods of volume measurements, cell lines, cell cycle synchronization (we studied non-synchronized cells, while other studies used starved cells), the substrate (only glass in our case), or substrate coating. Nevertheless, it is hard to imagine how the specific effect we described above – a volume loss due to spreading kinetics, thus probably related to the surface/membrane stress of the fast spreading cells – could lead to a long term correlation between shape and volume, since all the surface stress associated to spreading should relax for timescales longer than tens of minutes. It is thus also possible that the methods used to measure cell volume in the other studies induced measurement artifacts.

3. Volume modulation during imposed deformation by mechanical confinement

a. Cell shape imposed by 2D confinement

Our working model, drawn from the results of the cell spreading experiments described above, is based on the hypothesis that cell deformation leads to surface/membrane tension, if the rate of deformation is faster than the actin cortex and plasma membrane turnover rates. A way to test this hypothesis is to impose a deformation to non-adhesive cells. This will also test the involvement of cell/substrate adhesion in the volume modulation response observed during cell spreading.

To do this we used a 6-well confiner device previously developed in our lab (Le Berre et al. 2014), described in Materials and methods. Briefly, suspended cells are plated on the glass bottom of the 6-well plate. Cover glasses with incompressible microfabricated pillars of desired height are sticked to soft pistons attached to the lid of the 6-well plate. By closing the lid of the plate we instantaneously (~ tens of ms) confine cells between the bottom and cover surfaces. The distance between the two surfaces is equal to the height of the spacer pillars. As the mean diameter of HeLa cells is about 17 µm, we considered confinement with pillars height (will call it "confinement height") of 20 µm as a non-confined state, and with less than 17 µm height as actual confinement. An advantage of this technique is that we can have six different experimental conditions on the same plate and operate with a large number of cells. However, we are not able to follow dynamic changes of single cells – we can observe the effect of confinement only at the level of the population.

First, we characterized the shape of the confined cells. As expected, non-confined cells have a spherical shape, and confined cells are rather cylindrical with round edges (Fig. 3.1a-c), very similar to confinement with a flat AFM cantilever (Elisabeth Fischer-Friedrich et al. 2014). We could also quantify the contact area using IRM (Fig. 3.1d).

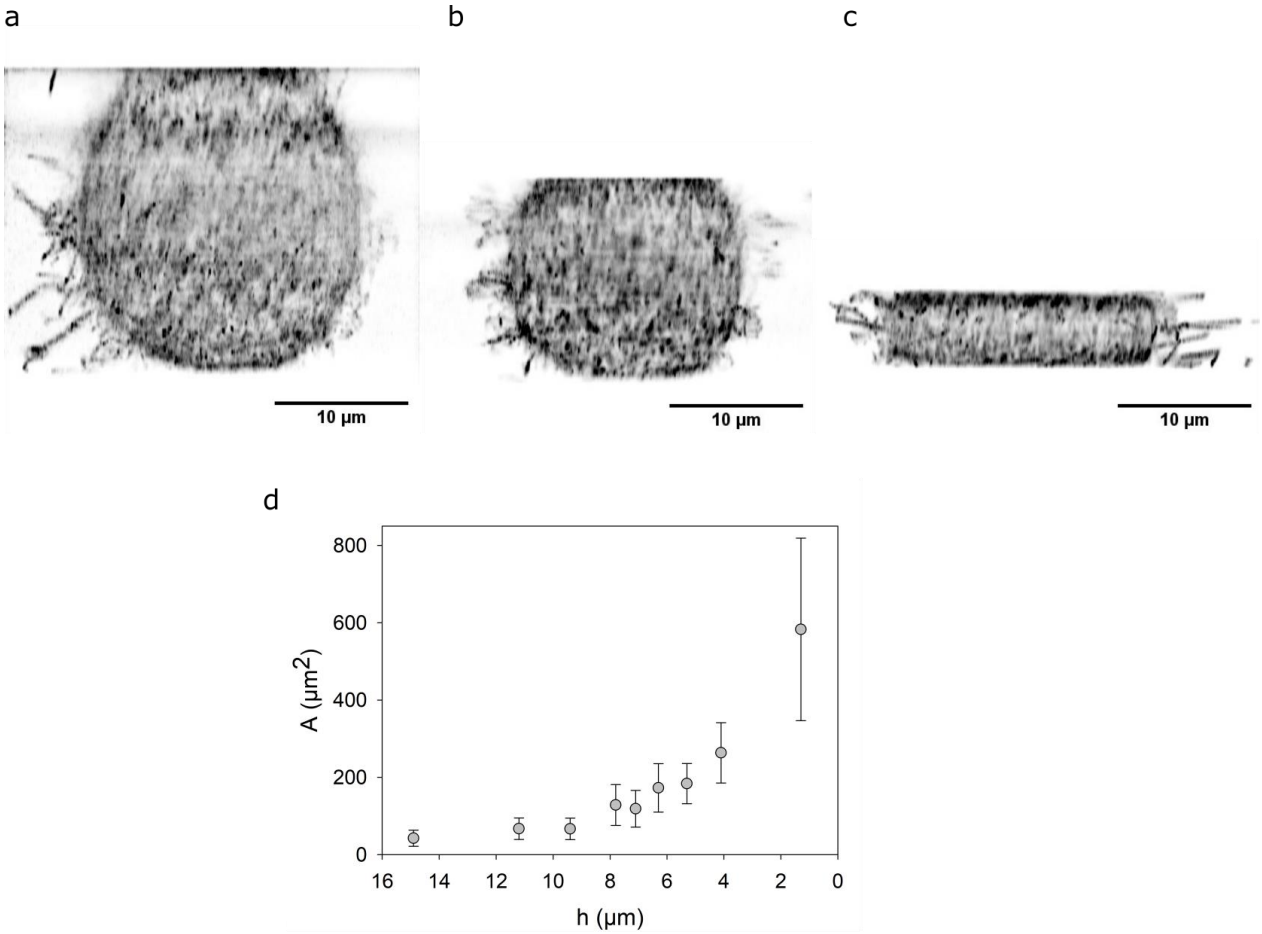

Figure 3.1: *Confinement change shape of rounded HeLa MyrPalm-GFP cells.*

Membrane marker MyrPalm is shown in black.

(a): spherical non-confined cell; (b): cell under 11 µm confinement; (c): cell under 5 µm confinement

(d): contact area between cells and bottom glass plotted as a function of confinement height. The number of cells in each conditions n= 24-162. Error bars represent standard deviation.

b. Confinement induces volume loss

We measured the volume of non-adhesive HeLa cells confined at different heights. As in the first part, we used FXm for the volume measurements, a detailed experimental procedure is described in Materials and methods. An important point to note is that the confinement pressure could deform the holding pillars and introduce small deviations in the height of the chamber and thus the absolute volume measurement. We have thus taken extreme care of calibrating heights for each experiments and discarded the confinements in which the height deviated too much from the expected value (typically, we use a

fluorescent marker in the medium, and its intensity should be proportional to the height, so comparing the various wells gives a linear relation and deviation from that gives a correction factor, or a criterium to eliminate a well).

The average cell volume decreased with the confinement height (Fig. 3.2a), to reach large volume losses: cells at 5µm confinement have 35% less volume than non-confined cells. Because we know the confinement height and mean volume of cells from the FXm measure, we can calculate the apparent surface area by using geometrical assumption of simple cell shape – sphere and cylinder (here we call surface area, the area of the apparent surface of the cell, or of its cortical part, which is not the same as the total surface area of the plasma membrane, which has a lot of folds and protrusions not taken into account in this measure –see the section 4 of the results). The analysis of the surface area indirect measure showed that cells kept surface area constant down to 5 µm confinement, accommodating the shape change mostly through the loss of volume (Fig. 3.2b). Lower confinement (less than 5 µm) induced strong morphological change in HeLa cells, as previously reported (Liu et al. 2015) – cells displayed a strong and sustained blebbing activity (Fig.3.2c). This made it much more difficult to measure a surface area (see images in Fig 3.2c), nevertheless, assuming a simple surface (blebs are small), showed that the apparent surface area increased a lot, meaning that the adaptation to the shape change involved in this case both volume loss and surface extension.

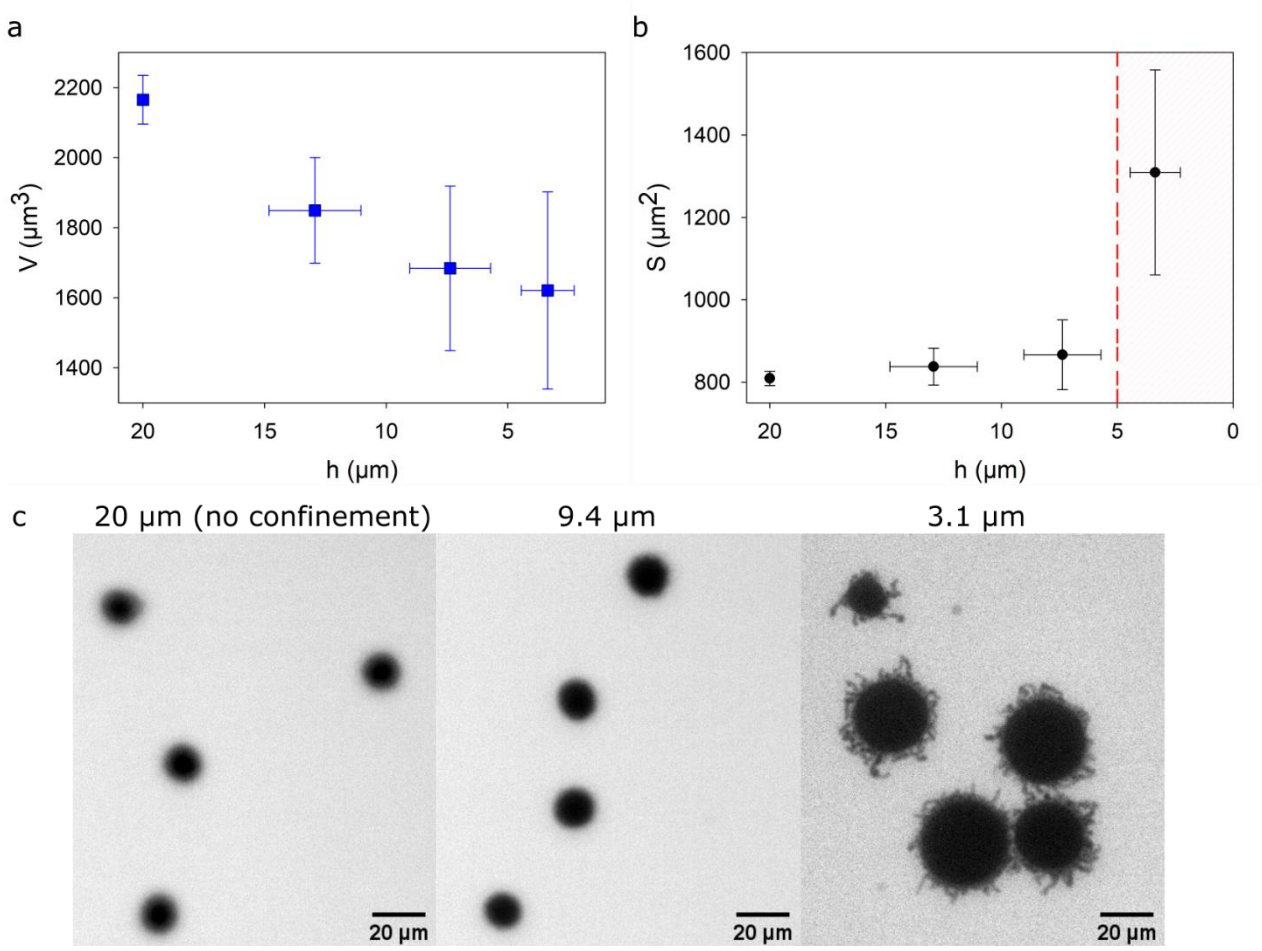

Figure 3.2: *Average volume and apparent surface of cells confined by different height.*

20µm represent non-confined cells.

(a): Each data point obtained by averaging the mean volume values of independent experiments (N=14-17), error bars represent standard deviation. Mean volume values of an independent experiment were obtained by averaging volume of individual cells in the population (n ~ 100).

(b): Each data point represents projected surface area extracted from volume values at panel A. Error bars represent standard deviation.

(c): FXm images of non-confined cells (left), confined with 9.4 µm (middle) and with 3.1 µm (right). Low confinement induces cell blebbing.

These results fit the working model proposed for the cell spreading experiments: confinement was performed at a very fast rate, it thus corresponds to the case of fast and large deformations which cannot be accommodated thanks to actin and membrane turnover. In order to maintain a homeostatic value of surface/membrane tension, to avoid membrane ruptures, cells would decrease volume (~20% volume loss for 5-15 µm confinement range) rather than increase apparent surface area (~5% surface extension for 5-

15 µm confinement range). This could be because the acto-myosin cortex limits the release of membrane stored in membrane reservoirs and folds (Fig.3.3).

However, when the applied deformation reached height lower than 5 µm, it induces not only volume loss, but also a detachment of the plasma membrane from the cortex (formation of blebs) allowing surface area extension. Note that the reason for extensive blebbing at low height corresponds to another study performed in the Piel team, not described here – it is due to an active response of the cell, corresponding to a sudden and sustained increase in contractility, caused by the deformation of the nucleus and the activation of a specific pathway at the level of the nuclear envelope. To avoid such an effect, it is possible to use enucleated cells (cytoplasts), but the study of their volume upon confinement has not been performed yet.

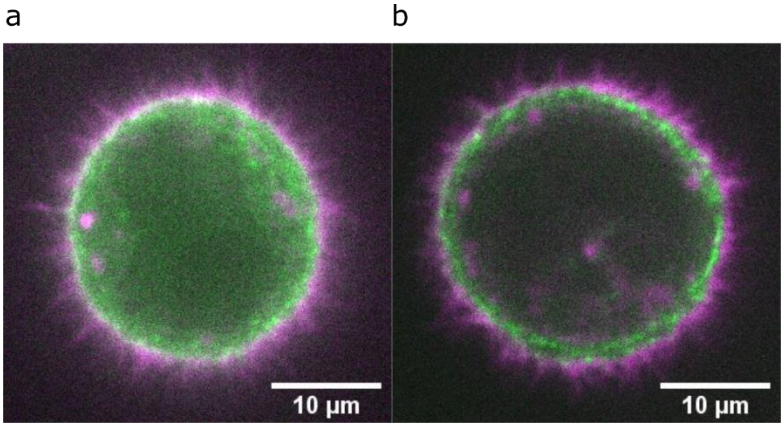

Figure 3.3: *Middle Z-plane of non-confined cell (a) and cell confined with 7.6 µm (b).*

Myosin (MYH9-GFP) is shown in green, membrane marker (CellMask) in magenta. Performed with 63X objective.

c. Actin disruption prevents volume loss under confinement

To test the hypothesis that the link between the plasma membrane and the actin cortex is responsible for the restriction in surface area expansion and this for the volume loss in response to confinement, we disrupted the actin cortex by Lat treatment. The advantage of the confinement experiment, compared to spreading, is that the deformation is externally imposed and it is thus easy to compare control and Lat treated cells, while for spreading cells the comparison was made more difficult because the Lat treatment affected the spreading speed. Treatment of cells with 2 µm Lat A induced a strong blebbing phenotype (Fig3.4a). Confined Lat treated cells also displayed large blebs (Fig3.4).

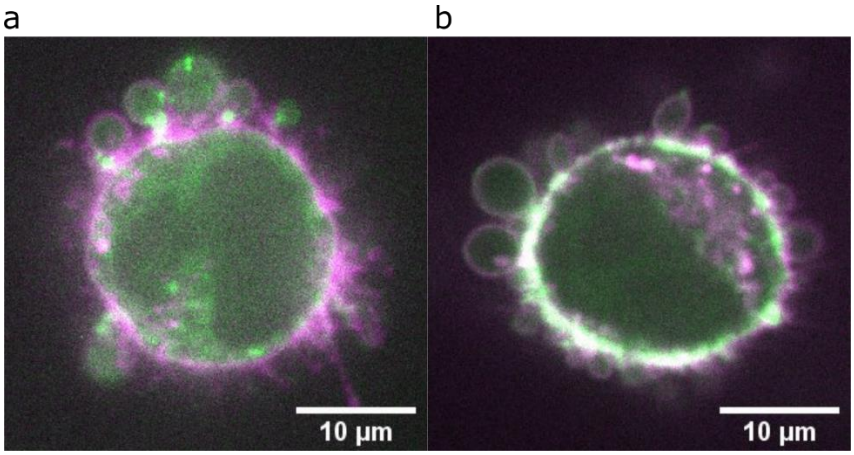

Figure 3.4: *Middle Z-plane of non-confined cell (a) and cell confined with 7.6 µm treated with 2 µM Lat A. Myosin (MYH9-GFP) is shown in green, membrane marker (CellMask) in magenta. Performed with 63X objective.*

We treated cells with two different concentrations of Lat (2 and 5 µM), then confined and measured their volume (Fig.3.5). Lat A treatment did not significantly increase volume (~3%) of non-confined cells, confinement cells treated with Lat lost much less volume than control cells.

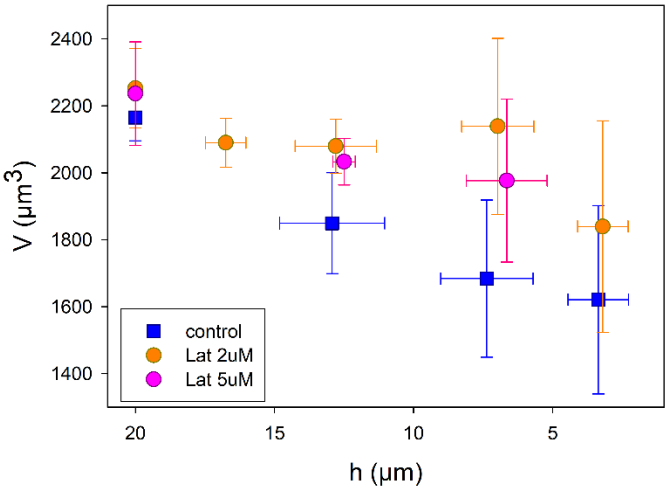

Figure 3.5: *Average volume of control and Lat treated cells confined with the different heights. For Lat 2 µM N=4-8 for different conditions, for Lat 5 µM N=2-7 for different conditions. Error bars represent standard deviation.*

These results are consistent with the hypothesis that volume loss upon deformation is due to the attachment of the plasma membrane to the actin cortex: Lat A treatment would allow deformation at constant volume because it facilitates opening of membrane reservoirs upon fast deformation, avoiding an increase of tension of the membrane upon confinement. The effect of Lat A should thus be to make the cell easier to deform (would deform more for a given force).

To test this hypothesis we measured cell deformability in collaboration with the lab of Dr. Jochen Guck. Real-time deformability cytometry (Otto et al. 2015) allows the mechanical characterization of large cell populations. Briefly, cells are flowed through a microfluidic channel constriction and deformed without contact by fluid shear stresses and pressure gradients (Fig.3.6a-e). Deformation (D = 1 − circularity) and size (cross-sectional area) displays the results in a scatter plot. We measured deformation and size of control cells and cells treated with different concentration of Lat (100 nM and 500 nM). We obtained that Lat treatment did not change cell size, which was consistent with FXm volume measurements, but, indeed, increased cell deformability (Fig.3.6f).

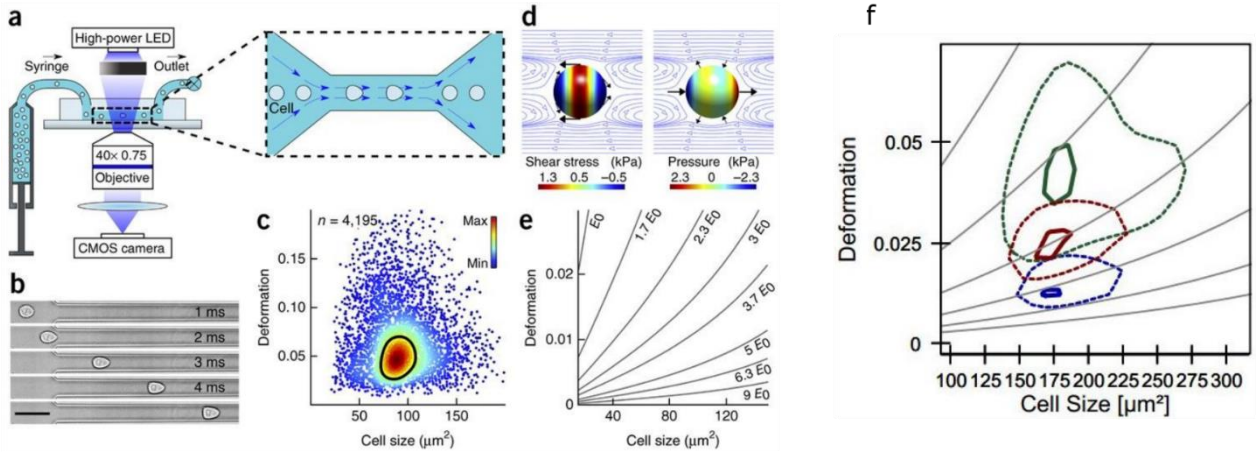

Figure 3.6: *Real-time deformability cytometry*

(a) Setup and measurement principle (inset shows a top view of constriction). (b) Time series of a cell deformed through constriction. Scale bar, 50 µm. (c) Scatter plot of deformation versus cell size (cross-sectional area) of 4.195 cells (dots) obtained in 45 s. Color indicates a linear density scale; black line, 50%-density contour. No cells were smaller than 20 µm^2. (d) Shear stress (left) and pressure (right) on the cell surface inside the constriction. Black arrows indicate stress directions; surface color indicates magnitude; blue lines show the flow profile in a co-moving reference frame. (e) Isoelasticity lines divide the size-deformation scatter plots into areas of identical stiffness for multiples of a given elastic modulus E_0. Panels a-e are reproduced from (Otto et al. 2015)

(f): Lat treated cells are more deformable than control cells. Control is shown in blue (n=2532), Lat 100 nM in red (n=355), Lat 500 nM in green (n=905).

d. Confinement induces volume loss in tens of milliseconds

At the population level, confined cells have a smaller volume than non-confined. However, with the setup used in the previous section, we were not able to follow dynamic volume change at the level of individual cells. To do this we used another confiner device developed in our lab (Le Berre et al. 2014), which allows to measure the volume of the same cells before and after confinement (from unconfined to ~10 µm for this experiment, see Materials and methods). We obtained that control cells lost on average ~13% of volume right after confinement (Fig.3.7a), while Lat treated cells lost only ~1% of volume (Fig. 3.7b). This is similar to what we observed before, but gives us access to the initial size of confined cells, and the dynamics of volume loss. Duration of the recording was limited for technical reasons; however, we did not observe any volume change for the few seconds following the immediate volume loss upon confinement. The striking observation from this experiment is that, in control cells, volume loss occurs between two consecutive images, separated by 500 ms. In these 500 ms, both the confinement step and the volume loss occurred. We observed the same volume loss in experiments performed at maximal frame rate (30 ms timelapse) and the volume loss and confinement occurred between two frames. Therefore, we conclude that confinement induces volume loss in a few tens of milliseconds, and that this volume loss requires an intact actin cytoskeleton (in the frame of our working model, this would be mostly the actin cortex, but bulk actin could also contribute to a bulk viscoelastic property of the cell leading to volume loss upon confinement).

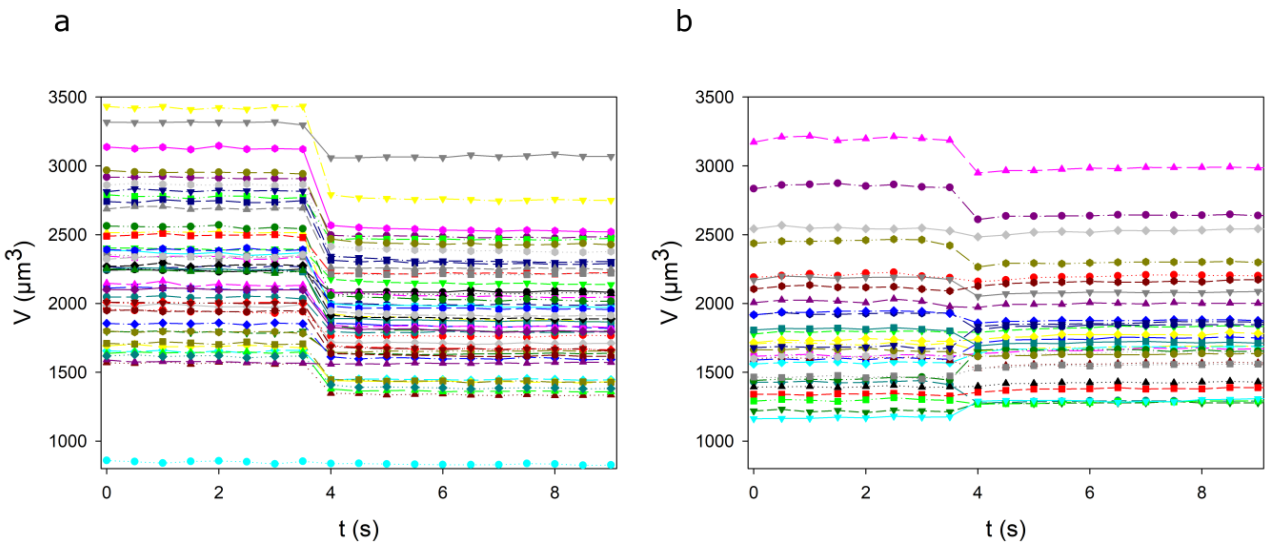

Figure 3.7: *Volume dynamic of individual control (a) and Lat treated (b) cells. Time frame 500 ms. Confinement was induced between 3.5 and 4s, cells lost volume within 500 ms.*

(a): All control cells lost volume when were compressed (11.2 µm), except the small cell which had an initial diameter almost equal to the confinement height. This cell kept its initial volume.

(b): Lat treated cells lost less volume than control under confinement (10.2 µm). Non-significant volume increase of some cells can come from the error introduced by confinement height estimations.

The speed at which volume loss occurs raises the question of the mechanism of volume loss induced by confinement – is it the same as during adhesion driven cell spreading?

1) Is volume loss an active process regulated by specific water and ion channels/pumps (regulatory volume adaptation) or the result of transient membrane rupture or increase in permeation?

2) What do cells lose under confinement: only water and ions (this would more likely correspond to the opening of specific pores/channels which filter large molecules, or activation of pumps) or full cytoplasmic content, resulting in loss of dry mass (this would be more compatible with membrane rupture and opening of large pores)?

Performing fast confinement experiments and recording images with a high NA objective at high frame rate, we observed a transient dilution of the fluorescent dye around the cells, with long trails of dimer regions emanating from the cells. Before confinement is applied, the chamber roof is a few tens of microns above the cells, and the cells appear as almost black objects in a bright background (Fig. 3.8a). At the first timeframe after confinement (here 100 ms), cells are compressed and long trails emanating from each cells are observed (Fig. 3.8b). These trails disappear in a few hundreds of ms (Fig. 3.8c). They could

correspond to the non labelled water coming out of the cells upon confinement, moving away with the stream lines of the fluorescent external fluid, which also has to flow due to the confinement step.

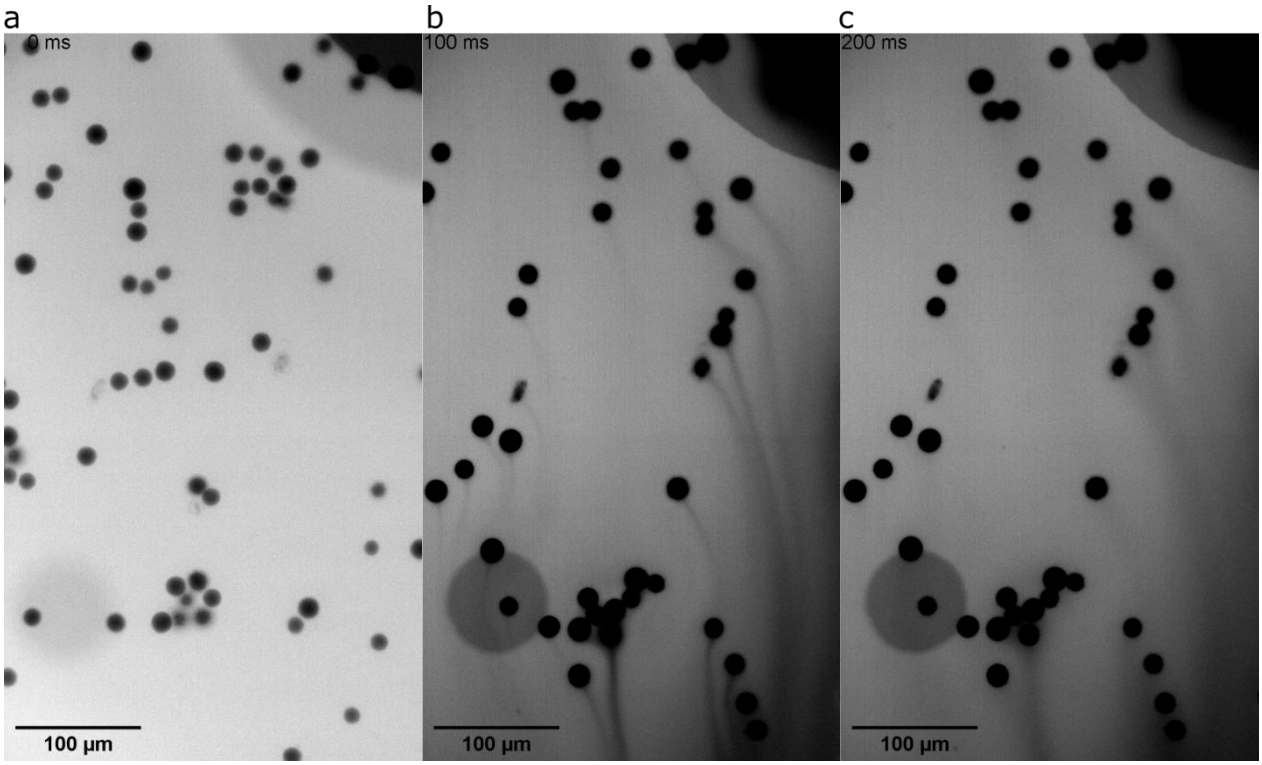

Figure 3.8: *Example of leakage induced by confinement*

(a): 0 ms non-confined cells

(b): 100ms cells are just compressed before this and previous frame

(c): 200ms ms after compression

e. Cells do not lose dry mass upon confinement

To distinguish between a leakage of cytoplasm or a loss of water/ions, we measured both volume and dry mass of confined cells. Cell dry mass is mostly due to large organic molecules that compose organelles, cytoskeleton, membrane, it can be measured by quantifying the phase shift of the light passing through the cells using quantitative phase microscopy (Aknoun et al. 2015). The result showed that, upon a confinement to 10 µm and 5 µm, cells decrease volume by ~10% and 30%, but their dry mass remains almost constant (Fig.3.9).

These results suggest that cells only loose water and possibly ions when they loose volume upon fast confinement. This rules out the hypothesis of cytosolic leakage or large membrane holes and rather favors the hypothesis of water/ion loss through specific channels/pumps/pores which do not let large molecules pass. To confirm this interpretation, we would need to have an experiment demonstrating the detection of dry mass loss upon an induced cytoplasmic leakage. This might be achieved with a strong osmotic shock leading to plasma membrane rupture.

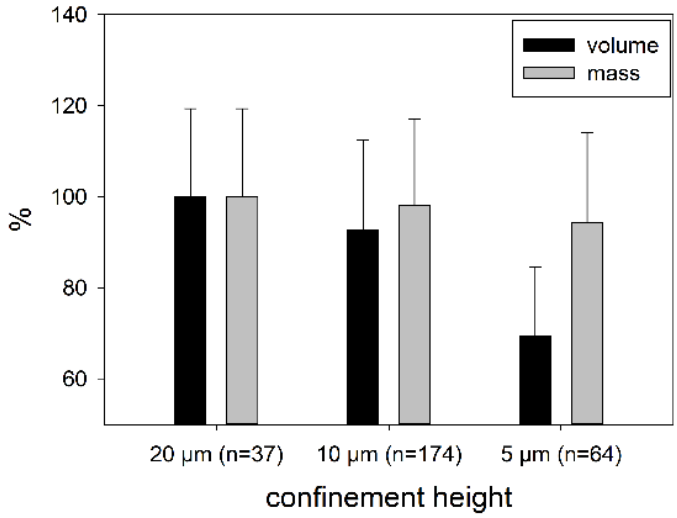

Figure 3.9: *Relative cell volume and dry mass upon confinement. Volume and mass normalized respectively by the values of non-confined cells (20 µm confinement height). Error bars represent standard deviation.*

f. Confinement induces death of ATP depleted cells, but not of control cells

Previous results from our lab showed that even strong confinement does not lead to cell death for a wide variety of cell types (Liu et al. 2015). Opening of the plasma membrane and cell death can be visualize live using propidium iodide, a molecule that cannot pass the plasma membrane and becomes fluorescent when bound to nucleic acids. Cells with ruptured plasma membrane and dead cells thus become strongly fluorescent.

We hypothesize that volume loss, by ensuring a reduced extension of the surface area and thus avoiding an excess is surface/membrane tension, could be a mechanism ensuring cell survival or integrity upon fast

confinement. Because our results using dry mass measurements suggest that volume loss might be an active process involving ion pumps, we decided to first poison all active processes in the cell by performing a depletion of ATP. We incubated cells in glucose-free medium supplemented with 6 mM 2-deoxy-D-glucose and 10 mM NaN_3. Cells incubated in just glucose-free medium were used as an additional control condition. We tested the effect of ATP-depletion on mitochondria of adherent cells (Fig. 3.10) and confirmed that the chosen experimental condition affect ATP-production and presence in the cells (Westermann 2012).

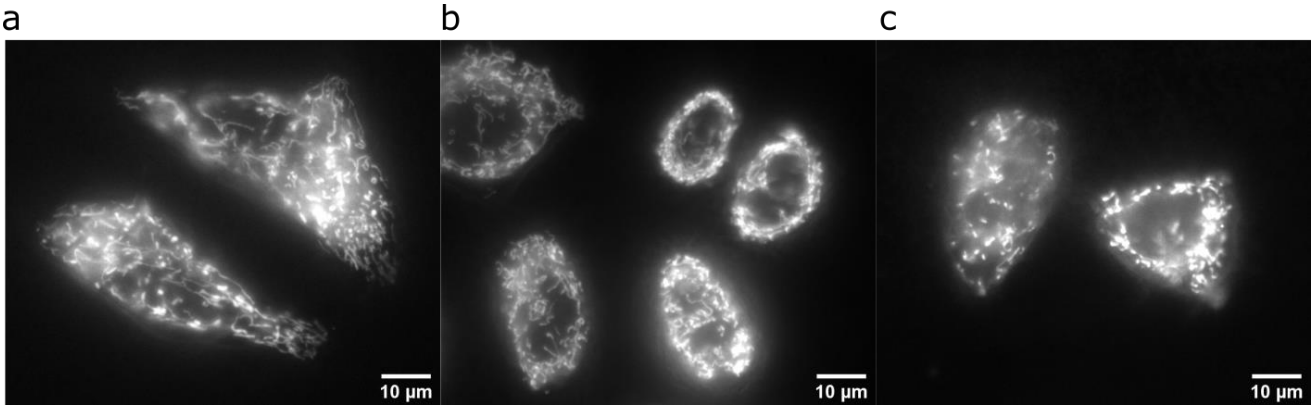

Figure 3.10: *Mitochondria of adherent HeLa stained with membrane potential dye TMRM*

(a): control cells have long mitochondria. Cells incubated in glucose-free medium (b) and ATP-depleted cells (c) have fragmented mitochondria, suggesting that ATP depletion treatment was efficient.

We measured the volume of suspended non-confined cells and found that ATP-depletion did not change the mean volume of the cell population, at least for the duration of treatment (30 min) assayed (Fig. 3.11a), and induced a minor level of cell death, not very different from the glucose free medium (less than 10% dead cells). Using propidium iodide as a marker of cell death (Fig. 3.11c), we found that ATP depletion increases the proportion of dead cells up to 27% under 5 µm confinement (only 2.5% for control cells and 12 % for cells in glucose free medium) (Fig. 3.11b).

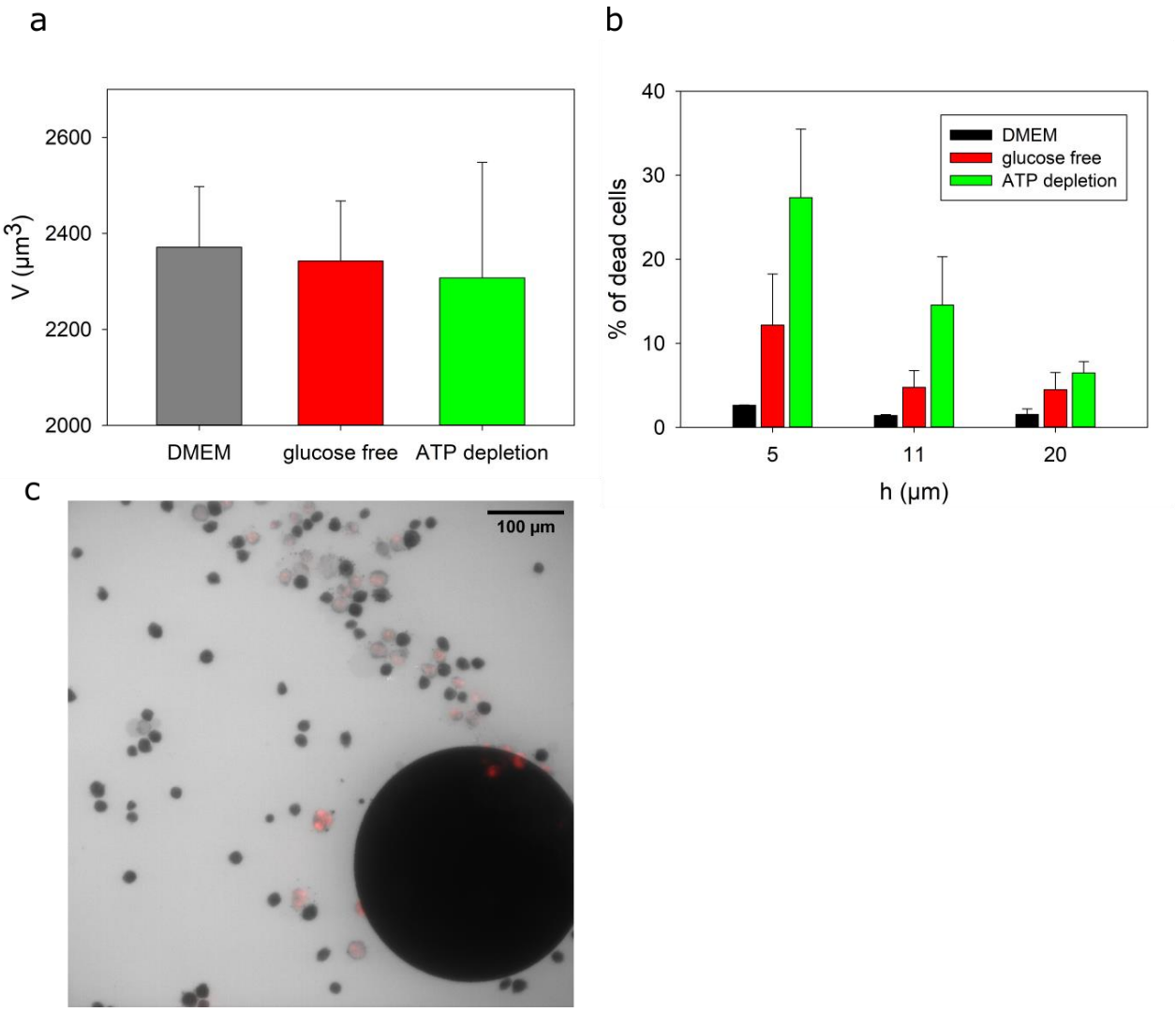

Figure 3.11: *Effect of ATP depletion on cell volume and viability*

(a): ATP depletion and incubation in glucose-free medium do not change mean cell volume. For each conditions N=4-7 independent experiments were performed, n~100 individual cells were measured for each experiment. Data points represent average values on independent experiments, error bars indicate standard deviation

(b): Percentage of propidium iodide positive cells for control cells and cells incubated in glucose-free medium/ATP-depleted under different confinement. Viability of control cells is not affected by confinement. Viability of ATP-depleted cells decreases with confinement height. N=2-5, n~100. Data points represent average values on independent experiments, error bars indicate standard deviation.

(c): ATP-depleted cells under 5 µm confinement, propidium iodide staining (red) indicates dead cells. Merge of GFP channel (for FXm) and mCherry (for propidium iodide), 20X.

ATP depletion thus alters the survival of cells upon confinement. However, this result can have different interpretations:

1) Decrease in ATP production reduces the efficiency of ion transport and, therefore, water flux (Demaurex and Grinstein 1994; Feranchak et al. 1998), and cell integrity is compromised because there is no volume loss – this would lead to a preferential death of the largest cells in the population, thus depleting it from a certain range of cell sizes – this is something we can test on the distribution of cells alive after confinement. We could also perform a dynamic confinement experiment to follow directly cell death and volume loss in single cells depleted for ATP and check if it is compatible with this hypothesis.

If this hypothesis is right, cell death in ATP depleted cells should be rescued in conditions in which cells do not loose volume upon confinement, for example with Lat treated cells. The issue with this experiment is the multiple treatments which might end up killing the cells independently of confinement.

2) ATP depletion could increase cell fragility by changing membrane composition, e.g. due to cholesterol depletion (Tilley et al. 1986). If this was the case, mechanical deformation could induce immediate cell death due to multiple membrane ruptures.

To disentangle these hypothesis, we need to apply more specific perturbations to affect the volume loss mechanism. Based on the results from the cell spreading experiments, we could test the inhibition of Arp2/3, or of ion transport.

g. Other cell lines

To confirm our findings, we also assayed RPE-1 cells. We also observed cell volume loss in RPE-1 upon confinement (Fig.3.12a). Volume loss was of the same order (about 25% for 5 µm confinement).

Additionally, we used human red blood cells (RBCs) that have biconcave shape under isoosmotic conditions. Human RBCs have unique property compared to most other mammalian cells. In particular, they lack any regulatory volume adaptation upon osmotic shocks and rather behave as perfect osmometers (Ponder 1935; Pafundo et al. 2010). Regulatory volume adaptation is a process by which, after an initial passive response to the osmotic shock (shrinking or swelling), cells return to their initial volume (Hoffmann, Lambert, and Pedersen 2009). Contrary to other cell types, when they are exposed to non-

isoosmotic conditions, human RBCs rapidly change their volume proportionally to the external osmolarity and do not come back to their initial volume.

RBCs are very small cells (about 90 μm^3). Therefore, we exposed them to an hypotonic medium to make them swell (50% of water). Cells were twice bigger than under isoosmotic conditions and we were able to confine them with the range of confinement heights accessible with our confiner method. Pre-swelled RBCs decreased their volume upon confinement (Fig.3.12b). Confinement induced rupture in some cells ("ghosts"), the volume of these cells was no taken into account.

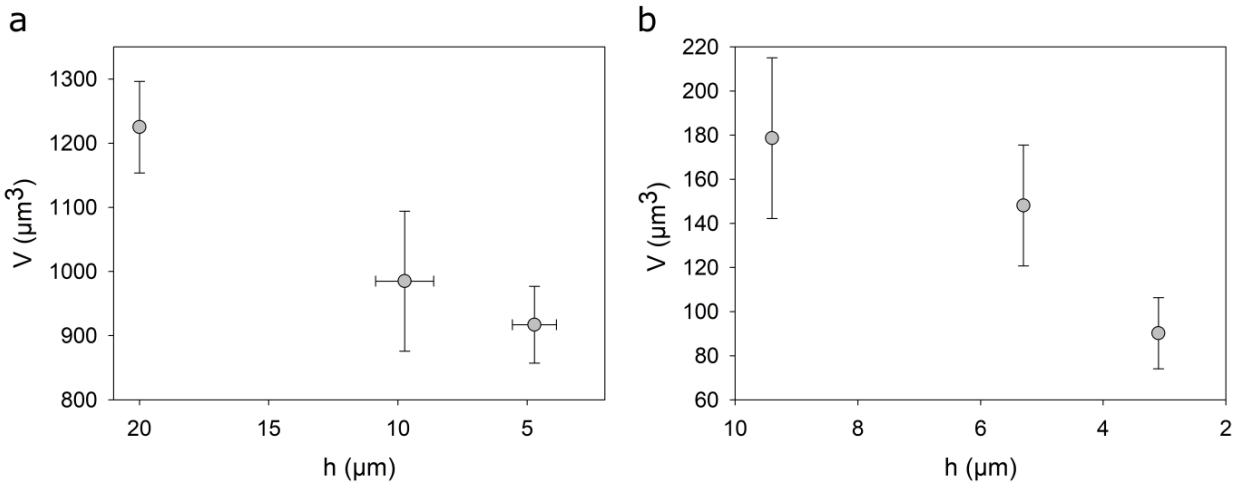

Figure 3.12: *Average volume of RPE-1 (a) and human RBCs (b) confined with different heights.*

(a): RPE-1 cells lose volume under confinement. 20 µm confinement can be considered as non-confined state. N=3-5 indicates independent experiments for different conditions, n=49-355 individual cells in each condition. Data points represent average values on independent experiments, error bars indicate standard deviation.

(b): Pre-swelled human RBCs lose volume under confinement. 9 µm confinement can be considered as non-confined state. Data points represent average values obtained from single experiment, n=158-275 for each conditions.

Volume loss upon confinement seem to be a general phenomenon, even in cells like RBCs. Depending on whether we consider that they have the same or a different behavior compared to HeLa and RPE1 cells, could orient our hypothesis regarding the mechanism regulating this volume loss: if we consider they show a similar behavior, we would tend to conclude that the mechanism ensuring volume regulatory decrease upon an hypoosmotic shock cannot be the same as the one involved here – another point in this direction is the very high speed of this volume loss.

h. Conclusion

We found that we can imposes strong and reproducible shape changes to non-adherent cells without killing them, using our confiner device. Those changes are accompanied by fast (less than 100ms) and large volume loss while cell dry mass remains almost constant. That volume loss increases with confinement height and can reach 35%, while the apparent cell surface area remains almost constant. We hypothesized that due to the binding of the plasma membrane to the actin cortex, and the slow turnover rate of the cortex and membrane compared to the deformation speed, membrane reservoirs/folds could not easily open upon such large and fast deformations. Volume loss would then avoid to stress the surface too much upon deformation. To test this hypothesis, we disrupted the actin cortex by Lat treatment, inducing large regions of membranes detached from the cortex (blebbing). Lat treatment did not change significantly the volume of non-confined cells, but confinement induced almost no volume loss in treated cells. A more specific test of our hypothesis would be to affect ERM-proteins, which are specifically involved in ensuring the binding of the plasma membrane to the cytoskeleton.

Another interesting direction for further investigation would be to impose a slow compression at timescales similar to cell spreading. We also lack direct force measurements to prove our model. This could be achieved using a flat AFM cantilever devices (Elisabeth Fischer-Friedrich et al. 2014). With this system however, the volume is not possible to measure with great precision.

We also observed that ATP depletion induced cell death under confinement while control cells had almost 100% viability. To interpret this result better, we need to perform these experiments with high temporal resolution: an increased fragility of the cell would lead to an immediate rupture upon confinement, while a defect in active ion regulation would lead to excessive intracellular pressure, or increased cell surface tension, leading to blebs, or membrane pores without inducing an immediate death.

Another perspective of this project is to monitor the fate of confined cells on longer timescale. Because we observed that these cells are able to survive and proliferate under confinement for tens of hours (other studies in the lab), but that they have lost water and not dry mass, we have thus produced cells which are much more dense than control cells. We could thus ask how this affect their growth, and whether and how they come back to a normal density.

One of the most intriguing observation is the timescale of volume loss induced by fast confinement. Our measurements are limited by 30 ms time resolution but they mean that cells lose more than 10% of their volume in less than 30 ms. This is much faster than volume changes induced by osmotic shocks (described

in the next section of results), which is supposed to provide a measure of volume permeation rate through the plasma membrane. Uniaxial compression could have a different mechanism than isotropic osmotic compression. For instance, we can speculate that the surface tension increase induced by confinement could lead to an increase of membrane permeability, potentially involving also opening of water channels. Another possibility is that confinement, by pulling on the membrane/cortex cohesive structure, thus potentially inducing fast movements of transmembrane proteins in the lipid bilayer, could induce a change in the lipid ordering, or very small transient membrane ruptures, to allow a faster efflux of water. To test the hypothesis of formation of pores/holes we could use membrane rupture markers, like CHMP4B-GFP (ESCRT III), or propidium iodide, previously used in the lab to study closure of laser induced pores (Jimenez et al. 2014).

Finally, we think that this mechanism of volume loss can be necessary for cell survival in response to fast and large deformations. Volume loss could release transient surface tension increase and bring tension to the homeostatic values that would prevent cell bursting.

Such fast and large deformations could be relevant for cells in the blood circulation, when crossing capillaries. Circulation carries a number of proliferating cells, such as white blood cells (immune cells), but also potentially cancer cells (Nath et al. 2018), as circulation is thought to be one of the routes for metastatic dissemination. The mechanisms allowing cells to survive large and fast deformations could thus be important to ensure survival of circulating cells, and could serve as targets to eliminate circulating cancer cells.

4. Osmotic shocks

a. Estimation of total plasma membrane area

Our results with cell compression raised some questions about cell permeability to water and plasma membrane availability. We decided to investigate these aspects of cell volume modulation using osmotic shock, which for decades has been the classical way to study cell volume regulation.

First, we wanted to estimate how much available plasma membrane area HeLa cells have. We used suspended HeLa cells placed in a volume measurement chamber coated with poly-L-lysine – with this surface treatment cells remained spherical but were stuck to the bottom plate even when the surrounding medium was exchanged to perform an osmotic shock. We measured the initial cell volume V_i before the shock and extracted the apparent surface area S_i for a sphere (Fig4.1a). Although the overall cell shape is a sphere, membrane staining shows, as expected, numerous membrane extensions/protrusions which could constitute large reservoirs (Fig.4.1b). When we replaced isotonic medium by pure distilled water, cells swelled rapidly (Fig.4.1d) and unfolded the plasma membrane protrusions, leading to a smooth surface (Fig.4.1c), and finally, burst. We measured cell volume V_{max} before bursting and extracted the surface area (Fig.4.1a). We obtained that cells maximum average increase volume is 6.3 times before bursting and their surface area 3.4 times compared to the initial apparent surface area of the sphere. This is similar to previously published data (Ping Ting-Beall, Needham, and Hochmuth 1993; Guilak, Erickson, and Ting-Beall 2002) and shows that we could easily access this potentially important parameter, also in other contexts described in the previous sections, by adding pure water at the end of the experiment to measure the total plasma membrane area. We concluded that the plasma membrane of cells in the isotonic medium is mostly stored in membrane reservoirs (folds, protrusions, etc…), as the apparent area is less than a third of the total available surface area of the plasma membrane.

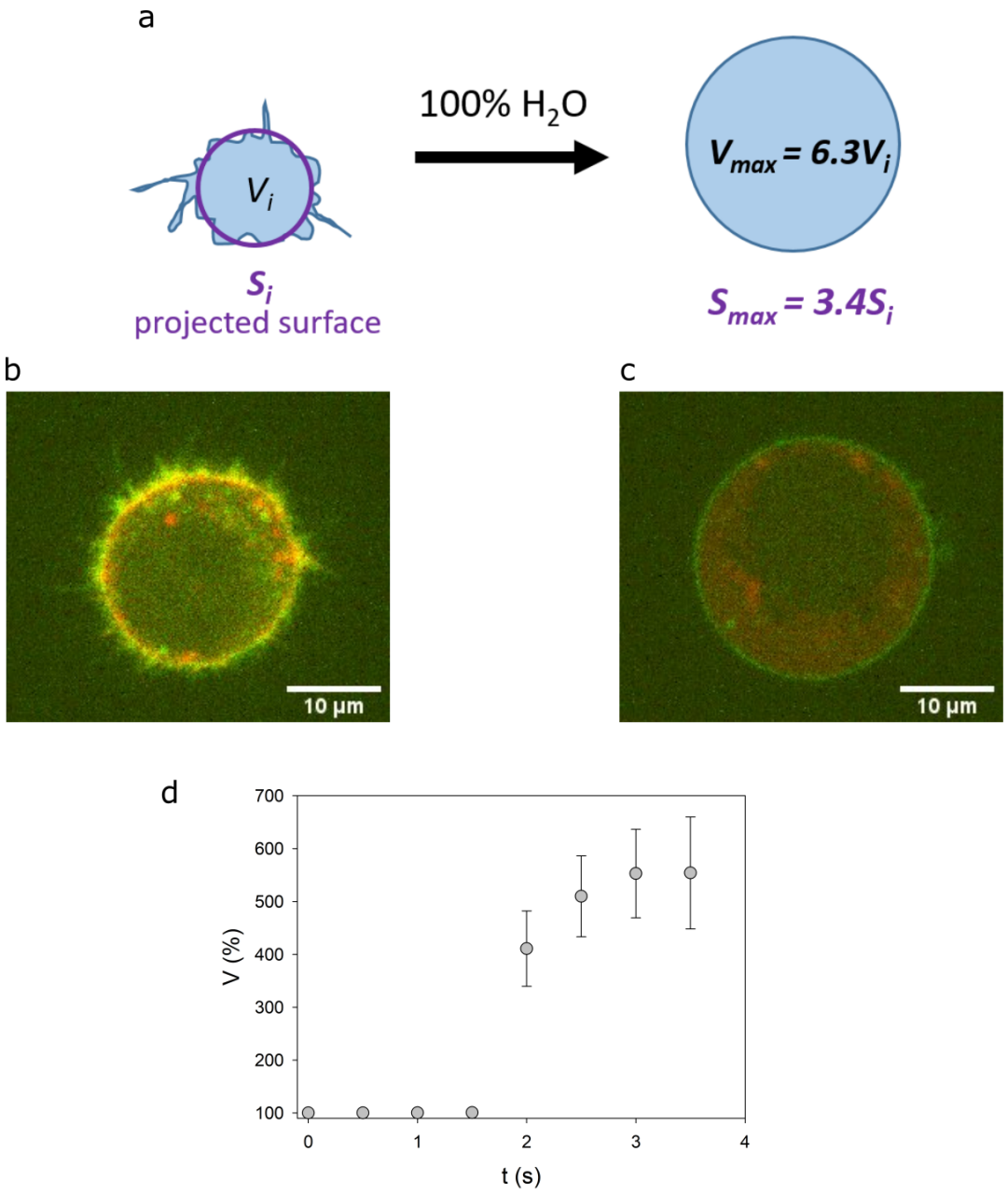

Figure 4.1: *Cells unfold their plasma membrane in response to extreme hypoosmotic shock.*

(a): schematic representation of the experiment

(b, c): The same cell in isotonic medium and before bursting. LifeAct is shown in red, plasma membrane stained with Cell mask is shown in green. The cell in isotonic medium has a spherical shape and contains membrane reservoirs. Swelling led to membrane unfolding and actin cortex disruption.

(d): Averaged normalized volume of n=26 cells exposed to distilled water. The isotonic medium was exchanged to water between 1.5 s and 2 s. Error bars represent standard deviation.

b. Initial passive response to osmotic shocks at the level of the cell population

When external osmolarity rapidly changes, cells passively swell/shrink with respect to osmotic pressure difference (Ponder's relation (Ponder 1935)). After this initial volume response, cells tend to come back to the volume values, which they had before the shock – regulatory volume decrease/increase (RVD/RVI).

First, we wanted to compare our results for passive response obtained with FXm to previously published data. This is also a way to validate our volume measurement method. The isotonic medium was quickly exchanged to a medium with a different osmolarity by flowing the medium over the cells – the speed of medium exchange was checked using a fluorescent dye in the medium (see Materials and methods). For the hypotonic shock, we used a mix of medium and water, for hypertonic, medium with addition of PEG400. Each solution was measured, for all experiments, using an osmometer, so we use the real osmolarity value and not an estimated one from the dilution/addition. One aspect which could be improved for hypoosmotic shocks (especially for the study of the active response) would be to ensure that only osmolarity changes and not the concentration of other important species (sugars, other nutrients, ions (Fernández et al. 2013)). Here we performed hypo-osmotic shocks, like in most other papers, by just diluting the medium with water.

Our results showed that, on average (averaging the response of many single cells for each osmolarity), the cell volume follows, as expected the Ponder's relation (Figure 4.2) (Eq.10): where V_{iso} and P_{iso} indicate initial volume and isotonic pressure, V indicates volume of the cell at the next time frame after exchange of isotonic medium to the medium with osmotic pressure P; R indicates the so called osmotically active volume fraction; and $(1-R)$ is an osmotically inactive volume fraction (excluded volume).

Similar to the previously published results we found that R=0.68 for control cells (Fig.4.2). Cells with depolymerized actin (by 2 µM Lat treatment) displayed a similar slope (R=0.71), which is also coherent with previous studies (Pritchard and Guilak 2004; Zhou et al. 2009).

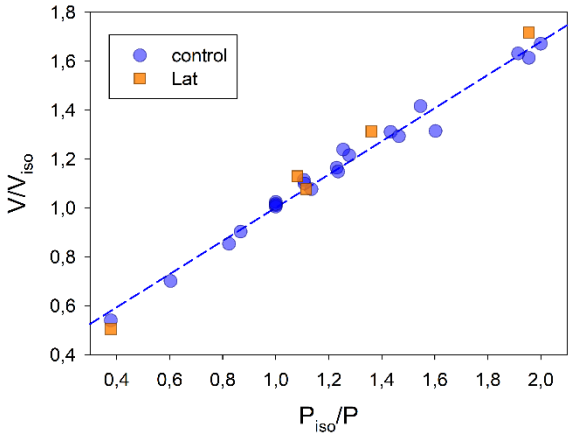

Figure 4.2: *Average passive volume response of the cell population to osmotic shock. Each point represents the mean of independent experiment; n~54 individual cells were measured in each experiment. Linear fit for control data points gives slope 0.71 with correlation 0.99.*

c. Diversity of passive response at the level of individual cells

Although when averaging for a cell population, the volume response to osmotic shock perfectly follows the Ponder's relation with a slope R=0.71, there is more diversity at the single cell level. For instance, there is a large distribution of individual cell volume increase in response to the same hypotonic shock in the same experiment (Fig.4.3a). We thus decided to calculate the osmotically active fraction R for individual cells from different experiments (Fig.4.3b). We obtained that, as expected, R did not depend on the magnitude of the shock both for control and Lat A treated cells (Fig.4.3c). However, we found an interesting tendency: smaller cells had a larger osmotically active fraction than bigger cells (Fig.4.3d). We can speculate that bigger cells have a larger fraction of solid components occupying the total cell volume than smaller cells; in other words, smaller cells might be more diluted than bigger cells. Because smaller cells are more likely to be early in their cell division cycle, it could be associated with the cell cycle-dependent dry mass production. Nevertheless, recording of mass and volume in single cycling cells (performed for another study in the lab and not shown here) rather suggest that during a few hours following mitosis, cells tend to be more dense. Another hypothesis is that the passive response is not defined only by the applied pressure, but also by other intrinsic cell properties, for example affecting plasma membrane permeability, or the speed of the trigger of the active response (which might limit the total volume gained in the passive phase – there is not a clear separation between the two phases, making it unclear, for single cells, whether they reached their passive equilibrium volume before the active

response starts). That could indicate that the initial volume response is not fully passive in individual cells, but that the cell-to-cell variability in the active part averages out at the population level, resulting in a good agreement with the Ponder's relation when averaging over many cells.

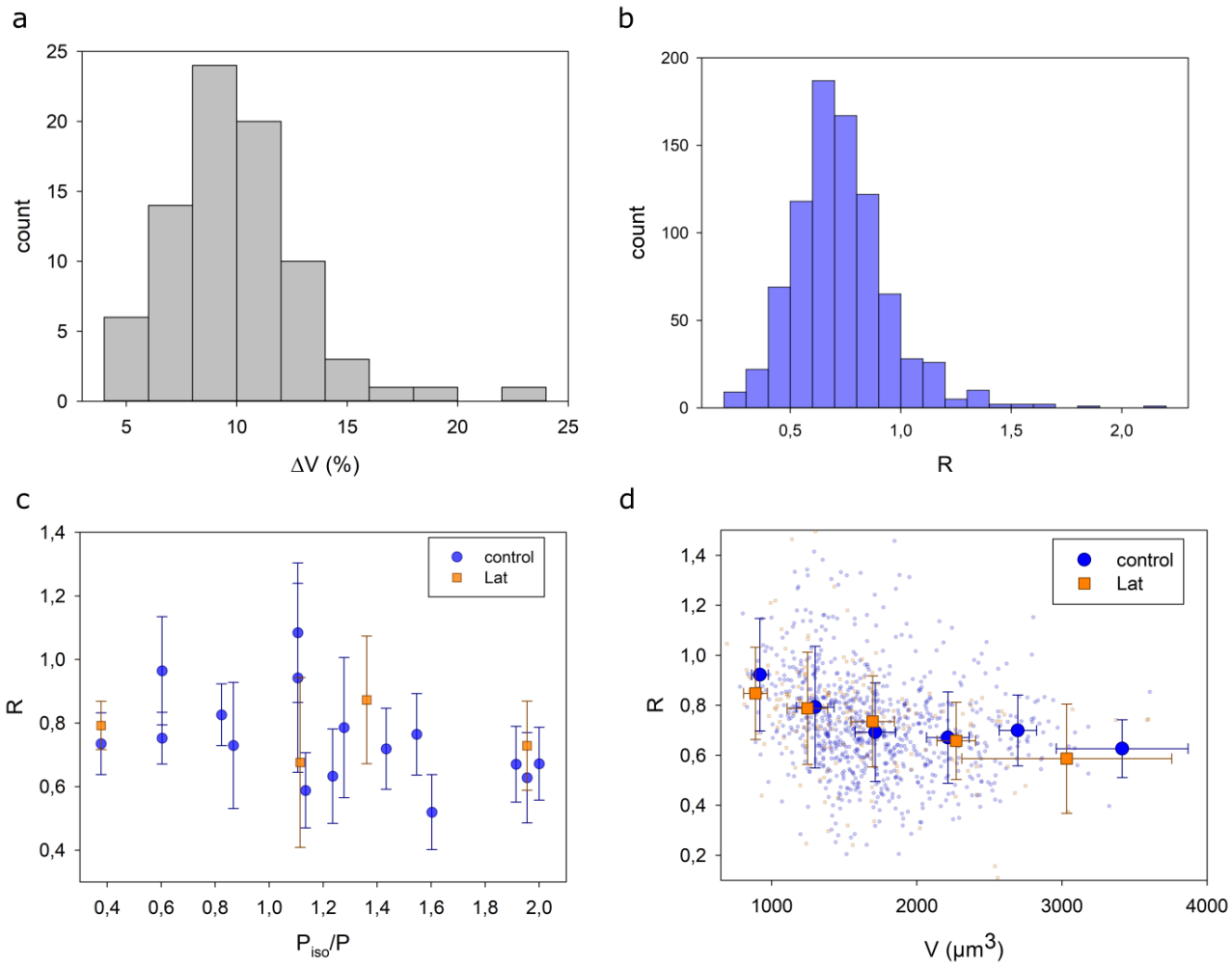

Figure 4.3: *Diversity in single cell response*

(a): Distribution of relative volume increase in response to the hypoosmotic shock $\frac{P_{iso}}{P} = 1.1$ *within a single experiment.*

(b): Distribution of osmotically active fraction R for individual cells from different experiments.

(c): Mean R values for individual experiments plotted as a function of applied osmotic pressure. Error bars represent standard deviation.

(d): Mean R values for different ranges of initial absolute cell volume. Small cells tend to have larger R, than big cells. Error bars represent standard deviation.

d. Dynamics of the passive response to hypoosmotic shock

The passive response to osmotic shocks is fast (a few seconds) and in most studies, there is no access to a good temporal resolution so the response is seen almost as a step increase/decrease in volume. In studies with good time resolution, the measure is usually not made to follow individual cells. Our method has no limitation in the speed of acquisition other than the speed of image transfer from the camera, and it gives single cell measures. We thus thought that it could be interesting to re-investigate with a good time resolution, the kinetics of volume change in the passive response. This could clarify what limits the speed of volume change, a question that remains open so far: is it limited rather by permeation through the membrane (and should thus be proportional to surface area – but which one? Apparent or total?) or is it limited by bulk volume expansion (e.g. due to the poroelastic properties of the cytoplasm)? Is there a contribution of the cell cortex for the very initial response, before the membrane detaches?

We used high temporal resolution (100 ms time frame). We observed that control cells increased their volume (in %) faster when the shock was stronger (Fig. 4.4a). To quantify it we calculated the initial speed of swelling for individual cells by performing a linear fit on the first time points. We obtained that on average the speed of swelling increased with the magnitude of the shock (Fig.4.4b). For Lat A treated cells this trend was not so obvious, but we cannot conclude at this point because the dataset is not complete (too few measures for the two points which do not follow the general trend).

To obtain a swelling time constant τ we used exponential fitting for individual cells:

$$V_t = V_i + (V_{max} - V_i)(1 - e^{-\frac{t}{\tau}}) \qquad \textit{(Eq. 23)}$$

where V_{max} is the maximum volume reached after shock and V_i is an initial cell volume before the shock – note that the individual cell curves are not always very well fitted by this equation and that V_{max} is not always well defined.

For both control and Lat A treated cells we observed some increase of τ with the magnitude of the shock (Fig.4.4c). However, this result has to be confirmed with more experimental data and more work on the fitting and sorting of individual cells – the longer time constant observed for Lat A cells could be due to the fact that they show less volume regulatory decrease and thus display more curves with no clear inflexion point to define V_{max}.

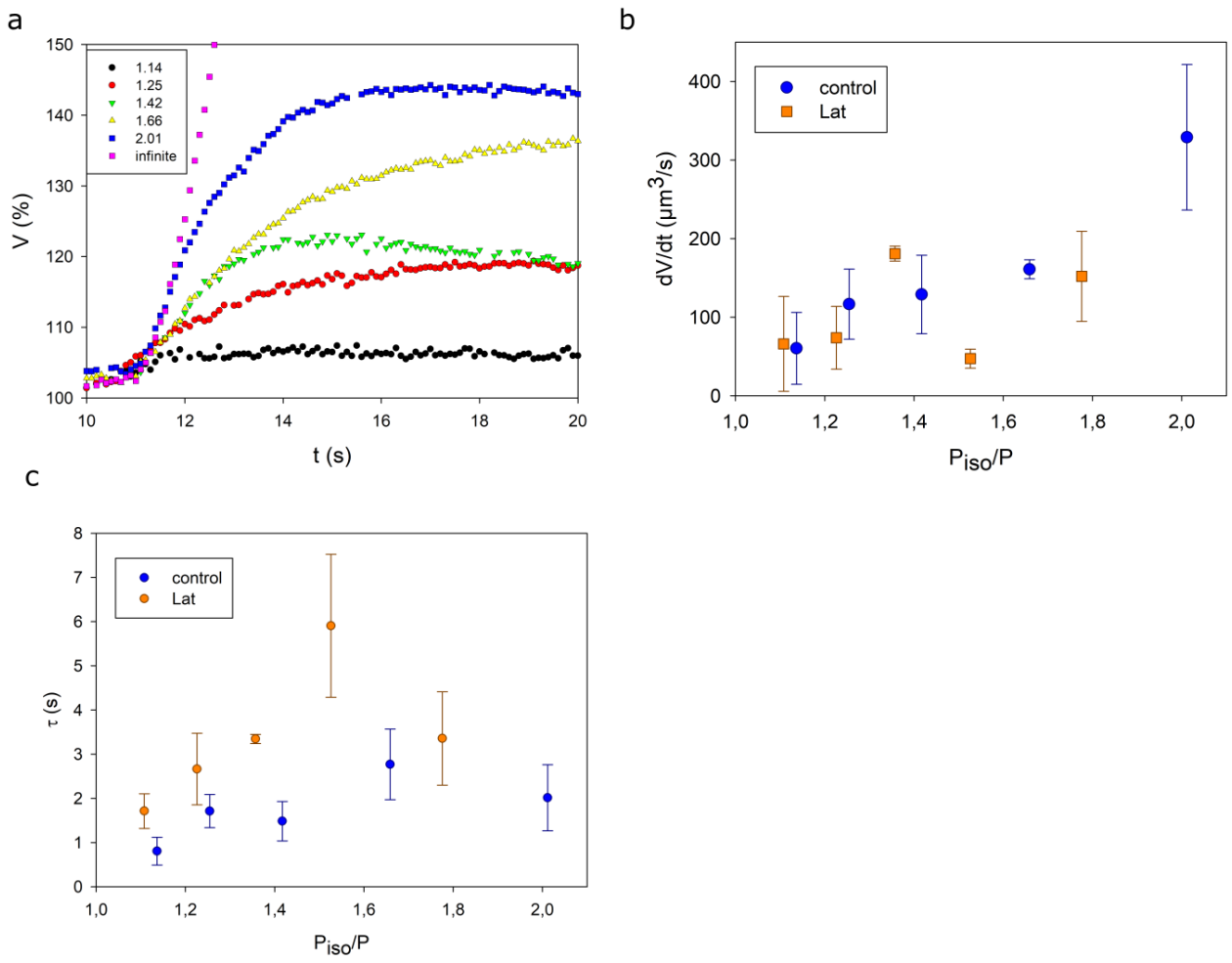

Figure 4.4: *Initial response to hypoosmotic shock*

(a): Examples of typical volume dynamic of individual cells in response to the osmotic shock of different magnitudes. The value at the legend indicates P_{iso}/P, "infinite" corresponds to the 100% of H_2O as P=0 mOsm.

(b): Median values of swelling speed of individual cells plotted as a function of applied pressure. n~10 individual cells were measured for each condition. Error bars represent standard deviation.

(c): Median values of swelling time of the same cells as in (b) plotted as a function of applied pressure. Error bars represent standard deviation.

Unlike cell confinement between two horizontal plates, we were able to follow the initial cell volume response to the osmotic shock. Classically hypoosmotic swelling is considered as a passive process that takes a constant time, which is independent of the shock magnitude and F-actin. We observed that swelling for control cells on average had a typical time of 1.76±0.64 s and we observed some increase of swelling time with the increase of the magnitude of the shock. Our data also showed that actin disruption

increases the swelling time if compared with control cells for a similar magnitude of the shock. But the interpretation of this typical swelling time is not yet clear (Fig.4.5). For instance, if water movement is limited by poroelastic cytoplasm, swelling time should be scaled with cell radius $\tau \sim R^2$. Although we need more experimental data, our results (sections **c** and **d**) suggest that swelling kinetics could also depend on a variety of other parameters. One problem which prevented us to reach a conclusive statement is that the range of initial cell radius was not large enough. To improve this, we will produce larger cells using cell cycle progression inhibitors such as Roskovitin (Clotilde Cadart et al. 2018).

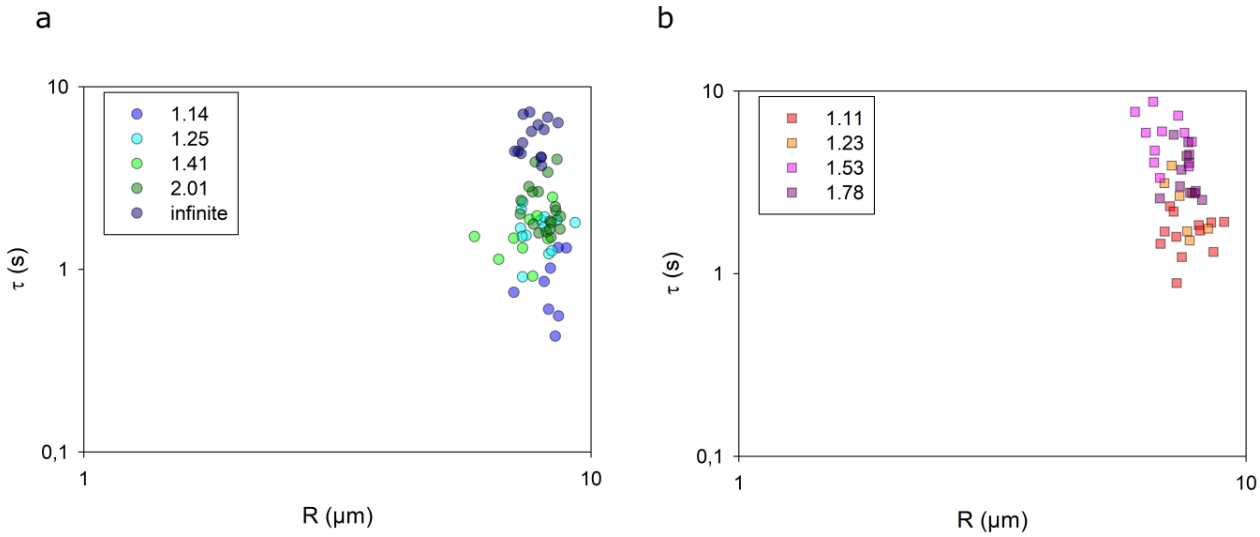

Figure 4.5: *Swelling time as a function of initial cell radius for control (a) and Lat treated cells (b). The values at the legend correspond to P_{iso}/P. Each point represents an individual cell.*

We will complete this study with hyperosmotic shocks, and with ATP depleted cells, or cells treated with drugs inhibiting the volume regulatory responses (NHE1 or VRAC inhibition) to avoid the complication in measuring the swelling time due to the initiation of the volume regulatory increase/decrease overlapping with the passive response.

e. Regulatory volume decrease/increase

Finally, we investigated the active adaptation, regulatory volume decrease/increase (RVD/RVI), by following the cell volume during 1 h after the osmotic shock (Fig.4.2). We observed that, on average, cells exposed to hypertonic shock (mix of medium with PEG400) recovered their initial volume, showing perfect

adaptation (Fig.4.6a,c). RVI was uniform with a standard deviation of ~5% for all shock magnitudes. On the contrary, cells exposed to hypoosmotic shocks (mix of medium and water) did not recover their initial volume on average (Fig.4.6b,d). We noticed that during this adaptation individual cells had very diverse behaviors, and the standard deviation for the adapted volume was increasing with the increase of the shock magnitude from 7 to 18%. Fig.4.6d almost suggest a bimodal behavior, with a population of cells showing perfect adaptation, and a population showing no adaptation at all, resulting in an average behavior of partial adaptation with large standard deviation. This shows that previous experiments, which did not follow single cells in time (most of them), might lead to misinterpretation of the result.

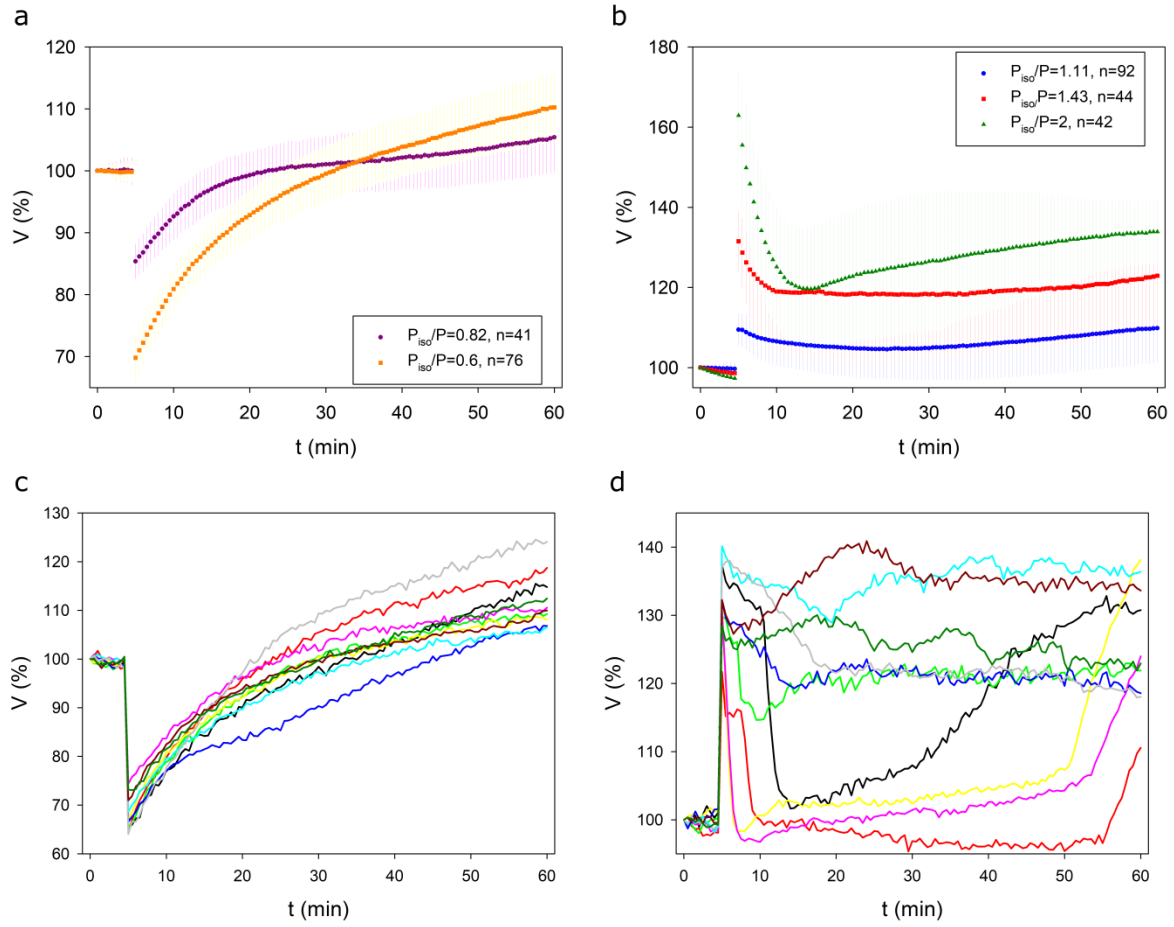

Figure 4.6: *Volume adaptation dynamic.*

(a): Average normalized volume dynamics in response to hyperosmotic shock. Error bars represent standard deviation.

(b): Average normalized volume dynamics in response to hypoosmotic shock. Error bars represent standard deviation.

(c): Examples of normalized cell volume dynamics of individual cells in response to hyperosmotic shock $P_{iso}/P=0.6$

(d): Examples of normalized cell volume dynamics of individual cells in response to hypoosmotic shock $P_{iso}/P=1.43$

To quantify these single cell behaviors, we decided to analyze the relative volume change of individual cells at a given time points (10 min after the osmotic shock, because at this time most cells have completed the volume adaptation) as a function of the initial passive volume change. This graph clearly shows the two population of non-adapting and perfectly adapting cells (Fig.4.7), with more complex behaviors appearing for large shocks.

1) No adaptation. The percentage of cells that did not adapt at all decreased with the magnitude of the shock both for control and Lat treated cells. We can speculate that small shocks do not significantly increase surface tension or other activators of the regulatory volume decrease pathway. It could be coherent with the fact that also slow osmotic changes do not activate RVD (Mola et al. 2016).

2) Partial adaptation: cells decrease their volume, but do not come back to the initial values. Most of the cells adapt partially after osmotic shocks with high magnitudes. It could be because strong osmotic shock induce F-actin disassembly (Pritchard and Guilak 2004). Lat A treated cells have a larger percentage of cells that adapt partially to the high magnitude of shock.

3) Perfect adaptation: cells recover initial volume values or decrease their volume even below initial volume

Note that for passive volume increase of 50% or above (horizontal axis), it seems that the two main behaviors remain but shifted to lower values of adapted volume.

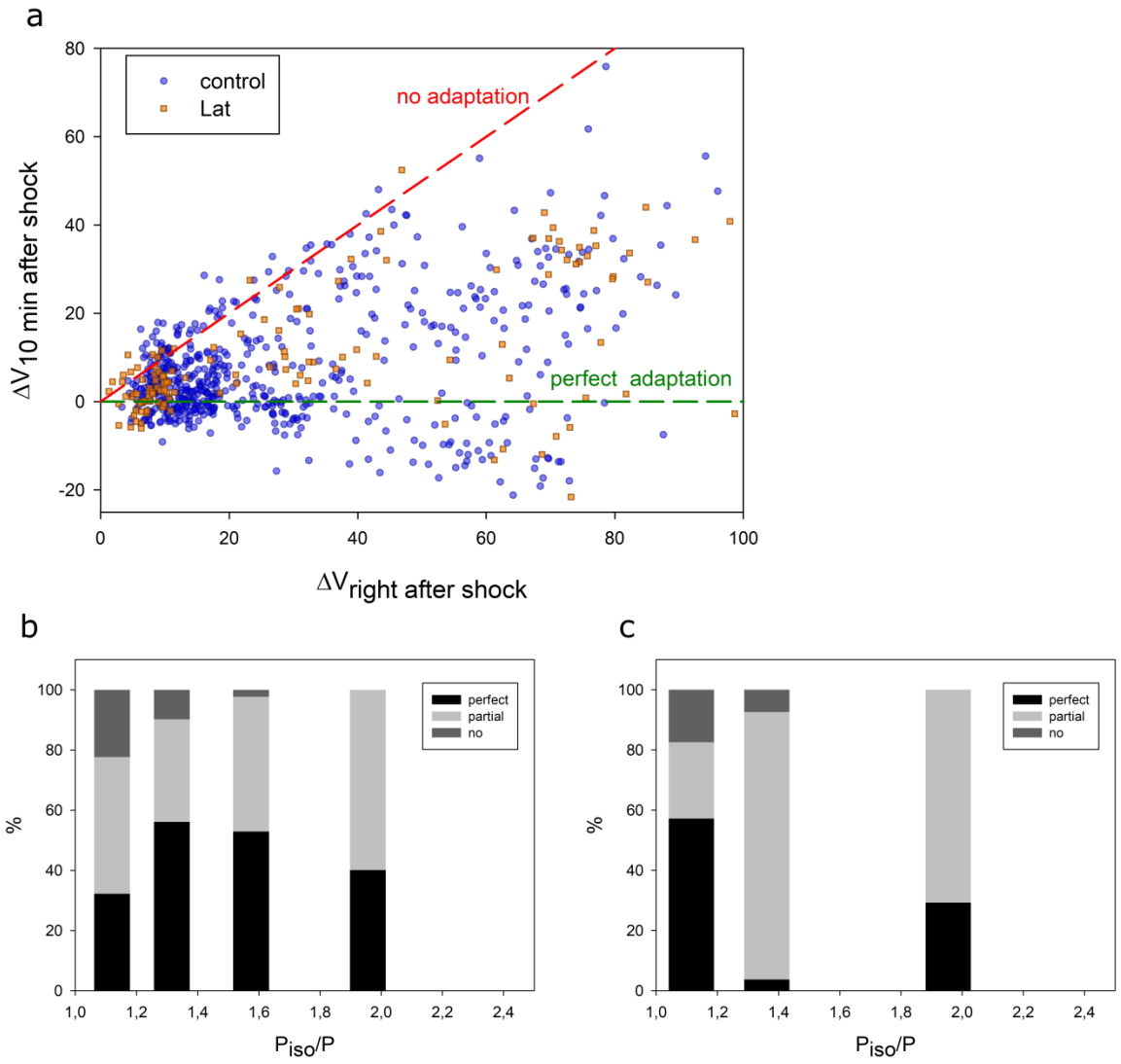

Figure 4.7: *RVD at the level of individual cells.*

(a): relative volume change in 10 min after shock as a function of initial volume increase for control and Lat treated cells for the different magnitude of the shock. Each point represents an individual cell.

Percentage of control (b) and Lat treated (c) cells with different adaptation regimes for.

Additionally, we analyzed the adaptation time τ extracted from an exponential fitting of volume curves for individual cells (in cases in which an exponential fit was possible):

$$V_t = V_{max} - (V_{max} - V_f)(1 - e^{-\frac{t}{\tau}}) \qquad \textit{(Eq. 24)}$$

where V_{max} is the volume right after shock (passive volume increase) and V_f is the final volume after adaptation.

We observed that for shocks of low magnitude, RVD was slower than for high magnitudes. Partial actin disruption tended to decrease the duration of the recovery phase.

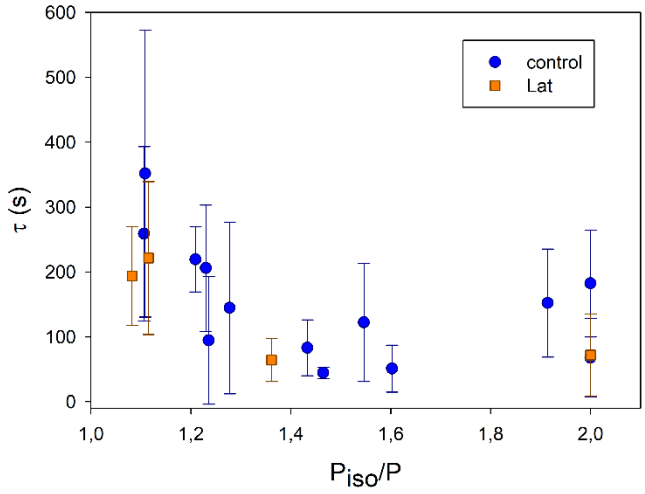

Figure 4.8: *RVD time.*

Median values of adaptation time. n~45 individual cells were measured in each condition. Error bars represent standard deviation.

f. Conclusion

Taken together, our results show that the rather simple picture given by the averaged behavior of many cells hides a complexity of behaviors at the single cell level, which cannot be clearly explained with the current knowledge on cell responses to osmotic shocks. Besides further experimentation to consolidate the results, this study will also require new theoretical developments and new sets of experiments to decipher the origin of the variability in the single cell responses. Although this field was studied for decades, there are still plenty of open questions.

We could also draw some clear conclusions, confirming previous results: cells have a large amount of plasma membrane stored in reservoirs. That helped us to understand better our results with cell confinement and cell spreading, and our method allowed us to reproduce very clearly the Ponder relation.

Immediate volume response to the change of extracellular osmolarity was described almost a century ago on RBCs by Ponder (Ponder 1935). Since this time, initial volume response is considered as a passive process, where the cell can be described as a "perfect osmometer". We obtained that this model works well at the level of the cell population; however, we observed a big diversity at the level of the cell population. Our results showed that osmotically active volume fraction is larger for small cells, a result which we cannot explain at the moment. We mostly focused on hypoosmotic swelling; however, we would need to study the dynamic of cell shrinking as well, as it seems less variable from cell to cell.

We observed that hypotonic swelling has a timescale of 1.76±0.64 s. Our preliminary results showed that hypertonic shrinking also has a timescale of the same magnitude (example at Fig.4.9a showed that loss of 10% volume takes about 500 ms), whereas we were not able to detect dynamics of volume loss for confinement experiment, suggesting that it was much faster. Similar with spreading experiments we plotted volume-surface balance for cells exposed to those 3 deformation types: hypo-, hyperosmotic shock, and confinement (Fig.4.9b). It shows that, for a similar range of volume loss as for hyperosmotic shocks, confined cells extended their surface in the range of what is observed in hypoosmotic swelling. This illustrate that uniaxial confinement could share aspects of both hypoosmotic response (membrane/surface extension) and hyperosmotic shocks (volume loss and increase in density).

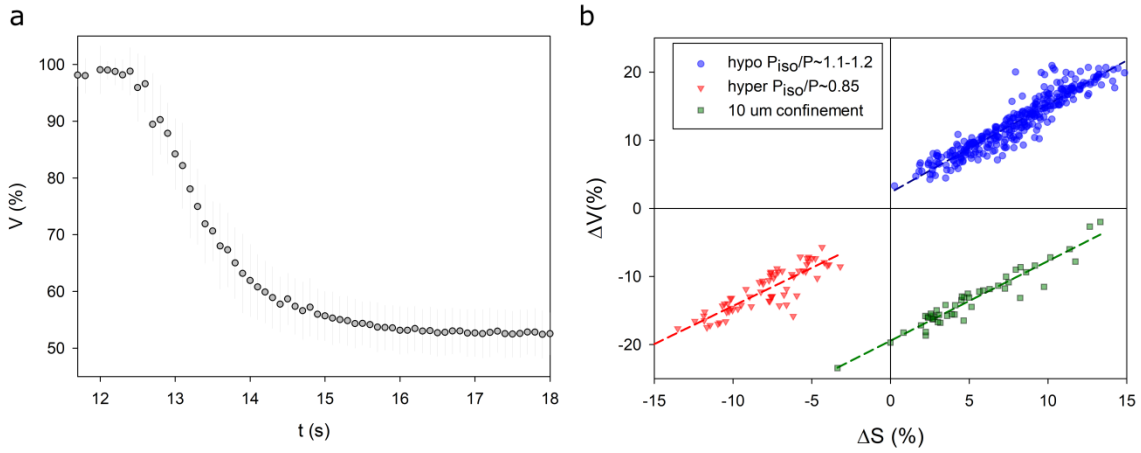

Figure 4.9: *Comparison of osmotic shock and confinement.*

(a): Average volume of n=16 cells in response to hypertonic shock.

(b): Relative volume change plotted versus relative surface change (surface was extracted from volume) of cells exposed to hypo/hyperosmotic shock and confinement.

We finally looked at active volume adaptation following an osmotic shock. We observed that HeLa cells uniformly recovered their initial volume after hyperosmotic shocks induced by PEG400, whereas hypoosmotic shock lead to a variety of single cell responses: no adaptation, partial adaptation, perfect adaptation. We observed that shocks of high magnitude (leading to actin disruption) and actin disruption by Lat A treatment increased the percentage of cells showing partial adaptation.

We also observed that adaptation time is faster for shocks of higher magnitude and for Lat A treated cells. This result is similar to previously published data (Pritchard and Guilak 2004). It indicates that the state of the actin cytoskeleton can modulate volume adaptation, probably, through activation of ion transport (S F Pedersen, Hoffmann, and Mills 2001).

There are two possible explanations for the origin of the variable single cell behaviors in terms of adaptation to an hypoosmotic shock: 1) either it is a process involving stochastic elements, or 2) the response depends on some cell properties that vary from cell to cell. A way to test this is to perform sequential osmotic shocks on the same cell. We chose to subject cells to two consecutive shocks of small amplitude, where we see a clear bimodal behavior (Fig.4.10). We observed that 70% of cells adapted (partially or perfectly) after the first shock. When these cells were exposed to the second osmotic shock, about half of them adapted (Fig.4.10a). 100% of the cells that did not adapt after the first shock did not adapt after the second shock as well (Fig.4.10b). This suggests that the answer could be more complicated, with a memory effect on top of a stochastic process. The shock itself could alter the cell in a stochastic manner, leading to cells which adapt or not. Once a cell is in a non-adaptive state, it stays in this state, at least in the timescale we studied.

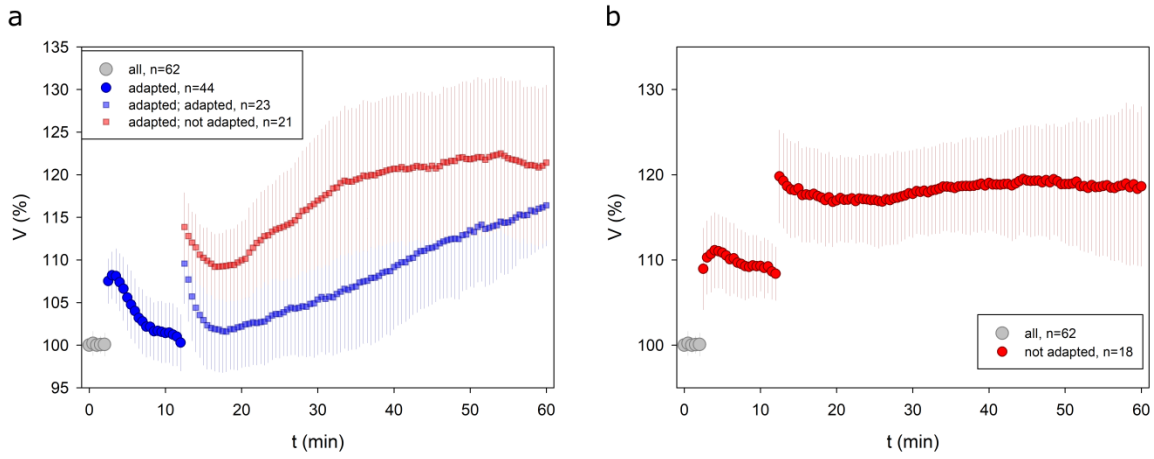

Figure 4.10: *Two hypoosmotic shock.*

For the first shock $P_{iso}/P_1=1.11$, for the second shock $P_1/P_2=1.08$.

A: 70% of cells adapted after the first shock. After the second shock, only half of these cells adapted.

B: 30% of cells did not adapt either after the first shock or after second.

Because the timescale of adaptation is of the order of several minutes, cell volume recovery can be determined not only by active ion transport but also affected by phenomena related to cell growth, at least for small shocks which change volume by less than 10% (growth is about 5% per hour). Moreover, osmotic shock can have an effect on cell growth rates (Buda et al. 2016; Rojas and Huang 2018). This field is still poorly investigated for mammalian cells due to the complexity of cell volume measurements and relatively long cell division cycles. We think that our measurement method and the preliminary data we obtained with it can open new perspectives for this old field of research.

IV. Discussion and perspectives

1. Osmotic shock

Animal cell volume regulation has been extensively studied mostly in the context of osmotic shock and usually at the level of cell population. Measurements on the level of individual cells, however, are scarce due to technical limitations. It has been shown that mammalian cells with few exceptions (like human RBCs) have a two-step response to the osmotic shock.

First, cells swell/shrink with respect to osmotic pressure difference when external osmolarity rapidly changes. Physicists investigated this process almost 100 years ago and concluded that cell volume change with subtraction of volume fraction occupied by solid components (excluded volume) is a simple function of osmotic pressure change (Ponder 1935). Later it was shown that this relative volume change does not depend on actin polymerization and adherence to the substrate (Zhou et al. 2009). Excluded volume for different cell lines was estimated from 15% (Benson, Chicone, and Critser 2011) to 30% (Zhou et al. 2009) of the total volume.

Our experimental data shows that for non-adherent HeLa cells on average excluded volume is about 30%. However, we observed a large diversity at single cell level. Interestingly, big cells had a larger fraction of excluded volume than small cells. Additionally, we found that excluded volume does not depend on the magnitude of the shock or actin polymerization.

Therefore, we hypothesized that our observation, that that larger cells have more excluded volume, could be related to either initial cell density or to membrane permeability/availability. If the fist hypothesis were true (which can be checked experimentally), it would simply mean that small cells are more dilute than big cells. This could be associated with cell cycle dependent protein production. Nevertheless, preliminary observations made in our lab and experimental study performed on yeasts (Neurohr et al. 2019) suggest that this hypothesis is not correct.

We thus also consider that the final volume cells reach in response to osmolarity changes could be limited by membrane availability. We showed that large amount of membrane of non-adherent cells is stored in membrane reservoirs consistent with previous observation (Ping Ting-Beall, Needham, and Hochmuth 1993; Groulx et al. 2006). These reservoirs are attached to acto-myosin cortex and thus not easily accessible (Pietuch and Janshoff 2013). As a consequence, the amount a cell swells could depend on the amount of membrane that can be released fast enough from such membrane stores, especially for small

magnitude shocks that do not lead to massive cortex disruption (Pritchard and Guilak 2004). However, we did not notice any difference in excluded volume between control cells and cells with partial actin disruption, ruling out our hypothesis of limited membrane availability due to attachment to actin cortex.

Another possible explanation of observed diversity of osmotically active fraction is that cells may have different membrane permeability, which could be defined by ion channel activity, that, for example, can vary depending on cell cycle stage, and hence, cell size (Blackiston, McLaughlin, and Levin 2009). In this case, water transport occurring as a response to change in osmolarity could not be considered as a passive process, which was commonly accepted in the field (Pritchard and Guilak 2004).

The following question is if the kinetics of water transport inside the cell induced by osmotic shock is basically a diffusion process (Minkov et al. 2013). Then, in principle, water propagation could be limited by poroelastic nature of cytoplasmic bulk, and timescale of water movement is $\tau = R^2/D$, where R is cell radius, and D is diffusion coefficient; $D \sim E\varepsilon^2/\mu$, E is elastic modulus, ε is pore size, μ is cytosol viscosity (Moeendarbary et al. 2013). Additionally, water movement inside the cell could be affected by the nucleus. For instance, the nucleus was shown to have non-linear osmotic properties unlike the cell: cell volume increases with increasing magnitude of osmotic shock following Ponder's relation, but nuclear volume reaches a plateau (Finan et al. 2009). Another possible limitation is membrane permeability, that is, how fast water can permeate through lipid bilayer.

Previous studies have shown that typical time of osmotic swelling is about 1 min (Fernández et al. 2013) and it does not depend on actin polymerization (Pritchard and Guilak 2004). Our experimental results showed that osmotic swelling and shrinking have a timescale of a few seconds that is similar to values estimated for water movement inside the cell (G. T. Charras, Mitchison, and Mahadevan 2009). We were not able to observe scaling of swelling time with cell radius – although there is large distribution of initial cell volume in population, cell radius varies in the range 7-9 μm. Therefore, to make a conclusive statement we would need to further increase the distribution of a cell radii, which is possible by cell cycle arrest or cell fusion.

We observed a strong increase in swelling speed and slight increase in swelling time with increase of shock magnitude. We could speculate that increase of swelling speed for large shock magnitude could be due to membrane permeability increase induced by high tension, e.g. by aquaporins activation (Ozu et al. 2018; Lisjak et al. 2017).

To test further the hypothesis of poroelastic constrain we disrupted actin network, aiming to increase internal network pore size and increase the diffusion coefficient. Contrary to our expectations, actin depolymerization increased swelling time. The possible explanation would be that tension generated in actin network is required to activate ion channels (Sasaki, Yui, and Noda 2014; Martinac 2014) thus increasing membrane permeability. If this hypothesis were correct, that would confirm the idea, that osmotic swelling is not a passive process.

Regulatory volume adaptation followed by initial swelling/shrinking (RVI or RVD) is a relatively long process – initial volume recovery usually takes tens of minutes. It is an active process as it relies on activity of ion pumps that require energy. Thus, there are a lot of factors that influence this process including cell growth and specific osmotic shock protein production. In contrast to initial volume response, adaptation was mostly investigated by biologists.

We found that cells perfectly recovered their volume (RVI) after hypertonic shock of different magnitudes (mix of medium and PEG400). The behavior of individual cells was uniform. On the contrary, cells exposed to hypoosmotic shocks (mix of medium and water) did not recover their initial volume on average and showed three type of behavior: perfect adaptation to initial volume, partial adaptation, no adaptation. Typical adaptation time was larger for small shock magnitudes (~5 min) than for high magnitudes (~2 min). Cells with depolymerized actin had smaller adaptation time than control. This result is similar to previously published data (Pritchard and Guilak 2004) and could indicate that the state of the actin cytoskeleton can modulate RVD, probably, through activation of ion transport (S F Pedersen, Hoffmann, and Mills 2001).

This part of the project is in its initial stage and requires more experimental data to be conclusive. We did not investigate hyperosmotic shrinking in detail, focusing more on hypoosmotic swelling. However, it is clear that our results, which were possible to obtain due to precise volume measurements of live individual cells performed with high temporal resolution, challenge established and commonly accepted assumptions.

2. Confinement

It is commonly accepted that cells do not change volume in response to uniaxial mechanical compression. This assumption is crucial for extraction of cell mechanical parameters from AFM indentation experiments

(Brückner and Janshoff 2015). One theoretical study predicted that cells can lose volume only when loading rate is slow enough (>1 μm/s) to provide ion transport (Jiang and Sun 2013).

Our results show that fast, in order of milliseconds, compression induces large volume loss, up to 30%. Very intriguing part is that we were not able to observe it dynamically – volume loss occurred less than in 30 ms, which was our time resolution limit. That made us think that loss of volume under confinement could have a different regulation to RVD followed by hypoosmotic shock (take minutes), and even not initial hyperosmotic shrinkage (~0.5 s). Thus, our current hypothesis is that confinement increases membrane permeability by increasing the distance between lipids in membrane bilayer by stretching, or aquaporin/ion channels opening, or transient holes formation. We need to test this hypothesis by markers indicating membrane reparation (Jimenez et al. 2014). ATP-depleted cell death induced by confinement likely can be explain by membrane fragility and thus irreversible rupture; it is also should be checked experimentally by altering membrane composition.

On the other hand, uniaxial compression (by a half of cell diameter) seemed to share the features of both hyper- and hypoosmotic challenges: cells lost volume and extended their surface by only a few percent. This small surface extension could be provided be membrane reservoirs flattening, however, without actin cortex disruption like in case of hypoosmotic shock (Pritchard and Guilak 2004), so membrane is attached to the cortex. Therefore, volume loss under confinement can be a protective mechanism preventing unstretchable membrane from irreversible rupture when available membrane reservoirs were already flattened. Consistent with this idea, actin cortex disruption leading to membrane detachment prevented large volume loss under confinement. Importantly, depolymerization of actin cortex per se increased cell volume only by few percent, consistent with (Salbreux, Charras, and Paluch 2012). Moreover, large compressive deformation (3-5 μm) induced both volume loss and membrane detachment, that would follow by complete cortex reformation (Le Berre, Aubertin, and Piel 2012).

Currently we do not have any force measurements – our confinement is geometrical constrain that allowed us to do volume measurements as well, but it is hard to combine it with force measurements technique. Another experimental approach that we did not perform is controlled loading. For instance, we expect that slow confinement would not lead to sudden cell shape change and consequent volume loss as cells could reorganize acto-myosin cortex and membrane.

Another question that we did not access is whether there is a volume adaptation after volume loss. In experiments with high temporal resolution, cells did not show volume increase right after confinement. The volume of confined cells was smaller than for control cells in experiments with static confinement –

measurements were done in 10-15 min after confinement. It would be interesting to check if cells are able to recover initial volume, if confinement is maintained or released. Confinement also could affect growth rate, would it be similar with hyperosmotic shock, which can inhibit cell growth (Copp et al. 2005)? Cell density increased after confinement (volume decreases, mass is constant). This would affect molecular crowding and protein synthesis (Delarue et al. 2018).

3. Spreading

Recently research group of Dr. David Weitz found that when suspended cells spread on substrate their lose 25% of volume in 1 hour - cell volume decreases with spreading area (Guo et al. 2017). Our data showed that on average HeLa cells lose 5% of volume in the first 20 min of spreading and then increase their volume with the rate similar to the cell growth. Importantly, we found that volume loss primarily depended on spreading speed, but not on spreading area, and the faster cells spread the more volume they lost. Cells that spread slowly could do it without volume loss and even with volume increase presumable due to the cell growth. Moreover, RPE-1 cells had a transient small volume increase at the initial stage of spreading. The difference between our results and previously published could be explained by either experimental procedure like cell lines or cell synchronization, or artifacts due to 3D reconstruction from confocal imaging, which relate the volume measure very much to the cell height, and suggests that they did not measure the volume but the height of the cells.

Next, we affected spreading kinetics by cytoskeleton perturbations and confirmed our observation: volume loss depends on spreading speed. Our model is that fast lamellipodia driven spreading induces volume loss due to the tension generated by branched actin that activate ion transport and volume loss. The mechanism of volume loss could be similar with RVD followed by hypoosmotic shock; we can test it experimentally by inhibition of ion channels and pump involved in RVD (e.g. VRAC). We also were able to modulate fast spreading without volume loss by inhibition of branched actin or NHE1 in low contractile cells, possibly due to inhibition of lamellipodia formation or direct interaction of branched actin with ion channels.

We also found that steady state cell volume does not correlate with shape and size of spreading area in cell population. It was different from previously published result: two studies showed negative correlation, another one – positive. This could be again different experimental procedure or volume measurements.

We studied cell volume regulation while attachment and spreading of rounded cells on a glass substrate, it allows us to observe us large shape changes with wide range of spreading speed. However, some cell types exhibit dramatic shape changes during migration not only on a substrate, but also in 3D environment, like dendritic cells (Vargas et al. 2017). We measured cell volume of dendritic cells, which were platted inside a collagen gel. Preliminary analysis showed that cell that were migrating (Fig.1.1a) had a larger volume fluctuations than non-motile cells (Fig.1.1b). This could indicate that active shape fluctuations during migration lead to volume changes. We would like to test in future if disability of cells decrease their volume while spreading (like combined Arp2/3 and contractility inhibition) would affect migratory properties of cells and/or potentially induces cell ruptures.

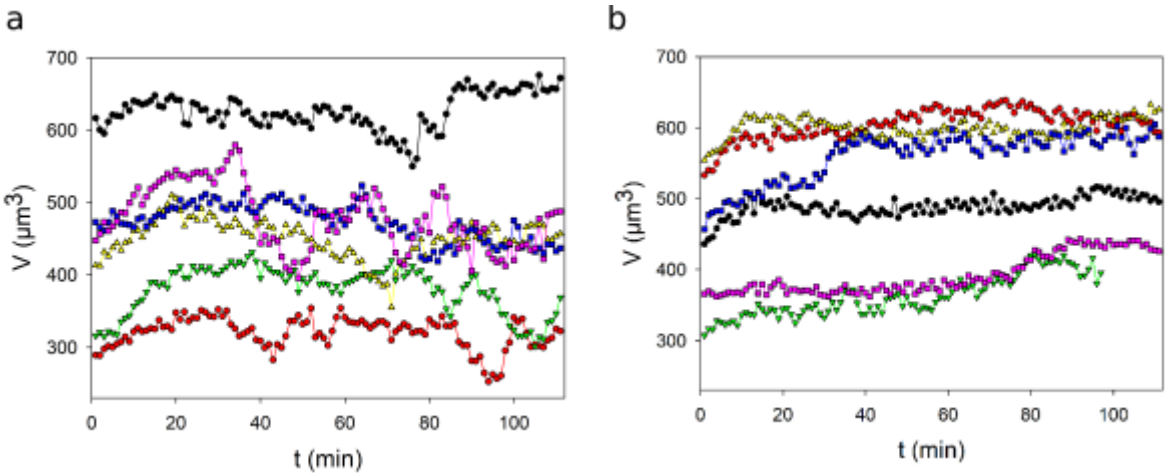

Fig.1.1 *Volume of single dendritic cells plated inside a collagen gel. Motile (a) and non-motile (b) cells.*

Migration and spreading on a substrate could explain volume fluctuation during cell growth observed in another project from our lab (Clotilde Cadart et al. 2018). We also observed that when cells lose volume during spreading, dry mass remains constant and start to grow together with volume (~20 min of spreading). It could mean that either spreading by itself or decrease in cell density delay protein production and, therefore, cell dry mass accumulation.

4. Conclusion

In this project, we studied cell volume modulation in response to mechanical deformations of different timescales. We showed that cells decrease, do not change or increase volume depending on kinetics of

deformation and the state of actomyosin cortex. It means that depending on the context cells have different material properties, for instance, Poisson's ratio.

It is important to notice that previously mammalian cell volume regulation was mostly studied in the context of osmotic shock (short time scale) or cell cycle (long time scale). We found new aspects for isotropic osmotic compression thanks to the FXm allowed us precise cell volume measurements with high temporal resolution. We also found that cells decrease volume in response to uniaxial compression challenging common assumption that cell volume is constant while mechanical confinement. We showed that cell modulate their volume while spreading (intermediate timescale). Taken together these results provide new insights in understanding of cell volume regulation of mammalian cells.

Bibliography

Aknoun, Sherazade, Julien Savatier, Pierre Bon, Frédéric Galland, Lamiae Abdeladim, Benoit Wattellier, and Serge Monneret. 2015. "Living Cell Dry Mass Measurement Using Quantitative Phase Imaging with Quadriwave Lateral Shearing Interferometry: An Accuracy and Sensitivity Discussion." https://doi.org/10.1117/1.JBO.20.

Armstrong, C. M. 2003. "The Na/K Pump, Cl Ion, and Osmotic Stabilization of Cells." *Proceedings of the National Academy of Sciences* 100 (10): 6257–62. https://doi.org/10.1073/pnas.0931278100.

Arpin, Monique, Dafne Chirivino, Alexandra Naba, and Ingrid Zwaenepoel. 2011. "Emerging Role for ERM Proteins in Cell Adhesion and Migration." *Cell Adhesion and Migration*. Taylor and Francis Inc. https://doi.org/10.4161/cam.5.2.15081.

Balijepalli, Ravi C., and Timothy J. Kamp. 2008. "Caveolae, Ion Channels and Cardiac Arrhythmias." *Progress in Biophysics and Molecular Biology*. https://doi.org/10.1016/j.pbiomolbio.2009.01.012.

Barbier, Lucie, Pablo J. Sáez, Rafaele Attia, Ana Maria Lennon-Duménil, Ido Lavi, Matthieu Piel, and Pablo Vargas. 2019. "Myosin II Activity Is Selectively Needed for Migration in Highly Confined Microenvironments in Mature Dendritic Cells." *Frontiers in Immunology* 10 (APR). https://doi.org/10.3389/fimmu.2019.00747.

Beckham, Yvonne, Robert J. Vasquez, Jonathan Stricker, Kareem Sayegh, Clement Campillo, and Margaret L. Gardel. 2014. "Arp2/3 Inhibition Induces Amoeboid-like Protrusions in MCF10A Epithelial Cells by Reduced Cytoskeletal-Membrane Coupling and Focal Adhesion Assembly." *PLoS ONE* 9 (6). https://doi.org/10.1371/journal.pone.0100943.

Benson, James D., Carmen C. Chicone, and John K. Critser. 2011. "A General Model for the Dynamics of Cell Volume, Global Stability, and Optimal Control." *Journal of Mathematical Biology*. https://doi.org/10.1007/s00285-010-0374-4.

Berre, Maël Le, Johannes Aubertin, and Matthieu Piel. 2012. "Fine Control of Nuclear Confinement Identifies a Threshold Deformation Leading to Lamina Rupture and Induction of Specific Genes." *Integrative Biology*. https://doi.org/10.1039/c2ib20056b.

Berre, Maël Le, Ewa Zlotek-Zlotkiewicz, Daria Bonazzi, Franziska Lautenschlaeger, and Matthieu Piel. 2014. "Methods for Two-Dimensional Cell Confinement." *Methods in Cell Biology*. https://doi.org/10.1016/B978-0-12-800281-0.00014-2.

Berthaud, Alice, François Quemeneur, Maxime Deforet, Patricia Bassereau, Françoise Brochard-Wyart, and Stéphanie Mangenot. 2016. "Spreading of Porous Vesicles Subjected to Osmotic Shocks: The Role of Aquaporins." *Soft Matter*. https://doi.org/10.1039/C5SM01654A.

Biswas, Arikta, Purba Kashyap, Sanchari Datta, Titas Sengupta, and Bidisha Sinha. 2019. "Cholesterol Depletion by MβCD Enhances Cell Membrane Tension and Its Variations-Reducing Integrity." *Biophysical Journal* 116 (8): 1456–68. https://doi.org/10.1016/j.bpj.2019.03.016.

Blackiston, Douglas J., Kelly A. McLaughlin, and Michael Levin. 2009. "Bioelectric Controls of Cell Proliferation: Ion Channels, Membrane Voltage and the Cell Cycle." *Cell Cycle (Georgetown, Tex.)* 8 (21): 3527–36. https://doi.org/10.4161/cc.8.21.9888.

Bonn, Daniel, Jens Eggers, Joseph Indekeu, Jacques Meunier, and Etienne Rolley. 2009. "Wetting and

Spreading." *Reviews of Modern Physics* 81: 739.

Bottier, Céline, Chiara Gabella, Benoît Vianay, Lara Buscemi, Ivo F. Sbalzarini, Jean-Jacques Meister, and Alexander B. Verkhovsky. 2011. "Dynamic Measurement of the Height and Volume of Migrating Cells by a Novel Fluorescence Microscopy Technique." *Lab on a Chip*. https://doi.org/10.1039/c1lc20807a.

Boudreault, Francis, and Ryszard Grygorczyk. 2004. "Cell Swelling-Induced ATP Release Is Tightly Dependent on Intracellular Calcium Elevations." *Journal of Physiology* 561 (2): 499–513. https://doi.org/10.1113/jphysiol.2004.072306.

Brückner, Bastian R., and Andreas Janshoff. 2015. "Elastic Properties of Epithelial Cells Probed by Atomic Force Microscopy." *Biochimica et Biophysica Acta - Molecular Cell Research* 1853 (11): 3075–82. https://doi.org/10.1016/j.bbamcr.2015.07.010.

Buda, Renata, Yunxiao Liu, Jin Yang, Smitha Hegde, Keiran Stevenson, Fan Bai, and Teuta Pilizota. 2016. "Dynamics of *Escherichia Coli* 's Passive Response to a Sudden Decrease in External Osmolarity." *Proceedings of the National Academy of Sciences*. https://doi.org/10.1073/pnas.1522185113.

Bun, Philippe, Serge Dmitrieff, Julio M Belmonte, François J Nédélec, and Péter Lénárt. 2018. "A Disassembly-Driven Mechanism Explains F-Actin-Mediated Chromosome Transport in Starfish Oocytes." *ELife* 7 (January). https://doi.org/10.7554/elife.31469.

Burg, Maurice B, and Arlyn Garcia-Perez. 1992. "How Tonicity Regulates Gene Expression." *Journal of the American Society of Nephrology* 3 (2): 121–27.

Cadart, C., E. Zlotek-Zlotkiewicz, L. Venkova, O. Thouvenin, V. Racine, M. Le Berre, S. Monnier, and M. Piel. 2017. "Fluorescence EXclusion Measurement of Volume in Live Cells." *Methods in Cell Biology*. https://doi.org/10.1016/bs.mcb.2016.11.009.

Cadart, C, L Venkova, P Recho, M Cosentino Lagomarsino, and M Piel. 2019. "The Physics of Cell-Size Regulation across Timescales." *Nature Physics*, August. https://doi.org/10.1038/s41567-019-0629-y.

Cadart, Clotilde, Sylvain Monnier, Jacopo Grilli, Pablo J. Sáez, Nishit Srivastava, Rafaele Attia, Emmanuel Terriac, Buzz Baum, Marco Cosentino-Lagomarsino, and Matthieu Piel. 2018. "Size Control in Mammalian Cells Involves Modulation of Both Growth Rate and Cell Cycle Duration." *Nature Communications* 9 (1): 3275. https://doi.org/10.1038/s41467-018-05393-0.

Cartagena-Rivera, Alexander X., Jeremy S. Logue, Clare M. Waterman, and Richard S. Chadwick. 2016. "Actomyosin Cortical Mechanical Properties in Nonadherent Cells Determined by Atomic Force Microscopy." *Biophysical Journal* 110 (11): 2528–39. https://doi.org/10.1016/j.bpj.2016.04.034.

Charras, G. T. 2008. "A Short History of Blebbing." In *Journal of Microscopy*, 231:466–78. https://doi.org/10.1111/j.1365-2818.2008.02059.x.

Charras, G. T., T. J. Mitchison, and L. Mahadevan. 2009. "Animal Cell Hydraulics." *Journal of Cell Science*. https://doi.org/10.1242/jcs.049262.

Charras, Guillaume, and Ewa Paluch. 2008. "Blebs Lead the Way: How to Migrate without Lamellipodia." *Nature Reviews Molecular Cell Biology* 9 (9): 730–36. www.nature.com/reviews/molcellbio.

Charras, Guillaume T., Justin C. Yarrow, Mike A. Horton, L. Mahadevan, and T. J. Mitchison. 2005. "Non-Equilibration of Hydrostatic Pressure in Blebbing Cells." *Nature* 435 (7040): 365–69.

https://doi.org/10.1038/nature03550.

Chifflet, Silvia, and Julio A. Hernández. 2012. “The Plasma Membrane Potential and the Organization of the Actin Cytoskeleton of Epithelial Cells.” *International Journal of Cell Biology* 2012 (January): 1–13. https://doi.org/10.1155/2012/121424.

Chugh, Priyamvada, Andrew G Clark, Matthew B Smith, Davide A D Cassani, Kai Dierkes, Anan Ragab, Philippe P Roux, Guillaume Charras, Guillaume Salbreux, and Ewa K Paluch. 2017. “Actin Cortex Architecture Regulates Cell Surface Tension.” *Nat Cell Biol.* 19 (6): 689–97. https://doi.org/10.1038/ncb3525.

Chugh, Priyamvada, and Ewa K. Paluch. 2018. “The Actin Cortex at a Glance.” *Journal of Cell Science* 131 (14): jcs186254. https://doi.org/10.1242/jcs.186254.

Clapham, DE. 2007. “Calcium Signaling.” *Cell* 131 (6): 1047–58.

Clucas, J., and F. Valderrama. 2015. “ERM Proteins in Cancer Progression.” *Journal of Cell Science* 128 (6): 1253–1253. https://doi.org/10.1242/jcs.170027.

Copp, Jeremy, Sandra Wiley, Manus W Ward, and Peter Van Der Geer. 2005. “Hypertonic Shock Inhibits Growth Factor Receptor Signaling, Induces Caspase-3 Activation, and Causes Reversible Fragmentation of the Mitochondrial Network.” *Am J Physiol Cell Physiol* 288: 403–15. https://doi.org/10.1152/ajpcell.

Cramer, Louise P. 2010. “Forming the Cell Rear First: Breaking Cell Symmetry to Trigger Directed Cell Migration.” *Nature Cell Biology* 12 (7): 628–32. https://doi.org/10.1038/ncb0710-628.

Cuvelier, Damien, and Pierre Nassoy. 2004. “Hidden Dynamics of Vesicle Adhesion Induced by Specific Stickers.” *Physical Review Letters*. https://doi.org/10.1103/PhysRevLett.93.228101.

Cuvelier, Damien, Manuel Théry, Yeh-Shiu Chu, Sylvie Dufour, Jean-Paul Thiéry, Michel Bornens, Pierre Nassoy, and L. Mahadevan. 2007. “The Universal Dynamics of Cell Spreading.” *Current Biology*. https://doi.org/10.1016/j.cub.2007.02.058.

Dahl, Kris Noel, Alexandre J.S. Ribeiro, and Jan Lammerding. 2008. “Nuclear Shape, Mechanics, and Mechanotransduction.” *Circulation Research*. https://doi.org/10.1161/CIRCRESAHA.108.173989.

Day, Rebecca E., Philip Kitchen, David S. Owen, Charlotte Bland, Lindsay Marshall, Alex C. Conner, Roslyn M. Bill, and Matthew T. Conner. 2014. “Human Aquaporins: Regulators of Transcellular Water Flow.” *Biochimica et Biophysica Acta - General Subjects* 1840 (5): 1492–1506. https://doi.org/10.1016/j.bbagen.2013.09.033.

Delarue, M., G. P. Brittingham, S. Pfeffer, I. V. Surovtsev, S. Pinglay, K. J. Kennedy, M. Schaffer, et al. 2018. “MTORC1 Controls Phase Separation and the Biophysical Properties of the Cytoplasm by Tuning Crowding.” *Cell* 174 (2): 338-349.e20. https://doi.org/10.1016/j.cell.2018.05.042.

Demaurex, Nicolas, and Sergio Grinstein. 1994. “Na + /H + ANTIPORT: MODULATION BY ATP AND ROLE IN CELL VOLUME REGULATION.” *J. Exp. Biol*. Vol. 196.

Denker, Sheryl P., and Diane L. Barber. 2002. “Cell Migration Requires Both Ion Translocation and Cytoskeletal Anchoring by the Na-H Exchanger NHE1.” *Journal of Cell Biology* 159 (6): 1087–96. https://doi.org/10.1083/jcb.200208050.

Diz-Muñoz, Alba, Daniel A Fletcher, and Orion D Weiner. 2013. “Use the Force: Membrane Tension as an

Organizer of Cell Shape and Motility." *Trends in Cell Biology* 23 (2): 47–53. https://doi.org/10.1016/j.tcb.2012.09.006.

Echarri, A., and M. A. Del Pozo. 2015. "Caveolae - Mechanosensitive Membrane Invaginations Linked to Actin Filaments." *Journal of Cell Science* 128 (15): 2747–58. https://doi.org/10.1242/jcs.153940.

Essig, Alvin. 1968. "The 'Pump-Leak' Model and Exchange Diffusion." *Biophysical Journal* 8 (1): 53–63. https://doi.org/10.1016/S0006-3495(68)86474-4.

Fehon, Richard G., Andrea I. McClatchey, and Anthony Bretscher. 2010. "Organizing the Cell Cortex: The Role of ERM Proteins." *Nature Reviews Molecular Cell Biology*. https://doi.org/10.1038/nrm2866.

Feranchak, Andrew P., Richard M. Roman, Erik M. Schwiebert, and J. Gregory Fitz. 1998. "Phosphatidylinositol 3-Kinase Contributes to Cell Volume Regulation through Effects on ATP Release." *Journal of Biological Chemistry*. https://doi.org/10.1074/jbc.273.24.14906.

Fernández, Juan M., Gisela Di Giusto, Maia Kalstein, Luciana Melamud, Valeria Rivarola, Paula Ford, and Claudia Capurro. 2013. "Cell Volume Regulation in Cultured Human Retinal Müller Cells Is Associated with Changes in Transmembrane Potential." *PLoS ONE*. https://doi.org/10.1371/journal.pone.0057268.

Finan, John D., Kevin J. Chalut, Adam Wax, and Farshid Guilak. 2009. "Nonlinear Osmotic Properties of the Cell Nucleus." *Annals of Biomedical Engineering*. https://doi.org/10.1007/s10439-008-9618-5.

Fischer-Friedrich, E, Y Toyoda, C J Cattin, D J Müller, A A Hyman, and F Jülicher. 2016. "Rheology of the Active Cell Cortex in Mitosis." *Biophysical Journal* 111 (3): 589-600.

Fischer-Friedrich, Elisabeth, Anthony A. Hyman, Frank Jülicher, Daniel J. Müller, and Jonne Helenius. 2014. "Quantification of Surface Tension and Internal Pressure Generated by Single Mitotic Cells." *Scientific Reports* 4 (6213). https://doi.org/10.1038/srep06213.

Fouchard, J., C. Bimbard, N. Bufi, P. Durand-Smet, A. Proag, A. Richert, O. Cardoso, and A. Asnacios. 2014. "Three-Dimensional Cell Body Shape Dictates the Onset of Traction Force Generation and Growth of Focal Adhesions." *Proceedings of the National Academy of Sciences*. https://doi.org/10.1073/pnas.1411785111.

Frisch, Thomas, and Olivier Thoumine. 2002. "Predicting the Kinetics of Cell Spreading." *Journal of Biomechanics*. https://doi.org/10.1016/S0021-9290(02)00075-1.

Fritzsche, Marco, Christoph Erlenkämper, Emad Moeendarbary, Guillaume Charras, and Karsten Kruse. 2016. "Actin Kinetics Shapes Cortical Network Structure and Mechanics." *Science Advances* 2 (4): e1501337. https://doi.org/10.1126/sciadv.1501337.

Gadsby, David C, and Patrick A Gerschel. 2009. "Ion Channels versus Ion Pumps: The Principal Difference, in Principle." *Nature Reviews Molecular Cell Biology* 10 (5): 344–52. https://doi.org/10.1038/nrm2668.

Gauthier, N. C., M. A. Fardin, P. Roca-Cusachs, and M. P. Sheetz. 2011. "Temporary Increase in Plasma Membrane Tension Coordinates the Activation of Exocytosis and Contraction during Cell Spreading." *Proceedings of the National Academy of Sciences*. https://doi.org/10.1073/pnas.1105845108.

Gauthier, N. C., O. M. Rossier, A. Mathur, J. C. Hone, and M. P. Sheetz. 2009. "Plasma Membrane Area Increases with Spread Area by Exocytosis of a GPI-Anchored Protein Compartment." *Molecular*

Biology of the Cell. https://doi.org/10.1091/mbc.E09-01-0071.

Ginzberg, Miriam B, Ran Kafri, and Marc Kirschner. 2015. "On Being the Right (Cell) Size." *Science* 348 (6236): 1245075. https://doi.org/10.1126/science.1245075.

Goudarzi, Mohammad, Aleix Boquet-Pujadas, Jean Christophe Olivo-Marin, and Erez Raz. 2019. "Fluid Dynamics during Bleb Formation in Migrating Cells in Vivo." *PLoS ONE* 14 (2). https://doi.org/10.1371/journal.pone.0212699.

Groulx, Nicolas, Francis Boudreault, Sergei N. Orlov, and Ryszard Grygorczyk. 2006. "Membrane Reserves and Hypotonic Cell Swelling." *Journal of Membrane Biology* 214 (1): 43–56. https://doi.org/10.1007/s00232-006-0080-8.

Guilak, Farshid. 1995. "Compression-Induced Changes in the Shape and Volume of the Chondrocyte Nucleus." *Journal of Biomechanics* 28 (12): 1529–41. https://doi.org/doi.org/10.1016/0021-9290(95)00100-X.

Guilak, Farshid, Geoffrey R Erickson, and H Ping Ting-Beall. 2002. "The Effects of Osmotic Stress on the Viscoelastic and Physical Properties of Articular Chondrocytes." *Biophysical Journal* 82.

Guo, Ming, Adrian F Pegoraro, Angelo Mao, Enhua H Zhou, Praveen R Arany, Yulong Han, Dylan T Burnette, et al. 2017. "Cell Volume Change through Water Efflux Impacts Cell Stiffness and Stem Cell Fate." *Proceedings of the National Academy of Sciences of the United States of America* 114 (41): E8618–27. https://doi.org/10.1073/pnas.1705179114.

Haase, Kristina, and Andrew E. Pelling. 2015. "Investigating Cell Mechanics with Atomic Force Microscopy." *Journal of the Royal Society Interface*. Royal Society of London. https://doi.org/10.1098/rsif.2014.0970.

Hale, Christopher M., Sean X. Sun, and Denis Wirtz. 2009. "Resolving the Role of Actoymyosin Contractility in Cell Microrheology." *PLoS ONE* 4 (9). https://doi.org/10.1371/journal.pone.0007054.

Hamill, O P, and B Martinac. 2001. "Molecular Basis of Mechanotransduction in Living Cells." *Physiological Reviews* 81 (2): 685–740. https://doi.org/10.1152/physrev.2001.81.2.685.

Harris, A, and G Charras. 2011. "Experimental Validation of Atomic Force Microscopy-Based Cell Elasticity Measurements." *Nanotechnology* 22 (34): 345102.

Haswell, Elizabeth S, Rob Phillips, and Douglas C Rees. 2011. "Mechanosensitive Channels: What Can They Do and How Do They Do It?" *Structure* 19 (10): 1356–69. https://doi.org/10.1016/j.str.2011.09.005.

Helfand, Brian T, Melissa G Mendez, S N Prasanna Murthy, Dale K Shumaker, Boris Grin, Saleemulla Mahammad, Ueli Aebi, et al. 2011. "Vimentin Organization Modulates the Formation of Lamellipodia." https://doi.org/10.1091/mbc.E10-08-0699.

Hell, S., G. Reiner, C. Cremer, and E. H.K. Stelzer. 1993. "Aberrations in Confocal Fluorescence Microscopy Induced by Mismatches in Refractive Index." *Journal of Microscopy*. https://doi.org/10.1111/j.1365-2818.1993.tb03315.x.

Henson, John H., Mesrob Yeterian, Richard M. Weeks, Angela E. Medrano, Briana L. Brown, Heather L. Geist, Mollyann D. Pais, Rudolf Oldenbourg, and Charles B. Shuster. 2015. "Arp2/3 Complex Inhibition Radically Alters Lamellipodial Actin Architecture, Suspended Cell Shape, and the Cell

Spreading Process." *Molecular Biology of the Cell* 26 (5): 887–900. https://doi.org/10.1091/mbc.e14-07-1244.

Hochmuth, Robert M. 2000. "Micropipette Aspiration of Living Cells." *Journal of Biomechanics*. Vol. 33.

Hoffmann, E. K., I. H. Lambert, and S. F. Pedersen. 2009. "Physiology of Cell Volume Regulation in Vertebrates." *Physiological Reviews*. https://doi.org/10.1152/physrev.00037.2007.

Höglund, Anna Stina. 1985. "The Arrangement of Microfilaments and Microtubules in the Periphery of Spreading Fibroblasts and Glial Cells." *Tissue and Cell* 17 (5): 649–66. https://doi.org/10.1016/0040-8166(85)90002-3.

Holzer, Peter. 2009. "Acid-Sensitive Ion Channels and Receptors." *Handbook of Experimental Pharmacology* 194: 283–332. https://doi.org/10.1007/978-3-540-79090-7_9.

Houk, Andrew R, Alexandra Jilkine, Cecile O Mejean, Rostislav Boltyanskiy, Eric R Dufresne, Sigurd B Angenent, Steven J Altschuler, Lani F Wu, and Orion D Weiner. 2012. "Membrane Tension Maintains Cell Polarity by Confining Signals to the Leading Edge during Neutrophil Migration." *Cell* 148 (1–2): 175–88. https://doi.org/10.1016/j.cell.2011.10.050.

Hua, Susan Z., Philip A. Gottlieb, Jinseok Heo, and Frederick Sachs. 2010. "A Mechanosensitive Ion Channel Regulating Cell Volume." *American Journal of Physiology-Cell Physiology* 298 (6): C1424–30. https://doi.org/10.1152/ajpcell.00503.2009.

Hui, T. H., Z. L. Zhou, J. Qian, Y. Lin, A. H W Ngan, and H. Gao. 2014. "Volumetric Deformation of Live Cells Induced by Pressure-Activated Cross-Membrane Ion Transport." *Physical Review Letters* 113 (118101). https://doi.org/10.1103/PhysRevLett.113.118101.

Ibata, Keiji, Shinichi Takimoto, Toshinori Morisaku, Atsushi Miyawaki, and Masato Yasui. 2011. "Analysis of Aquaporin-Mediated Diffusional Water Permeability by Coherent Anti-Stokes Raman Scattering Microscopy." *Biophysical Journal*. https://doi.org/10.1016/j.bpj.2011.08.045.

Jarsch, Iris K., Frederic Daste, and Jennifer L. Gallop. 2016. "Membrane Curvature in Cell Biology: An Integration of Molecular Mechanisms." *Journal of Cell Biology*. Rockefeller University Press. https://doi.org/10.1083/jcb.201604003.

Jiang, Hongyuan, and Sean X. Sun. 2013. "Cellular Pressure and Volume Regulation and Implications for Cell Mechanics." *Biophysical Journal* 105 (3): 609–19. https://doi.org/10.1016/j.bpj.2013.06.021.

Jiao, Runsheng, Dan Cui, Stephani C. Wang, Dongyang Li, and Yu-Feng Wang. 2017. "Interactions of the Mechanosensitive Channels with Extracellular Matrix, Integrins, and Cytoskeletal Network in Osmosensation." *Frontiers in Molecular Neuroscience* 10 (April). https://doi.org/10.3389/fnmol.2017.00096.

Jimenez, Ana Joaquina, Paolo Maiuri, Julie Lafaurie-Janvore, Séverine Divoux, Matthieu Piel, and Franck Perez. 2014. "ESCRT Machinery Is Required for Plasma Membrane Repair." *Science*. https://doi.org/10.1126/science.1247136.

Kadir, Lina Abdul, Michael Stacey, and Richard Barrett-Jolley. 2018. "Emerging Roles of the Membrane Potential: Action beyond the Action Potential." *Frontiers in Physiology*. Frontiers Media S.A. https://doi.org/10.3389/fphys.2018.01661.

Karatekin, Erdem, Hicham Guitouni, Nicolas Borghi, Pierre-Henri Puech, Françoise Brochard-Wyart, and Olivier Sandre. 2003. "Cascades of Transient Pores in Giant Vesicles: Line Tension and Transport."

Biophysical Journal 84 (3): 1734–49. https://doi.org/10.1016/S0006-3495(03)74981-9.

Kay, Alan R. 2017. "How Cells Can Control Their Size by Pumping Ions." *Frontiers in Cell and Developmental Biology*. https://doi.org/10.3389/fcell.2017.00041.

Klumpp, Stefan, Matthew Scott, Steen Pedersen, and Terence Hwa. 2013. "Molecular Crowding Limits Translation and Cell Growth." *Proceedings of the National Academy of Sciences of the United States of America* 110 (42): 16754–59. https://doi.org/10.1073/pnas.1310377110.

Köhler, Simone, Kurt M. Schmoller, Alvaro H. Crevenna, and Andreas R. Bausch. 2012. "Regulating Contractility of the Actomyosin Cytoskeleton by PH." *Cell Reports* 2 (3): 433–39. https://doi.org/10.1016/j.celrep.2012.08.014.

Koivusalo, Mirkka, Christopher Welch, Hisayoshi Hayashi, Cameron C. Scott, Moshe Kim, Todd Alexander, Nicolas Touret, Klaus M. Hahn, and Sergio Grinstein. 2010. "Amiloride Inhibits Macropinocytosis by Lowering Submembranous PH and Preventing Rac1 and Cdc42 Signaling." *Journal of Cell Biology* 188 (4): 547–63. https://doi.org/10.1083/jcb.200908086.

Kumar, Rinku, and Bidisha Sinha. 2017. "Regulation of Thickness of Actomyosin Cortex in Well-Spread Cells by Contractility and Spread Area." *BiorXiv*. https://doi.org/10.1101/205138.

Lancaster, OscarM, Maël LeBerre, Andrea Dimitracopoulos, Daria Bonazzi, Ewa Zlotek-Zlotkiewicz, Remigio Picone, Thomas Duke, Matthieu Piel, and Buzz Baum. 2013. "Mitotic Rounding Alters Cell Geometry to Ensure Efficient Bipolar Spindle Formation." *Developmental Cell*. https://doi.org/10.1016/j.devcel.2013.03.014.

Lee, Hong-pyo, Luo Gu, David J. Mooney, Marc E. Levenston, and Ovijit Chaudhuri. 2017. "Mechanical Confinement Regulates Cartilage Matrix Formation by Chondrocytes." *Nature Materials*. https://doi.org/10.1038/nmat4993.

Lee, Hong-pyo, Ryan Stowers, and Ovijit Chaudhuri. 2019. "Volume Expansion and TRPV4 Activation Regulate Stem Cell Fate in Three-Dimensional Microenvironments." *Nature Communications*. https://doi.org/10.1038/s41467-019-08465-x.

Lieber, Arnon D., Yonatan Schweitzer, Michael M. Kozlov, and Kinneret Keren. 2015. "Front-to-Rear Membrane Tension Gradient in Rapidly Moving Cells." *Biophysical Journal* 108 (7): 1599–1603. https://doi.org/10.1016/j.bpj.2015.02.007.

Lieber, Arnon D., Shlomit Yehudai-Resheff, Erin L. Barnhart, Julie A. Theriot, and Kinneret Keren. 2013. "Membrane Tension in Rapidly Moving Cells Is Determined by Cytoskeletal Forces." *Current Biology*. https://doi.org/10.1016/j.cub.2013.05.063.

Limozin, Laurent, and Kheya Sengupta. 2009. "Quantitative Reflection Interference Contrast Microscopy (RICM) in Soft Matter and Cell Adhesion." *ChemPhysChem*. https://doi.org/10.1002/cphc.200900601.

Lisjak, Marjeta, Maja Potokar, Boštjan Rituper, Jernej Jorgačevski, and Robert Zorec. 2017. "AQP4e-Based Orthogonal Arrays Regulate Rapid Cell Volume Changes in Astrocytes." *The Journal of Neuroscience* 37 (44): 10748–56. https://doi.org/10.1523/jneurosci.0776-17.2017.

Liu, Yan Jun, Maël Le Berre, Franziska Lautenschlaeger, Paolo Maiuri, Andrew Callan-Jones, Mélina Heuzé, Tohru Takaki, Raphaël Voituriez, and Matthieu Piel. 2015. "Confinement and Low Adhesion Induce Fast Amoeboid Migration of Slow Mesenchymal Cells." *Cell*.

https://doi.org/10.1016/j.cell.2015.01.007.

Louvet-Vallée, Sophie. 2000. “ERM Proteins: From Cellular Architecture to Cell Signaling.” *Biology of the Cell*. Elsevier Masson SAS. https://doi.org/10.1016/S0248-4900(00)01078-9.

Lumpkin, Ellen A., and Michael J. Caterina. 2007. “Mechanisms of Sensory Transduction in the Skin.” *Nature*. https://doi.org/10.1038/nature05662.

Martinac, Boris. 2014. “The Ion Channels to Cytoskeleton Connection as Potential Mechanism of Mechanosensitivity.” *Biochimica et Biophysica Acta - Biomembranes* 1838 (2): 682–91. https://doi.org/10.1016/j.bbamem.2013.07.015.

McGrail, Daniel J., Kathleen M. McAndrews, Chandler P. Brandenburg, Nithin Ravikumar, Quang Minh N. Kieu, and Michelle R. Dawson. 2015. “Osmotic Regulation Is Required for Cancer Cell Survival under Solid Stress.” *Biophysical Journal*. https://doi.org/10.1016/j.bpj.2015.07.046.

McGrath, James L. 2007. “Cell Spreading: The Power to Simplify.” *Current Biology*. https://doi.org/10.1016/j.cub.2007.03.057.

McNeil, Paul L., and Richard A. Steinhardt. 1997. “Loss, Restoration, and Maintenance of Plasma Membrane Integrity.” *Journal of Cell Biology*. https://doi.org/10.1083/jcb.137.1.1.

Minkov, Ivan L., Emil D. Manev, Svetla V. Sazdanova, and Kiril H. Kolikov. 2013. “Equilibrium and Dynamic Osmotic Behaviour of Aqueous Solutions with Varied Concentration at Constant and Variable Volume.” *The Scientific World Journal* 2013. https://doi.org/10.1155/2013/876897.

Miroshnikova, Yekaterina A., Michele M. Nava, and Sara A. Wickström. 2017. “Emerging Roles of Mechanical Forces in Chromatin Regulation.” *Journal of Cell Science* 130 (14): 2243–50. https://doi.org/10.1242/jcs.202192.

Miyamoto, Tatsuya, Tsutomu Mochizuki, Hiroshi Nakagomi, Satoru Kira, Masaki Watanabe, Yasunori Takayama, Yoshiro Suzuki, Schuichi Koizumi, Masayuki Takeda, and Makoto Tominaga. 2014. “Functional Role for Piezo1 in Stretch-Evoked Ca2+ Influx and ATP Release in Urothelial Cell Cultures.” *Journal of Biological Chemistry* 289 (23): 16565–75. https://doi.org/10.1074/jbc.M113.528638.

Model, Michael A. 2018. “Methods for Cell Volume Measurement.” *Cytometry A* 93 (3): 281-296. https://doi.org/10.1002/cyto.a.23152.

Moeendarbary, Emad, Léo Valon, Marco Fritzsche, Andrew R. Harris, Dale A. Moulding, Adrian J. Thrasher, Eleanor Stride, L. Mahadevan, and Guillaume T. Charras. 2013. “The Cytoplasm of Living Cells Behaves as a Poroelastic Material.” *Nature Materials*. https://doi.org/10.1038/nmat3517.

Mola, Maria Grazia, Angelo Sparaneo, Concetta Domenica Gargano, David C. Spray, Maria Svelto, Antonio Frigeri, Eliana Scemes, and Grazia Paola Nicchia. 2016. “The Speed of Swelling Kinetics Modulates Cell Volume Regulation and Calcium Signaling in Astrocytes: A Different Point of View on the Role of Aquaporins.” *GLIA*. https://doi.org/10.1002/glia.22921.

Mori, Yoichiro. 2012. “Mathematical Properties of Pump-Leak Models of Cell Volume Control and Electrolyte Balance.” *Journal of Mathematical Biology* 65 (5): 875–918. https://doi.org/10.1007/s00285-011-0483-8.

Moriarty, Rebecca A., and Kimberly M. Stroka. 2018. “Physical Confinement Alters Sarcoma Cell Cycle Progression and Division.” *Cell Cycle* 17 (19–20): 2360–73.

https://doi.org/10.1080/15384101.2018.1533776.

Morishita, Kazuhiro, Kengo Watanabe, and Hidenori Ichijo. 2019. “Cell Volume Regulation in Cancer Cell Migration Driven by Osmotic Water Flow.” *Cancer Science*, July, cas.14079. https://doi.org/10.1111/cas.14079.

Nath, Binita, Asif Raza, Vishal Sethi, Amaresh Dalal, Siddhartha Sankar Ghosh, and Gautam Biswas. 2018. “Understanding Flow Dynamics, Viability and Metastatic Potency of Cervical Cancer (HeLa) Cells through Constricted Microchannel.” *Scientific Reports* 8 (1). https://doi.org/10.1038/s41598-018-35646-3.

Nawaz, Schanila, Paula Sánchez, Kai Bodensiek, Sai Li, Mikael Simons, and Iwan A.T. Schaap. 2012. “Cell Visco-Elasticity Measured with AFM and Optical Trapping at Sub-Micrometer Deformations.” *PLoS ONE* 7 (9). https://doi.org/10.1371/journal.pone.0045297.

Neurohr, Gabriel E, Rachel L Terry, Folkert J Van Werven, Liam J Holt, Angelika Amon Correspondence, Jette Lengefeld, Megan Bonney, et al. 2019. “Excessive Cell Growth Causes Cytoplasm Dilution And Contributes to Senescence Article Excessive Cell Growth Causes Cytoplasm Dilution And Contributes to Senescence.” *Cell* 176. https://doi.org/10.1016/j.cell.2019.01.018.

Newton, H, D E Pegg, R Barrass, and R G Gosden. 1999. “Osmotically Inactive Volume, Hydraulic Conductivity, and Permeability to Dimethyl Sulphoxide of Human Mature Oocytes.” *Journal of Reproduction and Fertility* 117 (1): 27–33.

Norman, Leann L., Jan Bruges, Kheya Sengupta, Pierre Sens, and Helim Aranda-Espinoza. 2010. “Cell Blebbing and Membrane Area Homeostasis in Spreading and Retracting Cells.” *Biophysical Journal* 99 (6): 1726–33. https://doi.org/10.1016/j.bpj.2010.07.031.

Norman, Leann, Kheya Sengupta, and H. Aranda-Espinoza Helim. 2011. “Blebbing Dynamics during Endothelial Cell Spreading.” *European Journal of Cell Biology* 90 (1): 37–48. https://doi.org/10.1016/j.ejcb.2010.09.013.

Nourse, Jamison L., and Medha M. Pathak. 2017. “How Cells Channel Their Stress: Interplay between Piezo1 and the Cytoskeleton.” *Seminars in Cell and Developmental Biology*. Elsevier Ltd. https://doi.org/10.1016/j.semcdb.2017.06.018.

Okada, Y, E Maeno, T Shimizu, K Dezaki, J Wang, and S Morishima. 2001. “Receptor-Mediated Control of Regulatory Volume Decrease (RVD) and Apoptotic Volume Decrease (AVD).” *The Journal of Physiology* 532: 3–16.

Oney, Izzet, Isil Aksan Kurnaz, and M. Levent Kurnaz. 2005. “Cytoplasmic-to-Nuclear Volume Ratio Affects AP-1 Complex Formation as an Indicator of Cell Cycle Responsiveness.” *FEBS Letters* 579 (2): 433–40. https://doi.org/10.1016/j.febslet.2004.11.104.

Otto, Oliver, Philipp Rosendahl, Alexander Mietke, Stefan Golfier, Christoph Herold, Daniel Klaue, Salvatore Girardo, et al. 2015. “Real-Time Deformability Cytometry: On-the-Fly Cell Mechanical Phenotyping.” *Nature Methods* 12 (3): 199–202. https://doi.org/10.1038/nmeth.3281.

Ozu, Marcelo, Luciano Galizia, Cynthia Acuña, and Gabriela Amodeo. 2018. “Aquaporins: More Than Functional Monomers in a Tetrameric Arrangement.” *Cells* 7 (11): 209. https://doi.org/10.3390/cells7110209.

Pafundo, Diego E., Cora L. Alvarez, Gerhard Krumschnabel, and Pablo J. Schwarzbaum. 2010. “A Volume

Regulatory Response Can Be Triggered by Nucleosides in Human Erythrocytes, a Perfect Osmometer No Longer." *Journal of Biological Chemistry*. https://doi.org/10.1074/jbc.M109.078246.

Pagliara, Stefano, Kristian Franze, Crystal R. McClain, George W. Wylde, Cynthia L. Fisher, Robin J. M. Franklin, Alexandre J. Kabla, Ulrich F. Keyser, and Kevin J. Chalut. 2014. "Auxetic Nuclei in Embryonic Stem Cells Exiting Pluripotency." *Nature Materials*. https://doi.org/10.1038/nmat3943.

Paul, Jonas, Stefan Romeis, Jürgen Tomas, and Wolfgang Peukert. 2014. "A Review of Models for Single Particle Compression and Their Application to Silica Microspheres." *Advanced Powder Technology*. Elsevier. https://doi.org/10.1016/j.apt.2013.09.009.

Pedersen, S F, E K Hoffmann, and J W Mills. 2001. "The Cytoskeleton and Cell Volume Regulation." *Comparative Biochemistry and Physiology Part A* 130: 385–99.

Pedersen, Stine F, Else K Hoffmann, Ivana Novak, Annarosa Arcangeli, and Jorge Arreola. 2013. "Cell Volume Regulation in Epithelial Physiology and Cancer." https://doi.org/10.3389/fphys.2013.00233.

Perez Gonzalez, Nicolas, Jiaxiang Tao, Nash D. Rochman, Dhruv Vig, Evelyn Chiu, Denis Wirtz, and Sean X. Sun. 2018. "Cell Tension and Mechanical Regulation of Cell Volume." *Molecular Biology of the Cell* 29 (21): 0–0. https://doi.org/10.1091/mbc.e18-04-0213.

Picas, Laura, Felix Rico, and Simon Scheuring. 2012. "Direct Measurement of the Mechanical Properties of Lipid Phases in Supported Bilayers." *Biophysical Journal* 102 (1). https://doi.org/10.1016/j.bpj.2011.11.4001.

Pietuch, Anna, Bastian R. Brückner, and Andreas Janshoff. 2013. "Membrane Tension Homeostasis of Epithelial Cells through Surface Area Regulation in Response to Osmotic Stress." *Biochimica et Biophysica Acta - Molecular Cell Research*. https://doi.org/10.1016/j.bbamcr.2012.11.006.

Pietuch, Anna, and Andreas Janshoff. 2013. "Mechanics of Spreading Cells Probed by Atomic Force Microscopy." *Open Biology* 3 (JUL). https://doi.org/10.1098/rsob.130084.

Ping Ting-Beall, By H, David Needham, and Robert M Hochmuth. 1993. "Volume and Osmotic Properties of Human Neutrophils." *Blood.* 81 (10): 2774–80. www.bloodjournal.org.

Ponder, Eric. 1935. "The Measurement of Red-cell Volume. Conductivity Measurements." *The Journal of Physiology* 85 (4): 439–49. https://doi.org/10.1113/jphysiol.1935.sp003330.

Potma, E. O., W. P. de Boeij, P. J. M. van Haastert, and D. A. Wiersma. 2012. "Real-Time Visualization of Intracellular Hydrodynamics in Single Living Cells." *Proceedings of the National Academy of Sciences* 98 (4): 1577–82. https://doi.org/10.1073/pnas.98.4.1577.

Prinz, William A., and Jenny E. Hinshaw. 2009. "Membrane-Bending Proteins." *Critical Reviews in Biochemistry and Molecular Biology* 44 (5): 278–91. https://doi.org/10.1080/10409230903183472.

Pritchard, Scott, and Farshid Guilak. 2004. "The Role of F-Actin in Hypo-Osmotically Induced Cell Volume Change and Calcium Signaling in Anulus Fibrosus Cells." *Annals of Biomedical Engineering*. https://doi.org/10.1023/B:ABME.0000007795.69001.35.

Rädler, Joachim, and Erich Sackmann. 1993. "Imaging Optical Thicknesses and Separation Distances of Phospholipid Vesicles at Solid Surfaces." *Journal de Physique II*.

Rape, Andrew D., Wei Hui Guo, and Yu Li Wang. 2011. "The Regulation of Traction Force in Relation to Cell Shape and Focal Adhesions." *Biomaterials*. https://doi.org/10.1016/j.biomaterials.2010.11.044.

Rappoport, Joshua Z, and Sanford M Simon. 2003. “Real-Time Analysis of Clathrin-Mediated Endocytosis during Cell Migration.” *Journal of Cell Science*. https://doi.org/10.1242/jcs.00289.

Raucher, Drazen, and Michael P. Sheetz. 2000. “Cell Spreading and Lamellipodial Extension Rate Is Regulated by Membrane Tension.” *Journal of Cell Biology* 148 (1): 127–36. https://doi.org/10.1083/jcb.148.1.127.

Rojas, Enrique R., and Kerwyn Casey Huang. 2018. “Regulation of Microbial Growth by Turgor Pressure.” *Current Opinion in Microbiology* 42: 62–70. https://doi.org/10.1016/j.mib.2017.10.015.

Roux, Aurélien. 2013. “The Physics of Membrane Tubes: Soft Templates for Studying Cellular Membranes.” *Soft Matter*. https://doi.org/10.1039/c3sm50514f.

Roux, Aurélien, Damien Cuvelier, Pierre Nassoy, Jacques Prost, Patricia Bassereau, and Bruno Goud. 2005. “Role of Curvature and Phase Transition in Lipid Sorting and Fission of Membrane Tubules.” *EMBO Journal* 24 (8): 1537–45. https://doi.org/10.1038/sj.emboj.7600631.

Sachs, Frederick, and Mettupalayam V. Sivaselvan. 2015. “Cell Volume Control in Three Dimensions: Water Movement without Solute Movement.” *The Journal of General Physiology* 145 (5): 373–80. https://doi.org/10.1085/jgp.201411297.

Salbreux, Guillaume, Guillaume Charras, and Ewa Paluch. 2012. “Actin Cortex Mechanics and Cellular Morphogenesis.” *Trends in Cell Biology*. https://doi.org/10.1016/j.tcb.2012.07.001.

Salzer, Ulrich, Julius Kostan, and Kristina Djinović-Carugo. 2017. “Deciphering the BAR Code of Membrane Modulators.” *Cellular and Molecular Life Sciences*. Birkhauser Verlag AG. https://doi.org/10.1007/s00018-017-2478-0.

Sasaki, Sei, Naofumi Yui, and Yumi Noda. 2014. “Actin Directly Interacts with Different Membrane Channel Proteins and Influences Channel Activities: AQP2 as a Model.” *Biochimica et Biophysica Acta - Biomembranes*. https://doi.org/10.1016/j.bbamem.2013.06.004.

Saxton, Michael J., and Ken Jacobson. 1997. “Single-Particle Tracking: Applications to Membrane Dynamics.” *Annual Review of Biophysics and Biomolecular Structure* 26 (1): 373–99. https://doi.org/10.1146/annurev.biophys.26.1.373.

Schäfer, Edith, Torben Tobias Kliesch, and Andreas Janshoff. 2013. “Mechanical Properties of Giant Liposomes Compressed between Two Parallel Plates: Impact of Artificial Actin Shells.” *Langmuir* 29 (33): 10463–74. https://doi.org/10.1021/la401969t.

Schwiebert, Erik M., and Akos Zsembery. 2003. “Extracellular ATP as a Signaling Molecule for Epithelial Cells.” *Biochimica et Biophysica Acta - Biomembranes*. Elsevier. https://doi.org/10.1016/S0005-2736(03)00210-4.

Shapiro, Herbert. 1948. “The Change in Osmotically Inactive Fraction Produced by Cell Activation.” *The Journal of General PHysiology*.

Shi, Zheng, Zachary T. Graber, Tobias Baumgart, Howard A. Stone, and Adam E. Cohen. 2018. “Cell Membranes Resist Flow.” *Cell*. https://doi.org/10.1016/j.cell.2018.09.054.

Shinoda, Wataru. 2016. “Permeability across Lipid Membranes.” *Biochimica et Biophysica Acta - Biomembranes* 1858 (10): 2254–65. https://doi.org/10.1016/j.bbamem.2016.03.032.

Singer, SJ, and GL Nicolson. 1972. “The Fluid Mosaic Model of the Structure of Cell Membranes.” *Science*

175 (4023): 720–31. http://science.sciencemag.org/.

Sinha, Bidisha, Darius Köster, Richard Ruez, Pauline Gonnord, Michele Bastiani, Daniel Abankwa, Radu V Stan, et al. 2011. “Cells Respond to Mechanical Stress by Rapid Disassembly of Caveolae.” *Cell* 144 (3): 402–13. https://doi.org/10.1016/j.cell.2010.12.031.

Spector, I., N. R. Shorlet, D. Blasberger, and Y. Kashman. 1989. “Latrunculins - Novel Marine Macrolides That Disrupt Microfilament Organization and Affert Cell Growth: I. Comparison with Cytochalasin D.” *Cell Motility and the Cytoskeleton* 13 (3): 127–44. https://doi.org/10.1002/cm.970130302.

Steffen, A., M. Ladwein, G. A. Dimchev, A. Hein, L. Schwenkmezger, S. Arens, K. I. Ladwein, et al. 2013. “Rac Function Is Crucial for Cell Migration but Is Not Required for Spreading and Focal Adhesion Formation.” *Journal of Cell Science* 126 (20): 4572–88. https://doi.org/10.1242/jcs.118232.

Stricker, Jonathan, Tobias Falzone, and Margaret L. Gardel. 2010. “Mechanics of the F-Actin Cytoskeleton.” *Journal of Biomechanics* 43 (1): 9–14. https://doi.org/10.1016/j.jbiomech.2009.09.003.

Stroka, Kimberly M., Hongyuan Jiang, Shih Hsun Chen, Ziqiu Tong, Denis Wirtz, Sean X. Sun, and Konstantinos Konstantopoulos. 2014. “Water Permeation Drives Tumor Cell Migration in Confined Microenvironments.” *Cell*. https://doi.org/10.1016/j.cell.2014.02.052.

Sugimoto, Asuna, Aya Miyazaki, Keita Kawarabayashi, Masayuki Shono, Yuki Akazawa, Tomokazu Hasegawa, Kimiko Ueda-Yamaguchi, et al. 2017. “Piezo Type Mechanosensitive Ion Channel Component 1 Functions as a Regulator of the Cell Fate Determination of Mesenchymal Stem Cells.” *Scientific Reports* 7 (1). https://doi.org/10.1038/s41598-017-18089-0.

Sukenik, Shahar, Pin Ren, and Martin Gruebele. 2017. “Weak Protein–Protein Interactions in Live Cells Are Quantified by Cell-Volume Modulation.” *Proceedings of the National Academy of Sciences* 114 (26): 6776–81. https://doi.org/10.1073/pnas.1700818114.

Sych, Taras, Yves Mély, and Winfried Römer. 2018. “Lipid Self-Assembly and Lectin-Induced Reorganization of the Plasma Membrane.” *Philosophical Transactions of the Royal Society B: Biological Sciences*. Royal Society Publishing. https://doi.org/10.1098/rstb.2017.0117.

Syeda, Ruhma, Zhaozhu Qiu, Adrienne E. Dubin, Swetha E. Murthy, Maria N. Florendo, Daniel E. Mason, Jayanti Mathur, et al. 2016. “LRRC8 Proteins Form Volume-Regulated Anion Channels That Sense Ionic Strength.” *Cell* 164 (3): 499–511. https://doi.org/10.1016/j.cell.2015.12.031.

Taloni, Alessandro, Elena Kardash, Oguz Umut Salman, Lev Truskinovsky, Stefano Zapperi, and Caterina A M La Porta. 2015. “Volume Changes during Active Shape Fluctuations in Cells.” *Physical Review Letters*. https://doi.org/10.1103/PhysRevLett.114.208101.

Thery, M. 2010. “Micropatterning as a Tool to Decipher Cell Morphogenesis and Functions.” *Journal of Cell Science*. https://doi.org/10.1242/jcs.075150.

Thilo, L., and G. Vogel. 1980. “Kinetics of Membrane Internalization and Recycling during Pinocytosis in Dictyostelium Discoideum.” *Proceedings of the National Academy of Sciences* 77 (2): 1015–19. https://doi.org/10.1073/pnas.77.2.1015.

Thottacherry, Joseph Jose, Anita Joanna Kosmalska, Amit Kumar, Amit Singh Vishen, Alberto Elosegui-Artola, Susav Pradhan, Sumit Sharma, et al. 2018. “Mechanochemical Feedback Control of Dynamin Independent Endocytosis Modulates Membrane Tension in Adherent Cells.” *Nature*

Communications 9 (1). https://doi.org/10.1038/s41467-018-06738-5.

Tilley, Leann, Sophie Cribier, Ben Roelofsen, Jos A F Op den Kamp, and Laurens L M van Deenen. 1986. "ATP-Dependent Translocation of Amino Phospholipids across the Human Erythrocyte Membrane." *FEBS Letters* 194 (1): 21–27. https://doi.org/10.1016/0014-5793(86)80044-8.

Tinevez, J.-Y., U. Schulze, G. Salbreux, J. Roensch, J.-F. Joanny, and E. Paluch. 2009. "Role of Cortical Tension in Bleb Growth." *Proceedings of the National Academy of Sciences* 106 (44): 18581–86. https://doi.org/10.1073/pnas.0903353106.

Tojkander, S., G. Gateva, and P. Lappalainen. 2012. "Actin Stress Fibers - Assembly, Dynamics and Biological Roles." *Journal of Cell Science* 125 (8): 1855–64. https://doi.org/10.1242/jcs.098087.

Tran, Duy T., Andrius Masedunskas, Roberto Weigert, and Kelly G. Ten Hagen. 2015. "Arp2/3-Mediated F-Actin Formation Controls Regulated Exocytosis in Vivo." *Nature Communications*. https://doi.org/10.1038/ncomms10098.

Vallés, Patricia G., Victoria Bocanegra, Andrea Gil Lorenzo, and Valeria Victoria Costantino. 2015. "Physiological Functions and Regulation of the Na+/H+ Exchanger [NHE1] in Renal Tubule Epithelial Cells." *Kidney and Blood Pressure Research*. S. Karger AG. https://doi.org/10.1159/000368521.

Vargas, Pablo, Lucie Barbier, Pablo José Sáez, and Matthieu Piel. 2017. "Mechanisms for Fast Cell Migration in Complex Environments." *Current Opinion in Cell Biology*. Elsevier Ltd. https://doi.org/10.1016/j.ceb.2017.04.007.

Verkman AS. 2013. "Aquaporins." *Curr Biol.* https://doi.org/10.1016/j.cub.2012.11.025.Aquaporins.

Voss, Felizia K., Florian Ullrich, Jonas Muñch, Katina Lazarow, Darius Lutte, Nancy Mah, Miguel A. Andrade-Navarro, Jens P. Von Kries, Tobias Stauber, and Thomas J. Jentsch. 2014. "Identification of LRRC8 Heteromers as an Essential Component of the Volume-Regulated Anion Channel VRAC." *Science*. https://doi.org/10.1126/science.1252826.

Wakatsuki, T. 2003. "Mechanics of Cell Spreading: Role of Myosin II." *Journal of Cell Science*. https://doi.org/10.1242/jcs.00340.

Wells, C. M. 2004. "Rac1-Deficient Macrophages Exhibit Defects in Cell Spreading and Membrane Ruffling but Not Migration." *Journal of Cell Science* 117 (7): 1259–68. https://doi.org/10.1242/jcs.00997.

Westermann, Benedikt. 2012. "Bioenergetic Role of Mitochondrial Fusion and Fission." In *Biochimica et Biophysica Acta - Bioenergetics*. https://doi.org/10.1016/j.bbabio.2012.02.033.

Wu, Jason, Amanda H. Lewis, and Jörg Grandl. 2017. "Touch, Tension, and Transduction – The Function and Regulation of Piezo Ion Channels." *Trends in Biochemical Sciences* 42 (1): 57–71. https://doi.org/10.1016/j.tibs.2016.09.004.

Wu, Pei Hsun, Dikla Raz Ben Aroush, Atef Asnacios, Wei Chiang Chen, Maxim E. Dokukin, Bryant L. Doss, Pauline Durand-Smet, et al. 2018. "A Comparison of Methods to Assess Cell Mechanical Properties." *Nature Methods* 15 (7). https://doi.org/10.1038/s41592-018-0015-1.

Xie, Kenan, Yuehua Yang, and Hongyuan Jiang. 2018. "Controlling Cellular Volume via Mechanical and Physical Properties of Substrate." https://doi.org/10.1016/j.bpj.2017.11.3785.

Yang, Ming, and William J. Brackenbury. 2013. "Membrane Potential and Cancer Progression." *Frontiers*

in Physiology. https://doi.org/10.3389/fphys.2013.00185.

Yang, Nicole J., and Marlon J. Hinner. 2015. “Getting across the Cell Membrane: An Overview for Small Molecules, Peptides, and Proteins.” *Methods in Molecular Biology* 1266: 29–53. https://doi.org/10.1007/978-1-4939-2272-7_3.

Yang, Qing, Xiao Feng Zhang, Thomas D. Pollard, and Paul Forscher. 2012. “Arp2/3 Complex-Dependent Actin Networks Constrain Myosin II Function in Driving Retrograde Actin Flow.” *Journal of Cell Biology* 197 (7): 939–56. https://doi.org/10.1083/jcb.201111052.

Zhou, E. H., X. Trepat, C. Y. Park, G. Lenormand, M. N. Oliver, S. M. Mijailovich, C. Hardin, D. A. Weitz, J. P. Butler, and J. J. Fredberg. 2009. “Universal Behavior of the Osmotically Compressed Cell and Its Analogy to the Colloidal Glass Transition.” *Proceedings of the National Academy of Sciences* 106 (26): 10632–37. https://doi.org/10.1073/pnas.0901462106.

Zlotek-Zlotkiewicz, Ewa, Sylvain Monnier, Giovanni Cappello, Mael Le Berre, and Matthieu Piel. 2015. “Optical Volume and Mass Measurements Show That Mammalian Cells Swell during Mitosis.” *Journal of Cell Biology* 211 (4): 765–74. https://doi.org/10.1083/jcb.201505056.

Annexe

Publications list

1. Cadart, C., E. Zlotek-Zlotkiewicz, **L. Venkova**, O. Thouvenin, V. Racine, M. Le Berre, S. Monnier, and M. Piel. 2017. “Fluorescence EXclusion Measurement of Volume in Live Cells.” Methods in Cell Biology 139: 103–20. https://doi.org/10.1016/bs.mcb.2016.11.009.

2. Cadart*, C., **L. Venkova***, P. Recho, M. Cosentino Lagomarsino, and M. Piel. 2019. “The Physics of Cell-Size Regulation across Timescales.” Nature Physics 15 (August): 993–1004. https://doi.org/10.1038/s41567-019-0629-y.

*- these authors contributed equally

3. Funk, J., F. Merino, **L. Venkova**, L. Heydenreich, J. Kierfeld, P. Vargas, S. Raunser, M. Piel, and P. Bieling. 2019. “Profilin and Formin Constitute a Pacemaker System.” ELife 8: e50963. https://doi.org/10.7554/eLife.50963.

université PARIS-SACLAY | ÉCOLE DOCTORALE Structure et dynamique des systèmes vivants (SDSV)

Titre : Régulation du volume cellulaire en réponse aux déformations

Mots clés : volume cellulaire, déformations, cytosquelette

Résumé : Les déformations mécaniques peuvent induire un changement de la surface et du volume cellulaires. Nous nous intéressons particulièrement à la régulation du volume cellulaire chez les cellules mammifères dans le contexte de déformations à différentes échelles de temps. Nous avons développé une méthode de mesure du volume cellulaire reposant sur l'exclusion de fluorescence, qui nous permet d'effectuer des mesures de volume précise au niveau de la cellules uniques. Dans cette étude, nous nous sommes concentrés sur la régulation du volume cellulaire au cours de l'étalement dynamique sur un substrat (échelle de temps : minutes). Nous avons démontré qu'il existe différents régimes de régulation du volume lors de l'étalement : les cellules réduisent, augmentent ou ne modifient pas leur volume, en fonction de l'état du cortex d'actomyosine et de la vitesse d'étalement. Nous avons également montré que la régulation du volume en réponse à une compression mécanique rapide (échelle de temps : millisecondes) indépendante de l'adhérence dépend également de l'état du cortex d'actomyosine. Enfin, nous avons montré que la réponse du volume à un choc osmotique (échelle de temps : secondes) est plus que complexe que décrite dans la littérature. En utilisant la technique du choc osmotique, nous avons également confirmé que les cellules ont un large excès de membrane repliée dans des réservoirs. Nos résultats montrent que le volume et l'aire cellulaires sont couplés par l'homéostasie de la tension de surface, et, étant donné que les déformations induisent une augmentation de la tension de surface, elles conduisent à des modifications du volume et de l'aire de la cellule.

Title : Cell volume regulation in response to deformations

Keywords : cell volume, deformations, cytoskeleton

Abstract : Mechanical deformations can lead to a change in cell surface area and volume. We are particularly interested in single mammalian cell volume regulation in the context of deformations of different timescales. We developed a method for cell volume measurements based on a fluorescent exclusion that allowed us to perform precise volume measurements of individual live cells. In the present study, we mainly focused on cell volume regulation while dynamic spreading on a substrate (timescale – minutes). We demonstrated that there are different regimes for volume regulation while spreading: cells decrease, increase or do not change volume, and a type of the regime depends on the state of the actomyosin cortex and spreading speed. We also showed that volume regulation in response to fast mechanical compression (timescale – milliseconds) independent of adhesion also depends on the actomyosin cortex state. Additionally, we showed that cell volume response to the osmotic shock (timescale – seconds) is more complex than it used to be known in the literature. Using osmotic shock technique, we also confirmed that cells have a large excess of membrane folded in reservoirs. Taken together, our data show that cell volume and surface area are coupled through surface tension homeostasis and as deformations induce surface tension increase, they lead to change volume and surface area.

Université Paris-Saclay
Espace Technologique / Immeuble Discovery
Route de l'Orme aux Merisiers RD 128 / 91190 Saint-Aubin, France